Understanding Complex Systems

Springer : COMPLEXITY

Christos Skiadas *Editor*

The Foundations of Chaos Revisited: From Poincaré to Recent Advancements

Springer

Springer Complexity

Springer Complexity is an interdisciplinary program publishing the best research and academic-level teaching on both fundamental and applied aspects of complex systems – cutting across all traditional disciplines of the natural and life sciences, engineering, economics, medicine, neuroscience, social and computer science.

Complex Systems are systems that comprise many interacting parts with the ability to generate a new quality of macroscopic collective behavior the manifestations of which are the spontaneous formation of distinctive temporal, spatial or functional structures. Models of such systems can be successfully mapped onto quite diverse "real-life" situations like the climate, the coherent emission of light from lasers, chemical reaction-diffusion systems, biological cellular networks, the dynamics of stock markets and of the internet, earthquake statistics and prediction, freeway traffic, the human brain, or the formation of opinions in social systems, to name just some of the popular applications.

Although their scope and methodologies overlap somewhat, one can distinguish the following main concepts and tools: self-organization, nonlinear dynamics, synergetics, turbulence, dynamical systems, catastrophes, instabilities, stochastic processes, chaos, graphs and networks, cellular automata, adaptive systems, genetic algorithms and computational intelligence.

The three major book publication platforms of the Springer Complexity program are the monograph series "Understanding Complex Systems" focusing on the various applications of complexity, the "Springer Series in Synergetics", which is devoted to the quantitative theoretical and methodological foundations, and the "SpringerBriefs in Complexity" which are concise and topical working reports, case-studies, surveys, essays and lecture notes of relevance to the field. In addition to the books in these two core series, the program also incorporates individual titles ranging from textbooks to major reference works.

Understanding Complex Systems

Founding Editor: S. Kelso

Future scientific and technological developments in many fields will necessarily depend upon coming to grips with complex systems. Such systems are complex in both their composition – typically many different kinds of components interacting simultaneously and nonlinearly with each other and their environments on multiple levels – and in the rich diversity of behavior of which they are capable.

The Springer Series in Understanding Complex Systems series (UCS) promotes new strategies and paradigms for understanding and realizing applications of complex systems research in a wide variety of fields and endeavors. UCS is explicitly transdisciplinary. It has three main goals: First, to elaborate the concepts, methods and tools of complex systems at all levels of description and in all scientific fields, especially newly emerging areas within the life, social, behavioral, economic, neuro- and cognitive sciences (and derivatives thereof); second, to encourage novel applications of these ideas in various fields of engineering and computation such as robotics, nano-technology and informatics; third, to provide a single forum within which commonalities and differences in the workings of complex systems may be discerned, hence leading to deeper insight and understanding.

UCS will publish monographs, lecture notes and selected edited contributions aimed at communicating new findings to a large multidisciplinary audience.

More information about this series at http://www.springer.com/series/5394

Christos Skiadas
Editor

The Foundations of Chaos Revisited: From Poincaré to Recent Advancements

Springer

Editor
Christos Skiadas
ManLab Technical University of Crete
Chania, Greece

ISSN 1860-0832 ISSN 1860-0840 (electronic)
Understanding Complex Systems
ISBN 978-3-319-29699-9 ISBN 978-3-319-29701-9 (eBook)
DOI 10.1007/978-3-319-29701-9

Library of Congress Control Number: 2016938786

Printed on acid-free paper

This Springer imprint is published by Springer Nature
The registered company is Springer International Publishing AG Switzerland

Preface

Henri Poincaré is considered to be one of the great minds of mathematics, physics, and astronomy. Apart from his rigorous mathematical and analytical style, he was also renowned for his deep insights into science and the philosophy of science. He developed and contributed to many important scientific achievements, and his works on the foundations of science, scientific hypothesis, and scientific method were written with elegance and style. Even more significantly, perhaps, he came to bear upon recent scientific achievements when he put forward the Poincaré conjecture, thereby introducing geometry and topology into the analysis of shape and form. The Poincaré conjecture and his work on the three-body problem are considered to constitute the foundations of the modern chaos theory.

This book *The Foundations of Chaos Revisited: From Poincaré to Recent Advancements* was motivated by the CHAOS 2015 International Conference at the Henri Poincaré Institute in Paris. This was undoubtedly the best place to gain insight into chaos theory as inspired by the Poincaré tradition in a place that must be considered as the home of Poincaré or, better, the home of mathematics in Paris.

In order to explore the foundations of chaos theory in greater depth, the aim was to approach the main theme with the style and elegance of Henri Poincaré, as exemplified in his mathematical-analytical formulation. Chaos theory provides a link between science and the humanities. It is one of the few scientific topics that tends to unify the different areas of science and to connect them with society as a whole and with a language, CHAOS, that is generally accepted as providing a common substrate, even if this substrate can be seen as mathematics, geometry, graphs, or linguistic material, depending on your viewing point. However, all would accept that chaos theory brings together a very broad range of fields.

Following a proposal by Christian Caron from Springer, we have asked the plenary and keynote speakers of the conference to contribute to a book with an extended version of their presentations, the aim being to connect Poincaré's contributions with today's achievements. We are happy that we have already received contributions of high caliber that will take the reader on a fascinating tour of chaos theory. Important applications integrating traditional and modern chaos theory are included in the final chapters of this book.

Ferdinand Verhulst has already published several contributions on the Henri Poincaré legacy. With his elegant style and deep understanding of the state of science, especially in mathematics and physics, both during and prior to the days when Poincaré was active, he presents a brilliant paper entitled "Henri Poincaré's Inventions in Dynamical Systems and Topology." He explains how Poincaré's broad knowledge of the existing literature led to such outstanding contributions to dynamical systems and topology. The latter achievement was also built upon the foundations in geometry and geometric representations of mathematical problems prevalent in the French school. The Poincaré map exemplifies Poincaré's deep insight into the way geometric visualization can lead to progress in mathematical modeling and especially chaotic modeling.

Jean-Mark Ginoux, a biographical expert on Poincaré who has made good use of the "Archives Henri Poincaré," has contributed a paper entitled "From Nonlinear Oscillations to Chaos Theory." Following on from the first chapter by Ferdinand Verhulst, he proceeds to explain how Poincaré's mathematical concept of limit cycle and the existence of sustained oscillations representing a stable regime of sustained waves contributed to the advancement of theory and practice in radio communications. The author provides documentation and an excellent presentation of the three main devices, the series-dynamo machine, the singing arc, and the triode, over a period ranging from the end of the nineteenth century till the end of the Second World War. He shows how Van der Pol's study of the oscillations of two coupled triodes and the forced oscillations of a triode led, at the end of the Second World War, to Mary Cartwright and John Littlewood's characterization of the related oscillating behavior as "bizarre." This behavior would later be identified as "chaotic." However, the basis of this achievement was set forty years earlier by Poincaré in his work *La Théorie de Maxwell et les oscillations Hertziennes: la télegraphie sans fil* (Gauthier-Villars, 3e ed. (Paris), 1907).

The early 1940s were a milestone for the characterization of nonlinear and "bizarre" oscillations, or better "fine structure solutions," to use the more elegant terminology for chaotic solutions in wave modeling in telecommunications. Then, in 1941 the Russian researcher A.N. Kolmogorov began modeling the chaotic phenomenon in fluid flow known as turbulence. It was an important step to pass from oscillations to waves in flows and turbulence. However, the limit cycles introduced by Poincaré in the solution of differential equations were a key achievement underpinning progress that would be made some decades later. And even more important was his paper on rotating fluids: "Sur la stabilité de l'équilibre des figures piriformes affectées par une masse fluide en rotation," Poincaré, H. (1901) *Philosophical Transactions A* **198**, 333–373. David Ruelle contributes to this important topic with an extended paper from the honorary presentation for his eightieth birthday at the CHAOS 2015 International Conference at the Henri Poincaré Institute in Paris. This paper follows up with further comments by Giovanni Gallavotti and Pedro Garrido, who also discuss related computer applications. From the early 1970s, with their seminal paper "On the Nature of Turbulence," Ruelle and Takens helped to bring forward Kolmogorov's ideas, while over the last few years (2012, 2014), David Ruelle has extended his contributions to the nonequilibrium statistical mechanics

of turbulence. Note that the related work of Kolmogorov was mainly on an ideal form of homogeneous and isotropic turbulence, whereas Ruelle is working on the problem of real nonhomogeneous turbulence, where the lack of homogeneity is called *intermittency*. According to David Ruelle, his paper integrates ideas of turbulence and heat flow:

> Translating a nonequilibrium problem (turbulence) into another nonequilibrium problem (heat flow) is in principle an interesting idea, but there are two obvious difficulties:
>
> - Expressing the fluid Hamiltonian as the Hamiltonian of a coupled system of nodes is likely to give complicated results.
> - The rigorous study of heat flow is known to be extremely hard.
>
> What we shall do is to use crude (but physically motivated) approximations, with the hope that the results obtained are in reasonable agreement with experiments. This is indeed the conclusion of our study, indicating that turbulence lies naturally within accepted ideas of nonequilibrium statistical mechanics.

Giovanni Gallavotti and Pedro Garrido follow Ruelle's paper "Non-equilibrium Statistical Mechanics of Turbulence" with "Comments on Ruelle's Intermittency Theory." Giovanni Gallavotti has made significant contributions to chaos theory and applications in the late 1970s and has published a book entitled *Foundations of Fluid Dynamics*. Here, in this joint paper with Garrido, they present an intermittency correction term to the classical Kolmogorov law. Many calculations are presented for various cases of turbulence and for different Reynold's numbers, thus strengthening the related theory.

Following the previous papers, Roger Lewandowski and Benoît Pinier contribute with a paper "The Kolmogorov Law of Turbulence: What Can Rigorously Be Proved?" They consider how homogeneity and isotropy are introduced into turbulence and give a mathematical proof of the famous -5/3 Kolmogorov law. Their aim is to:

1. Carefully express the appropriate similarity assumption that a homogeneous and isotropic turbulent flow must satisfy in order to derive the -5/3 law
2. Derive the -5/3 law theoretically from the similarity assumption
3. Discuss the numerical validity of such a law from a numerical simulation in a test case, using the software BENFLOW 1.0, developed at the Institute of Mathematical Research in Rennes

They use the Navier-Stokes equations and refer to work by Boussinesq: "Essai sur la théorie des eaux courantes." *Mémoires présentés par divers savants à l'Académie des Sciences* (Paris, 23.1.1877, 1–660). Another approach is given in "Sur la stabilité de l'équilibre des figures piriformes affectées par une masse fluide en rotation," Poincaré, H. (1901), *Philosophical Transactions A* **198**, 333–373.

Pierre Coullet and Yves Pomeau present a very important topic under the title "History of Chaos from a French Perspective." This is an exceptional paper, deserving much attention. Every point is presented with clarity and a deep insight into the subject. They start with Poincaré and the French tradition in dynamical systems. As they explain:

> The history of chaos begins with Poincaré. His PhD thesis can be seen as the very beginning of dynamics as we know it. He invented powerful geometrical methods to understand "qualitatively" the behavior of solutions of ordinary differential equations. His message remains alive, because of the power of his methods. As a side remark it is curious to see his basic concepts rediscovered again and again. The saddle-node bifurcation (noeud-col in Poincaré thesis) has grown popular in this respect and lately has acquired various fancy new names. Poincaré not only pioneered qualitative methods for the analysis of differential equations, but he also began to study dissipative dynamical systems that differed from the (far more complex) methods of Lagrangian dynamics (a topic where he also brought fundamental ideas).

In the same style they continue with a fascinating presentation, discussing authors and researchers, theoreticians and experimentalists, and the interaction between them, as well as scientific progress in the field of chaos. They conclude:

> Clearly, chaos theory and experiment has not suffered from lack of attractiveness. Nowadays it has morphed into the wider field of nonlinear science, drawing in many bright young colleagues. We hope this tree will continue to blossom.

Orbits and periodic orbits in a topological environment, maps, and related presentations all started with Poincaré, to be expanded later in a well-known paper by V. Arnold entitled: "Small Denominators. I. Mapping of the Circumference onto Itself" (*Amer. Math. Soc. Transl.* (2), 46:213–284, 1965). Quasiperiodicity is explored in the paper by Suddhasattwa Das, Yoshitaka Saiki, Evelyn Sander, and James A. Yorke. They provided a one-dimensional quasiperiodic map as an example and showed that their weighted averages converged far faster than the usual rate of O(1 N), provided f was sufficiently differentiable. They used this method for efficient numerical computation of rotation numbers, invariant densities, and conjugacies of quasiperiodic systems and also to provide evidence that the changes of variables were (real) analytic. James Yorke was an invited plenary speaker at the CHAOS 2015 International Conference. He is one of the main contributors to chaos theory with many papers to his name. Two of the best are "Period Three Implies Chaos," T.Y. Li, and J.A. Yorke, *American Mathematical Monthly* 82, 985 (1975), and "Controlling Chaos," E. Ott, C. Grebogi, and J.A. Yorke, *Phys. Rev. Lett.* 64, 1196–1199 (1990).

Alexander Ramm has explored the problem of heat transfer in a complex medium. He has already investigated the scattering of acoustic and electromagnetic waves by small bodies of arbitrary shapes and discussed applications to the creation of new engineered materials. These are very important contributions to a subject that has many practical applications in the production of modern materials with special characteristics.

Theory and practice suggests that time delays are connected with chaotic behavior, and this is explained in the paper by V.J. Law, W.G. Graham, and D.P. Dowling entitled "Plasma Hysteresis and Instability: A Memory Perspective". They start with a historical review of the significance of Duddell's "singing arc" and its application to deleterious effects in the control of both hysteresis and spatiotemporal stability as the two-electrode valve evolved into the three-electrode or triode vacuum tube. They illustrate the use of oscillograph Lissajous figures in the I-V plane,

the Q-V plane, and the harmonic plane to investigate these deleterious effects in modern low-pressure parallel-plate systems and atmospheric pressure plasma systems and compare the hysteresis and stability within the "singing arc." They discuss developments from the original oscillograph measurement to today's analog, digital, and software methods. They also ask whether the "singing arc" and other plasma systems fall in the category of a memory element. The authors explain Poincaré's achievements in this area:

> A recent reevaluation of the work of Henri Poincaré has revealed that he too played a significant role in the mathematical understanding of the arc's stable regime using limit cycles and their deviation from that regime. Even though Poincaré did not study the triode vacuum tube, the review claims that the two-electrode "singing arc" is analogous to the three-electrode or triode vacuum tube. Given the extended triode development time line, it would seem unlikely that, at Poincaré's wireless telegraphy conference in 1908 or at the time close to his death in 1912, he was able to deduce or describe the behavior of early triode vacuum tubes that operated under soft or hard vacuum conditions. Nevertheless, Poincaré's closed limit cycles do predate the work of Van de Pol and J. Van de Mark along with Andronov self-oscillations.

The Indian scientist Sir Chandrasekhara Venkata Raman earned the 1930 Nobel Prize in physics for his work in the field of light scattering and the development of the so-called Raman amplifiers. Following this discovery, several theoretical and applied studies led to the construction of new scientific fields, including the fiber Raman amplifiers presented in a paper by Vladimir L. Kalashnikov and Sergey V. Sergeyev entitled "Stochastic Anti-resonance in Polarization Phenomena." To treat this problem, the authors based their work on the classical Poincaré sphere, an analytic tool first developed in Poincaré's publication: "Les methodes nouvelles de la mecanique celeste" (Tome I, Paris, 1892, Gauthier-Villars). The authors put forward a more general analytic framework, useful in many topics, as discussed in their paper:

> Here we shall demonstrate a cooperation between analytical multi-scale techniques and direct numerical simulations of SDEs that reveals a quite nontrivial phenomenon, stochastic antiresonance (SAR). This can be characterized by different signatures, including the Hurst parameter, the Kramers length, the standard deviation, etc. This phenomenon can be treated as a noise-driven escape from a metastable state which is intrinsic to diffusion in crystals, protein-folding, activated chemical reactions, and many other contexts. As a test bed, we consider a fiber Raman amplifier with random birefringence, a device with a direct practical impact on the development of high-transmission-rate optical networks.

Many applications of chaos are based on differential equations and systems of differential equations. Right from the beginning, when methods were first introduced to solve differential equations, it was evident that exact solutions would not generally exist in the majority of applications. Still other scientific advancements relating to second-order differentials had to wait until Ito and Stratonovich came on the scene in the twentieth century, establishing the stochastic theory already introduced in another form by Paul Langevin (1908). Poincaré's great achievement is illustrated by the fact that, very early in his career, in fact, in his PhD dissertation, he had suggested a qualitative approach to solving differential equations, including limit cycles and singular or stationary points, while he had introduced the term

"bifurcation" in his first paper on mathematics (1885). It is interesting to see how important these tools have become today. The paper by Irene M. Moroz, Roger Cropp, and John Norbury entitled "A Simple Plankton Model with Complex Behaviour" includes all the recipes provided by Poincaré to deal with a coupled system of four nonlinear differential equations, including phase portraits, critical or equilibrium points, bifurcation diagrams, and chaotic oscillations. This paper is a typical example of the importance of Poincaré's findings across a broad range of theoretical and applied fields in science.

An interesting application, entitled "Fractal Radar: Towards 1980–2015," is included in the paper by Alexander A. Potapov, along with an interesting approach to the theory of fractional measure and nonintegral dimension. According to the author:

> The main feature of fractals is the nonintegral value of its dimension. The development of dimension theory began with the work of Poincaré, Lebesgue, Brauer, Urysohn, and Menger. Sets which are negligibly small and indistinguishable in one way or another in the sense of Lebesgue measure arise in different fields of mathematics. To distinguish such sets with a pathologically complicated structure, one should use unconventional characteristics of smallness, for example, Hausdorff's capacity, potential, measures, dimension, and so on. The application of the fractional Hausdorff dimension associated with entropy, fractals, and strange attractors has turned out to be most fruitful in dynamical systems theory.

Irina N. Pankratova and Pavel A. Inchin explore a "Simulation of Multidimensional Nonlinear Dynamics by One-Dimensional Maps with Many Parameters." They propose a class of discrete dynamical systems as nonlinear matrix models to describe multidimensional multiparameter nonlinear dynamics. In their article, they simulate the system's asymptotic behavior by introducing a two-step algorithm to compute ω-limit sets of dynamical systems. They propose a qualitative theory allocating invariant subspaces of the system matrix that contain cycles of rays on which the ω-limit sets of the dynamical systems are situated, and they introduce dynamical parameters to describe the system behavior. The ω-limit set of the system trajectory is computed using the analytical form of the one-dimensional nonlinear Poincaré map determined by the dynamical parameters.

The paper "Sudden Cardiac Death and Turbulence" authored by Guillaume Attuel, Oriol Pont, Binbin Xu, and Hussein Yahia is another important application of the theories presented in the first part of this book, including Poincaré's methods and Y. Pomeau's conjecture regarding hydrodynamic intermittency. This is a clear and concise discussion of one of the main causes of death in our societies. Many of the theoretical tools of chaos theory are used, including abnormal oscillations, fluctuations, and limit cycles. A system of four coupled differential equations is introduced, and Poincaré section plots are presented, along with an analysis of the onset of turbulence.

The paper by Philippe Beltrame entitled "Absolute Negative Mobility in a Ratchet Flow" relates to the papers of David Ruelle, Jean-Mark Ginoux, and Alexander Ramm. The problem is modeled by a simple system and by a system of four coupled nonlinear differential equations. Bifurcation diagrams, period-

doubling cascades, critical values, strange attractors, and Poincaré sections are presented along with a discussion of the chaotic transition.

Given the selection of papers in the book, the aim here is to reach a broad scientific and general audience. Indeed, it is directed not only at researchers and scientists in almost every field but also at a wider audience interested in discovering and exploring the way modern chaos theory was brought into being some 120 years ago by a brilliant scientist who had the intellectual ability and the scientific knowledge to reach both the heart and the boundaries of this theory.

We are grateful for the valuable support of Christian Caron, who first suggested this book devoted to the Poincaré legacy, and to Springer for publishing it. Our deepest thanks go to the authors and to the direction of the Henri Poincaré Institute in Paris for accepting to host the CHAOS 2015 International Conference, including the staff of the Institute who ensured the success of the conference in a scientifically inspiring environment.

Chania, Greece Christos Skiadas
December 2015

Contents

Chapter 1
Henri Poincaré's Inventions in Dynamical Systems and Topology

Ferdinand Verhulst

Abstract The purpose of this article is to trace the invention of images and concepts that became part of Poincaré's dynamical systems theory and the Analysis Situs. We will argue that these different topics are intertwined whereas for topology Riemann surfaces and automorphic functions play an additional part. The introduction explains the term *invention* in the context of Poincaré's philosophical ideas. Poincaré was educated in the school of Chasles and Darboux that emphasized the combination of analysis and geometry to perform mathematics fruitfully. This will be illustrated in the second section where we list his new concepts and inventions in dynamical systems, followed by the descriptions of theory available before Poincaré started his explorations and the theory he developed. The third section studies in the same way the development of Poincaré's topological thinking that took place in the same period of time as his research in dynamical systems theory.

1.1 Introduction

The purpose of this paper is to *trace the inventions of Poincaré regarding dynamical systems and topology* starting with the accepted knowledge of his time. As we will see, for topology we will have to discuss aspects of the theory of automorphic functions. The intertwining of analysis and geometry is typical for the scientific work of Henri Poincaré.

This paper will not be a systematic treatment of his achievements and their impact on later science. Such systematic descriptions and references can be found in the biographies [8] and [31].

The use of the word 'invention' in the title needs some explanation. One should note that the first meaning of *invention* in French, as Poincaré used it, is indeed the same as in English.

F. Verhulst (✉)
Mathematisch Instituut, University of Utrecht, PO Box 80.010, 3508 TA Utrecht, The Netherlands
e-mail: f.verhulst@uu.nl

C. Skiadas (ed.), *The Foundations of Chaos Revisited: From Poincaré to Recent Advancements*, Understanding Complex Systems,
DOI 10.1007/978-3-319-29701-9_1

A famous essay by Henri Poincaré in [16] has the title *"L'invention mathématique"*. In [31, p. 84] the essay is described as follows:

> In a wonderful piece of introspection, Poincaré describes in the essay how sudden insight came to him in solutions of mathematical problems. He conjectures that the unconscious mind, stimulated by intense but seemingly fruitless exploration of a problem by the conscious mind, considers many mathematical combinations and makes a choice on the basis of aesthetics and economy. An example that he gives of such an occurrence concerns the Fuchsian functions.

There has been a lot of confusion about the use of this term. The English translation of [16] uses "discovery" instead of "invention", see [18, p. 46]. Even recently in [8, p. 120] this produced the following mix-up:

> In 1908 Poincaré talked to the Société de Psychologie in Paris about the psychology of discovery of new results in mathematics. The published version in *L'enseignement mathématique*, "L'invention mathématique," became one of his more famous essays.

The mix-up of discovery and invention is repeated on p. 120 of [8].

People argue that, starting with a complete system of axioms, mathematics is not invented but *discovered*. Of course discovery applies to a result like:

Assuming Euclides' axioms in plane geometry, we have that the sum of the angles within a triangle is 180 degrees.

Such results were discovered by careful analysing and following up the given assumptions.

When Poincaré uses the term **invention** *he refers to the creation of new concepts or the identification of deep relations between different mathematical or physical concepts.*

Platonic reasoning would argue for instance that the integers or the prime numbers exist independently of the human mind. However, long after identifying three apples or nine trees, the human mind came up with the abstract notion of number, for instance 3 or 9, as an element of the set of integers. An integer (and the set of integers) has no relation to a physical phenomenon, it exists only as an abstraction in the human mind; it is an example of human invention. It became the inspiration for the concept of operations like multiplication, a subsequent invention. And this was followed by the concept of multiplication of elements of other sets, for instance complex numbers, quaternions, matrices, elements of vectorspaces, etc.

Closely related to the idea of invention is the importance Poincaré attributes to language in [15]. The scientist creates the language to describe phenomena; to find the most suitable verbal description is an essential element of understanding the phenomena, both in the natural sciences and in mathematics. The perception of the relation between concepts and phenomena needs expression in language, which is an ingredient of the process of scientific invention. An example given by Poincaré concerns the motion of the celestial bodies. Kepler's laws contain a description in terms of the motion of the planets in elliptical orbits; the geometric concept of an ellipse provided the language. The transition to Newton's laws produced a richer formulation resulting in deeper understanding; the analytic concept of differential equation provided the language.

A concept introduced in [17] gives another illustration of the language for a new concept. Poincaré reasons that the *classification* of scientific facts is a main part of the activity of scientists. One considers for instance in biology all living creatures on Earth and tries to classify them in various groups. Or one considers in mathematics the set of integers and tries to distinguish subsets as even or odd numbers. A classification makes sense if adding new elements to the set does not change the old classification. For instance in biology, the discovery of a new type of living creature in the deep oceans, does not change the 'definition' of birds or mammals. If a classification is not changed by adding new elements, it is called *predicative* by Poincaré. This is now an accepted concept in logic. A definition in mathematics is really a classification, a definition has to be predicative.

Poincaré gives a simple example. Consider the set of integers and as a subset H the first hundred integers. Classify them in two subsets: A, the numbers one through ten and B, the numbers larger than ten. Embedding H in a larger set, for instance the first 200 integers, does not change the classification in A and B, so it is predicative.

When Poincaré (1854–1912) started his career, his educational background was as follows:

He was a student at the Lycée of Nancy (1871–1875) where classical geometry, analysis, algebra and the humanities were taught. After this he was a student at L'École Polytechnique (1873–1875) with courses in analysis, geometry, mechanics and physics, chemistry, celestial mechanics. Then he attended L'École des Mines (1875–1878) where technical and geophysical lectures were given.

His dissertation on singularities of solutions of first order nonlinear partial differential equations was accepted at the Sorbonne in 1879, he became 25 in that year.

Poincaré was an enthusiastic reader of novels but not of scientific papers. He read the classics on celestial mechanics and special functions of that time, papers by Betti, Hermite, Laguerre, Bonnet, Halphen, Darboux, and later the writings of Riemann and Weierstraß whom he admired.

In the sequel we will start each section with a list of Poincaré's inventions and ideas, followed by descriptions of what was known at that time and a sketch of his ideas.

1.2 Dynamical Systems

New concepts and inventions:

1. Algebroid functions.
2. Index theory for plane dynamical systems i.e. autonomous second-order ordinary differential equations (ODEs).
3. The Poincaré-Bendixson theorem for plane dynamical systems.
4. Convergence of series solutions of ODEs, the use of the implicit function theorem, bifurcation theory (the Hopf bifurcation).

5. Asymptotic, divergent series.
6. Normalization, the Poincaré domain.
7. Fixed point theorems for dynamical systems.
8. The recurrence theorem for dynamical systems characterized by measure-preserving maps.
9. Homoclinic chaos.

1.2.1 Ordinary Differential Equations in the Nineteenth Century

Scientific treatises discussing ordinary differential equations in the nineteenth century are of three different types: books or papers on mathematical physics, on special functions and separate treatises on differential equations as we know them nowadays. We will leave aside the books that are completely application oriented. These books are of great interest but they merit a special study.

Special functions like the elliptic ones pose many difficult analytic problems. A typical and important example is the monograph by Jacobi [9]. The book is devoted to the analysis of elliptic functions (generalization of solutions of the mathematical pendulum equation).

George Boole's [4] is a text that deals mainly with elementary methods; it can be compared with introductions as taught at present. It discusses exact first order equations, integrating factors, special solutions and equations (Riccati equation) and methods for linear equations (sometimes tricks), variation of constants, geometric methods (involutes, curvature, tangencies).

A similar elementary treatise was written by Duhamel [7]. Duhamel lectured at the École Polytechnique, where Poincaré studied. Henri acquainted himself already with this course while still at the Nancy Lycée (see [31]). Part 4 on the integration of ODEs contains material as in Boole [4] but with more geometric problems and elementary Taylor series expansions for solutions.

We will pay special attention to the extensive treatises by Jordan [10] and Laurent [13]. Although at the year of their publication, Poincaré had been publishing on differential equations since 1879, his results are still ignored here. The books [10] and [13] are typical for the knowledge of ordinary differential equations in the nineteenth century before Poincaré.

Camille Jordan (1838–1922), see Fig. 1.1, was professor at L'École Polytechnique where he taught analysis. His three volumes Cours d'Analyse are a rich and didactical account of the analysis of his time. In vol. 3, pp. 1–296, two chapters deal with ordinary differential equations. The first chapter introduces again exact equations and integrating factors with examples from classical equations (Bernoulli, Clairaut), but interestingly, Jordan extends this to the cases in dynamics where one knows a number of integrals but not enough to solve the system. The integrals can be used to reduce the dimension of the system.

Attention is given to series expansions of solutions near regular and near singular points. Cases like

$$\frac{dy}{dx} = \frac{1}{f(x,y)} \quad \text{or} \quad x\frac{dy}{dx} = f(x,y)$$

with $f(0,0) = 0$ and series expansions near $(0,0)$ are discussed extensively, based on the theory of Briot and Bouquet [5]. It should be noted that in the subsequent chapter on partial differential equations, the topic of series expansions cannot be found (this would be the topic of Poincaré's doctoral thesis). The second chapter treats linear equations with variable and constant coefficients. The theory is illustrated by the discussion of a number of special functions.

Hermann Laurent (1841–1908) published his seven volumes Traité d'Analyse [13] in the period 1895–1891; he was "examinateur d'admission á l'École Polytechnique" and from 1889 on professor at the École Agronomique in Paris, see Fig. 1.1. Volume 5 of [13, pp. 1–320], contains an extensive didactical introduction to ordinary differential equations. It has also special value because of the many references and the exercises. The first three chapters follow the same path as present day introductions: special methods, first order equations, equations of Bernoulli, Clairaut, etc. The treatment of linear equations becomes more interesting as Laurent discusses for instance equations with periodic coefficients, Lamé's equation and Halphen's theory of invariants. Chapter 4 summarizes the theory of special functions but without the difficult questions raised by Riemann, see Sect. 1.3. Chapter 5 is on nonlinear equations with emphasis on special integrable cases. Interesting is the method attributed to Jacobi; consider the equation

$$\frac{d^2y}{dx^2} = F(x,y)$$

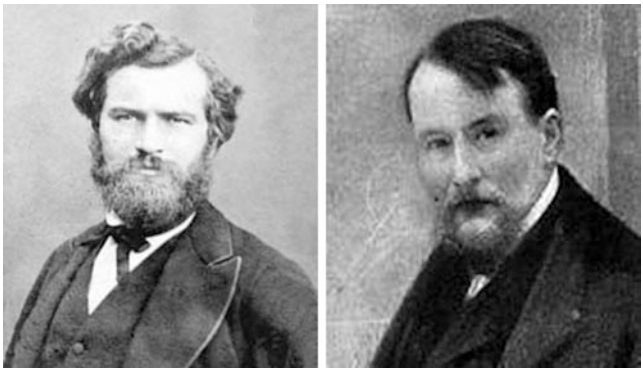

Fig. 1.1 Camille Jordan (1838–1922) and Hermann Laurent (1841–1908)

with first integral

$$\frac{dy}{dx} = \phi(x, y, c),$$

c a constant of integration. Jacobi shows that in this case the differential equation can be solved by quadrature. It can be considered a generalization of the method of d'Alembert that solves a similar problem for linear equations. The last chapter considers systems of first order linear equations including Cauchy's introduction of characteristic equations.

The exercises give an idea of the level of teaching and the requirements for students. Many exercises are concerned with geometrical questions for instance involving the curvature of certain solutions.

1.2.2 Poincaré's Thesis

Poincaré was educated in geometry and analysis, but he did not restrict himself to one particular mathematical discipline. His major contributions regarding dynamical systems, the *Mémoire* of 1881–82, the *prize essay* of 1889 and the *Méthodes Nouvelles de la Mécanique Célèste*, are clearly characterized by the interaction of analysis and geometry

The thesis [22] was presented in 1879 and is concerned with an extended study of the known concepts of critical points and singularities of nonlinear first-order partial differential equations of the form

$$F(z, x_1, \ldots, x_n, \frac{\partial z}{\partial x_1}, \ldots, \frac{\partial z}{\partial x_n}) = 0.$$

The method of characteristics reduces the problem to the integration of an n-dimensional system of nonlinear ODEs. If $n = 2$ we can write the phase-plane equation associated with the two characteristic equations as

$$x^m \frac{dy}{dx} = f(x, y)$$

with $f(x, y)$ a holomorphic function. If $m = 0$, $y(x)$ is holomorphic near $x = 0$ and can be described by a corresponding series expansion. If $m = 1$, we have a weakly singular case, if $m > 1$ and integer we have an irregular singularity. Poincaré introduces *algebroid function* as follows: The function z of n variables $x_1, \ldots, x_n$ is algebroid of degree m near $(0, \ldots, 0)$ if z satisfies an equation of the form

$$z^m + A_{m-1} z^{m-1} + \ldots + A_1 z + A_0 = 0,$$

where the functions $A_0, \ldots, A_{m-1}$ have a convergent power series in $x_1, \ldots, x_n$ near $(0, \ldots, 0)$. If we can prove that the solution of the partial differential equation is algebroid, we can formulate results on the existence of certain convergent series expansions near $(0, \ldots, 0)$.

This is a useful generalization of the results of Briot and Bouquet [5], but the thesis goes on with the treatment of more complicated cases. In this connection, Poincaré introduces series expansions that exclude resonances of the form

$$m_2\lambda_2 + m_3\lambda_3 + \ldots + m_n\lambda_n = \lambda_1,$$

where the λ_i are determined by the differential equation, the $m_2, \ldots, m_n$ are positive integers. In addition, the idea of non-resonance in celestial mechanics is generalized to requiring that the convex hull of the λ_i in the complex plane does not contain the origin. This precludes the theory of normal forms, see for instance Arnold [1], where for the location of the λ_i we would nowadays say "the spectrum is in the Poincaré domain".

1.2.3 The Mémoire of 1881–82

The Mémoire [20] of 1881–82 is mainly concerned with two-dimensional problems and so is very different from his three volumes *Méthodes Nouvelles de la Mécanique Célèste* [14] where the first general theory of dynamical systems is found. The Mémoire is restricted to autonomous second order equations as many articles on ODEs are in the nineteenth century, but the research programme sketched by Poincaré breaks with the traditions of his time; it is very general and at present the programme still dominates research. In ODE research, it is the first study of global behaviour of solutions. Poincaré unfolds here the philosophy of studying nonlinear dynamics as it is still practiced today:

> Unfortunately it is evident that in general these equations [ODEs] can not be integrated using known functions, for instance using functions defined by quadrature. So, if we would restrict ourselves to the cases that we could study with definite or indefinite integrals, the extent of our research would be remarkably diminished and the vast majority of questions that present themselves in applications would remain unsolved.

And a few sentences on:

> The complete study of a function [solution of an ODE] consists of two parts:
>
> 1. Qualitative part (to call it like this), or geometric study of the curve defined by the function;
> 2. Quantitative part, or numerical calculation of the values of the function.

Consider the two-dimensional system

$$\frac{dx}{dt} = X(x, y), \quad \frac{dy}{dt} = Y(x, y)$$

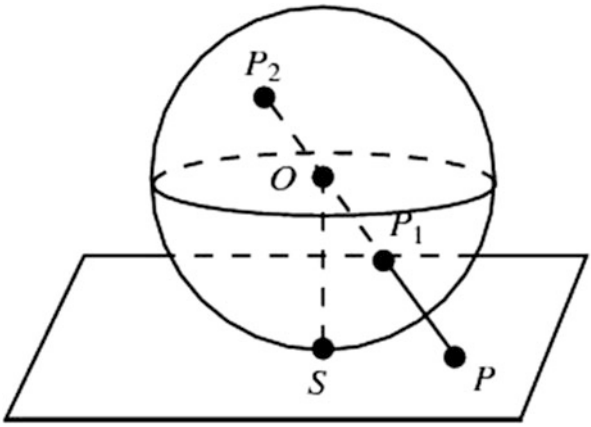

Fig. 1.2 Gnomonic projection of a plane onto a sphere

with orbits in the Euclidean (x, y)-phaseplane. For the analysis of the system, Poincaré uses gnomonic projection; this is a cartographic projection of a plane onto a sphere (in cartography of course the other way around), see Fig. 1.2.

The plane is tangent to the sphere and each point of the plane is projected through the centre of the sphere, producing two points on the spherical surface, one on the Northern hemisphere, one on the Southern. The equatorial plane separates the two hemispheres. A point on the great circle in the equatorial plane corresponds with infinity.

Each straight line in the plane projects onto a great circle. So a tangent to an orbit in the plane projects onto a great circle that has at least one point in common with the projection of the orbit on the sphere. Such a point will be called a *contact*. The advantage of this projection is that the plane is projected on a compact set which makes global treatment easier. We have to consider with special attention the equatorial great circle which corresponds with the points at infinity of the plane. A bounded set in the plane is projected on two sets, symmetric with respect to the centre of the sphere and located in the two hemispheres.

If in a point (x_0, y_0) we have not simultaneously $X = Y = 0$, (x_0, y_0) is a regular point of the system and we can obtain a power series expansion of the solution near (x_0, y_0).

If in a point (x_0, y_0) we have simultaneously $X = Y = 0$, (x_0, y_0) is a singular point. Under certain nondegeneracy conditions Poincaré finds four types for which he introduces the nowadays well-known names *saddle, node, focus and centre*. These are called singularities of first type. In the case of certain degeneracies we have singularities of the second type. Points on the equatorial great circle may correspond with singularities at infinity and can be investigated by simple transformations. The next section of the Mémoire is remarkable; it discusses the distribution and the number of singular points. Assuming that X and Y are polynomials and of the same degree and if X_m, Y_m indicate the terms of the highest degree, while we have *not* $xY_m - yX_m = 0$, then the number of singular points is

at least 2 (if the curves described by $X = 0$ and $Y = 0$ do not intersect on the two hemispheres after projection, there must be an intersection on the equatorial circle). In addition it is shown that a singular point on the equator has to be a node or a saddle, in the plane one cannot spiral to or from a singularity at infinity. An important new concept is *index*. Consider a closed curve, a cycle, located on one of the hemispheres. Taking one tour of the cycle in the positive sense, the expression Y/X jumps h times from $-\infty$ to $+\infty$, it jumps k times from $+\infty$ to $-\infty$. We call i with

$$i = \frac{h-k}{2}$$

the index of the cycle. It is then relatively easy to see that for cycles consisting of regular points one has:

- A cycle with no singular point in its interior has index 0.
- A cycle with exactly one singular point in its interior has index $+1$ if it is a saddle, index -1 if it is a node or a focus.
- If N is the number of nodes within a cycle, F the number of foci, C the number of saddles, the index of the cycle is $C - N - F$.
- If the number of nodes on the equator is $2N'$, the number of saddles $2C'$, the index of the equator is $N' - C' - 1$.
- The total number of singular points on the sphere is $2 + 4n,\ n = 0, 1, \cdots$.

A solution of the ODE may touch a curve or cycle in a point, a contact. In such a point the orbit and the curve have a common tangent. An algebraic curve or cycle has only a finite number of contacts with an orbit. Counting the number of contacts and the number of intersections for a given curve contains information about the geometry of the orbits.

A useful tool is the 'théorie des conséquents', what is now called the theory of Poincaré maps. We start with an algebraic curve parametrized by t so that $(x, y) = (\phi(t), \psi(t))$ with $\phi(t), \psi(t)$ algebraic functions; the endpoints A and B of the curve are given by $t = \alpha$ and $t = \beta$. Assume that the curve AB has no contacts and so has only intersections with the orbits. Starting on point M_1 with a semi-orbit (the orbit traced for $t \geq t_0$), we may end up again on the curve AB in point M_1 which is the 'conséquent' of M_0. Nowadays we would call M_1 the point generated by the Poincaré-map of M_0 under the phaseflow of the ODE. It plays an important part in understanding high-dimensional ODEs, anticipating the theory of fixed points of maps of differential topology.

If $M_0 = M_1$, the orbit is a cycle and Poincaré argues that returning maps correspond with either a cycle or a spiralling orbit. It is possible to discuss various possibilities with regards to the existence of cycles in which the presence or absence of singular points plays a part.

This analysis has important consequences for the theory of limit cycles. Semi-orbits will be a cycle, a semi-spiral not ending at a singular point, or a semi-orbit going to a singular point. Interior and exterior to a limit cycle there has always to be

at least one focus or one node. Of the various possibilities considered it is natural to select annular domains, not containing singular points and bounded by cycles without contact and so transversal to the phase-flow. Such annular domains are often used to prove the existence of one or more limit cycles (Poincaré-Bendixson theory).

In the Mémoire, the topology of two-dimensional domains, either $\mathbb{R}^2$ or for instance S^2, with the Jordan separation theorem as an ingredient, plays an essential role.

Poincaré gave a few examples that were reproduced in [31, pp. 116–117], however with disturbing misprints. We discuss the examples here.

Example 1 Consider the system with Euclidean variables x, y:

$$\begin{cases} \dot{x} &= x(x^2+y^2-2x-3)-y, \\ \dot{y} &= y(x^2+y^2-2x-3)+x. \end{cases} \tag{1.1}$$

The origin $(0,0)$ is a stable focus corresponding with two foci on the sphere. Using polar coordinates

$$x = r\cos\phi,\ y = r\sin\phi,$$

we find outside the origin:

$$\dot{r} = r(r^2-2r\cos\phi-3),\ \dot{\phi} = 1.$$

Elimination of time produces the equation:

$$\frac{dr}{d\phi} = r(r^2-2r\cos\phi-3).$$

As $dr/d\phi(r=1) = 2(\cos\phi-1) \leq 0$ and $r^2-2r\cos\phi < 3$ for $r<1$, we have that within the circle $r=1$ the flow is acyclic, the flow is contracting. As $dr/d\phi(r=3) = 18(1-\cos\phi) \geq 0$ and $r^2-2r\cos\phi > 3$ for $r>3$, we have that the flow outside the circle $r=3$ is also acyclic, the flow is expanding. Within the circle $r=1$ and outside the circle $r=3$ have opposite signs for $dr/d\phi$, so the annular region $1<r<3$ is cyclic. As $dr/d\phi$ changes sign only once in the annular region, the annular region is monocyclic and contains one (unstable) limit cycle.

The second example shows a different phenomenon.

Example 2 Consider the system with Euclidean variables x, y:

$$\begin{cases} \dot{x} &= 2x(x^2+y^2-4x+3)-y, \\ \dot{y} &= 2y(x^2+y^2-4x+3)+x. \end{cases} \tag{1.2}$$

The origin $(0, 0)$ is an unstable focus corresponding with two foci on the sphere. Using again polar coordinates we find outside the origin:

$$\dot{r} = 2r(r^2 - 4r\cos\phi + 3),\ \dot{\phi} = 1.$$

Elimination of time produces the equation:

$$\frac{dr}{d\phi} = 2r(r^2 - 4r\cos\phi + 3).$$

Rewrite the equation as

$$\frac{dr}{d\phi} = 2r[(r-1)(r-3) + 4r(1-\cos\phi)].$$

As $dr/d\phi(r = 1) = 8(1 - \cos\phi) \geq 0$ and $r^2 - 4r\cos\phi > -3$ within the circle $r = 1$, we have that within the circle $r = 1$ the flow is acyclic, the flow is expanding.

At $r = 3$ we have again $dr/d\phi \geq 0$; if $r > 3$, we have $dr/d\phi > 0$. The flow outside the circle $r = 3$ is acyclic, the flow is also there expanding. The annular region $1 < r < 3$ has to be considered more closely. By analyzing the expression $(r^2 - 4r\cos\phi + 3)$, we see that $dr/d\phi$ cannot change sign in the annular region, so the annular region is also acyclic. There exist no limit cycles in a finite domain of the system.

We add a note on the behaviour near infinity of the solutions of the two examples. The systems (1.1) and (1.2) can be written as:

$$\begin{cases} \dot{x} &= xA(x, y) - y, \\ \dot{y} &= yA(x, y) + x. \end{cases} \tag{1.3}$$

We add the initial conditions $x(0) = x_0 \neq 0,\ y(0) = y_0$. Putting $\eta = y/x$ we find:

$$\frac{d\eta}{dt} = 1 + \eta^2,\ \eta(0) = \frac{y_0}{x_0},$$

with solution

$$\eta(t) = \frac{y(t)}{x(t)} = \frac{y_0}{x_0} + tan(t).$$

Inside the limit cycle of Example 1, the rotation of the orbits toward the origin causes the orbits to cross the positive y-axis with period 2π (alternating with crossing the negative y-axis).

In both examples, the solutions starting at a point $r(0) > 3$ tend to infinity. The equation $\dot{\phi} = 1$ suggests rotation, but this is not the case as the solutions tend to

infinity in a finite time. Assuming $r(0) > 3$, this can be seen from the following estimates:

Example 1, $\dot{r} \geq r(r^2 - 2r - 3) \geq (r-3)^3$.

Example 2, $\dot{r} \geq 2r(r^2 - 4r + 3) \geq 2(r-3)^3$.

Integration of the differential inequalities (with $r(0) > 3$) gives the desired result.

At the equator of the Poincaré sphere, we find no limit cycles. Transforming $x = 1/u$ and $y = 1/v$, we find from the transformed system that the singularities at the equator are not regular.

1.2.4 The Prize Essay for Oscar II, 1888–89

The famous prize awarded by King Oscar II of Sweden and Norway on the occasion of his 60th birthday in 1889 has become a well-known story, mainly because Henri Poincaré, who won the prize (see [23]), had to admit and to correct an error after the event. For detailed accounts see [2] and [31]. Not so well-known is that apart from the error to be corrected, the first version of the prize essay contained already fundamental theorems. Important results from the prize essay involve series expansions, periodic solutions and bifurcations. Series expansions with respect to a small parameter were the main tool in celestial mechanics of that time, but these expansions were formal. Comparison with results of various authors was not easy as many different transformations of the equations of motion were in use. Poincaré gave explicit criteria for the convergence and divergence of such series based on holomorphic expansion theorems of differential equations and the implicit function theorem. At the same time, his insight in the causes of the break-up of validity of expansion procedures, inspired him to the first set-up of a very important field: bifurcation theory. All these topics would be treated more extensively in [14].

Series expansion produce always local information. An important global result is the *recurrence theorem*:

Consider a dynamical system defined on a compact set in $\mathbb{R}^n$ with the property that the flow induced by the system is measure-preserving. Poincaré uses the term volume-preserving as the notion of measure does not exist at this time. Examples are the motion of an incompressible fluid in a nondeformable vessel or the phase-flow induced by a time-independent Hamiltonian system without singularities on a compact domain. Using the invariance of the domain volume, it is proved that most particles or fluid elements return an infinite number of times arbitrarily close to their initial position. The recurrence time is not specified but depends in general on the required closeness to the initial position and of course on the dynamical system at hand.

The interpretation of the recurrence theorem in the case of a chaotic system is interesting. In a two degrees-of-freedom Hamiltonian system near stable equilibrium, the KAM theorem guarantees in most cases the existence of an infinite number of two-dimensional invariant tori that separate the energy manifold into small chaotic regions. In these systems the recurrence phenomena near stable equilibrium

are quite strong. Moving further away from stable equilibrium, the recurrence times will be more and more dependent on the initial positions.

In the case of more than two degrees-of-freedom, resonances will produce more active sets of chaotic orbits near stable equilibrium producing very different recurrence times.

Another basic result is the *non-integrability of conservative systems*.

In the corrected version of the prize essay [23], Poincaré overturned the general philosophy that Lagrangian or Hamiltonian systems are always integrable. The traditional idea was that if one could not find the integrals of for instance the gravitational three-body problem, this was caused only by lack of analytic skill. In fact, in his first submission of the prize essay, Poincaré set out to prove integrability of the circular, plane, restricted three-body problem. This can be written as a two degrees of freedom Hamiltonian system which takes the form of four first-order equations with periodic coefficients. He identified an unstable periodic solution and approximated its stable and unstable manifolds by series expansions. Poincaré calls these invariant manifolds "surfaces asymptotiques". He concluded (incorrectly in the first version) that the continuations of stable and unstable manifolds could be glued together to form integral surfaces corresponding with a second first integral of the system.

After a query of the editor of the Acta Mathematica asking for more details, Poincaré found out that this gluing was not possible in this particular example. He found an infinite number of intersections instead of merging of the manifolds. These results preclude the existence of homoclinic manifolds that would indicate the presence of a second integral. In the prize essay, the description of the geometry of the dynamics of the two degrees-of-freedom circular, plane, restricted three-body problem is tied in with the non-integrability results. In [14], the analysis will grow to its full generality for n degrees of freedom Hamiltonian systems.

1.2.5 Les Méthodes Nouvelles de la Mécanique Céleste 1892–1899

The three volumes of the Méthodes Nouvelles appeared in the same period (1892–1899) as the Analysis Situs and its supplements (1892–1905). The reference to celestial mechanics in the title of the three volumes is misleading, they contain the first general theory of dynamical systems describing both conservative and dissipative systems by analytical and geometric methods. Celestial mechanics is often used in [14] as an illustration of the theory.

To solve ODEs, in particular in problems of celestial mechanics, the use of series expansions is ubiquitous. Poincaré formulated and proved a basic series expansion theorem in vol. 1, Chap. 2 of [14]. At the same time he demonstrates how the convergence of such series can break down. This involves conditions of the implicit function theorem with consequences for the bifurcation of solutions.

The use of the implicit function theorem was known at that time for sets of polynomial equations, but to apply these ideas to ODEs was new. Poincaré introduces the notion of *bifurcation set* with modifications for the dissipative and the conservative case (for more details see [31]). Particularly interesting is that in Chap. 3 a very general discussion is presented of what is now called the Hopf bifurcation.

The flexibility of Poincaré's mind shows again when he introduces divergent or asymptotic series in Chap. 8 as a legitimate tool. This went against the general mathematical philosophy of that time that required series to be convergent, but it agreed with the practice of many scientists working in applications. Divergent series can be used to obtain approximations of solutions but the difficult question of concluding existence of solutions and other qualitative questions from asymptotic approximations were not touched upon by Poincaré, this came after his time.

In [14], the fundamental non-integrability theorem is formulated and proved in the general case of the time-independent $2n$ dimensional Hamiltonian equations of motion

$$\dot{x} = \frac{\partial F}{\partial y}, \ \dot{y} = -\frac{\partial F}{\partial x}$$

with small parameter μ and the convergent expansion $F = F_0 + \mu F_1 + \mu^2 F_2 + \cdots$; F_0 depends on x only and its Jacobian is non-singular, $|\partial F_0/\partial x| \neq 0$. Suppose $F = F(x, y)$ is analytic and periodic in y in a domain D; the first integral $\Phi(x, y)$ of the system is analytic in x, y in D, analytic in μ and periodic in y:

$$\Phi(x, y) = \Phi_0(x, y) + \mu\Phi_1(x, y) + \mu^2\Phi_2(x, y) + \cdots$$

The statement is then that with these assumptions, $\Phi(x, y)$ *can not be an independent first integral of the Hamiltonian equations of motion unless we impose further conditions.*

In the *Méthodes Nouvelles* [14, Chap. 5 of vol. 1], chapter 5 of volume 1, the technique is first analytic: a second integral should Poisson-commute with and be independent of the Hamiltonian; expanding the second integral with respect to a suitable small parameter and applying these conditions leads to a contradiction unless additional assumptions are made (see also [31]). It is understandable that the geometric aspects of non-integrability could not be understood at that time for more than two degrees of freedom. Very few contemporaries of Poincaré understood these aspects, even for two degrees of freedom (phase-space dimension 4). It is not clear whether Elie Cartan [6] understood non-integrability or, if he did, knew what to make of it. In his book [6] he recalls Poincaré's definition of integral invariant but he ignores existence questions.

There are more geometric details given in vol. 3, Chap. 32 of [14]. As in the prize essay, the analysis is inspired by the actual Hamiltonian dynamics of stable and unstable manifolds. Here we find the famous description of chaotic dynamical

behaviour when considering the Poincaré-section of an unstable periodic solution in a two degrees of freedom Hamiltonian system:

> If on tries to represent the figure formed by these two curves with an infinite number of intersections whereas each one corresponds with a double asymptotic solution, these intersections are forming a kind of lattice-work, a tissue, a network of infinite closely packed meshes. Each of the two curves must not cut itself but it must fold onto itself in a very complex way to be able to cut an infinite number of times through each mesh of the network.
>
> One will be struck by the complexity of this picture that I do not even dare to sketch. Nothing is more appropriate to give us an idea of the intricateness of the three-body problem and in general all problems of dynamics where one has not a uniform integral and where the Bohlin series are divergent.

In this case of two degrees of freedom, the energy manifold is 3-dimensional in 4-dimensional phase-space.The flow on the energy manifold is visualized by the corresponding Poincaré-maps ("théorie des conséquents"). The double asymptotic solutions are the remaining homoclinic solutions that are produced by the intersections. The Bohlin series mentioned in the citation are *formal* series obtained by Bohlin for periodic solutions in celestial mechanics.

The picture Poincaré sketches destroys the possibility of a complete foliation into tori of the energy manifold, topologically S^3, induced by a second independent integral of motion.

1.2.6 The Poincaré-Birkhoff Theorem

This theorem appeared in 1912, a long time after the Analysis Situs and its supplements. However, it is typical for Poincaré's interest in the global character of dynamical systems. It bothered him that so many results in this field are local, series expansions, normal forms, bifurcations, and he formulated a more global geometric theorem [24]. The reason to postpone its publication was that he found his reasoning not satisfactory; the actual proof was given by Birkhoff [3].

The idea is to characterize certain dynamical systems by an area-preserving, continuous twist-map of an annular region into itself. Such a map has at least two fixed points corresponding with periodic solutions of the dynamical system. The applications Poincaré had in mind were the global characterization of periodic solutions of time-independent Hamiltonian systems with two degrees of freedom. The dynamics of such a system restricted to a compact energy manifold is three-dimensional. The Poincaré maps of the orbits can provide the twist map described by the theorem. After 1912, fixed point theorems would play an important part in general and differential topology and in dynamical systems.

1.3 Topology

A number of topological concepts were known before Poincaré's time, but, as in the case of the theory of dynamical systems, he invented its questions and the modern form of this field single-handedly. Poincaré used the term *Analysis Situs* ('analysis of place') for topology in a paper that appeared in 1892. It was followed up in typical Poincaré 'second-thoughts' style by five supplements, the last one in 1905. A translation into English and an introduction can be found in [26]. As stated before, the three volumes on dynamical systems [14] and the Analysis Situs were written in the same period of time. Before this period, Poincaré started his work on automorphic (Fuchsian) functions. We will argue that automorphic functions and dynamical systems, in particular the step from local to global considerations, were both instrumental in the creation of the Analysis Situs.

New concepts and inventions:

1. Triangularization of manifolds, the Euler-Poincaré invariant
2. Homology
3. The fundamental group
4. Algebraic topology

1.3.1 Topology Before Poincaré

We will briefly describe topology before Poincaré and we will discuss in subsequent subsections various topics in Poincaré's work of the period 1878–1892 that might have inspired his ideas. We conclude with discussing some of his inventions of the Analysis Situs, see also [30]. A few aspects of our reasoning can be found in [32].

Leibniz
The term 'Analysis Situs' is attributed to Gottfried Wilhelm Leibniz (1648–1716) whose optimistic view considered our world the optimal one among possible worlds. The symbolism that he successfully applied in calculus was probably an inspiration for him to wish for symbolic 'calculus' in philosophy, sociology and geometry. For geometry this would imply an extension to forms and spaces characterized by algebraic symbols; this extension was called analysis situs, but the idea, although interesting, got no substance in Leibniz' subsequent work.

Euler
One of the mathematicians who thought about structures and forms in geometry was Leonhard Euler (1707–1783), see Fig. 1.3. He considered a convex two-dimensional polyhedron in Euclidean 3-space with V the number of vertices, E the number of edges and F the number of faces. The Euler characteristic for polyhedrons χ is an invariant of the form:

$$\chi = V - E + F = 2.$$

Fig. 1.3 Leonhard Euler (1707–1783), drawing by Giovanni Batista Bosio (1764–1827), engraved by Francesco Rebagli (courtesy private collection)

Interestingly, the Euler characteristic was generalized by Poincaré to more general closed, non-convex surfaces like tori or spheres with handles.

Abel, Möbius and Jordan

A handle, a 'look-through hole', in a surface is not so easy to characterize mathematically. Niels Henrik Abel (1802–1829) called the number of handles g, the genus of a surface in 3-space; for a sphere $g = 0$, for a torus $g = 1$ etc. August Ferdinand Möbius (1790–1868) developed ideas about non-orientable surfaces in Euclidean 3-space. Both Möbius and Camille Jordan (1838–1922) thought and formulated ideas about topological maps of surfaces. In their view, correspondence ("Elementarverwandschaft" in Möbius view) between two surfaces was not primarily characterized by point mappings but by considering the surfaces dissected in infinitesimal elements where neighboring elements of one surface correspond with neighboring elements of the other surface. For more details and references see [29].

Betti

Enrico Betti (1823–1892) gave a more precise description of tori and handles by defining his so-called Betti numbers. Betti uses the idea of connectivity and the number of closed curves separating a closed surface to characterize handles and more complicated structures.

The Influence of Riemann

The successes of analysis in dynamics, in particular in celestial mechanics, had its counterpart in applied mathematics in Germany, but meanwhile geometric thinking went there its autonomous course. This becomes clear in the mathematics of Bernhard Riemann (1826–1866), see Fig. 1.4. Poincaré notes in *La valeur de la science* [15]:

> Among the German mathematicians of this century, two names are particularly famous; these are the two scientists who have founded the general theory of functions, Weierstrass and Riemann. Weierstrass reduces everything to the consideration of series and their analytical transformations. To express it better, he reduces analysis to a kind of continuation of arithmetic; one can go though all his books without finding a picture. In contrast with this, Riemann calls immediately for the support of geometry, and each of his concepts presents an image that nobody can forget once he has understood its meaning. ([15], essay 'L'intuition et la logique en mathématiques')

It is interesting to consider Riemann's papers in the light of Poincaré's remarks.

At the occasion of his 'Habilitation' in Göttingen (1854), Riemann lectured on the foundations of geometry [28], see also [27] and for the historical context [29]. Riemann starts with experience and notes that the Euclidean foundations are not necessary, but that they have an acceptable certainty. He formulates a research plan for n-dimensional manifolds and spaces without precise descriptions. Weyl [28] links these considerations with later results in geometry, for instance by Klein, and with general relativity.

The collected works of Riemann [27] start with a treatise on the foundations of complex function theory, without figures but, as noted by Poincaré, "each of

Fig. 1.4 Bernhard Riemann (1826–1866) and Henri Poincaré (1854–1912)

its concepts presenting an image". The interpretation of a complex function in the neighbourhood of a singularity plays a prominent part. In Riemann's articles, analysis and geometry go hand in hand, producing new insights in both fields.

A long article on Abelian functions in [27] is written in the same style, it contains four figures. The integration of differential equations leads more often than not to solutions that are defined implicitly. We are then faced with an inversion problem to find the explicit solution. Consider for instance a simple implicit relation in complex variables: $w = z^2$ with inversion, $z = \sqrt{w}$; this leads to the well-known problem that, starting, say on the real axis, and moving on a circle around the origin (the singularity), will produce a different value when arriving again at the real axis. An ingenious solution for the problem of many-valuedness to obtain unique continuation of such a function was proposed by Riemann. Using several sheets (complex planes) when moving around the singularity and joining them, one obtains the so-called Riemann surface. In the example of the quadratic equation above, one needs two sheets to be joined. For more general algebraic implicit equations, one needs for such an inversion a finite number of sheets and so a more complicated Riemann surface. A clear and systematic treatment of Riemann surfaces with historical remarks can be found in [12].

A prominent mathematician after Riemann was Felix Klein (1849–1925). His papers, books and lectures have a strong intuitive and geometric flavor. His work on automorphic functions, although considerable, was overshadowed by the results of Poincaré at the same time; see also [8] and [31]. Both mathematicians elaborated on the geometric aspects of Riemann surfaces.

1.3.2 Local Versus Global in Poincaré's Fuchsian Functions

Many results on the local behaviour of functions were known in the 18th and 19th centuries. A few mathematicians aimed at a more global understanding ; Poincaré shared this ambition with Felix Klein (1849–1925). In his lecture notes on linear differential equations [11] Klein notes that we can make series expansions near the singularities of the coefficients, but this does not help global understanding. A basic tool for these problems is the geometric theory of automorphic functions developed both by Klein and Poincaré. Klein, while referring to an earlier lecture, states in the beginning of [11] (lecture of April 24, 1894):

> ... für hypergeometrische Functionen trat in meiner Vorlesung das Bestreben hervor den Gesamtverlauf der durch die Differentialgleichung definirten Funktionen zu erfassen.
>
> (... for hypergeometric functions, I wished to get a grip on the overall behaviour of the functions defined by the differential equation.)

The theory of Fuchsian (automorphic) functions is a successful synthesis of function theory and geometry, at the same time the concepts that were developed stimulated the emergence of topological concepts. Poincaré started to publish about Fuchsian functions in 1881, see vol. 2 of [19] and [25]. He was inspired by the

German mathematician Fuchs (1833–1902) who considered a second order, linear, ordinary differential equation of the form

$$y'' + A(z)y' + B(z)y = 0$$

with $A(z)$ and $B(z)$ holomorphic functions of the complex variable z in a region $S \subset \mathbb{C}$. There are two independent solutions $y_1(z)$ and $y_2(z)$ and Fuchs started to consider the ratio $\eta = y_1/y_2$. He was interested in the behaviour of the solutions near singular points of $A(z)$ and $B(z)$ and performed analytic continuation of $y_1(z)$ and $y_2(z)$ along a closed curve around such a singularity and inversion of the function $\eta(z)$. This led him to consider a linear transformation of η and, more in general, to look for functions that are invariant under a substitution of the form

$$z \to \frac{az + b}{cz + d}, \tag{1.4}$$

with coefficients a, b, c, d. So we have

$$f\left(\frac{az + b}{cz + d}\right) = f(z).$$

The substitution (1.4) (or transformation as we call it nowadays) is very rich; it consists of translations and rotations in the complex plane or, in the language of dynamical systems, expansions and contractions. The ratio $\eta(z)$ of the solutions should be invariant under these linear substitutions which is a more general property than periodicity that corresponds with the special case $a = c = d = 0$, $b \neq 0$ and real.

1.3.3 Fuchsian Groups

Poincaré put the results at a higher level of abstraction. He called the functions which are invariant under transformation (1.4) Fuchsian, they are now called automorphic. The group of transformations acts usually on the upper complex half-plane $Im(z) > 0$ or on the disk $|z| < 1$. It is still removed from our present abstract concept of a group as a set of elements with certain operations defined on it. For his analysis, Poincaré had to distinguish between continuous and discontinuous transformation groups. He understood by a flash of intuition that the continuation of these complex functions, the use of Riemann surfaces and transformations in the complex plane correspond with geometric structures that can be understood only in terms of non-Euclidean geometry. In fact, until Poincaré looked at these problems, non-Euclidean geometry was considered as an artificial playground without much relevance to mathematics in general.

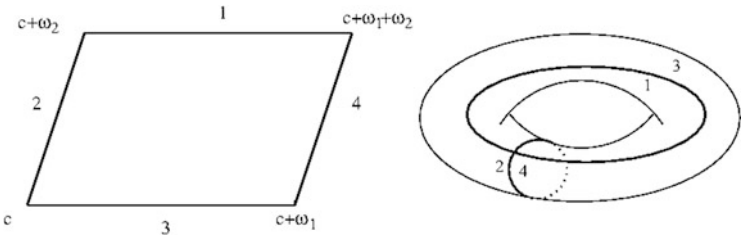

Fig. 1.5 Fundamental parallelogram corresponding with a torus

In the analysis of functions with singularities, fundamental polygons and coverings of Riemann surfaces by polygons play an important part. For some functions a covering by triangles is suitable. In the case of elliptic functions we have the inversion of an elliptic integral that produces double periodicity:

$$\eta(x + m_1\omega_1 + m_2\omega_2) = \eta(x)$$

which keeps $\eta(x)$ invariant ($m_1, m_2 \in \mathbb{Z}$). In this case one uses a covering of parallelograms. Identifying several parts of the boundary of a fundamental polygon leads for the triangle to genus zero (one can deform to a sphere), for the parallelogram to $g = 1$ (identifying the opposite sides two by two leads to a torus, see Fig. 1.5). Poincaré shows that fundamental polygons bounded by more sides lead to arbitrary large genus. For an introduction to polygon coverings see [12, Chap. 12]. In [11] Klein discusses the relations between a fundamental parallelogram and a torus (see Fig. 1.5) and between a fundamental octagonal and a surface with genus two.

Closely related to this is Poincaré's theory of uniformization problems. Differential equations lead to the integration and inversion of algebraic functions; their analytic continuations produce multi-valued analytic functions. Uniformization of such functions corresponds to obtaining a parametrization by single-valued meromorphic functions. The development has led to the relation between complex function theory and hyperbolic geometry, and also to many results in the study of quadratic forms and arithmetic surfaces. The theory of uniformization contains still many fundamental open questions.

1.3.4 Covering an Analytic Curve in 1883

In [21] Poincaré considers a complex vector function $y_1(x), y_2(x), \ldots, y_n(x)$; he lets the complex variable x describe a closed contour C on a Riemann surface S. When x traces the contour C, the function is restricted to an analytic curve on S. The idea is to show that there exists a transformation $x \to z$ such that after applying the

transformation, the vector field y can be parametrized by single-valued meromorphic functions of z. There are two types of contours:

1. When x traces C once, at least one of the components of y does not return to its starting value.
2. All components return to their starting value when tracing the contour C once. There are two subcases:
   1. By slight deformation of C this property persists;
   2. Applying slight deformation of C the property does not persist.

The proof that such a transformation exists rests on two ideas. First, one knows that if C is a closed contour, one can find a holomorphic function $u(\xi, \eta)$ inside C which takes prescribed values on C. This is based on solving the Dirichlet problem of the Laplace equation in two dimensions.

The second point concerns us here. Poincaré states in the proof that the analytic curve on the Riemann surface S is covered by an infinite number of *feuillets*, the infinitesimal elements of Möbius and Jordan. This construction of the covering is later used and extended by Poincaré as a general covering procedure for manifolds.

1.3.5 The Analysis Situs and Its Supplements

On reading the Analysis Situs of 1895 and its later supplements [26], one notes that the conciseness and abstraction of modern mathematics is missing; reading the text is relatively easy. This is deceptive as the ideas and new concepts go very deep. Its readability is misleading.

Introductions to Poincaré's topological papers are found in [29] and [26]. We will discuss a number of basic concepts from the papers referring sometimes to his earlier work. Poincaré was not an avid reader but usually gave carefully credit to ideas and results of colleagues if he knew about them. There are not many references in the Analysis Situs as the material was so new.

1. Introduction of the concept of manifold in arbitrary dimension (by construction).

   The idea of a manifold has a long history with contributions from many mathematicians. Poincaré introduced the covering of an analytic curve in [21]. It is generalized to two and higher-dimensional manifolds.

   In the first section of the Analysis Situs, manifolds are described by sets of algebraic equations in $\mathbb{R}^n$. A new approach is given in the third section where manifolds are defined by continuous parametrizations; they can be replaced by analytic parametrizations as we can approximate continuous functions by analytic ones. In this way, manifolds of the same dimension that have a common part can be considered an analytic continuation of each other.

   Thus far, the analysis of Poincaré of the treatment of manifolds was a natural extension of ideas of older mathematicians and the theory of complex functions on Riemannian surfaces, see [29].

2. The use of local parametrizations that become global by overlap like in analytic continuation was a new idea. Another new element arises in Sect. 10 of the Analysis Situs [26]: geometric representation by gluing together polyhedra identifying faces and manifolds. Consider a manifold M and replace the manifold by approximating simplexes with adjacent boundaries, forming a simplicial complex. In this way, using polygons like triangles, we obtain a triangulation of a manifold that makes it easier to apply homology (the next item).
3. Homology.

   Suppose a manifold M contains r-dimensional submanifolds, Poincaré calls them cycles. If M has a $(r+1)$-dimensional submanifold with as a boundary one given r-dimensional cycle, the cycle is homologous to zero in M. Consider as an illustration an annular region in the plane where $r = 1$, see Fig. 1.6.
4. Homology theory and the fundamental group.

   In Sect. 11 of [26], Poincaré considers domains in 4-space with 3-dimensional surfaces as boundaries that can be subdivided and homeomorphically transformed into polygons. Regarding such transformations, the inspiration from Fuchsian groups becomes explicit in the Sects. 10–14. In Sect. 11, Poincaré writes

   > The analogy with the theory of Fuchsian groups is too evident to need stressing. (transl. J. Stillwell [26])

   One of the results is the emergence of algebraic structures between Betti numbers and a generalized topological Euler invariant (usually called now Euler-Poincaré invariant). Consider a group Γ of translations γ of the complex plane $\mathbb{C}$ (or a suitable other domain) which is fixed-point free. A typical case is when Γ is generated by two Euclidean translations in different directions.

   Associated with Γ is a fundamental domain D which is a polygon. In the case of $\mathbb{C}$ we can take for the fundamental domain a parallelogram. The translations of this polygon in two directions fill $\mathbb{C}$, see Fig. 1.5.

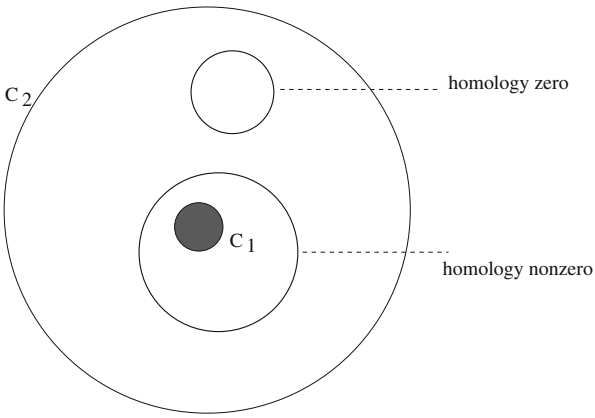

Fig. 1.6 Consider the annular region bounded by C_1 and C_2. A *closed curve* with interior in the annular region has homology zero, a *closed curve* encircling C_1 has nonzero homology

Another aspect brings us to algebraic topology: we can identify opposite sides of the fundamental parallelogram to obtain a torus which is in this special case $\mathbb{C}/\Gamma$. Considering other domains and polygons we may find manifolds with genus higher than one.

5. Associated with homology is also Poincaré duality. It was stated in terms of Betti numbers: The kth and $(n-k)$th Betti numbers of a closed, orientable n-manifold are equal. Criticism of his work by Poul Heegaard led him to discuss (so-called) torsion in the second supplement.

1.3.6 Conclusions

The Analysis Situs was created as a completely new mathematical theory. Its inventions are geometrical representation, triangulation of manifolds, homology and algebraic topology. In particular:

1. To study the connectedness of a manifold Poincaré developed a calculus of submanifolds. The relations involved were called homologies, they could be handled as ordinary equations. This started algebraic topology and what Leibniz would have called "an algebra of surfaces".
2. Technically, Fuchsian transformations and the fundamental group played an inspiring and important part in the set-up of the Analysis Situs.
3. Geometrically, the picture is more complex. Riemann surfaces, global considerations from ODEs and Hamiltonian dynamics were another inspiration. In the dynamical systems theory of Poincaré [20] and [14], an important part of the considerations are local like series expansions, bifurcation theory etc. The development of global insight in dynamical systems like the reasoning needed to describe homoclinic chaos and the use of fixed point results to find periodic solutions (Sect. 1.2.6) was new, it needed consideration of the dynamics on 3-dimensional compact manifolds embedded in 4-space.

References

1. V.I. Arnold, *Geometrical Methods in the Theory of Ordinary Differential Equations* (Springer, New York, 1983)
2. J. Barrow-Green, *Poincaré and the Three Body Problem*. History of Mathematics, vol. 11 (AMS, Providence; London Math. Soc., London, 1997)
3. G.D. Birkhoff, Proof of Poincaré's geometric theorem. Trans. Am. Math. Soc **14**, 14–22 (1913)
4. G. Boole, *A Treatise on Differential Equations* (Macmillan and Co., Cambridge, 1859), 2nd edn., ed. by I. Todhunter (1865)
5. C. Briot, T. Bouquet, Recherches sur les propriété's des fonctions définies par les équations différentielles. J. de lÉcole Polytechnique, Cahier **21**, 133–198 (1856)
6. E. Cartan, *Leçons sur les invariants intégraux*. Librarie Scientifique A (Hermann et Fils, Paris, 1922)
7. M. Duhamel, *Éléments de calcul infinitésimal*, vol. 2, part 4 (4th edn. revised and annotated by J. Bertrand) (Gauthier-Villars, Paris 1887)

8. J. Gray, *Henri Poincaré, a Scientific Biography* (Princeton University Press, Princeton, 2012)
9. C.G.J. Jacobi, *Fundamenta nova theoriae functionum ellipticarum* (Borntraeger, Regiomonti, 1829)
10. C. Jordan, *Cours d'Analyse*. Calcul Intégral, Équations Différentielles, vol. 3 (Gauthier-Villars, Paris, 1887)
11. F. Klein, *Ueber lineare Differentialgleichungen der zweiten Ordnung, Vorlesung, gehalten im Sommersemester 1894* (Ausgearbeitet von E. Ritter, Göttingen, 1894)
12. K. Lamotke, *Riemannsche Flächen*, 2nd edn. (Springer, New York, 2009)
13. H. Laurent, *Traité d'Analyse*. Calcul Intégral, Équations Différentielles Ordinaites, vol. 5 (Gauthier-Villars, Paris, 1890)
14. H. Poincaré, *Les Méthodes Nouvelles de la Mécanique Célèste*, 3 vols. (Gauthier-Villars, Paris, 1892, 1893, 1899)
15. H. Poincaré, *La Valeur de la Science* (Flammarion, Paris, 1905)
16. H. Poincaré, *Science et Méthode* (Flammarion, Paris, 1908)
17. H. Poincaré, *Dernières Pensées* (Flammarion, Paris, 1913)
18. H. Poincaré, *Science and Method*, translated by F. Maitland, preface by B. Russell (Thomas Nelson and Sons, London, 1914)
19. H. Poincaré, *Oeuvres de Henri Poincaré publiées sous les auspices de l'Académie des Sciences*, vols. 1–12 (Gauthier-Villars, Paris, 1916–1954)
20. H. Poincaré, Mémoire sur les courbes définies par une équation différentielle. J. de Mathématiques, 3e série **7**, 375–422 (1881); **8**, 251–296 (1882); Annalen **19**, 553–564 (1882); also in *Oeuvres de Henri Poincaré publiées sous les auspices de l'Académie des Sciences*, vol. 2, pp. 92–105 (Gauthier-Villars, Paris, 1916–1954)
21. H. Poincaré, Sur un théorème de la théorie générale des functions. Bull. Soc. Math. de France **11**, 112–125 (1881); also in *Oeuvres de Henri Poincaré publiées sous les auspices de l'Académie des Sciences*, vol. 4 (Gauthier-Villars, Paris, 1916–1954)
22. H. Poincaré, *Sur les propriétés des functions définies par les équations aux différences partielles*. Oeuvres de Henri Poincaré publiées sous les auspices de l'Académie des Sciences, vol. 1 (Gauthier-Villars, Paris, 1916)
23. H. Poincaré, Sur le probléme des trois corps et les équations de la dynamique. Act. Math. **13**, 1–270 (1890), also in *Oeuvres de Henri Poincaré publiées sous les auspices de l'Académie des Sciences*, vol. 7, pp. 262–479 (Gauthier-Villars, Paris, 1916–1954)
24. H. Poincaré, Sur un théorème de géometrie. Rend. Circolo Mat. Palermo **33**, 375–407 (1912); also in *Oeuvres de Henri Poincaré publiées sous les auspices de l'Académie des Sciences*, vol. 6, pp. 499–538 (Gauthier-Villars, Paris, 1916–1954)
25. H. Poincaré, *Papers on Fuchsian Functions*, translated and introduced by J. Stillwell (Springer, New York, 1985)
26. H. Poincaré, *Papers on Topology, Analysis Situs and Its Five Supplements*, translated and introduction by J. Stillwell. History of Mathematics, vol. 37 (American Mathematical Society, Providence; London Mathematical Society, London, 2010)
27. B. Riemann, *Gesammelte Mathematische Werke und wissenschaftlicher Nachlass* (Complete Works), ed. by H. Weber with cooperation of R. Dedekind (B.G. Teubner, Leipzig, 1876)
28. B. Riemann, *Über die Hypothesen, welche die Geometrie zu Grunde liegen*, Göttingen, June 1854, ed. and annotated by H. Weyl (Julius Springer, Berlin, 1921); also in *Gesammelte Mathematische Werke und wissenschaftlicher Nachlass* (Complete Works), ed. by H. Weber with cooperation of R. Dedekind (B.G. Teubner, Leipzig, 1876)
29. E. Scholz, *Geschichte des Mannigfaltigkeitsbegriffs von Riemann bis Poincaré* (Birkhäuser, Boston, 1980)
30. D. Siersma, Poincaré and analysis situs, the beginning of algebraic topology. Nieuw Archief voor Wiskunde, Centennial Issue **13**, 196–200 (2012)
31. F. Verhulst, *Henri Poincaré, Impatient Genius* (New York, Springer, 2012)
32. F. Verhulst, The interaction of geometry and analysis in Henri Poincaré's conceptions. Nieuw Archief voor Wiskunde, Centennial Issue **13**, 209–216 (2012)

Chapter 2
From Nonlinear Oscillations to Chaos Theory

Jean-Marc Ginoux

Abstract In this work we propose to reconstruct the historical road leading from nonlinear oscillations to chaos theory by analyzing the research performed on the following three devices: the *series-dynamo machine*, the *singing arc* and the *triode*, over a period ranging from the end of the nineteenth century till the end of the Second World War.

Thus, it will be shown that the *series-dynamo machine*, i.e. an electromechanical device designed in 1880 for experiments, enabled to highlight the existence of *sustained oscillations* caused by the presence in the circuit of a component analogous to a "negative resistance".

The *singing arc*, i.e. a spark-gap transmitter used in *Wireless Telegraphy* to produce oscillations and so to send messages, allowed to prove that, contrary to what has been stated by the historiography till recently, Poincaré made application of his mathematical concept of *limit cycle* in order to state the existence of *sustained oscillations* representing a stable regime of sustained waves necessary for radio communication.

During the First World War, the *singing arc* was progressively replaced by the *triode* and in 1919, an analogy between *series-dynamo machine*, *singing arc* and *triode* was highlighted. Then, in the following decade, many scientists such as André Blondel, Jean-Baptiste Pomey, Élie and Henri Cartan, Balthasar Van der Pol and Alfred Liénard provided fundamental results concerning these three devices. However, the study of these research has shown that if they made use of Poincaré's methods, they did not make any connection with his works.

In the beginning of the 1920s, Van der Pol started to study the oscillations of two coupled *triodes* and then, the forced oscillations of a *triode*. This led him to highlight some oscillatory phenomena which have never been observed previously. It will be then recalled that this new kind of behavior considered as "bizarre" at the end of the Second World War by Mary Cartwright and John Littlewood was later identified as "chaotic".

J.-M. Ginoux (✉)
Archives Henri Poincaré, CNRS, UMR 7117, Nancy, France

Laboratoire LSIS, CNRS, UMR 7296, Toulon, France
e-mail: ginoux@univ-tln.fr

C. Skiadas (ed.), *The Foundations of Chaos Revisited: From Poincaré to Recent Advancements*, Understanding Complex Systems,
DOI 10.1007/978-3-319-29701-9_2

2.1 Introduction

The aim of this work is to trace the history of the foundations of Chaos theory through the analysis of the works performed on the following three devices: the *series-dynamo machine*, the *singing arc* and the *triode*, over a period ranging from the end of the nineteenth century till the end of the Second World War.

In 1880, by sending the current produced by a dynamoelectrical into a magnetoelectrical machine forming thus a *series-dynamo machine*, the French engineer Jean-Marie Gérard Anatole Lescuyer highlighted a *nonlinear phenomenon* that will be later considered by Paul Janet as *sustained oscillations* and by Balthasar Van der Pol as *relaxation oscillations*.[1] If the cause of this phenomenon was rapidly identified as being the presence in the circuit of a component analogous to a "negative resistance", its mathematical modeling was out of reach at that time.

A quarter of a century later, at the time of the emergence of *Wireless Telegraphy*, it became of tremendous need to find the condition for which the oscillations produced by a spark-gap transmitter called *singing arc* were sustained. Actually, this condition representing a stable regime of sustained waves necessary for radio communication was established by Henri Poincaré in 1908 during a series of "forgotten lectures" he gave at the École Supérieure des Postes et Télécommunications (today Telecom ParisTech). Contrary to what was stated by the historiography till recently, Poincaré made thus the first correspondence between the existence of *sustained oscillations* and the concept of *limit cycle* that he had introduced in his second memoir "On the curves defined by differential equations". In other words, he proved that the *periodic solution* of the nonlinear ordinary differential equation characterizing the oscillations of the *singing arc* corresponds in the phase plane to an attractive *closed curve*, i.e. a *stable limit cycle*.

During the First World War, the *singing arc* was progressively replaced by the *triode* which was also able to sustain oscillations but even more importantly to amplify the electric signal.

In 1919, the French engineer Paul Janet established an analogy between the *series-dynamo machine*, the *singing arc* and the *triode* and stated thus that their *sustained oscillations* belong to the same *nonlinear phenomenon*. Then, in the following decade, many scientists such as André Blondel, Jean-Baptiste Pomey, Élie and Henri Cartan, Balthasar Van der Pol and Alfred Liénard provided fundamental results concerning these three devices. However, it appears that if they made use of Poincaré's methods, they did not make any connection with his works.

In the beginning of the 1920s, Van der Pol started to study the oscillations of two coupled *triodes* and then, the forced oscillations of a *triode*. This led him to highlight new oscillatory phenomena that he called *oscillation hysteresis*, *automatic*

[1] A brief history of *relaxation oscillations* can be found in Ginoux and Letellier [16]. However, let's notice that this article has been entirely republished by M. Letellier in the Chap. 2 of his last book while omitting to make correct reference to this work. For a detailed history of *relaxation oscillations*, see Ginoux [14, 19, 20].

synchronization and *frequency demultiplication*. Nevertheless, in this case, if the oscillations are still sustained, the solution is no more periodic but exhibits a new kind of behavior that will be called "bizarre" at the end of the Second World War by Mary Cartwright and John Littlewood and that will be later identified as "chaotic".

2.2 The Series-Dynamo Machine: The Expression of Nonlinearity

At the end of the nineteenth century, *magneto-* or *dynamo-electric machines* were used in order to turn mechanical work into electrical work and *vice versa*. With the former type of machine, the magnetic field is induced by a permanent magnet, whereas the latter uses an electromagnet. These machines produced either *alternating* or *direct current* indifferently. Thus, in 1880, a French engineer named Jean-Marie-Anatole Gérard-Lescuyer made an experiment by associating a *dynamo-electric machine* used as a generator with a *magneto-electric machine*, which in this case can be considered as the motor (Fig. 2.1).

Gérard-Lescuyer [21, 22] reports on the found effects in a note published in the *Comptes rendus de l'Académie des Sciences de Paris* and in the *Philosophical Magazine* in the following way:

> As soon as the circuit is closed the magnetoelectrical machine begins to move; it tends to take a regulated velocity in accordance with the intensity of the current by which it is excited; but suddenly it slackens its speed, stops, and start again in the opposite direction, to stop again and rotate in the same direction as before. In a word, it receives a regular reciprocating motion which lasts as long as the current that produces it.

While observing the periodical reversal of the magneto-electric machine's circular motion, despite the direct current, he wondered about the causes of this oscillatory phenomenon that he was unfortunately unable to isolate. Gérard-Lescuyer [21, 22] wrote in his conclusion:

> What are we to conclude from this? Nothing, except that we are confronted by a scientific paradox, the explanation of which will come, but which does not cease to be interesting.

It was actually proven by the count Théodose du Moncel [12] a few weeks later, then by Aimé Witz [50, 51], and by Paul Janet [24], that the gap situated between the brushes of the dynamo is the source of an electromotive force (e.m.f.), i.e. a potential

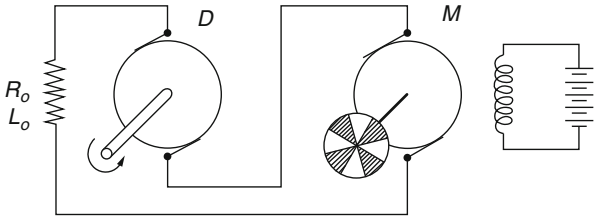

Fig. 2.1 The Gérard-Lescuyer's paradoxical experiment [26]

difference at its terminals symbolized by a nonlinear function of the intensity that flows through there. However, the mathematical modeling of this e.m.f. was out of reach at that time. Therefore the essence of Gérard-Lescuyer's paradox is the presence of an e.m.f, which has a *nonlinear current-voltage characteristic* acting as a *negative resistance* and leading to *sustained oscillations*.

Half a century later, the famous Dutch physicist Balthasar Van der Pol [46] noted:

> Relaxation oscillations produced by a motor powered by a D.C. series-dynamo. The fact that such a system is able to produce relaxation oscillations was already briefly discussed. In an article written by Mr. Janet (we find a reference to Gérard Lescuyer (CR 91, 226, 1880) where this phenomenon had already been described.

2.3 The Singing Arc: Poincaré's Forgotten Lectures

At the end of the nineteenth century a forerunner to the incandescent light bulb called *electric arc* was used for lighthouses and street lights. Regardless of its weak glow it had a major drawback: the noise generated by the electrical discharge which inconvenienced the population. In London, physicist William Du Bois Duddell (1872–1917) was commissioned in 1899 by the British authorities to solve this problem. He thought up the association of an oscillating circuit made with an inductor L and a capacitor C (F on Fig. 2.2) with the *electrical arc* to stop the noise (see Fig. 2.2). Duddell [10, 11] created a device that he named *singing arc*.

Duddell had actually created an oscillating circuit capable of producing not only sounds (hence its name) but especially electromagnetic waves. This device would therefore be used as an emitter for *wireless telegraphy* until the triode replaced it. The *singing arc* or *Duddell's arc* was indeed a "spark gap" device meaning that it produced sparks which generated the propagation of electromagnetic waves shown by Hertz's experiments as pointed out by Poincaré [36, p. 79]:

> If an electric arc is powered by direct current and if we put a self-inductor and a capacitor in a parallel circuit, the result is comparable to Hertz's oscillator... These oscillations are *sustained* exactly like those of the pendulum of a clock. We have genuinely an electrical escapement.

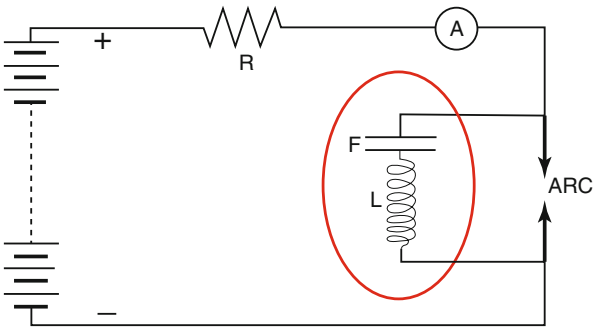

Fig. 2.2 Diagram of the singing arc's circuit, from Duddell [10, 11]

On July 4th 1902, Henri Poincaré became Professor of Theoretical Electricity at the École Supérieure des Postes et Télégraphes (Telecom ParisTech) in Paris where he taught until 1910. The director of this school, Édouard Éstaunié (1862–1942), then asked him to give a series of conferences every 2 years in May–June from 1904 to 1912. He told about Poincaré's first lecture of 1904:

> From the first words it became apparent that we were going to attend the research work of this extraordinary and awesome mathematician... Each obstacle encountered, a short break marked embarrassment, then a blow of shoulder, Poincaré seemed to defy the annoying function.

In 1908, Poincaré chose as the subject: Wireless Telegraphy. The text of his lectures was first published weekly in the journal *La Lumière Électrique* [37] before being edited as a book the year after [38]. In the fifth and last part of these lectures entitled: Télégraphie dirigée : oscillations entretenues (Directive telegraphy: sustained oscillations) Poincaré stated a necessary condition for the establishment of a stable regime of sustained oscillations in the *singing arc*. More precisely, he demonstrated the existence, in the phase plane, of a *stable limit cycle*.

To this aim Poincaré [37] studied Duddell's circuit that he represented by the following diagram (Fig. 2.3) consisting of an electromotive force (e.m.f.) of direct current E, a resistance R and a self-induction, and in parallel, a *singing arc* and another self-induction L and a capacitor.

Then, he called x the capacitor charge, x' the current intensity in the branch including the capacitor, $\rho x'$ the term corresponding to the internal resistance of the self and various damping and $\theta\,(x')$ the term representing the e.m.f. of the arc the mathematical modeling of which was also out of reach for Poincaré at that time. Nevertheless, Poincaré was able to establish the *singing arc equation*, i.e. the second order nonlinear differential equation (2.1) for the sustained oscillations in the *singing arc*:

$$Lx'' + \rho x' + \theta\left(x'\right) + Hx = 0 \tag{2.1}$$

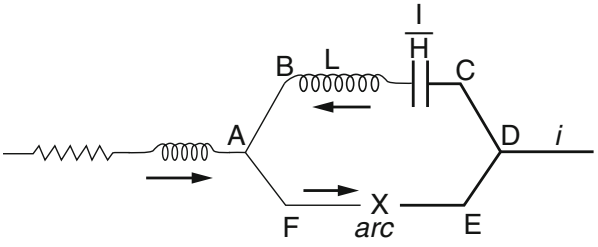

Fig. 2.3 Circuit diagram of the singing arc, from Poincaré [37, p. 390]

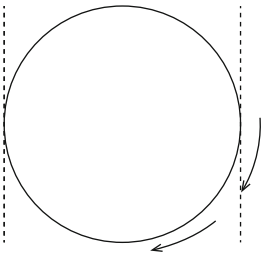

Fig. 2.4 Closed curve solution of the *sing arc equation*, from Poincaré [37, p. 390]

Then, by using the *qualitative theory of differential equations* that he developed in his famous memoirs [30–34], he stated that:

> One can construct curves satisfying this differential equation, provided that function θ is known. Sustained oscillations correspond to closed curves, if there exist any. But every closed curve is not appropriate, it must fulfill certain conditions of stability that we will investigate.

Thus, he plotted a representation of the solution of Eq. (2.1) (see Fig. 2.4):

Let's notice that this closed curve is only a *metaphor* of the solution since Poincaré does not use any graphical integration method such as *isoclines*. This representation led him to state the following *stability condition*:

> *Stability condition.* – Let's consider another non-closed curve satisfying the differential equation, it will be a kind of spiral curve approaching indefinitely near the closed curve. If the closed curve represents a stable regime, by following the spiral in the direction of the arrow one should be brought back to the closed curve, and provided that this condition is fulfilled the closed curve will represent a stable regime of sustained waves and will give rise to a solution of this problem.

Then, it clearly appears that the *closed curve* which represents a stable regime of sustained oscillations is nothing else but a *limit cycle* as Poincaré [31, p. 261] has introduced it in his own famous memoir "On the curves defined by differential equations" and as Poincaré [32, p. 25] has later defined it in the notice on his own scientific works [32]. But this, first *giant step* is not sufficient to prove the stability of the oscillating regime. Poincaré had to demonstrate now that the periodic solution of Eq. (2.1) (the *closed curve*) corresponds to a *stable limit cycle*. So, in the next part of his lectures, Poincaré gave what he calls a "condition de possibilité du problème". In fact, he established a stability condition of the periodic solution of Eq. (2.1), i.e. a stability condition of the limit cycle under the form of the following inequality.

$$\int \theta\left(x'\right) x' dt < 0 \tag{2.2}$$

It has been proved by Ginoux [13, 14, 17, 19, 20] that this stability condition (2.2) flows from a fundamental result introduced by Poincaré in the chapter titled "Exposants caractéristiques" ("Characteristics exponents") of his "New Methods of Celestial Mechanics" [35, vol. I, p. 180].

Until recently the historiography considered that Poincaré did not make any connection between sustained oscillations and the concept of limit cycle he had introduced and credited the Russian mathematician Aleksandr' Andronov [1, 2] for having been the "first" to establish this correspondence between periodic solution and limit cycle.

Concerning the *singing arc*, Van der Pol [49] also noted in the beginning of the thirties:

> In the electric field we have some very nice examples of relaxation oscillations, some are very old, such as spark discharge of a plate machine, the oscillation of the electric arc studied by Mr. Blondel in a famous memoir (1) or the experience of Mr. JANET, and other more recent...
> (1) BLONDEL, *Eclair. Elec.*, 44, 41, 81, 1905. See also *J. de Phys.*, 8, 153, 1919.

2.4 The Triode: From Periodic Solution to Limit Cycle

In 1907, the American electrical engineer Lee de Forest (1873–1961) invented the *audion*. It was actually the first *triode* developed as a radio receiver detector. Curiously, it found little use until its amplifying ability was recognized around 1912 by several researchers. Then, it progressively replaced the *singing arc* in the *wireless telegraphy* devices and underwent a considerable development during the First World War. Thus, in October 1914, a few months after the beginning of the conflict, the French General Gustave Ferrié (1868–1932), director of the *Radiotélégraphie Militaire* department, gathered a team of specialists whose mission was to develop a French *audion*, which should be sturdy, have regular characteristics, and be easy to produce industrially. Ferrié asked to the French physicist Henri Abraham (1868–1943) to recreate Lee de Forests' audions. However, their fragile structure and lack of stability made them unsuitable for military use. After several unsuccessful attempts, Abraham created a fourth structure in December 1914, which was put in operation from February to October 1915 (Fig. 2.5).

The original of this valve called "Abraham lamp" is still in the Arts et Métiers museum to this day (Fig. 2.5). It has a cylindrical structure, which appears to have been designed by Abraham. In November 1917, Abraham consequently invented with his colleague Eugene Bloch (1878–1944) a device able to measure wireless telegraphy emitter frequencies: the so-called *multivibrator* (see Ginoux [14, 17, 19, 20]).

Wireless telegraphy development, spurred by war effort, went from craft to full industrialization. The triode valves were then marketed on a larger scale. More reliable and stable than the *singing arc*, the consistency of the various components used in the triode allowed for exact reproduction of experiments, which facilitated research on sustained oscillations.

Fig. 2.5 Picture of the original lamp T.M. made by Abraham (1915)

2.4.1 Janet's Analogy

In April 1919, the French scientist Paul Janet (1863–1937) published an article entitled "Sur une analogie électrotechnique des oscillations entretenues" [25] which was of considerable importance on several levels. Firstly, it underscored the technology transfer taking place, consisting in replacing an electromechanical component (*singing arc*) with what would later be called an electronic tube. This represented a true revolution since the *singing arc*, because of its structure it made experiments complex and tricky, making it almost impossible to recreate. Secondly, it revealed "technological analogy" between *sustained oscillations* produced by a *series dynamo machine* like the one used by Gérard-Lescuyer [21, 22] and the oscillations of the *singing arc* or a three-electrode valve (*triode*). Janet [25, p. 764] wrote:

> It seemed to me interesting to mention the unexpected analogies of this experiment with the sustained oscillations so widely used to-day in wireless telegraphy, for example, those produced in Duddell's arc or in the lamp with three-electrodes lamps used as oscillators... Producing and sustaining oscillations in these systems mostly depends on the presence, in the oscillating circuit, of something comparable to a negative resistance. The dynamo-series acts as a negative resistance, and the engine with separated excitation acts as a capacity.

Thus, Janet considered that in order to have analogies in the effects, i.e. in order to see the same type of oscillations in the *series-dynamo machine*, the *triode* and the *singing arc*, there must be an analogy in the causes. Therefore, since the *series-dynamo machine* acts as a *negative resistance*, responsible for the oscillations,

there is indeed an analogy. Consequently, only one equation must correspond to these devices. In this article, Janet provided the nonlinear differential equation characterizing the oscillations noted during Gérard-Lescuyer's experiment:

$$L\frac{d^2i}{dt^2} + \left[R - f'(i)\right]\frac{di}{dt} + \frac{k^2}{K}i = 0 \tag{2.3}$$

where R corresponds to the resistance of the series dynamo machine, L is the self-induction of the circuit and K/k^2 is analogous to a capacitor and $f(i)$ is the electromotive force of the *series-dynamo machine*. However, as recalled by Janet [25, p. 765], its mathematical modeling was also out of reach at that time.

> But the phenomenon is limited by the characteristic's curvature, and regular, non-sinusoidal equations actually occur. They are governed by the equation (2.3), which could only be integrated if we knew the explicit for of the function $f(i)$.

By replacing in Eq. (2.3) i with x, R with ρ, $f'(i)$ with $\theta(x)$, and k^2/K with H, one find again Poincaré's *singing arc* equation (2.2). Thus, both ordinary differential equations are analogous but are not of the same order. Nevertheless, it appeared that Janet did make no connection with Poincaré's works.

2.4.2 Blondel's Triode Equation

According to the historiography, it is common knowledge the Dutch physicist Balathasar Van der Pol is credited for having stated the differential equation of the triode in his famous publication entitled "On relaxation oscillations" published in 1926 [45]. However, it was proved by Ginoux [14, 17, 18] on the one hand that the triode equation was actually stated by Van der Pol in 1920 in a publication entitled: "A theory of the amplitude of free and forced triode vibrations," [40] and on the other that the French engineer André Blondel sated the triode equation 1 year before him.

As previously pointed out, the main problem of these three devices was the mathematical modeling of their *oscillation characteristics*, i.e., the e.m.f. of the *series-dynamo machine*, of the *singing arc* and of the *triode*.

Thus, in a note published in the *Comptes Rendus* of the *Académie des Sciences* on the 17th of November 1919, Blondel proposed to model the *oscillation characteristic* of the triode as follows [3]:

$$i = b_1(u + kv) - b_3(u + kv)^3 - b_5(u + kv)^5 \ldots \tag{2.4}$$

Then, substituting i by its expression in the triode equation, neglecting the internal resistors and integrating once with respect to time, he obtained

$$C\frac{\mathrm{d}^2u}{\mathrm{d}t^2} - \left(b_1h - 3b_3h^3u^2 - \ldots\right)\frac{\mathrm{d}u}{\mathrm{d}t} + \frac{u}{L} = 0 \tag{2.5}$$

Let's notice that this equation is perfectly equivalent to those obtained by Poincaré and Janet. Nevertheless, if Blondel solved the problem of the mathematical modeling of the *oscillation characteristic* of the *triode* he did make no connection with Poincaré's works despite of the fact that he knew him personally.

2.4.3 Pomey's Contribution

Less than on year later, the French engineer Jean-Baptiste Pomey (1861–1943) proposed a mathematical modeling of the e.m.f. of the *singing arc* in his entitled: "Introduction à la théorie des courants téléphoniques et de la radiotélégraphie" and published on June 28th 1920 (this detail would be of great importance in the following). Pomey [39, p. 375] wrote:

> For the oscillations to be sustained it is not enough to have a periodic motion, it is necessary to have a stable motion.

Then, he proposed the following "law" for the e.m.f. of the *singing arc*:

$$E = E_0 + ai - bi^3 \tag{2.6}$$

and posing $i = x'$ (like Poincaré) he provided the nonlinear differential equation of the *singing arc*:

$$Lx'' + Rx' + \frac{1}{C}x = E_0 + ax' - bx'^3 \tag{2.7}$$

By posing $H = 1/C$, $\rho = R$ and $\theta\left(x'\right) = -E_0 - ax' + bx'^3$ it is obvious that Eqs. (2.1) and (2.7) are completely identical.[2] Moreover, it is striking to observe that Pomey has used exactly the same variable x' as Poincaré to represent the current intensity. Here again, there is no reference to Poincaré. This is very surprising since Pomey was present during the last lecture of Poincaré at the École Supérieure des Postes et Télégraphes in 1912 whose he had written the introduction. So, one can imagine that he could have attended the lecture of 1908.

At the same time, Van der Pol [40] proposed the following mathematical modeling of the *oscillation characteristic* of the *triode* in an article published on July 17, 1920:

$$i = \psi\left(kv\right) = \alpha v + \beta v^2 + \gamma v^3 \tag{2.8}$$

[2]For more details see Ginoux [17–20].

Van der Pol [40, p. 704] precised that, by symmetry consideration, one can choose $\beta = 0$ and provided the *triode* equation:

$$C\frac{d^2v}{dt^2} - \left(\alpha - 3\gamma v^2\right)\frac{dv}{dt} + \frac{1}{L}v = 0 \tag{2.9}$$

Taking into account that β can be chosen as equal to zero, one finds no difference between the Eqs. (2.6) and (2.8). Nevertheless, nothing proves that Van der Pol had read Pomey's book.

Five years later, on September 28th 1925, Pomey wrote a letter to the mathematician Élie Cartan (1869–1951) in which he asked him to provide a condition for which the oscillations of an electrotechnics device analogous to the *singing arc* and to the *triode* whose equation is exactly that of Janet (2.3) are sustained. Within ten days, Élie Cartan and his son Henri sent an article entitled: "Note sur la génération des oscillations entretenues" [4] in which they proved the existence of a periodic solution for Janet's equation (2.3). In fact, their proof was based on a diagram which corresponds exactly to a "first return map" diagram introduced by Poincaré in his memoir "Sur les Courbes définies par une équation différentielle" [31, p. 251].

2.4.4 Van der Pol's Relaxation Oscillations

Van der Pol's most famous publication is probably that entitled "On relaxation oscillations" [45]. However, what is least well-known is that he published four different versions of this paper in 1926 in the following order:

1. Over Relaxatietrillingen [42] (in Dutch);
2. Over Relaxatie-trillingen [43] (in Dutch);
3. Über Relaxationsschwingungen [44] (in German);
4. On relaxation-oscillations [45] (in English).

In these four articles, Van der Pol presents the following generic dimensionless nonlinear differential equation for *relaxation oscillations* which is neither attached to the *triode*, nor to any other device (*series-dynamo machine* or *singing arc*):

$$\ddot{v} - \varepsilon(1 - v^2)\dot{v} + v = 0. \tag{2.10}$$

Early on, Van der Pol [40, p. 179] realized that the Eq. (2.10) was not analytically integrable:

> It has been found to be impossible to obtain an approximate analytical solution for (2.10) with the supplementing condition ($\varepsilon \ll 1$), but a graphical solution may be found in the following way.

So, he used the *isoclynes* method to graphically integrate the nonlinear differential equation (2.10) for the *relaxation oscillations* (Fig. 2.6).

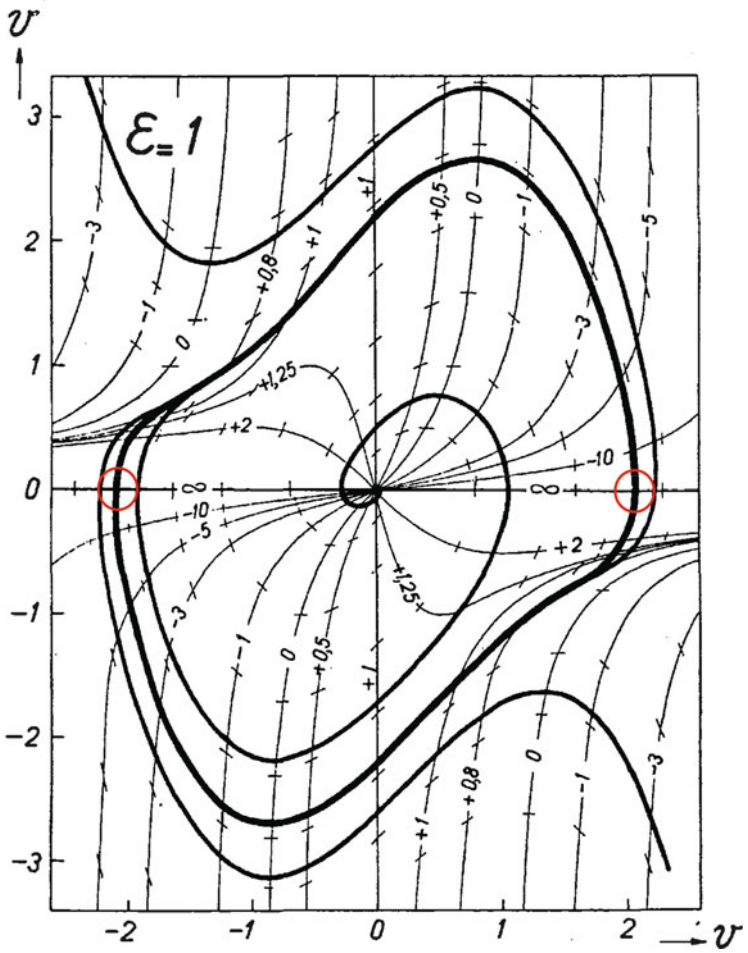

Fig. 2.6 Graphical integration of Eq. (2.10)

Obviously, the solution plotted on this figure is nothing else but a *limit cycle* of Poincaré. Nevertheless, contrary to a widespread view, Van der Pol didn't recognize this signature of a *periodic solution* and did make no connection with Poincaré's works till 1930! On the occasion of a series of lectures that he made at the École supérieure d'Électricité on March 10th and 11th 1930, Van der Pol wrote [49]:

> Note on each of these three figures a closed integral curve, which is an example of what Poincaré called a limit cycle, because the neighboring integral curves are approaching asymptotically.

Moreover, let's notice that he didn't make any reference to Poincaré's works but to Andronov's article [2].

2.4.5 *Liénard's Riddle*

On May 1928, the French engineer Alfred Liénard (1869–1958) published an article entitled "Étude des oscillations entretenues" in which he studied the solution of the following nonlinear differential equation:

$$\frac{d^2x}{dt^2} + \omega f(x)\frac{dx}{dt} + \omega^2 x = 0 \tag{2.11}$$

Such an equation is a generalization of the well-known Van der Pol's equation and of course of Janet's equation (2.4). Under certain assumptions on the function $F(x) = \int_0^x f(x)\,dx$ less restrictive than those chosen by Cartan [4] and Van der Pol [45], Liénard [27] proved the existence and uniqueness of a periodic solution of Eq. (2.11). Then, Liénard [27, p. 906] plotted this solution (Fig. 2.7) and wrote:

> All integral curves, interior or exterior, traveled in the direction of increasing time, tend asymptotically to the curve D, we say that the corresponding periodic motion is a stable motion.

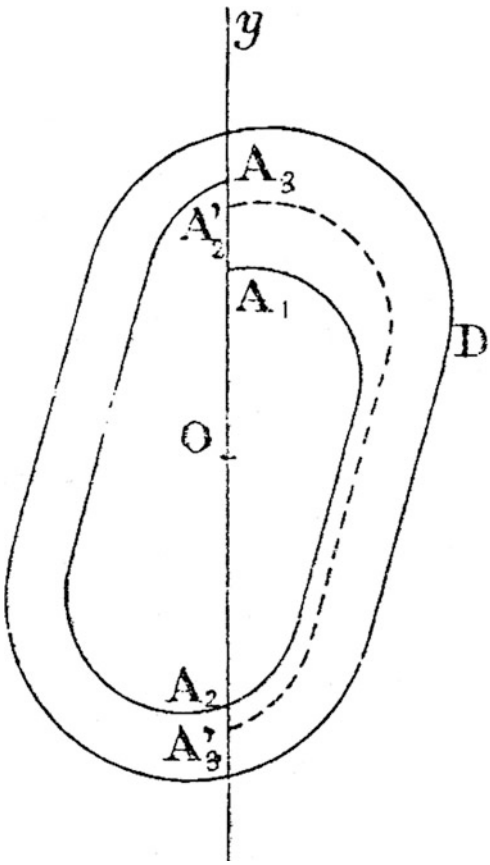

Fig. 2.7 Closed curve solution of Eq. (2.10), Liénard [27]

Then, Liénard [27, p. 906] explained that the condition for which the "periodic motion" is stable is given by the following inequality:

$$\int_{\Gamma} F(x)\, dy > 0 \tag{2.12}$$

By considering that the trajectory curve describes the closed curve clockwise in the case of Poincaré and counter clockwise in the case of Liénard, it is easy to show that both conditions (2.2) and (2.12) are completely identical[3] and represents an analogue of what is now called "orbital stability". Again, one can find no reference to Poincaré's works in Liénard's paper. Moreover, it is very surprising to observe that he didn't used the terminology "limit cycle" to describe its periodic solution. All these facts constitutes the Liénard's riddle.

2.4.6 *Andronov's Note at the Comptes Rendus*

On Monday 14 October 1929, the French mathematician Jacques Hadamard (1865–1963) presented to the Académie des Sciences de Paris a note which was sent to him by Aleksandr Andronov and entitled "Poincaré's limit cycles and the theory of self-sustained oscillation". In this work, Andronov [2] proposed to transform the second order nonlinear differential equation modeling the sustained oscillations by the *series-dynamo machine*, the *singing arc* or the *triode* into the following set of two first order differential equations:

$$\frac{dx}{dt} = P(x, y) \quad ; \quad \frac{dy}{dt} = Q(x, y) \tag{2.13}$$

Then, he explained that the periodic solution of this system (2.13) is expressed in terms of Poincaré's limit cycles:

> This results in self-oscillations which emerge in the systems characterized by the equation of type (2.13) corresponding mathematically to Poincaré's stable limit cycles.

It is important to notice that due to the imposed format of the *Comptes Rendus* (limited to four pages), Andronov did not provide any demonstration. He just claimed that the periodic solution of a non-linear second order differential equation defined by (2.13) "corresponds" to Poincaré's stable limit cycles. Then, Andronov provided a stability condition for the stability of the limit cycle:

$$\int_0^{2\pi} \left[f_x(R\cos\xi, -R\sin\xi; 0)\cos\xi + g_y(R\cos\xi, -R\sin\xi; 0)\sin\xi \right] d\xi < 0 \tag{2.14}$$

[3] For more details see Ginoux [14, 17–20].

In fact, this condition is based on the use of *characteristic exponents* introduced by Poincaré in his so-called *New Methods on Celestial Mechanics* [35, Vol. I, p. 161] and after by Lyapounov in his famous textbook *General Problem of Stability of the Motion* [28]. That's the reason why Andronov will call later the stability condition (2.14): stability in the sense of Lyapounov or Lyapounov stability. It has been stated by Ginoux [13, 14, 17, 19, 20] that both stability condition of Poincaré (2.2) and of Andronov (2.14) are totally identical. Thus by comparing Andronov's previous sentence with that of Poincaré (see above), it clearly appears that Andronov has stated the same correspondence as Poincaré 20 years after him. Nevertheless, it seems that Andronov may not have read Poincaré's article since at that time even if the first volume of his complete works had been already published it didn't contained Poincaré's lectures on *Wireless Telegraphy*.

2.4.7 The First "Lost" International Conference on Nonlinear Oscillations

From 28 to 30 January 1933 the first International Conference of Nonlinear Oscillations was held at the Institut Henri Poincaré (Paris) organized at the initiative of the Dutch physicist Balthasar Van der Pol and of the Russian mathematician Nikolaï Dmitrievich Papaleksi. This event, of which virtually no trace remains, was reported in an article written in Russian by Papaleksi at his return in USSR. This document, recently rediscovered by Ginoux [15], has revealed, on the one hand, the list of participants who included French mathematicians: Alfred Liénard, Élie and Henri Cartan, Henri Abraham, Eugène Bloch, Léon Brillouin, Yves Rocard ... and, on the other hand the content of presentations and discussions. The analysis of the minutes of this conference highlights the role and involvement of the French scientific community in the development of the theory of nonlinear oscillations.[4]

According to Papaleksi [29, p. 211], during his talk, Liénard recalled the main results of his study on sustained oscillations:

> Starting from its graphical method for constructing integral curves of differential equations, he deduced the conditions that must satisfy the nonlinear characteristic of the system in order to have periodic oscillations, that is to say for that the integral curve to be a closed curve, i.e. a limit cycle.

This statement on Liénard must be considered with great caution. Indeed, one must keep in mind that Papaleksi had an excellent understanding of the work of Andronov [2] and that his report was also intended for members of the Academy of the USSR to which he must justified his presence in France at this conference in order to show the important diffusion of the Soviet work in Europe. Despite the presence of MM. Cartan, Lienard, Le Corbeiller and Rocard it does not appear that

[4]For more details see Ginoux [14, 15, 17, 19, 20].

this conference has generated, for these scientists, a renewed interest in the problem of sustained oscillations and limit cycles.

2.5 The Triode: From Limit Cycle to "Bizarre" Solutions

At the end of the First World War, the development of wireless telegraphy led the engineers and scientists to turn to the study of self-sustained oscillations in a three-electrode lamp subjected to a periodic "forcing" or a "coupling". According to Mrs. Mary Lucy Cartwright [9]:

> The non-linearity [in the Van der Pol equation] may be said to control the amplitude in the sense that it allows it to increase when it is small but prevents it becoming too large. The general solution cannot be obtained by the combination of two linearly independent solutions and similar difficulties arise when we add a forcing term to this equation. This was brought out very clearly by the work of Van der Pol and Appleton, partly in collaboration, and partly independently, in a series of papers on radio oscillations published between 1920 and 1927. To me the work of the radio engineers is much more interesting and suggestive than that of the mechanical engineers. The radio engineers want their systems to oscillate, and to oscillate in a very orderly way, and therefore they want to know not only whether the system has a periodic solution, but whether it is stable, what its period and amplitude and harmonic content are, and how these vary with the parameters of the equation, and they sometimes want the period to be determined with a very small error. In the early days they wanted to explain why the amplitude was limited in a certain way and why in some cases the period lengthened as the harmonic content increased and not in others. The desire to know why and the insistence on how the various quantities such as amplitude and frequency vary with the parameters of the equation over fairly wide ranges meant that numerical and graphical solutions either failed to provide the answer or were far too cumbersome. Further, unless one knows something about the general behavior of the solutions, the numerical work, which is only approximate, may be misleading.

Thus, in the beginning of the 1920s, Van der Pol [40] studied the oscillations of a forced triode, i.e. a triode powered by a voltage generator with an f.e.m. of type $v(t) = E_s in(\omega_1 t)$ the equation of which reads then:

$$\ddot{v} - \alpha\left(1 - v^2\right)\dot{v} + \omega_0^2 v = \omega_1^2 E_s in(n\omega_1 t) \quad \text{with} \quad \varepsilon = \frac{\alpha}{\omega_0} \ll 1 \tag{2.15}$$

Four years later, while using the method of "slowly-varying amplitude" that he had developed, Van der Pol [41] was thus able on the one hand to obtain more directly the various approximations of the amplitude of this forced system, and on the other hand, to construct a solution to the equation more easily than by using the classical Poincaré-Lindstedt or Fourier methods.[5] In this paper, Van der Pol [47] highlights the fact that when the difference in frequency of the two signals is inferior to this value an *automatic synchronization* phenomenon occurs and the two circuits

[5]The English version of this article was published in 1927. See Van der Pol [47].

oscillate with the same frequency. This led him to evidence the phenomenon of *frequency entrainment*, which he defined thus:

> Hence the free frequency undergoes a correction in the direction of the forced frequency, giving the impression as if the free frequency were being attracted by the forced frequency.

In 1927, Van der Pol and his colleague Jan Van der Mark [48] published an article titled "Frequency Demultiplication," in which they again studied the forced oscillations of a triode, but in the field of *relaxation oscillations*. Then, they explained that the *automatic synchronization* phenomenon, observed in the case of the forced oscillations of a triode, can also occur for a range of the parameter corresponding to the *relaxation oscillations*, i.e. for $\varepsilon \gg 1$, but in a much wider frequency field. They also reported that the *resonance* phenomenon is almost non-existent in forced relaxation oscillations, and that consequently, the sinusoidal e.m.f. inducing the forcing influences the period (or frequency) of the oscillations more than it does their amplitude, and added:

> It is found that the system is only capable of oscillating with *discrete frequencies*, these being determined by whole *sub-multiples of the applied frequency*.

In their article, Van der Pol and Van der Mark [48] proposed, in order to evidence the *frequency demultiplication* phenomenon, the following construction (see Fig. 2.8) on which we can see a "jump" of the period for each increase in the value of the capacitor's capacitance.

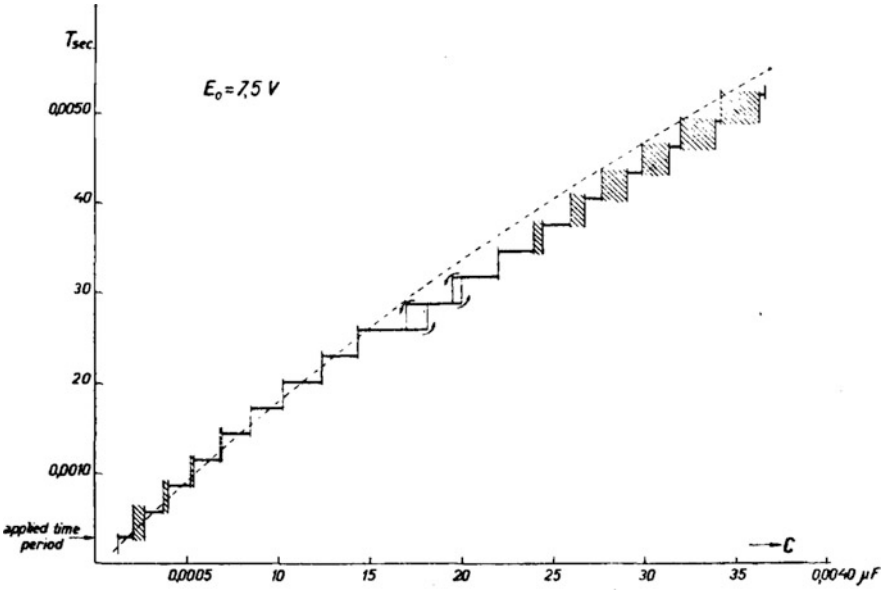

Fig. 2.8 Representation of the phenomenon of *frequency demultiplication*, from Van der Pol et Van der Mark [48, p. 364]

In order to evidence this *frequency demultiplication* phenomenon, Van der Pol and Van der Mark used a phone. They then described the phenomenon what they heard in the receiver:

> Often an irregular noise is heard in the telephone receivers before the frequency jumps to the next lower value. However, this is a subsidiary phenomenon, the main effect being the regular frequency multiplication.

This irregular noise they heard was actually the sound manifestation of the transition which was taking place. Indeed, as the frequency varied, the solution to the differential equation (2.15), which had been until now represented by a *limit cycle*, i.e. by a *periodic attractor*, would draw a "strange attractor" transcribing the *chaotic behavior* of the solution. Van der Pol seemed to have reached the limits of deterministic physics with how far he went in the exploration of nonlinear and non-autonomous systems. He "flirted", as Mary Lucy Cartwright and John Edensor Littlewood [5–8] did 20 years later with the first signs of chaos, when they called "bizarre" the behavior of the solution to the differential equation (2.15) for specific values of the parameters. Indeed, according to Guckenheimer et al. [23]:

> Van der Pol's work on nonlinear oscillations and circuit theory provided motivation for the seminal work of Cartwright and Littlewood. In 1938, just prior to World War II, the British Radio Research Board issued a request for mathematicians to consider the differential equations that arise in radio engineering. Responding to this request, Cartwright and Littlewood began studying the forced Van der Pol equation and showed that it does indeed have bistable parameter regimes. In addition, they showed that there does not exist a smooth boundary between the basins of attraction of the stable periodic orbits. They discovered what is now called chaotic dynamics by detailed investigation of this system.

2.6 Conclusion

Thus, the analysis of the research performed on the following three devices: the *series-dynamo machine*, the *singing arc* and the *triode*, over a period ranging from the end of the nineteenth century till the end of the Second World War, has enabled to reconstruct the historical road leading from nonlinear oscillations to chaos theory. The *series-dynamo machine* has highlighted a new kind of oscillations generated by the presence of a nonlinear component in the circuit, i.e. a *negative resistance*. Poincaré's work on the *singing arc* has provided an analytical condition for the sustaining of these oscillations, i.e. for the existence of a stable limit cycle. Moreover, this has proved that Poincaré has established 20 years before Andronov the correspondence between periodic solution and stable limit cycle. In his research on the *triode*, Blondel has solved the question of the mathematical modeling of its *oscillation characteristic*, i.e. of its *negative resistance* and stated thus, 1 year before Van der Pol, the *triode*'s equation. Then, Janet highlighted an analogy between the oscillations sustained by the *series-dynamo machine*, the *singing arc* and the *triode* and Van der Pol deduced that they were belonging to the same oscillatory phenomenon that he called *relaxation oscillations*. Though he plotted the solution

of the equation that now bears his name, he didn't recognize that it was obviously a Poincaré's limit cycle. Thereafter, Cartan and then Liénard proved the existence and uniqueness of this periodic solution but did not make either a connection with Poincaré's works. Immediately after Andronov established this connection, Van der Pol and Papaleksi organized the first *International Conference on Nonlinear Oscillations* in Paris. Nevertheless, this meeting did not lead to any development or research in this field. At the same time, Van der Pol and Van der Mark highlighted that the forced triode was the source of a strange phenomenon that they called *frequency demultiplication*. At the end of the Second World War, Cartwright and Littlewood investigated this system and considered its oscillations as "bizarre". Many years later, it appeared that they had actually observed the first *chaotic behavior*.

References

1. A.A. Andronov, Предельные циклы Пуанкаре и теория колебаний, in IVs'ezd ruskikh fizikov (5-16.08, p. 23–24). (Poincaré's limit cycles and the theory oscillations), this report has been read guring the IVth congress of Russian physicists in Moscow between 5 to 16 August 1928, p. 23–24
2. A.A. Andronov, Les cycles limites de Poincaré et la théorie des oscillations auto-entretenues. C. R. Acad. Sci. **189**, 559–561 (1929)
3. A. Blondel, Amplitude du courant oscillant produit par les audions générateurs. C. R. Acad. Sci. **169**, 943–948 (1919)
4. E. Cartan, H. Cartan, Note sur la génération des oscillations entretenues. Ann. P. T. T. **14**, 1196–1207 (1925)
5. M.L. Cartwright, J. Littlewood, On non-linear differential equations of the second order, I: the equation $\ddot{y} - k\left(1 - y^2\right)\dot{y} + y = b\lambda kcos\left(\lambda t + a\right)$, k large. J. Lond. Math. Soc. **20**, 180–189 (1945)
6. M.L. Cartwright, J. Littlewood, On nonlinear differential equations of the second order, II: the equation $\ddot{y} - kf\left(y\right)\dot{y} + g\left(y,k\right) = p\left(t\right) = p_1\left(t\right) + kp_2\left(t\right); k > 0, f\left(y\right) \geq 1$. Ann. Math. **48**, 472–494 (1947)
7. M.L. Cartwright, J. Littlewood, Errata. Ann. Math. **49**, 1010 (1948)
8. M.L. Cartwright, J. Littlewood, Addendum. Ann. Math. **50**, 504–505 (1949)
9. M.L. Cartwright, Non-linear vibrations: a chapter in mathematical history. Presidential address to the mathematical association, January 3, 1952. Math. Gazette **36**(316), 81–88 (1952)
10. W. du Bois Duddell, On rapid variations in the current through the direct-current arc. J. Inst. Electr. Eng. **30**(148), 232–283 (1900)
11. W. du Bois Duddell, On rapid variations in the current through the direct-current arc. J. Inst. Electr. Eng. **46**, 269–273, 310–313 (1900)
12. Th. du Moncel, Réactions réciproques des machines dynamo-électriques et magnéto-électriques. La Lumière Électrique **2**(17), 352 (1880)
13. J.M. Ginoux, L. Petitgirard, Poincaré's forgotten conferences on wireless telegraphy. Int. J. Bifurcation Chaos **20**(11), 3617–3626 (2010)
14. J.M. Ginoux, Analyse mathématiques des phénomènes oscillatoires non linéaires. Thèse, Université Pierre & Marie Curie, Paris VI (2011)
15. J.M. Ginoux, The first "lost" international conference on nonlinear oscillations (I.C.N.O.). Int. J. Bifurcation Chaos **4**(22), 3617–3626 (2012)

16. J.M. Ginoux, C. Letellier, Van der Pol and the history of relaxation oscillations: toward the emergence of a concepts. Chaos **22**, 023120 (2012)
17. J.M. Ginoux, Self-excited oscillations: from Poincaré to Andronov. Nieuw Archief voor Wiskunde (New Archive for Mathematics). Journal published by the Royal Dutch Mathematical Society (Koninklijk Wiskundig Genootschap) **13**(3), 170–177 (2012)
18. J.M. Ginoux, R. Lozi, Blondel et les oscillations auto-entretenues. Arch. Hist. Exact Sci. **66**(5), 485–530 (2012)
19. J.M. Ginoux, *Histoire de la théorie des oscillations non linéaires* (Hermann, Paris, 2015)
20. J.M. Ginoux, *History of Nonlinear Oscillations Theory*. Archimede, New Studies in the History and Philosophy of Science and Technology (Springer, New York, 2016)
21. J.M.A. Gérard-Lescuyer, Sur un paradoxe électrodynamique. C. R. Acad. Sci. **168**, 226–227 (1880)
22. J.M.A. Gérard-Lescuyer, On an electrodynamical paradox. Philos. Mag V **10**, 215–216 (1880)
23. J. Guckenheimer, K. Hoffman, W. Weckesser, The forced Van der Pol equation i: the slow flow and its bifurcations. SIAM J. Appl. Dyn. Syst. **2**(1), 1–35 (2003)
24. P. Janet, Sur les oscillations électriques de période moyenne. J. Phys. Theor. Appl. **2**(1), 337–352 (1893)
25. P. Janet, Sur une analogie électrotechnique des oscillations entretenues. C. R. Acad. Sci. **168**, 764–766 (1919)
26. Ph. Le Corbeiller, Non-linear theory of maintenance of oscillations. J. Inst. Electr. Eng. **79**, 361–378 (1936)
27. A. Liénard, Étude des oscillations entretenues. Revue générale de l'Electricité **23**, 901–912, 946–954 (1928)
28. A. Lyapounov, Problème général de la stabilité du mouvement. Annales de la faculté des sciences de Toulouse, Sér. 2 **9**, 203–474 (1907) [Originally published in Russian in 1892. Translated by M. Édouard Davaux, Engineer in the French Navy à Toulon]
29. N. Papaleksi, Международная нелинейным конференция, in *Internatinal Conference On Nonlinear Process*, Paris, 28–30 January 1933. Z. Tech. Phys. **4**, 209–213 (1934)
30. H. Poincaré, Sur les courbes définies par une équation différentielle. Journal de mathématiques pures et appliquées **3**(7), 375–422 (1881)
31. H. Poincaré, Sur les courbes définies par une équation différentielle. Journal de mathématiques pures et appliquées **3**(8), 251–296 (1882)
32. H. Poincaré, *Notice sur les Travaux Scientifiques de Henri Poincaré* (Gauthier-Villars, Paris, 1884)
33. H. Poincaré, Sur les courbes définies par une équation différentielle. Journal de mathématiques pures et appliquées **4**(1), 167–244 (1885)
34. H. Poincaré, Sur les courbes définies par une équation différentielle. Journal de mathématiques pures et appliquées **4**(2), 151–217 (1886)
35. H. Poincaré, *Les Méthodes Nouvelles de la Mécanique Céleste*, vols. I–III (Gauthier-Villars, Paris, 1892, 1893, 1899)
36. H. Poincaré, La théorie de Maxwell et les oscillations hertziennes: la télégraphie sans fil, 3rd edn. (Gauthier-Villars, Paris, 1907)
37. H. Poincaré, Sur la télégraphie sans fil. La Lumière Électrique **2**(4), 259–266, 291–297, 323–327, 355–359, 387–393 (1908)
38. H. Poincaré, in *Conférences sur la télégraphie sans fil* (La Lumière Électrique éd., Paris, 1909)
39. J.B. Pomey, *Introduction à la théorie des courants téléphoniques et de la radiotélégraphie* (Gauthier-Villars, Paris, 1920)
40. B. Van der Pol, A theory of the amplitude of free and forced triode vibrations. Radio Rev. **1**, 701–710, 754–762 (1920)
41. B. Van der Pol, Gedwongen trillingen in een systeem met nietlineairen weerstand (Ontvangst met teruggekoppelde triode). Tijdschrift van het Nederlandsch Radiogenootschap **2**, 57–73 (1924)
42. B. Van der Pol, Over Relaxatietrillingen. Physica **6**, 154–157 (1926)

43. B. Van der Pol, Over “Relaxatie-trillingen”. Tijdschrift van het Nederlandsch Radiogenootschap **3**, 25–40 (1926)
44. B. Van der Pol, Über “Relaxationsschwingungen”. Jahrbuch der drahtlosen Telegraphie und Telephonie **28**, 178–184 (1926)
45. B. Van der Pol, On “relaxation-oscillations”. Lond. Edinb. Dublin Philos. Mag. J. Sci. VII **2**, 978–992 (1926)
46. B. Van der Pol, Über Relaxationsschwingungen II. Jahrbuch der drahtlosen Telegraphic und Telephonie **29**, 114–118 (1927)
47. B. Van der Pol, Forced oscillations in a circuit with non-linear resistance (reception with reactive triode). Lond. Edinb. Dublin Philos. Mag. J. Sci. VII **3**, 65–80 (1927)
48. B. Van der Pol, J. van der Mark, Frequency demultiplication. Nature **120**, 363–364 (1927)
49. B. Van der Pol, Oscillations sinusoïdales et de relaxation. Onde Électrique **9**, 245–256, 293–312 (1930)
50. A. Witz, Des inversions de polarités dans les machines série-dynamos. C. R. Acad. Sci. **108**, 1243–1246 (1889)
51. A. Witz, Recherches sur les inversions de polarité des série-dynamos. J. Phys. Theor. Appl. **8**(1), 581–586 (1889)

Chapter 3
Hydrodynamic Turbulence as a Nonstandard Transport Phenomenon

David Ruelle

Abstract The hydrodynamic time evolution is Hamiltonian in the inertial range (i.e., in the absence of viscosity). From this we obtain that the macroscopic study of hydrodynamic turbulence is equivalent, at an abstract level, to the microscopic study of a heat flow in a nonstandard geometry. In the absence of fluctuations this means that the Kolmogorov theory of turbulence is equivalent to a heat flow for a suitable mechanical system. Turbulent fluctuations (intermittency) correspond to thermal fluctuations for the heat flow. A relatively crude estimate of the thermal fluctuations, based on standard ideas of nonequilibrium statistical mechanics is presented: this agrees remarkably well with what is observed in several turbulence experiments. A logical relation with the lognormal theory of Kolmogorov and Obukhov is also indicated, which shows what fails in this theory, and what can be rescued.

3.1 Introduction

In the present paper we give a relatively informal presentation of some new ideas on hydrodynamic turbulence which have been introduced in two papers by the author [1, 2]. Here we insist on the physical ideas; the reader will find calculations and details in the above references. Furthermore, relevant computer calculations by Gallavotti and Garrido are presented in a companion paper [3]. Our basic idea is to consider hydrodynamic turbulence as a physical phenomenon, not a chapter in the study of nonlinear partial differential equations.

A remarkable experimental fact about turbulence is that it is chaotic (see Ruelle-Takens [4], Gollub and Swinney [5], Libchaber [6], etc.). This means that the time evolution (f^t) of a turbulent fluid system belongs to a much studied class of deterministic dynamics with sensitive dependence on initial conditions (see Lorenz [7], and the reprint collections by Cvitanović [8] and Hao Bai-Lin [9]). In particular,

D. Ruelle (✉)
Mathematics Department, Rutgers University, New Brunswick, NJ, USA

Institut des Hautes Études Scientifiques, 91440 Bures sur Yvette, France
e-mail: ruelle@ihes.fr

C. Skiadas (ed.), *The Foundations of Chaos Revisited: From Poincaré to Recent Advancements*, Understanding Complex Systems,
DOI 10.1007/978-3-319-29701-9_3

the time dependence of turbulence is not quasi-periodic: the frequency spectrum is not discrete. There are natural measures used for the description of chaotic physical systems, these are called SRB measures (Ia.G. Sinai, D. Ruelle, R. Bowen, see [10, 11] for a discussion of this topic). In fact, a useful idea is to assume that the physical system behaves as if it had uniformly hyperbolic dynamics (that it is an Anosov flow: this is the Gallavotti-Cohen [12] *chaotic hypothesis*).

In view of the above remarks, we obtain a statistical theory of turbulence simply by determining a SRB measure for a dynamical system describing the time evolution of a fluid. There are several perfectly decent mathematical definitions of SRB measures. However, the technical problem of finding SRB measures for the time evolution defined by the Navier-Stokes equations at moderate or high Reynolds numbers appears totally beyond reach. For that reason, I shall not bother to discuss the precise definition of SRB measures. The problem of understanding the statistical structure of hydrodynamic turbulence has a straight answer, but this answer cannot in practice be implemented. I have come to this conclusion several decades ago, and it is only recently that I have seen a way out of that difficulty. Here is the idea: the turbulent energy cascade is conceptually just a special case of a heat transport problem. In other words, the macroscopic turbulent energy cascade is mathematically the same thing as a microscopic heat flow problem in a nonstandard geometry.

As it turns out, the studying the nonequilibrium statistical mechanics of heat flows is an extremely hard problem, and it would seem that we have replaced the intractable problem of turbulent energy cascade by a heat flow problem which is equally intractable. If we try to gain physical understanding rather than mathematical proof, the situation is better because we have some physical understanding of the statistical structure of a heat flow, at least if we are not too far from equilibrium. Instead of using SRB measures, we shall thus follow more traditional ideas of nonequilibrium statistical mechanics. Our aim will be to predict certain features of the turbulent energy cascade from the study of a heat flow. Specifically we shall be interested in:

- the intermittency exponents ζ_p (large Reynolds number $\mathcal{R}$ limit)
- the probability distribution of velocity gradients (moderate $\mathcal{R}$)
- understanding what works (doesn't work) in the Kolmogorov-Obukhov lognormal turbulence theory.

We shall be led to making rather crude approximations to obtain explicit results. In spite of this we shall be surprisingly successful in understanding the physics of turbulence. To the present author this means that hydrodynamic turbulence can be naturally understood on the basis of generally accepted (or acceptable) ideas on Hamiltonian dynamics, dimensional analysis (à la Kolmogorov) and nonequilibrium ergodic theory. No subtle results about nonlinear PDE's will play a role in our discussion.

3.2 Turbulent Fluid as a Physical System: A Problem in Nonequilibrium Statistical Mechanics

We shall discuss incompressible fluids in three dimensions. We think of a body of fluid contained in a bounded box. It is known that the incompressible approximation is reasonable for many problems. The dynamics of our incompressible fluid is Hamiltonian, modified by dissipation due to viscosity. The viscous dissipation occurs at small scales, and we shall discuss it separately, as is often done. We shall act on the fluid by some external forces, which keep the fluid in motion in spite of energy dissipation. Since dissipation occurs at small scales, it is customary to assume that the external forces act at large spatial scales.

In the equations describing fluid time evolution, the inviscid (Hamiltonian) part is naturally and uniquely defined: it is just an analytic expression of the acceleration, and the adjective *inertial* is often used to denote this part. The viscous term describing self-friction is based on response theory: there is a viscous force which resists deformations of the fluid. In the Navier-Stokes equation linear response is used to express self-friction, but this is an approximation and the viscous term doesn't have the same universal character as the inertial term. The question of existence and uniqueness of solutions of the Navier-Stokes equation, while mathematically interesting, is thus of limited interest from the physical viewpoint which we adopt here. The viscous terms become important only for small spatial scales (this follows from a dimensional argument), so that energy dissipation occurs at small spatial scales.

The inviscid time evolution for a D-dimensional fluid has a very different character if $D = 2$ and $D = 3$. In 2 dimensions there are many conserved quantities because the vorticity (curl of the velocity) is scalar, and the distribution of values of this scalar vorticity is time-independent. The time evolution of a 2-dimensional fluid is thus very non-ergodic. In 3 dimensions we may make the opposite assumption of high ergodicity (the time evolution is ergodic and mixing in a suitable sense). It is therefore natural (as we shall see) that in three dimension the energy goes from large to small spatial scales: this is the *turbulent energy cascade*. The adjective "turbulent" refers to the manner in which the energy transfer is seen experimentally to proceed: via complicated irregular velocity fluctuations. That the situation is very different in 2 dimensions is not astonishing in view of the highly non-ergodic nature of the time evolution (one speaks of an inverse cascade). The natural situation is that observed in 3 dimensions, and which we shall study.

Let our fluid be contained in a cubic box with side ℓ_0. We decompose this box into sub-boxes of side $\ell_n = \kappa^{-n}\ell_0$ (these will be called *nodes*) where the positive integer κ will be specified later. We can use wavelets to associate $\approx 2\kappa^3$ modes to each node. Remember now that our fluid is a Hamiltonian system. We may think of this Hamiltonian system as formed of interacting sub-systems corresponding to the nodes, each with $\approx \kappa^3$ degrees of freedom. In this manner, the turbulent energy cascade starting at the node 0 and ending by dissipation at nodes of high level n, is equivalent to a heat flow through a Hamiltonian system of coupled nodes, with heat

flowing from node 0 to (many) nodes of high level. This equivalence of turbulent cascade to heat flown a non-standard geometry is in principle exact, although not formulated precisely here.

Translating a nonequilibrium problem (turbulence) into another nonequilibrium problem (heat flow) is in principle an interesting idea, but there are two obvious difficulties:

- expressing the fluid Hamiltonian as Hamiltonian of a coupled system of "nodes" is likely to give complicated results,
- the rigorous study of a heat flow is known to be extremely hard (see for instance [13, 14]).

What we shall do is to use crude (but physically motivated) approximations, with the hope that the results obtained are in reasonable agreement with experiments. This is indeed the conclusion of our study, indicating that turbulence fits naturally within accepted ideas of nonequilibrium statistical mechanics.

3.3 Statistical Mechanics of Turbulence Without Fluctuations

A fundamental step forward in the understanding of turbulence has been achieved by Kolmogorov [15–17]. He noticed that if turbulence is assumed to be spatially homogeneous and isotropic, then many features of the energy cascade are determined by dimensional analysis.[1] The experimental study of fluids has shown that turbulence is in fact not homogeneous: this lack of homogeneity is known as *intermittency*.

Let us now look at the heat flow interpretation of the turbulent energy cascade. The macroscopic description of a heat flow, ignoring the microscopic structure of the heat conductor and the microscopic fluctuations leads to an answer in terms of heat conductivity. We can give a heat flow equivalent version of the Kolmogorov turbulent cascade theory: the heat flows from the site 0 towards high level sites, respecting the nonstandard geometry of the system, and a prescribed amount of energy (heat) leaving 0 per unit time. We have thus a complete equivalence between the Kolmogorov turbulent energy cascade and a heat flow in a nonstandard geometry where microscopic structure and fluctuations are ignored.

The Hamiltonian description than we have obtained in terms of interacting nodes, each with $\approx \kappa^3$ degrees of freedom has a discrete structure, and must have fluctuations. If we had a finite temperature equilibrium state, the energy fluctuations would be given by Boltzmann's law. Outside of equilibrium the situation is not as

[1] Dimensional analysis says how various quantities (like velocity or energy) depend on certain variables (like spatial distance, and time): velocity is spatial distance divided by time, energy is mass times velocity squared, etc. Dimensional analysis appears somewhat trivial, but for the turbulent energy cascade it has led to spectacular predictions.

well understood, but there are fluctuations, which must correspond to intermittency for the turbulent cascade.

3.4 Statistical Mechanics of Turbulence with Fluctuations

To proceed with the study of fluctuations we shall make crude approximations based on physical ideas that we have about turbulence and about the nonequilibrium statistical mechanics of heat flows. We shall assume that a given constant κ can be chosen so that (allowing some approximations) the dynamical structure is particularly simple. First we shall neglect interactions between nodes except those between nodes corresponding to a cube of size ℓ_n and the cubes of size ℓ_{n+1} that it contains. If we consider a graph with nodes as vertices, and interacting nodes as edges, this graph is thus a tree. A similar approximation has been made in models of intermittency (see [18, 19]) where one would think of eddies rather than nodes.

We can assume that the flow of energy is overwhelmingly from a node of level n towards the nodes of level $n+1$ with which it interacts: this corresponds to the differences of temperature at various levels which can be obtained from the theory without fluctuations, and corresponds to the direction of the turbulent energy cascade. We now make the strong but natural assumption that the nodes of level $n+1$ interacting with a given node of level n are in (approximate) thermal equilibrium with the fluctuating energy of this node. We assume thus the κ can be chosen such that there is a Boltzmannian energy distribution at each node, with a condition between neighboring nodes which expresses that energy flows overwhelmingly from level n to level $n+1$, and that energy is conserved.

For a node of level n, let $\mathbf{v}_{ni}$ be the fluctuation velocity at one of the next order modes (box i of size ℓ_{n+1}) and write

$$V_n = V_{ni} = |\mathbf{v}_{ni}|^3$$

The kinetic energy corresponding to the velocity $\mathbf{v}_{ni}$ is $\kappa^{-3(n+1)}.|\mathbf{v}_{ni}|^2/2$. The residence time at the node of level n is $\sim \ell_n/|\mathbf{v}_{n-1}|$ by dimensional analysis. Energy conservation requires that the rate of flow of energy out of the node of level n is equal to the rate of flow into that node:

$$\kappa^{-3}\sum_i \frac{|\mathbf{v}_{ni}|^3}{\ell_{n+1}} = \frac{|\mathbf{v}_{n-1}|^3}{\ell_n} \qquad \text{or} \qquad \kappa^{-3}\sum_i |\mathbf{v}_{ni}|^3 = \frac{V_{n-1}}{\kappa}$$

Given V_{n-1}, this relation may be interpreted as a microcanonical ensemble condition on the $|\mathbf{v}_{ni}|^3$. We replace this by a canonical distribution such that each $\mathbf{v}_{ni}$ has a distribution

$$\sim \exp\Big(-\frac{|\mathbf{v}_n|^3}{\kappa^{-1}V_{n-1}}\Big)d^3\mathbf{v}_n$$

Therefore, given V_{n-1}, we find that V_n has the distribution

$$\frac{\kappa\, dV_n}{V_{n-1}} \exp\Big(-\frac{\kappa V_n}{V_{n-1}}\Big).$$

For a decreasing sequence of boxes of sizes $\ell_0, \dots, \ell_n$ we obtain that, if V_0 is fixed, we have a probability distribution

$$\frac{\kappa\, dV_1}{V_0} e^{-\kappa V_1/V_0} \dots \frac{\kappa\, dV_n}{V_{n-1}} e^{-\kappa V_n/V_{n-1}} \tag{3.1}$$

for $V_1, \dots, V_n$. Note that this distribution extends naturally to a probability measure ϖ on sequences $(V_n)_{n=1}^{\infty}$. Physically however, the validity of (1) is limited by dissipation due to the viscosity ν. We want ℓ_n to be larger than the length at which dissipation due to viscosity takes place (Kolmogorov length); this is expressed by

$$|\mathbf{v}_{ni}|\, \ell_n > \nu \qquad \text{or} \qquad V_n^{1/3} \ell_n > \nu \tag{3.2}$$

3.5 Applications of (3.1)

- (a) The exponents ζ_n.
  Let us now discuss the structure functions, i.e., the moments

$$\langle |\mathbf{v}_n|^p \rangle = \langle V_n^{p/3} \rangle$$

for positive integer p, and the exponents ζ_p such that

$$\langle |\mathbf{v}_n|^p \rangle \sim \ell_n^{\zeta_p} \qquad \text{or} \qquad \zeta_p \ln \ell_n \sim \ln \langle V_n^{p/3} \rangle = -n \cdot \frac{p}{3} \ln \kappa + \ln \langle W_n^{p/3} \rangle$$

where we have written $W_k = \kappa^k V_k$. We have here

$$\langle W_n^{p/3} \rangle = \int dW_1 \frac{e^{-W_1/W_0}}{W_0} \int \cdots \int dW_{n-1} \frac{e^{-W_{n-1}/W_{n-2}}}{W_{n-2}} \int dW_n \frac{e^{-W_n/W_{n-1}}}{W_{n-1}} \cdot W_n^{p/3}$$

and also

$$\int_0^\infty dW_n \frac{e^{-W_n/W_{n-1}}}{W_{n-1}} \cdot W_n^{p/3} = W_{n-1}^{p/3} \int_0^\infty d\xi\, e^{-\xi} \xi^{p/3} = W_{n-1}^{p/3} \Gamma(\frac{p}{3} + 1)$$

so that by induction we find

$$\langle W_n^{p/3} \rangle = [\Gamma(\tfrac{p}{3}+1)]^n W_0^{p/3}, \quad \zeta_p \approx \frac{-n\frac{p}{3} \ln \kappa + \ln \langle W_n^{p/3} \rangle}{-n \ln \kappa} \approx \frac{p}{3} - \frac{1}{\ln \kappa} \ln \Gamma(\tfrac{p}{3}+1)$$

In conclusion we have the (approximate) prediction

$$\zeta_p = \frac{p}{3} - \frac{1}{\ln \kappa} \ln \Gamma(\frac{p}{3} + 1) \tag{3.3}$$

Using either the heat propagation or the eddy cascade picture, we see that κ should be chosen such that the initial W_n distribution concentrated on one value for (n, i) thermalizes to values of W_{n+1} for the systems $(n + 1, j)$ distributed according to

$$\frac{1}{W_n} e^{-W_{n+1}/W_n} dW_{n+1}$$

This requires κ sufficiently large. However, if the value of κ is too large, several different temperatures will be present among the systems $(n + 1, j)$ connected with (n, j), and the W_{n+1}-distribution will not be Boltzmannian. Of course a rigorous justification of this picture is well beyond the power of current mathematical methods. We can only claim this: κ should be such that when an eddy of size r has decayed to eddies of size r/κ their energies have a thermal distribution, after which the process can start again. In the dissipative range the distribution of V_n should be cut off at large V_n. Numerically, one finds that the above formula fits the experimental data [20] well with $1/\log \kappa = 0.32 \pm 0.01$, i.e., κ between 20 and 25.

Note also that (3.3) gives $\zeta_3 = 1$ independently of κ. This is in agreement with studies based on the Navier-Stokes equation.

- (b) Radial velocity increment $u = \Delta_r v = \sum_k u_k$.

If $r \approx \ell_n$ we have $u \approx u_n \approx$ radial component of $\mathbf{v}_n$. Therefore, given V_0, a rough estimate of the probability distribution $F_\Delta(u)\, du$ of u is given by:

$$F_\Delta(u) = \Big(\prod_{k=1}^{n} \int_0^\infty \frac{\kappa\, dV_k}{V_{k-1}} e^{-\kappa V_k / V_{k-1}} \Big) \frac{1}{2V_n^{1/3}} \chi_{[-V_n^{1/3}, V_n^{1/3}]}(u)$$

$$= \frac{1}{2} (\frac{\kappa^n}{V_0})^{1/3} \int \cdots \int_{w_1 \cdots w_n > (\kappa^n/V_0)|u|^3} \prod_{k=1}^{n} \frac{dw_k\, e^{-w_k}}{w_k^{1/3}}$$

(One compares with experimental data for $\xi = \text{const.}u$ with $|\xi|$ normalized by $\langle \xi^2 \rangle = 1$, therefore the approximation $u \approx$ radial component of $\mathbf{v}_n$ is not as terrible as might seem).

Instead of $F_\Delta(u)\, du$ we consider the distribution $G_n(y)\, dy$ of $y = (\kappa^n/V_0)^{1/3}|u|$, so that

$$G_n(y) = \int \cdots \int_{w_1 \cdots w_n > y^3} \prod_{k=1}^{n} \frac{dw_k\, e^{-w_k}}{w_k^{1/3}}$$

$$e^t G_n(e^t) = (\phi^{*(n-1)} * \psi)(t) \tag{3.4}$$

where

$$\phi(t) = 3\exp(3t - e^{3t}) \quad , \quad \psi(t) = e^t \int_t^\infty e^{-s}\phi(s)\, ds$$

From this one obtains that $G_n(y)$ is a decreasing function of y.

Using the formula (3.2) for the dissipation length we obtain $n = (3/4)\ln \mathcal{R}/\ln \kappa \approx 0.24 \ln \mathcal{R}$. $G_n(y)$ gives then a reasonable fit of the numerical data for small y. However, a comparison with the Navier-Stokes results of Schumacher [21] shows that the behavior at large y is not as simple. This can be understood because the dissipation length is not fixed by the Reynolds number $\mathcal{R}$, but fluctuates. In fact the probability distribution $P(\xi)\, d\xi$ of the radial velocity gradient ξ (normalized by $\langle \xi^2 \rangle = 1$) which is computed in [2] has contributions of various values of n (one can show that there are no contribution of $n \leq j$ if $\kappa^{2j} \leq \xi\mathcal{R}$). For a study taking into account the fluctuations of the dissipation length see the paper by Gallavotti and Garrido [3] in this volume.

- (c) Relation with the Kolmogorov-Obukhov lognormal theory.

  The above formula (3.5) implies that $G_n(e^t)$ as a function of e^t is a convolution product of many factors for large n, which suggests an asymptotic Gaussian distribution, i.e., a lognormal distribution with respect to t. This would be in agreement with the well-known ideas of Kolmogorov [22] and Oboukhov for introducing intermittency in Kolmogorov theory. However, the very explicit forms given above for ϕ and ψ show that these functions do not tend very rapidly to zero at infinity (only exponentially). This means that we do not have an asymptotic lognormal distribution. In particular we need not trust the prediction for the exponents ζ_n made by the lognormal theory, and it is satisfactory that (3.3) gives a better fit to the experimental data.

References

1. D. Ruelle, Hydrodynamic turbulence as a problem in nonequilibrium statistical mechanics. PNAS **109**, 20344–20346 (2012)
2. D. Ruelle, Non-equilibrium statistical mechanics of turbulence. J. Stat. Phys. **157**, 205–218 (2014)
3. G. Gallavotti, G. Garrido, Non-equilibrium statistical mechanics of turbulence: comments on Ruelle's intermittency theory, in *The Foundations of Chaos Revisited: From Poincaré to Recent Advancements*, ed. by C. Skiadas (Springer, Heidelberg, 2016). doi:10.1007/978-3-319-29701-9
4. D. Ruelle, F. Takens, On the nature of turbulence. Commun. Math. Phys. **20**, 167–192 (1971) and **23**, 343–344 (1971)
5. J.P. Gollub, H.L. Swinney, Onset of turbulence in a rotating fluid. Phys. Rev. Lett. **35**, 927–930 (1975)
6. A. Libchaber, From chaos to turbulence in Benard convection. Proc. R. Soc. Lond. **A**413, 63–69 (1987)
7. E.N. Lorenz, Deterministic nonperiodic flow. J. Atmos. Sci. **20**, 130–141 (1963)
8. P. Cvitanović (ed.), *Universality in Chaos*, 2nd edn. (Adam Hilger, Bristol, 1989)

9. B.-L. Hao (ed.), *Chaos II* (World Scientific, Singapore, 1990)
10. L.-S. Young, What are SRB measures, and which dynamical systems have them? J. Stat. Phys. **108**, 733–754 (2002)
11. C. Bonatti, L.J. Díaz, M. Viana, *Dynamics Beyond Uniform Hyperbolicity* (Springer, Berlin, 2005)
12. G. Gallavotti, E.G.D. Cohen, Dynamical ensembles in stationary states. J. Stat. Phys. **80**, 931–970 (1995)
13. D. Dolgopyat, C. Liverani, Energy transfer in a fast-slow Hamiltonian system. Commun. Math. Phys. **308**, 201–225 (2011)
14. D. Ruelle, A mechanical model for Fourier's law of heat conduction. Commun. Math. Phys. **311**, 755–768 (2012)
15. A.N. Kolmogorov, The local structure of turbulence in incompressible viscous fluid for very large Reynolds number. Dokl. Akad. Nauk SSSR **30**, 301–305 (1941)
16. A.N. Kolmogorov, On degeneration (decay) of isotropic turbulence in an incompressible viscous liquid. Dokl. Akad. Nauk SSSR **31**, 538–540 (1941)
17. A.N. Kolmogorov, Dissipation of energy in locally isotropic turbulence. Dokl. Akad. Nauk SSSR **32**, 16–18 (1941)
18. G. Parisi, U. Frisch, On the singularity structure of fully developed turbulence, in *Turbulence and Predictability in Geophysical Fluid Dynamics*, ed. by M. Ghil, R. Benzi, G. Parisi (North-Holland, Amsterdam, 1985), pp. 84–88
19. R. Benzi, G. Paladin, G. Parisi, A. Vulpiani, On the multifractal nature of fully developed turbulence and chaotic systems. J. Phys. A **17**, 3521–3531 (1984)
20. F. Anselmet, Y. Gagne, E.J. Hopfinger, R.A. Antonia, High-order velocity structure functions in turbulent shear flows. J. Fluid Mech. **140**, 63–89 (1984)
21. J. Schumacher, J. Scheel, D. Krasnov, D. Donzis, K. Sreenivasan, V. Yakhot, Small-scale universality in turbulence. Proc. Natl. Acad. Sci. USA **111**(30), 10961–10965 (2014)
22. A.N. Kolmogorov, A refinement of previous hypotheses concerning the local structure of turbulence in a viscous incompressible fluid at high Reynolds number. J. Fluid Mech. **13**, 82–85 (1962)

Chapter 4
Non-equilibrium Statistical Mechanics of Turbulence

Comments on Ruelle's Intermittency Theory

Giovanni Gallavotti and Pedro Garrido

Abstract The recent proposal by D. Ruelle for a theory of the corrections to the OK theory ("intermittency corrections") is to take into account that the Kolmogorov scale itsef should be regarded as a fluctuating variable. Some quantitative aspects of the theory can be quite easily studied also via computer and will be presented.

4.1 A Hierarchical Turbulence Model

The proposal [7, 8] for a theory of the corrections to the OK theory ("intermittency corrections") is to take into account that the Kolmogorov scale itself should be regarded as a fluctuating variable.

The OK theory is implied by the assumption, for n large, of zero average work due to interactions between wave components with wave length $< \kappa^{-n}\ell_0 \equiv \ell_n$ and components with wave length $> \kappa\,\kappa^{-n}\ell_0$ (ℓ_0 being the length scale where the energy is input in the fluid and κ a scale factor to be determined) together with the assumption of independence of the distribution of the components with inverse wave length ("momentum") in the shell $[\kappa^n, \kappa\kappa^n]\ell_0^{-1}$, [5, p. 420].

It is represented by the equalities

$$\frac{\mathbf{v}_{ni}^3}{\ell_n} = \frac{\mathbf{v}_{(n+1)i'}^3}{\ell_{n+1}}, \qquad \mathbf{v} = |v|,\ v \in R^3 \tag{4.1}$$

G. Gallavotti (✉)
INFN-Roma1, Roma, Italy
Rutgers University, New Brunswick, NJ, USA
e-mail: giovanni.gallavotti@roma1.infn.it

P. Garrido
Physics Department, University of Granada, Avda. del Hospicio, S/N, 18010 Granada, Spain
e-mail: garrido@onsager.ugr.es

C. Skiadas (ed.), *The Foundations of Chaos Revisited: From Poincaré to Recent Advancements*, Understanding Complex Systems,
DOI 10.1007/978-3-319-29701-9_4

interpreted as stating an *equality up to fluctuations* of the velocity components of scale $\kappa^{-n}\ell_0$, i.e. of the part of the velocity field which can be represented by the Fourier components in a basis of plane waves localized in boxes, labeled by $i = 1, \dots \kappa^{3n}$, of size $\kappa^{-n}\ell_0$ into which the fluid (moving in a container of linear size ℓ_0) is imagined decomposed (a wavelet representation) so that $(n+1, i')$ labels a box contained in the box (n, i).

The length scales are supposed to be separated by a suitably large scale factor κ (i.e. $\ell_n = \kappa^{-n}\ell_0 = \kappa^{-1}\ell_{n-1}$) so that the fluctuations can be considered independent, however not so large that more than one scalar quantity (namely $\mathbf{v}^3_{n,i}$) suffices to describe the independent components of the velocity (small enough to avoid that "several different temperatures will be present among the systems $(n+1, j')$" inside the containing box labeled (n, j), and the $\mathbf{v}_{n+1,j}$ distribution "will not be Boltzmannian for a constant temperature inside",[7, p. 2]).

The distribution of $\mathbf{v}^3_{n+1,j}$ is then simply chosen so that the average of the $\mathbf{v}^3_{n+1,j}$ is the value $\mathbf{v}^3_{n,i}\kappa$ if the $\mathbf{v}^3_{n+1,j}$ on scale $n+1$ gives a finer description of the field in a box named j contained in the box named i of scale larger by one unit.

Among the distributions with this property is selected the one which maximizes entropy[1] and is:

$$W_{ni} \stackrel{def}{=} |v_{ni}|^3, \qquad \prod_{m=0}^{n}\prod_{i=1}^{\kappa^m} \frac{dW_{i,m+1}}{W_{i'm}} \kappa\, e^{-\kappa \frac{W_{i,m+1}}{W_{i',m}}} \tag{4.2}$$

with W_0 a constant that parameterizes the fixed energy input at large scale: the motion will be supposed to have a 0 average total velocity at each point; hence $W_0^{\frac{1}{3}}$ can be viewed as an imposed average velocity gradient at the largest scale ℓ_0.

The $\mathbf{v}_{in} = W_{in}^{\frac{1}{3}}$ is then interpreted as a velocity variation on a box of scale $\ell_0\kappa^{-n}$ or κ^{-n} as ℓ_0 will be taken 1. The index i will be often omitted as we shall mostly be concerned about a chain of boxes, one per each scale $\kappa^{-n}, n = 0, 1, \dots$, totally ordered by inclusion (i.e. the box labeled (i, n) contains the box labeled $(i', n+1)$).

The distribution of the energy dissipation $W_{n,i} \stackrel{def}{=} \mathbf{v}^3_{n,i}$ in the hierarchically arranged sequence of cells is therefore close in spirit to the hierarchical models that have been source of ideas and so much impact, at the birth of the *renormalization group* approach to multiscale phenomena, in quantum field theory, critical point statistical mechanics, low temperature physics, Fourier series convergence to name a few, and to their nonperturbative analysis, either phenomenological or mathematically rigorous, [1–4, 10–12].

The present turbulent fluctuations model can therefore be called *hierarchical model for turbulence* in the inertial scales. It will be supposed to describe the

[1] If the box $\Delta = (n, j) \subset \Delta' = (n-1, j')$ then the distribution $\Pi(W|W_{\Delta'})$ of $W_\Delta \equiv \mathbf{v}^3_\Delta$ is conditioned to be such that $\langle W \rangle = \kappa^{-1} W_{\Delta'}$; therefore the maximum entropy condition is that $-\int \Pi(W|W') \log \Pi(W|W') dW - \lambda_\Delta \int W \Pi(W|W') dW$, where λ_Δ is a Lagrange multiplier, is maximal under the constraint that $\langle W \rangle = W'\kappa^{-1}$: this gives the expression, called *Boltzmannian* in [7], for $\Pi(W|W')$.

velocity fluctuations at scales n at which the Reynolds number is larger than 1, i.e. as long as $\frac{\mathbf{v}_n \kappa^{-n} \ell_0}{\nu} > 1$.

The description will of course be approximate, [8, Sect. 3]: for instance the correlations of the velocity gradient components are not considered (and skewness will still rely on the classic OK theory, [6, Sect. 34]).

Given the distribution (and the initial parameter W_0) it "only" remains to study its properties assuming the distribution valid for velocity profiles such that $\mathbf{v}_n \kappa^{-n} \ell_0 > \nu$ after fixing the value of κ in order to match data in the literature (as explained in [8, Eq. (12)]). As a first remark the scaling corrections proposed in [12] can be rederived.

The average energy dissipation in a box of scale n can be defined as the average of $\varepsilon_n \stackrel{def}{=} W_n \ell^{-n}$, $\ell_n = \ell_0 \kappa^{-n}$: the latter average and its p"th order moments can be readily computed to be, for $p > 0$:

$$\begin{aligned} &\frac{\log \langle\, \varepsilon_n^p \,\rangle}{-\log \ell_n} \xrightarrow[n\to\infty]{} \tau_p = -\frac{\log \Gamma(1+p)}{\log \kappa}, \qquad \langle\, \varepsilon_n^p \,\rangle \sim \kappa^{n\tau_p}, \\ &\langle\, (\frac{W_n}{\ell_n})^{\frac{p}{3}} \,\rangle \sim \kappa^{n\tau_{\frac{p}{3}}}, \qquad \langle\, \mathbf{v}_n^p \,\rangle \sim \ell_0^{\frac{p}{3}} \kappa^{-n\zeta_p}, \qquad \zeta_p = \frac{p}{3} + \tau_p \end{aligned} \tag{4.3}$$

The $W_n^{\frac{1}{3}}$ being interpreted as a velocity variation on a box of scale $\ell_0 \kappa^{-n}$, the last formula can also be read as expressing the $\langle\, (\frac{|\Delta_r v|}{r})^p \,\rangle \sim r^{\zeta_p}$ with $\zeta_p = \frac{1}{3} - \frac{\log \Gamma(\frac{p}{3}+1)}{\log \kappa}$.

The τ_p is the intermittency correction to the value $\frac{1}{3}$: the latter is the standard value of the OK theory in which there is no fluctuation of the dissipation per unit time and volume $\frac{W_n}{\ell_n}$; this gives us one free parameter, namely κ, to fit experimental data: its value, universal within Ruelle's theory, turns out to be quite large, $\kappa \sim 22.75$, [7], fitting quite well all experimental p-values ($p < 18$).

Other universal predictions are possible. In [8] a quantity has been studied for which accurate simulations are available.

If $\mathbf{W}$ is a sample $(W_0, W_1, \ldots)$ of the dissipations at scales $0, 1, \ldots$ for the distribution in the hierarchical turbulence model, the smallest scale $n(\mathbf{W})$ at which $W_n^{\frac{1}{3}} \ell_0 \kappa^{-n} \simeq \nu$ occurs is the scale at which the Kolmogorov scale is attained (i.e. the Reynolds number $\frac{W_n^{\frac{1}{3}} \ell_n}{\nu}$ becomes < 1).

Taking $\ell_0 = 1, \nu = 1$, at such (random) Kolmogorov scale the actual dissipation is $\xi = W_{n(\mathbf{W})} \kappa^{n(\mathbf{W})}$ with a probability distribution with density $P^*(\xi)$. If $w_k = \frac{W_k}{W_{k-1}}$ then $W_n = W_0 w_1 \cdots w_n$ and the computation of $P^*(\xi)$ can be seen as a problem on extreme events about the value of a product of random variables. Hence is natural that the analysis of P^* involves the Gumbel distribution $\phi(t)$ (which appears with parameter 3), [8].

The P^* is a distribution (universal once the value of κ has been fixed to fit the mentioned intermittency data) which is interesting because it can be related to a quantity studied in simulations.

It has been remarked, [8], that, assuming a symmetric distribution of the velocity increments on scale κ^{-n} whose modulus is $W_{n,i}^{\frac{1}{3}}$, the hierarchical turbulence model

can be applied to study the distribution of the velocity increments: for small velocity increments the calculation can be performed very explicitly and quantitatively precise results are derived, that can be conceivably checked at least in simulations. The data analysis and the (straightforward) numerical evaluation of the distribution P^* is described below, following [8].

4.2 Data Settings

Let $\ell_0, \nu = 1$ and let $\mathbf{W} = (W_0, W_1, \ldots)$ be a sample chosen with the distribution

$$p(d\mathbf{W}) = \prod_{i=1}^{\infty} \frac{\kappa\, dW_i}{W_{i-1}}\, e^{-\kappa \frac{W_i}{W_{i-1}}} \tag{4.4}$$

with W_0, κ given parameters; and let $\mathbf{v} = (v_0, v_1, \ldots) = (W_0^{\frac{1}{3}}, W_1^{\frac{1}{3}}, \ldots)$.

Define $n(\mathbf{W}) = n$ as the smallest value of i such that $W_i^{\frac{1}{3}}\kappa^{-i} \equiv v_i\kappa^{-i} < 1$: $n(\mathbf{W})$ will be called the "dissipation scale" of $\mathbf{W}$.

Imagine to have a large number $\mathcal{N}$ of p-distributed samples of $\mathbf{W}$'s. Given $h > 0$ let

$$P_n^*(\xi) \stackrel{def}{=} \frac{1}{h}\frac{1}{\mathcal{N}}\Big((\#\,\mathbf{W} \text{ with } n(\mathbf{W}) = n) \cap (\xi < (W_n/W_0)^{\frac{1}{3}}\kappa^n < \xi + h)\Big) \tag{4.5}$$

hence $hP_n^*(\xi)$ is the probability that the dissipation scale n is reached with ξ in $[\xi, \xi+h]$. Then $P^*(\xi) \stackrel{def}{=} \sum_{n=0}^{\infty} P_n^*(\xi)$ is the probability density that, at the dissipation scale, the velocity gradient $\frac{v_n}{v_0}\kappa^n$ is between ξ and $\xi + h$.

The velocity component in a direction is $v_n \cos\vartheta$: so that the probability that it is in $d\xi$ with gradient $\frac{v_n}{v_0}\kappa^n$ and that this happens at dissipation scale $= n$ is $d\xi$ times

$$\int P_n^*(\frac{v_n}{v_0}\kappa^n = \xi_0)d\xi_0\delta(\xi_0|\cos\vartheta| - \xi)\frac{\sin\vartheta\, d\vartheta\, d\varphi}{4\pi} = \int_{\xi}^{\infty} \frac{P_n^*(\xi_0)}{\xi_0}d\xi_0 \tag{4.6}$$

Let

$$P(\xi) \stackrel{def}{=} \int_{\xi_0 > \xi} \frac{d\xi_0}{\xi_0} \sum_{n=1}^{\infty} P_n^*(\xi_0) \tag{4.7}$$

that is the probability distribution of the (normalized radial velocity gradient) and

$$\sigma_m = \int_0^{\infty} d\xi P(\xi)\xi^m \tag{4.8}$$

its momenta. To compare this distribution to experimental data [9] it is convenient to define

$$p(z) = \frac{1}{2}\sigma_2^{1/2} P(\sigma_2^{1/2}|z|) \tag{4.9}$$

We have used the following computational algorithm to $P(\xi)$:

1. Build a sample (i) $\mathbf{W}^{(i)} = (W_0, W_1, \ldots, W_n, \ldots)$
2. Stop when $n = \bar{n}_i$ such that $W_{n-1}^{1/3}\kappa^{-(n-1)} > 1 > W_n^{1/3}\kappa^{-n}$
3. Evaluate $\bar{m}_i = int(\xi_i/h) + 1$ where $\xi_i = \kappa^{\bar{n}_i}(W_{\bar{n}_i}/W_0)^{1/3}$
4. goto to (1) during N times

Then, the distribution $P(\xi)$ is given by

$$P(mh - h/2) = h^{-1}\bar{P}(m) \quad , \quad \bar{P}(m) = \frac{1}{N}\sum_{i=1}^{N}\frac{1}{\bar{m}_i}\chi(\bar{m}_i \geq m) \tag{4.10}$$

where $\chi(A) = 1$ if A is true and 0 otherwise. It is convenient to define the probability to get a given m value as

$$\overline{Q}(m) = \frac{1}{N}\sum_{i=1}^{N}\delta(\bar{m}_i, m) \tag{4.11}$$

where $\delta(n, m)$ is the Kronecker delta. Once obtained $\overline{Q}(m)$, we can get recursively $\bar{P}(m)$:

$$\bar{P}(m+1) = \bar{P}(m) - \frac{1}{m}\overline{Q}(m) \quad , \quad \bar{P}(1) = \sum_{m=1}^{\infty}\frac{1}{m}\overline{Q}(m) = \frac{1}{N}\sum_{i=1}^{N}\frac{1}{\bar{m}_i} \tag{4.12}$$

and the momenta distribution is then given by:

$$\sigma_m = h^m \frac{1}{N}\sum_{i=1}^{N}\frac{1}{\bar{m}_i}\sum_{l=1}^{\bar{m}_i} l^m \tag{4.13}$$

Finally, the error bars of a probability distribution (for instance $\bar{P}$) are computed by considering that the probability that in N elements of a sequence there are n in the box m is given by the binomial distribution:

$$D_m(n, N) = \binom{N}{n}\bar{P}(m)^n\left(1 - \bar{P}(m)\right)^{N-n} \tag{4.14}$$

From it we find

$$\langle n\rangle_m = N\bar{P}(m) \quad , \quad \langle (n-\langle n\rangle_m)^2\rangle_m = \bar{P}(m)\left(1-\bar{P}(m)\right)/N \tag{4.15}$$

where $\langle . \rangle = \sum_n . D_m(n,N)$. Therefore, the error estimation for the $\bar{P}$ probability is given by

$$\bar{P}(m) \pm 3\left(\bar{P}(m)\left(1-\bar{P}(m)\right)/N\right)^{1/2} \tag{4.16}$$

We have done 15 simulations with $\kappa = 22$, $N = 10^{12}$ realizations (10^4 cycles of size 10^7) and different values of W_0: 10^7, 10^8, 5×10^8, 10^9, 2×10^9, 3×10^9, 4×10^9, 5×10^9, 10^{10}, 2×10^{10}, 5×10^{10}, 7×10^{10}, 10^{11}, 2×10^{11} and 5×10^{11}. We also use the Reynold's number $R = W_0^{1/3}$.

The size of κ has been chosen to fit the data for the intermittency exponents ζ_p and it is quite large ($\kappa = 22$, [7]): this has the consequence that the Kolmogorov scale is reached at a scale κ^{-n} with $n = 2, 3$ and very seldom for higher scales, at the considered Reynolds numbers. That can be seen in Fig. 4.1 where we show the obtained distributions of $\bar{n}_i$, $i = 1, \ldots, N$. In Fig. 4.2 we see the average value of $\bar{n}$ and its second momenta. We see that for low Reynold's numbers the values is almost constant equal to 2 and from $R \simeq 2000$ it begins to grow. The second momenta shows a minimum for $R \simeq 1000$ where almost all events are in $\bar{n}_i = 2$.

The measured distribution of $Q(\xi)$ (see Fig. 4.3) reflects the superposition of two distributions: the values of ξ associated to the $\bar{n}_i = 2$ and to $\bar{n}_i = 3$ events. Moreover, for small values of R the overall distribution is dominated by the events $\bar{n}_i = 2$ and for large Reynold's numbers it is dominated by the $\bar{n}_i = 3$ events. At each case the form of the distribution is different: for small R, $log_{10}Q(\xi)$ is quadratic in ξ and for large R is linear in ξ.

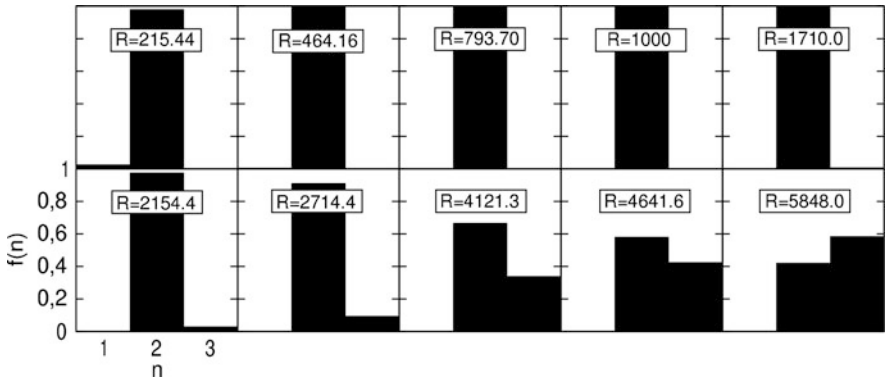

Fig. 4.1 Distribution of events that reach the Kolmogorov scale κ^{-n} for different values of the Reynold's numbers R and $\kappa = 22$. The total number of events is 10^{12}

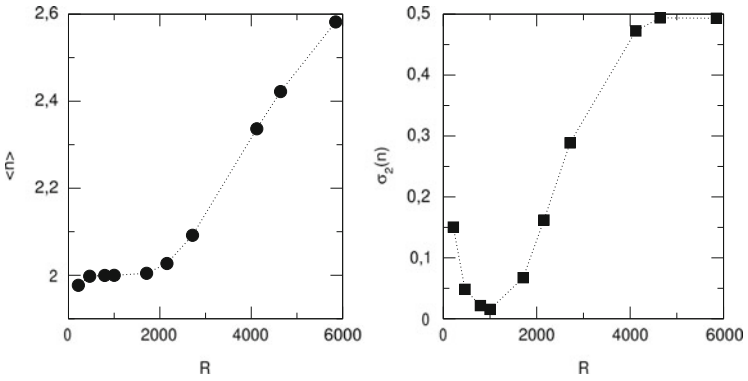

Fig. 4.2 Momenta of the $\bar{n}$-distribution. *Left*: average value. *Right*: second momenta

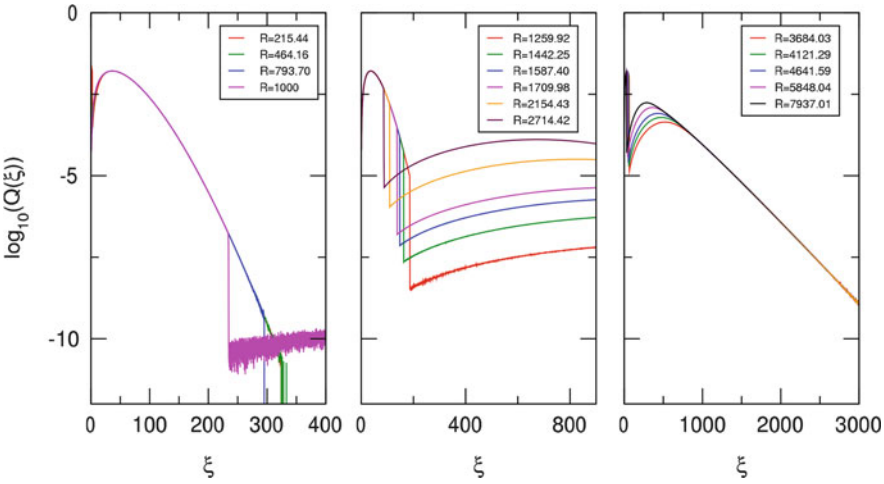

Fig. 4.3 Plot as a function of $\xi = mh$ of the logarithm of the probability, $\log_{10} Q(\xi)$, with $Q(\xi) = \overline{Q}(\frac{\xi}{h})$, that the Kolmogorov scale is reached at scale $m = \frac{\xi}{h}$, for different Reynold's numbers and $h = 10^{-3}\langle\, \xi \,\rangle$

The behavior of Q defines the behavior of $p(z)$. In Fig. 4.4 we see the $p(z)$ behavior. We again see clearly how for low R values the distribution is non sensitive to the values of R and it is Gaussian. For intermediate values of R the exponential of a quadratic function is a good fit for the measured distribution and large enough values of z but its parameters depend on R. Finally for R large of 3000 the distribution changes and its behavior for large z values seems to be fitted very well by a linear function with a R-depending slope.

It is interesting to show the dependence of the momenta of $\bar{P}$, σ_n, as a function of R. In Fig. 4.5 we see their behavior. We can naturally identify three regions: Region I ($R \in [0, 1000]$) where the momenta are almost constant, Region II

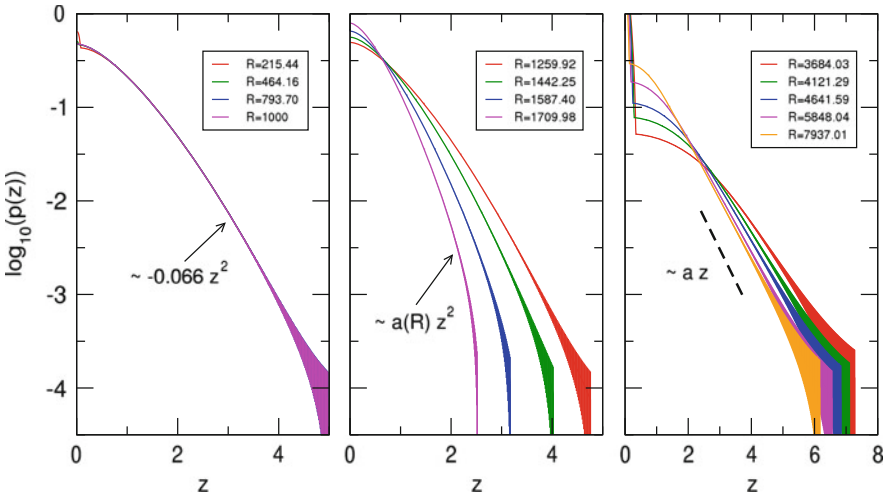

Fig. 4.4 $log_{10}p(z)$ distribution for different Reynold's numbers. *Central figure*: $a(1259.92) = -0.08$, $a(1442.25) = -0.12$, $a(1587.40) = -0.24$ and $a(1709.98) = -0.52$. *Right figure*: $a(3684.03) = -0.51$, $a(4121.29) = -0.55$, $a(4621.59) = -0.58$, $a(5848.04) = -0.61$ and $a(7937.01) = -0.64$

($R \in [1000, 4000]$) where the moments grow with R and Region III ($R \in [4000, \infty]$) where relative moments tend to some asymptotic value.

Experimental data can be found in [9] and are illustrated by the two plots in Fig. 4.6 taken from the cited work which give the function $\log_{10} p(z)$. I.e. the probability density for observing a normalized radial gradient z as a function of $z = \xi/\sqrt{\langle \xi^2 \rangle}$ in the case of homogeneous isotropic turbulence (HIT) (i.e. Navier-Stokes in a cube with periodic boundaries) or in the case of Raleigh-Benard convection (RBC) (NS+heat transport in a cylinder with hot bottom and cold top). The results of Fig. 4.6, for $z > 0$ should be compared with those of Fig. 4.4 at the corresponding Reynolds numbers. In both cases we see that the distribution for high Reynold numbers have linear-like behavior for large z-values. In fact for the HIT case and $R = 2243$ we can fit a line with slope -0.77 in the interval $z \in [3.3, 5.57]$. Also in the RBC case we can do a linear fit with slope -0.42 ($z \in 5.14, 9.69$]) for $R = 4648$. The value obtained is similar to the ones we computed on Fig. 4.4.

In Fig. 4.7, we can compare the measured *flatness* in our numerical experiment with the observed by Schumacher et al. [9]. We see that the values are similar for small and large Reynold's numbers but there is a peaked structure for intermediate values due to the relevant discontinuity when passing from $\bar{n}_i = 2$ to $\bar{n}_i = 3$ events.

All these results shows that the important aspect of the experiments is quite well captured with the only parameter κ available for the fits, i.e. a strong deviation from Gaussian behavior and the agreement of the location of the abscissae of the

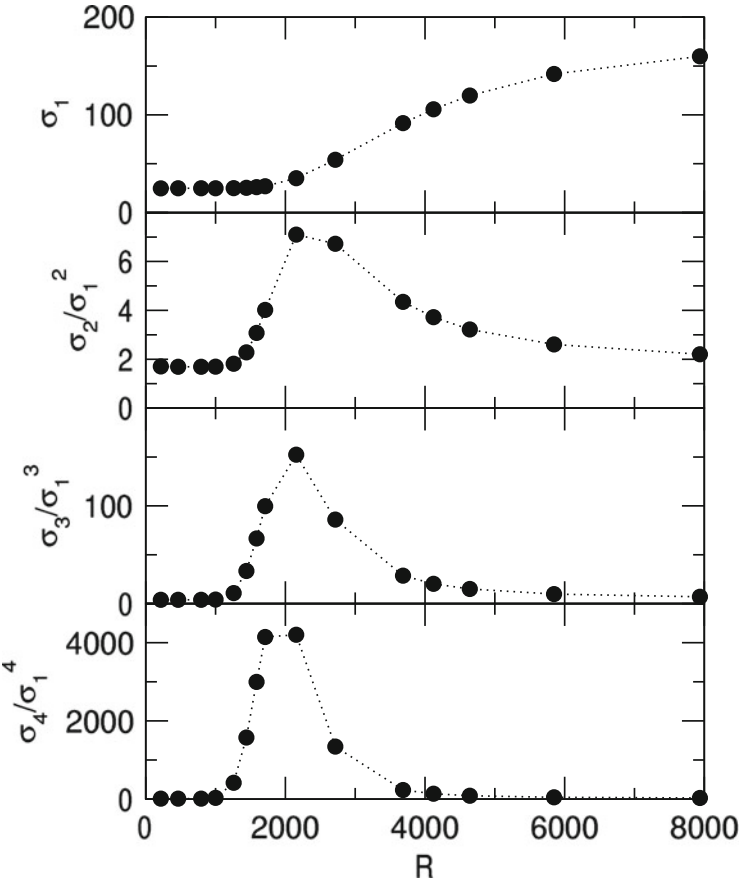

Fig. 4.5 Measured momenta of the distribution $P(\xi)$, σ_n, vs Reynold's number

minima of the tails in the second case at the maximal W_0; this feature fails in the first case (HIT) as the abscissa is about 30: is it due to a too small Reynolds number? This seems certainly a factor to take into account as the curve appears to become independent of R, hence universal as it should on the basis of the theory, for $R > 4000$.

In conclusion the results are compatible with the OK theory but show important deviations for large fluctuations because the Gumbel distribution does not show a Gaussian tail.

All this has a strong conceptual connotation: the basic idea (ie the proposed hierarchical and scaling distribution of the kinetic energy dissipation per unit time) is fundamental.

The need to assign a value to the scaling parameter κ is quite interesting: in the renormalization group studies the actual value of κ is usually not important

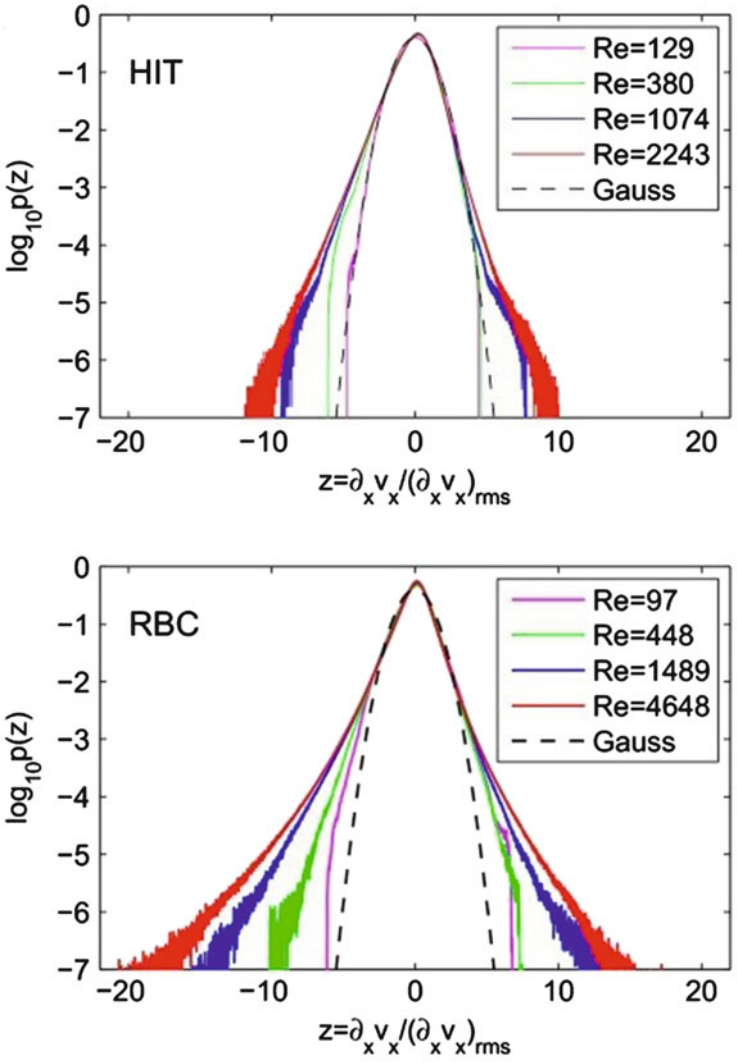

Fig. 4.6 Measured $p(z)$ by Schumacher et al. [9] for different Reynold's numbers

as long as it is $\kappa > 1$. Here the value of κ is shown to be relevant (basically it appears explicitly in the end results and its value ~ 20 must, in principle, be fixed by comparison with simulations on fluid turbulence).

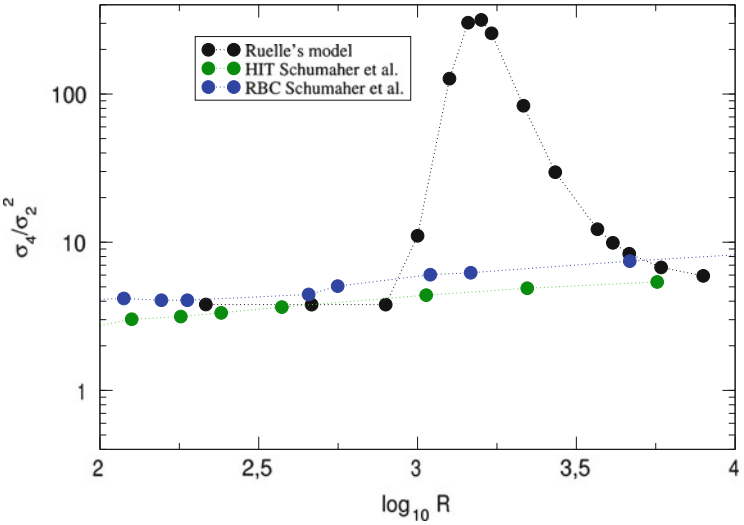

Fig. 4.7 Measured flatness (σ_4/σ_2^2) compared with the results by Schumacher et al. [9] for different Reynold's numbers

Acknowledgements The above comments are based on numerical calculations first done by P. Garrido and confirmed by G. Gallavotti. This is the text of our comments (requested by the organizers) to the talk by D. Ruelle at the CHAOS15 conference, Institut Henri Poincaré, Paris, May 26–29, 2015.

References

1. G. Benfatto, G. Gallavotti, *Renormalization Group* (Princeton University Press, Princeton, 1995)
2. P. Bleher, Y. Sinai, Investigation of the critical point in models of the type of Dyson's hierarchical model. Commun. Math. Phys. **33**, 23–42 (1973)
3. F. Dyson, Existence of a phase transition in a one-dimensional Ising ferromagnet. Commun. Math. Phys. **12**, 91–107 (1969)
4. G. Gallavotti, On the ultraviolet stability in statistical mechanics and field theory. Annali di Matematica **CXX**, 1–23 (1979)
5. G. Gallavotti, *Foundations of Fluid Dynamics*, 2nd edn. (Springer, Berlin, 2005)
6. L.D. Landau, E.M. Lifschitz, *Fluid Mechanics* (Pergamon, Oxford, 1987)
7. D. Ruelle, Hydrodynamic turbulence as a problem in nonequilibrium statistical mechanics. Proc. Natl. Acad. Sci. **109**, 20344–20346 (2012)
8. D. Ruelle, Non-equilibrium statistical mechanics of turbulence. J. Stat. Phys. **157**, 205–218 (2014)
9. J. Schumacher, J.D. Scheel, D. Krasnov, D.A. Donzis, V. Yakhot, K.R. Sreenivasan, Small-scale universality in fluid turbulence. Proc. Natl. Acad. Sci. **111**, 10961–10965 (2014)

10. K. Wilson, Model Hamiltonians for local quantum field theory. Phys. Rev. **140**, B445–B457 (1965)
11. K. Wilson, Model of coupling constant renormalization. Phys. Rev. D **2**, 1438–1472 (1970)
12. K. Wilson, The renormalization group. Rev. Mod. Phys. **47**, 773–840 (1975)

Chapter 5
The Kolmogorov Law of Turbulence What Can Rigorously Be Proved? Part II

Roger Lewandowski and Benoît Pinier

Abstract We recall what are the different known solutions for the incompressible Navier-Stokes Equations, in order to fix a suitable functional setting for the probabilistic frame that we use to derive turbulence models, in particular to define the mean velocity and pressure fields, the Reynolds stress and eddy viscosities. Homogeneity and isotropy are discussed within this framework and we give a mathematical proof of the famous $-5/3$ Kolmogorov law, which is discussed in a numerical simulation performed in a numerical box with a non trivial topography on the ground.

MCS Classification : 76D05, 76F65, 65M60

5.1 Introduction

We focus in this paper on the law of the $-5/3$, which attracted a lot of attention from the fluid mechanics community these last decades, since it is a basis for many turbulence models, such as Large Eddy Simulation models (see for instance in [20, 21, 44, 50]). Although it is usually known as the Kolmogorov law, it seems that it appears for the first time in a paper by Onsager [42] in 1949, and not in the serie of papers published by Kolmogorov in 1941 (see in [56]), where the author focuses on the $2/3$'s law, by introducing the essential scales related to homogeneous and isotropic turbulent flows (see formula (5.33) below). In this major contribution to the field, Kolmogorov opened the way for the derivation of laws based on similarity principles such as the $-5/3$'s law (see also in [11, 32]).

R. Lewandowski • B. Pinier (✉)
IRMAR, UMR 6625, Université Rennes 1, and Fluminance Team INRIA, Campus Beaulieu, 35042 Rennes cedex, France
e-mail: Roger.Lewandowski@univ-rennes1.fr; benoit.pinier@inria.fr
http://perso.univ-rennes1.fr/roger.lewandowski

C. Skiadas (ed.), *The Foundations of Chaos Revisited: From Poincaré to Recent Advancements*, Understanding Complex Systems,
DOI 10.1007/978-3-319-29701-9_5

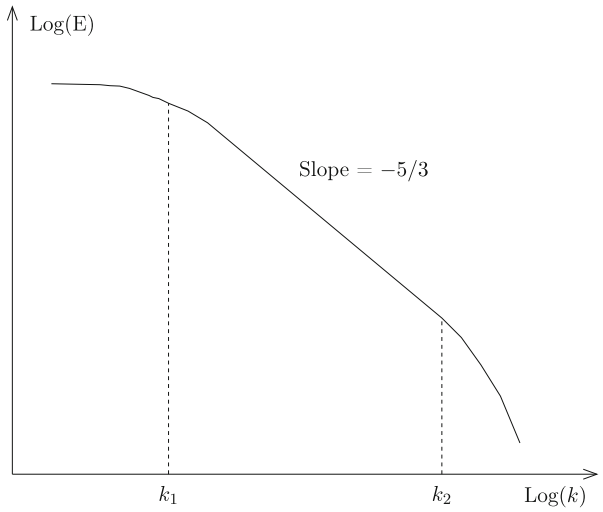

Fig. 5.1 Energy spectrum log-log curve

Roughly speaking, the $-5/3$'s law states that in some inertial range $[k_1, k_2]$, the energy density of the flow $E(k)$ behaves like $C^{te}k^{-5/3}$, where k denotes the current wave number [see Fig. 5.1 below and the specific law (5.40)].

This paper is divided in a theoretical part and a numerical part, in which we aim at:

1. carefully express what is the appropriate similarity assumption that must satisfy an homogeneous and isotropic turbulent flow in order to derive the $-5/3$'s law (Assumptions 5.4.1 and 5.4.2 below),
2. to theoretically derive the $-5/3$ law from the similarity assumption (see Theorem 5.4.2 below),
3. to discuss the numerical validity of such a law from a numerical simulation in a test case, using the software BENFLOW 1.0, developed at the Institute of Mathematical Research of Rennes.

Before processing items (1) and (2), we discuss on different results about the Navier-Stokes equations (5.1) (NSE in what follows), that are one of the main tools in fluid mechanics, as well as the Reynolds stress (5.13) derived by taking the expectation of the NSE, once the appropriate probabilistic frame is specified. We then define the density energy $E(k)$, which is the energy of the flow in the sphere $\{k = |\mathbf{k}|\}$ in the Fourier space. Furthermore, we introduce the concept of dimensional bases in order to properly set Assumptions 5.4.1 and 5.4.2.

The numerical simulation takes place in a computational box (see Fig. 5.2) with a non trivial topography (see Fig. 5.3), by using the mean NSE (5.12), the $k - \mathscr{E}$ model (5.20), and appropriate boundary conditions supposed to model the dynamics

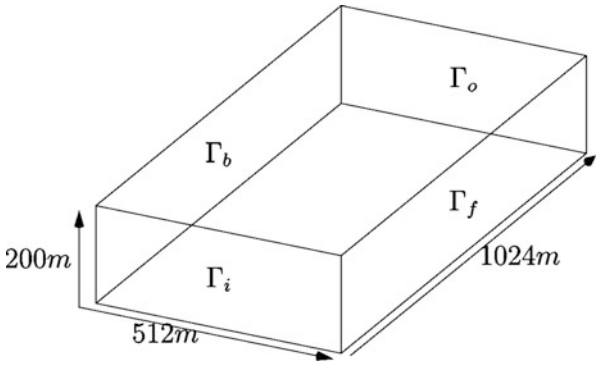

Fig. 5.2 Computational box

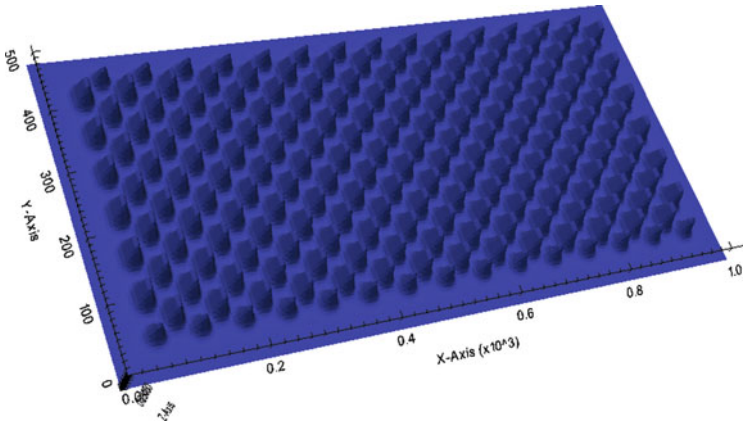

Fig. 5.3 View of the ground

of the atmospheric boundary layer. Atmospheric boundary layer modeling is a modern challenge because of its significance in climate change issues. We find in the literature many simulations carried out in different configurations, such as for example the case of a flat ground [1, 5, 13, 45], the case of stable or convective boundary layers [38, 59], urban simulations where building are modeled by parallelipipeds [39], wind farms [46], realistic configurations including mountains [37, 58]. Of course, this flows is not homogeneous nor isotropic. However, the simulations shows that the curve of $\log_{10}(E(k))$ exhibits an inertial range over 4 decades, in which the regression straight line has a slope equal to $-2.1424 \neq -5/3$ (see Fig. 5.6), suggesting that the $-5/3$'s law is not satisfied in this case.

5.2 About the 3D Navier Stokes Equations

5.2.1 Framework

Let $\Omega \subseteq \mathbb{R}^3$ be a C^1 bounded convex smooth domain, Γ its boundary, $T \in \mathbb{R}_+$ (eventually $T = +\infty$), and $Q = [0, T] \times \Omega$. The velocity of the flow is denoted by $\mathbf{v}$, its pressure by p. The incompressible Navier Stokes equation satisfied by $(\mathbf{v}, p)$ (NSE in the remainder) are as follows:

$$\begin{cases} \partial_t \mathbf{v} + (\mathbf{v} \cdot \nabla)\, \mathbf{v} - \nabla \cdot (2\nu D\mathbf{v}) + \nabla p = \mathbf{f} & \text{in } Q, \quad \text{(i)} \\ \nabla \cdot \mathbf{v} = 0 & \text{in } Q, \quad \text{(ii)} \\ \mathbf{v} = 0 & \text{on } \Gamma, \quad \text{(iii)} \\ \mathbf{v} = \mathbf{v}_0 & \text{at } t = 0, \quad \text{(iv)} \end{cases} \tag{5.1}$$

where $\mathbf{v}_0$ is any divergence free vector fields such that $\mathbf{v}_0 \cdot \mathbf{n}|_\Gamma = 0$, $\nu > 0$ denotes the kinematic viscosity, that we suppose constant for the simplicity, $\mathbf{f}$ is any external force (such as the gravity for example), $D\mathbf{v}$ denotes the deformation tensor, $\nabla\cdot$ the divergence operator and $(\mathbf{v} \cdot \nabla)\, \mathbf{v}$ is the nonlinear transport term, specifically

$$\begin{aligned} &D\mathbf{v} = \frac{1}{2}\left(\nabla \mathbf{v} + \nabla \mathbf{v}^t\right), \quad \nabla \mathbf{v} = (\partial_j v_i)_{1 \le ij \le 3}, \quad \mathbf{v} = (v_1, v_2, v_3), \quad \partial_i = \partial \partial x_i, \\ &\nabla \cdot \mathbf{v} = \partial_i v_i, \\ &[(\mathbf{v} \cdot \nabla)\, \mathbf{v}]_i = v_j \partial_j v_i, \end{aligned}$$

by using the Einstein summation convention. We recall that it is easily deduced from the incompressibility condition (see [11]):

$$\begin{aligned} &(\mathbf{v} \cdot \nabla)\, \mathbf{v} = \nabla \cdot (\mathbf{v} \otimes \mathbf{v}), \quad \mathbf{v} \otimes \mathbf{v} = (v_i v_j)_{1 \le i,j \le 3}, \\ &\nabla \cdot (2\nu D\mathbf{v}) = \nu \Delta \mathbf{v}. \end{aligned}$$

In the following, we will consider the functional spaces

$$\mathbf{W} = \{\mathbf{v} \in H_0^1(\Omega)^3, \nabla \cdot \mathbf{v} = 0\} \hookrightarrow \mathbf{V} = \{\mathbf{v} \in L^2(\Omega)^3,\ \mathbf{v} \cdot \mathbf{n}|_\Gamma = 0, \nabla \cdot \mathbf{v} = 0\}, \tag{5.2}$$

Throughout the paper, we assume $\mathbf{v}_0 \in \mathbf{V}$.

5.2.2 Strong Solutions to the NSE

Let P be the orthogonal projection $L^2(\Omega)^3 \hookrightarrow \mathbf{V}$, A and F the operators

$$A\mathbf{v} = -\nu P \Delta \mathbf{v}, \quad F\mathbf{v} = P((\mathbf{v} \cdot \nabla)\, \mathbf{v}).$$

By applying P to (5.1.i) in noting that $P(\nabla p) = 0$, we are led to the following initial value problem

$$\begin{cases} \dfrac{d\mathbf{v}}{dt} = -A\mathbf{v} + F\mathbf{v} + P\mathbf{f}(t), & \text{(i)} \\ \mathbf{v}(0) = \mathbf{v}_0, & \text{(ii)} \end{cases} \tag{5.3}$$

where $t \to \mathbf{v}(t)$ and $t \to \mathbf{f}(t)$ are considered as functions valued in $\mathbf{W}$ and $\mathbf{V}$ respectively.

Definition 5.2.1 We say that $\mathbf{v} = \mathbf{v}(t)$ is a strong solution to the NSE in a time interval $[0, T^\star]$ if $d\mathbf{v}/dt$ and $A\mathbf{v}$ exist and are continuous in $[0, T^\star]$ and (5.3.i) is satisfied there.

Remark 5.2.1 In Definition 5.2.1, the pressure is not involved. It can be reconstructed by the following equation

$$\Delta p = -\nabla \cdot ((\mathbf{v} \cdot \nabla)\, \mathbf{v}) + \nabla \cdot \mathbf{f}, \tag{5.4}$$

derived from Eq. (5.1.i) by taking its divergence.

The existence of a strong solution is proved in Fujita-Kato [18]. It is subject to regularity conditions regarding the initial data $\mathbf{v}_0$ and the source $\mathbf{f}$. The result is stated as follows.

Theorem 5.2.1 *We assume*

(i) $\mathbf{v}_0 \in \mathbf{V} \cap H^{1/2}(\Omega)^3$,
(ii) $\mathbf{f}$ *is Hölder continuous in* $[0, T]$.

Then there exists $T^\star = T^\star(\nu, ||\mathbf{v}_0||_{1/2,2,\Omega}, ||\mathbf{f}||_{C^{0,\alpha}(\Omega)})$ *such that the NSE admits a unique strong solution* $\mathbf{v} = \mathbf{v}(t)$. *Moreover, if* $\mathbf{f} = \mathbf{f}(t, \mathbf{x})$ *is Hölder continuous in* $Q = [0, T^\star] \times \Omega$, *then* $\mathbf{v}(t, \mathbf{x})$, $\nabla \mathbf{v}(t, \mathbf{x})$, $\Delta \mathbf{v}(t, \mathbf{x})$ *and* $\partial \mathbf{v}(t, \mathbf{x})/\partial t$ *are Hölder continuous in* $]0, T^\star[\times \Omega$.

Remark 5.2.2 The strong solution is solution of the equation

$$\mathbf{v}(t) = e^{-tA}\mathbf{v}_0 - \int_0^t e^{-(t-s)A} F(\mathbf{v}(s))ds + \int_0^t e^{-(t-s)A} P\mathbf{f}(s)ds, \tag{5.5}$$

which is approached by the sequence $(\mathbf{v}_n)_{n \in \mathbb{N}}$ expressed by

$$\mathbf{v}_n(t) = e^{-tA}\mathbf{v}_0 - \int_0^t e^{-(t-s)A} F(\mathbf{v}_{n-1}(s))ds + \int_0^t e^{-(t-s)A} P\mathbf{f}(s)ds, \tag{5.6}$$

The reader is referred to [9, 12, 28] for more details concerning the question of strong solutions.

5.2.3 Turbulent Solutions

Definition 5.2.2 We say that $\mathbf{v}$ is a turbulent solution of NSE (5.1) in $[0,T]$ if

(i) $\mathbf{v} \in L^2([0,T],\mathbf{W}) \cap L^\infty([0,T],L^2(\Omega))$,

(ii) $\partial_t \mathbf{v} \in L^{4/3}([0,T],\mathbf{W}') = [L^4([0,T],\mathbf{W})]'$ (by writing $\partial_t = \dfrac{\partial}{\partial t}$ for the simplicity),

(iii) $\lim\limits_{t\to 0} ||\mathbf{v}(\cdot,t) - \mathbf{v}_0(\cdot)||_{0,2,\Omega} = 0$,

(iv) $\forall\, \mathbf{w} \in L^4([0,T],\mathbf{W})$,

$$\int_0^T < \partial_t \mathbf{v}, \mathbf{w} > dt + \int_0^T \int_\Omega (\mathbf{v}\otimes\mathbf{v}) : \nabla \mathbf{w}\, d\mathbf{x}dt + \int_0^T \int_\Omega \nabla \mathbf{v} : \nabla \mathbf{w}\, d\mathbf{x}dt$$
$$= \int_0^T < \mathbf{f}, \mathbf{w} > dt,$$

where for $\mathbf{u} \in \mathbf{W}$, $\mathbf{F} \in \mathbf{W}'$, $< \mathbf{F}, \mathbf{u} >$ denotes the duality pairing between $\mathbf{F}$ and $\mathbf{u}$,

(v) $\mathbf{v}$ satisfies the energy inequality at each $t > 0$,

$$\frac{1}{2}\int_\Omega |\mathbf{v}(t,\mathbf{x})|^2 d\mathbf{x} + \nu \int_0^t \int_\Omega |\nabla \mathbf{v}(t',\mathbf{x})|^2 d\mathbf{x}dt' \le \int_0^t < \mathbf{f}, \mathbf{v} > dt'.$$

Remark 5.2.3 Once again, the pressure is not involved in this formulation. It this frame, it is recovered by the De Rham Theorem (see for instance in [55]).

The existence of a turbulent solution was first proved by Leray [29] in the whole space, then by Hopf [22] in the case of a bounded domain with the no slip boundary condition, which is the case under consideration here. This existence result can be stated as follows.

Theorem 5.2.2 *Assume that* $\mathbf{v}_0 \in \mathbf{V}$, $\mathbf{f} \in L^{4/3}([0,T],\mathbf{W}')$. *Then the NSE (5.1) has a turbulent solution.*

Remark 5.2.4 The turbulent solution is global in time, which means that it may be extended to $t \in [0,\infty[$ depending on a suitable assumption on $\mathbf{f}$. However it is not known whether it is unique or not. Moreover, it is not known if the energy inequality is an equality.

The reader is also referred to [14, 16, 36, 55] for further results on turbulent (also weak) solutions of the NSE.

5.3 Mean Navier-Stokes Equations

5.3.1 Reynolds Decomposition

Based on strong or turbulent solutions, it is known that it is possible to set a probabilistic framework in which we can decompose the velocity $\mathbf{v}$ and the pressure as a the sum of the statistical mean and a fluctuation, namely

$$\mathbf{v} = \overline{\mathbf{v}} + \mathbf{v}', \quad p = \overline{p} + p'. \tag{5.7}$$

More generally, any tensor field ψ related to the flow can be decomposed as

$$\psi = \overline{\psi} + \psi'. \tag{5.8}$$

The statistical filter is linear and subject to satisfy the Reynolds rules:

$$\overline{\partial_t \psi} = \partial_t \overline{\psi}, \tag{5.9}$$

$$\overline{\nabla \psi} = \nabla \overline{\psi}, \tag{5.10}$$

as well as

$$\overline{\overline{\psi}} = \overline{\psi} \text{ leading to } \overline{\psi'} = 0. \tag{5.11}$$

We have studied in [11] different examples of such filters. Historically, such a decomposition was first considered in works by Stokes [53], Boussinesq [6], Reynolds [49], Prandtl [47], in the case of the « long time average »(see also in [31]). Later on, Taylor [54], Kolmogorov [25] and Onsager [42] have considered such decompositions when the fields related to the flow are considered as random variables, which was one of the starting point for the development of modern probability theory.

5.3.2 Reynolds Stress and Closure Equations

We take the mean of the NSE (5.1) by using (5.9)–(5.11). We find out the following system:

$$\begin{cases} \partial_t \overline{\mathbf{v}} + (\overline{\mathbf{v}} \cdot \nabla)\, \overline{\mathbf{v}} - \nu \Delta \overline{\mathbf{v}} + \nabla \overline{p} = -\nabla \cdot \boldsymbol{\sigma}^{(\mathrm{r})} + \mathbf{f} & \text{in } Q, \\ \nabla \cdot \overline{\mathbf{v}} = 0 & \text{in } Q, \\ \overline{\mathbf{v}} = 0 & \text{on } \Gamma, \\ \overline{\mathbf{v}} = \overline{\mathbf{v}_0} & \text{at } t = 0, \end{cases} \tag{5.12}$$

where

$$\boldsymbol{\sigma}^{(\mathrm{R})} = \overline{\mathbf{v}' \otimes \mathbf{v}'} \tag{5.13}$$

is the Reynolds stress. The big deal in turbulence modeling is to express $\boldsymbol{\sigma}^{(\mathrm{R})}$ in terms of averaged quantities. The most popular model is derived from the Boussinesq assumption which consists in writing:

$$\boldsymbol{\sigma}^{(\mathrm{R})} = -\nu_t D\overline{\mathbf{v}} + \frac{2}{3}k\,\mathrm{Id}, \tag{5.14}$$

where

1. $k = \dfrac{1}{2}\mathrm{tr}\,\boldsymbol{\sigma}^{(\mathrm{R})} = \dfrac{1}{2}\overline{|\mathbf{v}'|^2}$ is the turbulent kinetic energy (TKE),
2. ν_t is an eddy viscosity.

In order to close the system, the eddy viscosity remains to be modeled. To do so, many options are available (see in [4, 10, 11, 24, 26, 30, 40, 50]).

One of the most popular model is the Smagorinsky's model (see for instance in [20, 21, 24, 34, 44, 48, 50–52]), in which

$$\nu_t = C_s\delta^2|D\mathbf{v}|, \tag{5.15}$$

where $C_s \approx 0.1$ or 0.2 is an universal dimensionless constant, and δ a characteristic scale, ideally the size of the smallest eddies in the flow the model is supposed to catch. This model is the foundation of the wide class of Large Eddy Simulation models. The reader will find various mathematical results concerning the Smagorinsky's model in [3, 11, 24, 35, 43].

We next mention the so-called TKE model, given by

$$\nu_t = C_k\ell\sqrt{k}, \tag{5.16}$$

which gives accurate results for the simulation of realistic flows (see for instance [33]). In model (5.16), ℓ denotes the Prandtl mixing length, C_k is a dimensionless constant that must be fixed according to experimental data. In practice, ℓ is taken to be equal to the local mesh size in a numerical simulation, and k is computed by using the closure equation (see in [11, 40])

$$\partial_t k + \overline{\mathbf{v}}\cdot\nabla k - \nabla\cdot(\nu_t\nabla k) = \nu_t|D\overline{\mathbf{v}}|^2 - \frac{k\sqrt{k}}{\ell}. \tag{5.17}$$

The reader will find a bunch of mathematical result concerning the coupling of the TKE equation to the mean NSE in [7, 8, 11, 19, 27, 30].

Finally, we mention the famous $k-\mathscr{E}$ model that is used for the numerical simulations carried out in Sect. 5.5. In this model, $\mathscr{E}$ denotes the turbulent dissipation

$$\mathscr{E} = 2\nu\overline{|D\mathbf{v}'|^2}, \tag{5.18}$$

and dimensional analysis leads to write

$$\nu_t = C_\mu \frac{k^2}{\mathscr{E}}. \tag{5.19}$$

The coupled system used to compute k and $\mathscr{E}$ is the following (see [11, 40] for the derivation of these equations):

$$\begin{cases} \partial_t k + \overline{\mathbf{v}} \cdot \nabla k - \nabla \cdot (\nu_t \nabla k) = \nu_t |D\overline{\mathbf{v}}|^2 - \mathscr{E}. \\ \partial_t \mathscr{E} + \overline{\mathbf{v}} \cdot \nabla \mathscr{E} - \nabla \cdot (\nu_t \nabla \mathscr{E}) = c_\eta k |D\overline{\mathbf{v}}|^2 - c_{\mathscr{E}} \dfrac{\mathscr{E}^2}{k}, \end{cases} \tag{5.20}$$

where $C_\nu = 0.09$, $c_{\mathscr{E}} = 1.92$ and $c_\eta = 1.44$ are dimensionless constants.

5.4 Law of the −5/3

The idea behind the law of the $-5/3$ for homogeneous and isotropic turbulence is that in the « inertial range », the energy density $E = E(k)$ at a given point $(t, \mathbf{x})$ is driven by the dissipation $\mathscr{E}$. In this section, we properly define the energy density E for homogeneous and isotropic turbulent flows. We then set the frame of the dimensional bases and the similarity principle in order to rigorously derive the law of the $-5/3$.

Remark 5.4.1 For homogeneous and isotropic turbulence, one can show the identity $\mathscr{E} = 2\nu \overline{|D\mathbf{v}'|^2} = 2\nu |\overline{D\mathbf{v}}|^2$ (see in [11]).

5.4.1 Energy Density of the Flow

Roughly speaking, homogeneity and isotropy means that the correlations in the flows are invariant under translations and isometries (see in [2, 11, 32]), which we assume throughout this section, as well as the stationarity of the mean flow for simplicity. Let

$$\mathbb{E} = \frac{1}{2} \overline{|\mathbf{v}|^2}, \tag{5.21}$$

be the total mean kinetic energy at a given point $\mathbf{x} \in \Omega$, which we not specify in what follows.

Theorem 5.4.1 *There exists a measurable function $E = E(k)$, defined over $\mathbb{R}_+$, the integral of which over $\mathbb{R}_+$ is finite, and such that*

$$\mathbb{E} = \int_0^\infty E(k)dk. \tag{5.22}$$

Proof Let $\mathbb{B}_2$ be the two order correlation tensor expressed by:

$$\mathbb{B}_2 = \mathbb{B}_2(\mathbf{r}) = (\overline{v_i(\mathbf{x})v_j(\mathbf{x}+\mathbf{r})})_{1\le i,j\le 3} = (B_{ij}(\mathbf{r}))_{1\le i,j\le 3}, \tag{5.23}$$

which only depend on $\mathbf{r}$ by the homogeneity assumption, nor on t because of the stationarity assumption. It is worth noting that

$$\mathbb{E} = \frac{1}{2}\mathrm{tr}\mathbb{B}_2(0). \tag{5.24}$$

Let $\widehat{\mathbb{B}}_2$ denotes the Fourier transform of $\mathbb{B}$ expressed by

$$\forall\, \mathbf{k} \in \mathbb{R}^3, \quad \widehat{\mathbb{B}}_2(\mathbf{k}) = \frac{1}{(2\pi)^3}\int_{\mathbb{R}^3} \mathbb{B}_2(\mathbf{r})e^{-i\mathbf{k}\cdot\mathbf{r}}d\mathbf{r}, \tag{5.25}$$

We deduce from the Plancherel formula,

$$\forall\, \mathbf{r} \in \mathbb{R}^3, \quad \mathbb{B}_2(\mathbf{r}) = \frac{1}{(2\pi)^3}\int_{\mathbb{R}^3} \widehat{\mathbb{B}}_2(\mathbf{k})e^{i\mathbf{k}\cdot\mathbf{r}}d\mathbf{k}, \tag{5.26}$$

which makes sense for both types of solutions to the NSE, strong or turbulent (see the Sect. 5.2). It is easily checked that the isotrpoy of $\mathbb{B}_2$ in $\mathbf{r}$ yields the isotropy of $\widehat{\mathbb{B}}_2$ in $\mathbf{k}$. Therefore, according to Theorem 5.1 in [11] we deduce the existence of two real valued functions $\widetilde{B}_d$ and $\widetilde{B}_n$ of class C^1 such that[1]

$$\forall\, \mathbf{k} \in \mathbb{R}^3, \quad |\mathbf{k}| = k, \quad \widehat{\mathbb{B}}_2(\mathbf{k}) = (\widetilde{B}_d(k) - \widetilde{B}_n(k))\frac{\mathbf{k}\otimes\mathbf{k}}{k^2} + \widetilde{B}_n(k)\mathrm{I}_3. \tag{5.27}$$

Using formula (5.27) yields

$$\widehat{B}_{ii}(\mathbf{k}) = \widetilde{B}_d(k) + 2\widetilde{B}_n(k), \tag{5.28}$$

which combined with Fubini's Theorem, (5.24) and (5.26), leads to

$$\int_{\mathbb{R}^3} \widehat{B}_{ii}(\mathbf{k})\, d\mathbf{k} = \int_0^\infty \left(\int_{|\mathbf{k}|=k} \widehat{B}_{ii}(\mathbf{k})d\boldsymbol{\sigma}\right) dk = \int_0^\infty 4\pi k^2(\widetilde{B}_d(k) + 2\widetilde{B}_n(k))\, dk, \tag{5.29}$$

[1] k already denotes the TKE, and from now also the wavenumber, $k = |\mathbf{k}|$. This is commonly used in turbulence modeling, although it might sometimes be confusing.

by noting $d\boldsymbol{\sigma}$ the standard measure over the sphere $\{|\mathbf{k}| = k\}$. This proves the result, where $E(k)$ is given by

$$E(k) = \left(\frac{k}{2\pi}\right)^2 (\widetilde{B}_d(k) + 2\widetilde{B}_n(k)). \tag{5.30}$$

□

Remark 5.4.2 From the physical point of view, $E(k)$ is the amount of kinetic energy in the sphere $S_k = \{|\mathbf{k}| = k\}$. As such, it is expected that $E \geq 0$ in $\mathbb{R}$, and we deduce from (5.22) that $E \in L^1(\mathbb{R}_+)$. Unfortunately, we are not able to prove that $E \geq 0$ from formula (5.30), which remains an open problem.

5.4.2 *Dimensional Bases*

Only length and time are involved in this frame, since we do not consider heat transfers and the fluid is incompressible. Therefore, any field ψ related to the flow has a dimension $[\psi]$ encoded as:

$$[\psi] = (\text{length})^{d_\ell(\psi)}(\text{time})^{d_\tau(\psi)}, \tag{5.31}$$

which we express through the couple

$$\mathbb{D}(\psi) = (d_\ell(\psi), d_\tau(\psi)) \in \mathbb{Q}^2. \tag{5.32}$$

Definition 5.4.1 A length-time basis is a couple $b = (\lambda, \tau)$, where λ is a given constant length and τ a constant time.

Definition 5.4.2 Let $\psi = \psi(t, \mathbf{x})$ (constant, scalar, vector, tensor…) be defined on $Q = [0, T] \times \Omega$. Let ψ_b be the dimensionless field defined by:

$$\psi_b(t', \mathbf{x}') = \lambda^{-d_\ell(\psi)} \tau^{-d_\tau(\psi)} \psi(\tau t', \lambda \mathbf{x}'),$$

where

$$(t', \mathbf{x}') \in Q_b = \left[0, \frac{T}{\tau}\right] \times \frac{1}{\lambda}\Omega,$$

is dimensionless. We say that $\psi_b = \psi_b(t', \mathbf{x}')$ is the b-dimensionless field deduced from ψ.

5.4.3 Kolmogorov Scales

Let us consider the length-time basis $b_0 = (\lambda_0, \tau_0)$, given by

$$\lambda_0 = \nu^{\frac{3}{4}} \mathscr{E}^{-\frac{1}{4}}, \quad \tau_0 = \nu^{\frac{1}{2}} \mathscr{E}^{-\frac{1}{2}}, \tag{5.33}$$

where $\mathscr{E}$ is the dissipation defined by (5.18) (see also Remark 5.4.1). The scale λ_0 is known as the Kolmogorov scale. The important point here is that

$$\mathscr{E}_{b_0} = \nu_{b_0} = 1. \tag{5.34}$$

Moreover, for all wave number k, and because

$$\mathbb{D}(E) = (3, -2), \tag{5.35}$$

we get

$$E(k) = \lambda_0^3 \tau_0^{-2} E_{b_0}(\lambda_0 k) = \nu^{\frac{5}{4}} \mathscr{E}^{\frac{1}{4}} E_{b_0}(\lambda_0 k), \tag{5.36}$$

by using (5.33). We must determine the universal profile E_{b_0}.

5.4.4 Proof of the −5/3's Law

The law of the $-5/3$ is based on two assumptions about the flow:

1. the separation of the scales (Assumption 5.4.1 below),
2. the similarity assumption (Assumption 5.4.2 below).

Assumption 5.4.1 *Let ℓ be the Prandtl mixing length. Then*

$$\lambda_0 << \ell. \tag{5.37}$$

Assumption 5.4.2 *There exists an interval*

$$[k_1, k_2] \subset \left[\frac{2\pi}{\ell}, \frac{2\pi}{\lambda_0}\right] \ \textit{s.t.}\ \ k_1 << k_2 \ \textit{and on}\ \ [\lambda_0 k_1, \lambda_0 k_2],$$
$$\forall\, b_1 = (\lambda_1, \tau_1),\ b_2 = (\lambda_2, \tau_2)\ \ \textit{s.t.}\ \ \mathscr{E}_{b_1} = \mathscr{E}_{b_2},\ \ \textit{then}\ \ E_{b_1} = E_{b_2}. \tag{5.38}$$

Theorem 5.4.2 *Scale separation and similarity Assumptions 5.4.1 and 5.4.2 yield the existence of a constant C such that*

$$\forall\, k' \in [\lambda_0 k_1, \lambda_0 k_2] = J_r, \quad E_{b_0}(k') = C(k')^{-\frac{5}{3}}. \tag{5.39}$$

Corollary 5.4.1 *The energy spectrum satisfies the* $-5/3$ *law*

$$\forall\, k \in [k_1, k_2], \quad E(k) = C\mathscr{E}^{\frac{2}{3}} k^{-\frac{5}{3}}, \tag{5.40}$$

where C is a dimensionless constant.

Proof Let

$$b^{(\alpha)} = (\alpha^3 \lambda_0, \alpha^2 \tau_0).$$

As

$$\mathscr{E}_{b^{(\alpha)}} = 1 = \mathscr{E}_{b_0},$$

the similarity assumption yields

$$\forall\, k' \in J_r, \quad \forall \alpha > 0, \quad E_{b^{(\alpha)}}(k') = E_{b_0}(k'),$$

which leads to the functional equation,

$$\forall\, k' \in J_r, \quad \forall\, \alpha > 0, \quad \frac{1}{\alpha^5} E_{b_0}(k') = E_{b_0}(\alpha^3 k'),$$

whose unique solution is given by

$$\forall\, k' \in J_r, \quad E_{b_0}(k') = C(k')^{-\frac{5}{3}}, \quad C = \left(\frac{k_1}{\lambda_0}\right)^{\frac{5}{3}} E_0\left(\frac{k_1}{\lambda_0}\right),$$

hence the result. Corollary 5.4.1 is a direct consequence of (5.36) combined with (5.39).

Remark 5.4.3 It can be shown that the law of $-5/3$ yields the Smagorinsky's model (5.15) (see in [11]).

5.5 Numerical Experiments

5.5.1 Simulation Setting

The computational domain Ω is a box, the size $L_x \times L_y \times L_z$ of which is equal to (1024 m, 512 m, 200 m) (see Fig. 5.3). The number of nodes is $(256, 128, 64)$. The bottom of the box, plotted in Fig. 5.3, has a non trivial topography modeled by gaussian smooth domes, the height of which being equal to 50 m. We perform the simulation with $\nu = 2 \times 10^{-5}\,\mathrm{m^2\,s^{-1}}$, which yields a Reynolds number equal

to 9.10^7. We use the mean NSE with the Boussinesq assumption, coupled to the $k - \mathscr{E}$ model, namely the PDE system (5.12)–(5.14)–(5.19)–(5.20). We specify in what follows the boundary conditions, by considering the following decomposition of $\Gamma = \partial\Omega$:

$$\Gamma = \Gamma_t \cup \Gamma_f \cup \Gamma_b \cup \Gamma_g \cup \Gamma_i \cup \Gamma_o,$$

where

- Γ_t is the top of the box,
- Γ_f is the front face,
- Γ_b is the back face,
- Γ_g is the bottom of the box (the ground),
- Γ_i is the inlet,
- Γ_o is the outlet.

The condition on Γ_i is prescribed by the Monin Obukhov similitude law [41]:

$$\mathbf{v}(x, y, z, t)|_{\Gamma_i} = \left(\frac{u_\star}{\kappa} \ln\left(\frac{z + z_0}{z_0}\right), 0, 0\right)^t, \tag{5.41}$$

where $\kappa = 0.4$ is the Von Karman constant, z denotes the distance from the ground level, the aerodynamic roughness length z_0 is equal to 0.1 m, the friction velocity is expressed by:

$$u_\star = \kappa U_{ref} \left[\ln\left(\frac{H_{ref} + z_0}{z_0}\right)\right]^{-1}, \tag{5.42}$$

by taking $U_{ref} = 36\,\mathrm{ms}^{-1}$ and $H_{ref} = 200\,\mathrm{m}$. The turbulent kinetic energy and turbulent dissipation are setted by

$$\begin{cases} k|_{\Gamma_i} = u_\star^{1/2} C_\nu^{-1/2}, \\ \mathscr{E}|_{\Gamma_i} = \dfrac{u_\star^3}{\kappa(z + z_0)}. \end{cases} \tag{5.43}$$

On Γ_b, velocity, TKE and turbulent dissipation are subject to verify the no slip and homogeneous boundary conditions,

$$\begin{cases} \mathbf{v}|_{\Gamma_g} = (0, 0, 0)^t, \\ k|_{\Gamma_g} = 0, \\ \mathscr{E}|_{\Gamma_g} = 0. \end{cases} \tag{5.44}$$

On the top and lateral boundaries, we put

$$\begin{cases} \mathbf{v}\cdot\mathbf{n} &= 0 \quad on \quad \Gamma_t \cup \Gamma_b \cup \Gamma_f, \\ \nabla k\cdot\mathbf{n} &= 0 \quad on \quad \Gamma_t \cup \Gamma_b \cup \Gamma_f, \\ \nabla \mathscr{E}\cdot\mathbf{n} &= 0 \quad on \quad \Gamma_t \cup \Gamma_b \cup \Gamma_f. \end{cases} \tag{5.45}$$

Finally a null gradient condition is prescribed at the outlet Γ_o

$$\begin{cases} \nabla(\mathbf{v}\cdot\mathbf{n}) &= 0 \quad on \quad \Gamma_o, \\ \nabla k\cdot\mathbf{n} &= 0 \quad on \quad \Gamma_o, \\ \nabla \mathscr{E}\cdot\mathbf{n} &= 0 \quad on \quad \Gamma_o. \end{cases} \tag{5.46}$$

Remark 5.5.1 The PDE system (5.12)–(5.14)–(5.19)–(5.20) with the boundary conditions (5.41)–(5.43)–(5.44)–(5.45)–(5.46) yields a very hard mathematical problem. The existence and the uniqueness of a solution is a difficult issue, whether for global weak solutions or local time strong solutions.

5.5.2 Results

The numerical scheme we use for the simulation is based on the standard finite volume method (FVM) in space, and an Implicit Euler for the time discretization. For the simplicity, we will not write here this technical part of the work. The reader will find comprehensive presentations of the FVM in [15, 17, 23, 57].

The simulation reaches a statistical equilibrium in about 180 physical seconds, which is the time at which the results are displayed. In Figs. 5.4 and 5.5, are plotted the values of the streamwise and spanwise components of the velocity at $z = 50\,\mathrm{m}$, which corresponds to the dome height.

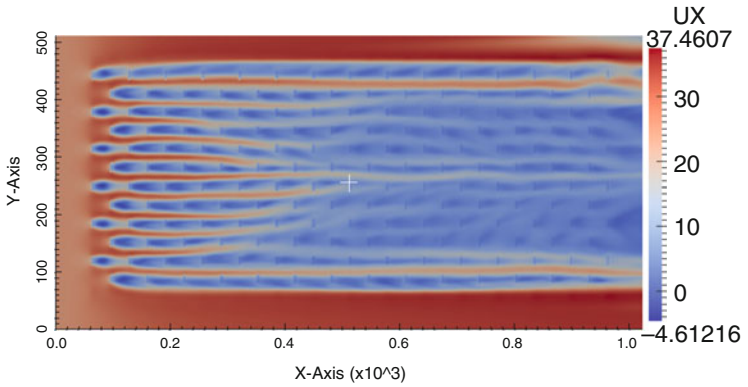

Fig. 5.4 Streamwise direction of the flow at the $z = 50\,\mathrm{m}$ cutplane

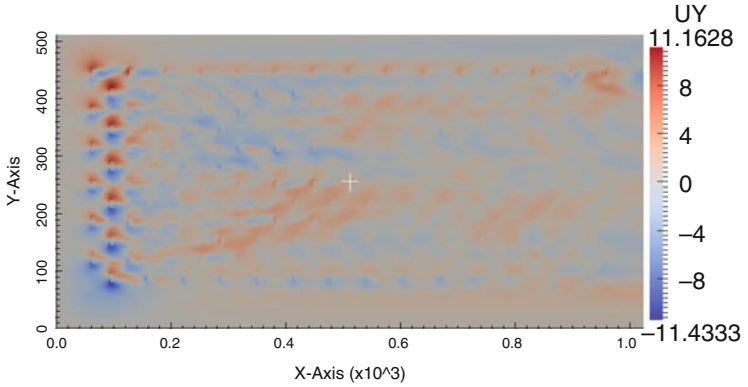

Fig. 5.5 Spanwise direction at the $z = 50$ m cutplane

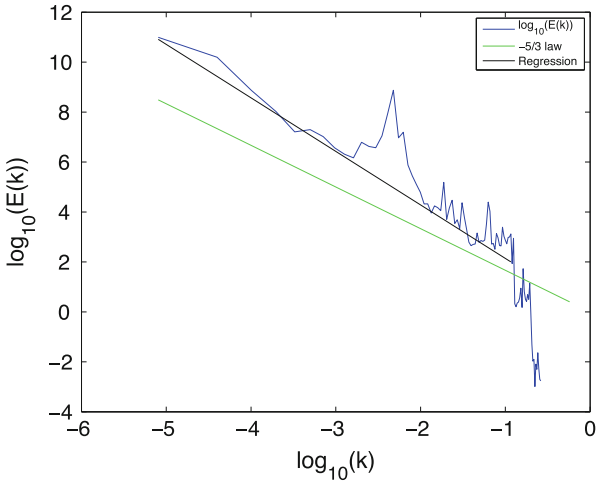

Fig. 5.6 Energy spectrum at the point $(x, y, z) = (500, 200, 50)$

In Fig. 5.6, we have plotted the energy spectrum of the flow at $(x, y, z) = (500, 200, 50)$ using a log-log scale, together with a straight line whose slope is equal to $-5/3 = -1,666\ldots$ and the regression straight line of $\log_{10}(E(k))$, whose slope is about equal to -2.1424. The results call for the following comments.

1. The simulation reveals a certain reliability of the code, which suggests the convergence of the numerical method. However, the mathematical convergence of the scheme remains an open question, closely related to the question of the existence of solutions mentioned in Remark 5.5.1.
2. The curve $\log_{10}(E(k))$ is an irregular curve which substantially differs from a straight line, so that we cannot conclude that numerically $E(k)$ behaves like $C^{te}k^{\alpha}$ in some interval $[k_1, k_2]$. Moreover, there is a gap between the slope of

the regression straight line of the curve and $-5/3$. However, something that looks like an inertial range can be identified between $k = 10^{-5}\,\mathrm{m}^{-1}$ and $k = 10^{-1}\,\mathrm{m}^{-1}$. This departure from the $-5/3$ law asks for the following comments and questions.

- The case under consideration yields a turbulence which is not homogeneous nor isotropic, which may explain the slope equal to -2.1424 we found.
- This simulation does not validate the Kolmogorov law or any law like $E(k) \approx C^{te}k^{\alpha}$. We cannot infer that such a law holds or not. Many parameters may generate the oscillations we observe in the curve $\log_{10}(E(k))$, such as any eventual numerical dissipation, a wrong choice of the constants in the $k - \mathscr{E}$ model which also may be not accurate, the boundary conditions we used and which may be questionable.

References

1. D. Apsley, I. Castro, A limited-length-scale k-epsilon model for the neutral and stably-stratified atmospheric boundary layer. Bound.-Layer Meteorol. **83**(1), 75–98 (1997)
2. G.K. Batchelor, *The Theory of Homogeneous Turbulence*. Cambridge Monographs on Mechanics and Applied Mathematics (Cambridge University Press, New York, 1959)
3. H. Beirão da Veiga, On the Ladyzhenskaya-Smagorinsky turbulence model of the Navier-Stokes equations in smooth domains. The regularity problem. J. Eur. Math. Soc. **11**(1), 127–167 (2009)
4. L.C. Berselli, T. Iliescu, W.J. Layton, *Mathematics of Large Eddy Simulation of Turbulent Flows*. Scientific Computation (Springer, Berlin, 2006)
5. E. Bou-Zeid, Large-eddy simulation of neutral atmospheric boundary layer flow over heterogeneous surfaces: blending height and effective surface roughness. Water Resour. Res. **40**(2), 1–18 (2004)
6. J. Boussinesq, Essai sur la théorie des eaux courantes. Mémoires présentés par divers savants à l'Académie des Sciences **23**(1), 1–660 (1877)
7. F. Brossier, R. Lewandowski, Impact of the variations of the mixing length in a first order turbulent closure system. Math. Model. Numer. Anal. **36**(2), 345–372 (2002)
8. M. Bulíček, R. Lewandowski, J. Málek, On evolutionary Navier-Stokes-Fourier type systems in three spatial dimensions. Comment. Math. Univ. Carolin. **52**(1), 89–114 (2011)
9. M. Cannone, Harmonic analysis tools for solving the incompressible Navier-Stokes equations, in *Handbook of Mathematical Fluid Dynamics*, vol. III (North-Holland, Amsterdam, 2004), pp. 161–244
10. T. Chacón-Rebollo, R. Lewandowski, A variational finite element model for large-eddy simulations of turbulent flows. Chin. Ann. Math. Ser. B **34**(5), 667–682 (2013)
11. T. Chacón Rebollo, R. Lewandowski, *Mathematical and Numerical Foundations of Turbulence Models and Applications*. Modeling and Simulation in Science, Engineering and Technology (Birkhäuser/Springer, New York, 2014)
12. J.-Y. Chemin, I. Gallagher, Wellposedness and stability results for the Navier-Stokes equations in $\mathbf{R}^3$. Ann. Inst. H. Poincaré Anal. Non Linéaire **26**(2), 599–624 (2009)
13. F.K. Chow, R.L. Street, M. Xue, J.H. Ferziger, Explicit filtering and reconstruction turbulence modeling for large-eddy simulation of neutral boundary layer flow. J. Atmos. Sci. **62**, 2058–2077 (2005)
14. P. Constantin, C. Foias, *Navier-Stokes Equations*. Chicago Lectures in Mathematics (University of Chicago Press, Chicago, IL, 1988)

15. R. Eymard, T. Gallouet, R. Herbin, Finite volume methods, in *Solution of Equation in Rn (Part 3), Techniques of Scientific Computing (Part 3)*. Handbook of Numerical Analysis, vol. 7 (Elsevier, Amsterdam, 2000), pp. 713–1018
16. E. Feireisl, *Dynamics of Viscous Compressible Fluids*. Oxford Lecture Series in Mathematics and its Applications, vol. 26 (Oxford University Press, Oxford, 2004)
17. J.H. Ferziger, M. Peric, *Computational Methods for Fluid Dynamics* (Springer Science & Business Media, Berlin, 2012)
18. H. Fujita, T. Kato, On the Navier-Stokes initial value problem. i. Arch. Ration. Mech. Anal. **16**(4), 269–315 (1964)
19. T. Gallouët, J. Lederer, R. Lewandowski, F. Murat, L. Tartar, On a turbulent system with unbounded eddy viscosities. Nonlinear Anal. **52**(4), 1051–1068 (2003)
20. M. Germano, Fundamentals of large eddy simulation, in *Advanced Turbulent Flow Computations (Udine, 1998)*. CISM Courses and Lectures, vol. 395 (Springer, Vienna, 2000), pp. 81–130
21. M. Germano, U. Piomelli, P. Moin, W. Cabot, A dynamic subgrid-scale eddy viscosity model. Phys. Fluids A **3**(7), 1760–1765 (1991)
22. E. Hopf, Über die Anfangswertaufgabe für die hydrodynamischen Grundgleichungen. Math. Nachr. **4**(1–6), 213–231 (1950). doi:10.1002/mana.3210040121. http://dx.doi.org/10.1002/mana.3210040121
23. H. Jasak, *Error Analysis and Estimation for the Finite Volume Method with Applications to Fluid Flows* (Imperial College London [University of London], London, 1996)
24. V. John, *Large Eddy Simulation of Turbulent Incompressible Flows: Analytical and numerical results for a class of LES models.* Lecture Notes in Computational Science and Engineering, vol. 34 (Springer, Berlin, 2004)
25. A.N. Kolmogorov, The local structure of turbulence in incompressible viscous fluid for very large Reynolds' numbers. Dokl. Akad. Nauk SSSR **30**, 301–305 (1941)
26. B.E. Launder, D.B. Spalding, The numerical computation of turbulent flows. Comput. Methods Appl. Mech. Eng. **3**(2), 269–289 (1974)
27. J. Lederer, R. Lewandowski, A RANS 3D model with unbounded eddy viscosities. Ann. Inst. H. Poincaré Anal. Non Linéaire **24**(3), 413–441 (2007)
28. P.-G. Lemarié-Rieusset, *Recent Developments in the Navier-Stokes Problem*. Chapman & Hall/CRC Research Notes in Mathematics, vol. 431 (Chapman & Hall/CRC, Boca Raton, FL, 2002)
29. J. Leray, Sur le mouvement d'un liquide visqueux emplissant l'espace. Acta Math. **63**(1), 193–248 (1934)
30. R. Lewandowski, The mathematical analysis of the coupling of a turbulent kinetic energy equation to the Navier-Stokes equation with an eddy viscosity. Nonlinear Anal. **28**(2), 393–417 (1997)
31. R. Lewandowski, Long-time turbulence model deduced from the Navier-Stokes equations. Chin. Ann. Math. Ser. B **36**(5), 883–894 (2015)
32. R. Lewandowski, *The Kolmogorov-Taylor Law of Turbulence: What can Rigorously be Proved?* Handbook of Applications of Chaos Theory (Taylor and Francis, London, 2016)
33. R. Lewandowski, G. Pichot, Numerical simulation of water flow around a rigid fishing net. Comput. Methods Appl. Mech. Eng. **196**(45–48), 4737–4754 (2007)
34. D.K. Lilly, Numerical simulation and prediction of atmospheric convection, in *Mécanique des Fluides Numérique (Les Houches, 1993)* (North-Holland, Amsterdam, 1996), pp. 325–374
35. J.-L. Lions, *Quelques Méthodes de Résolution des Problèmes aux Limites Non linéaires* (Dunod, Gauthier-Villars, 1969)
36. P.-L. Lions, *Mathematical Topics in Fluid Mechanics: Incompressible Models*, vol. 1. Oxford Lecture Series in Mathematics and its Applications, vol. 3 (Clarendon Press, Oxford University Press, Oxford, New York, 1996)
37. N. Marjanovic, S. Wharton, F.K. Chow, Investigation of model parameters for high-resolution wind energy forecasting: case studies over simple and complex terrain. J. Wind Eng. Ind. Aerodyn. **134**, 10–24 (2014)

38. P.J. Mason, Large-eddy simulation of the convective atmospheric boundary layer. J. Atmos. Sci. **46**, 1492–1516 (1989)
39. T. Michioka, A. Sato, K. Sada, Large-eddy simulation coupled to mesoscale meteorological model for gas dispersion in an urban district. Atmos. Environ. **75**(x), 153–162 (2013)
40. B. Mohammadi, O. Pironneau, *Analysis of the k-Epsilon Turbulence Model*. Research in Applied Mathematics (Wiley, Masson, Chichester, 1994)
41. A.S. Monin, A.M. Obukhov, Basic laws of turbulent mixing in the surface layer of the atmosphere. Contrib. Geophys. Inst. Acad. Sci. USSR **24**(151), 163–187 (1954)
42. L. Onsager, Statistical hydrodynamics. Nuovo Cimento (9) **6**(Supplemento, 2(Convegno Internazionale di Meccanica Statistica)), 279–287 (1949)
43. C. Pares Madroñal, Étude mathématique et approximation numérique de quelques problèmes aux limites de la mécanique des fluides incompressibles. Institut National de Recherche en Informatique et en Automatique (INRIA), Rocquencourt (1992)
44. S.B. Pope, *Turbulent Flows* (Cambridge University Press, Cambridge, 2000)
45. F. Porté-Agel, C. Meneveau, M.B. Parlange, A scale-dependent dynamic model for large-eddy simulation: application to a neutral atmospheric boundary layer. J. Fluid Mech. **415**, 261–284 (2000)
46. F. Porté-Agel, Y.-T. Wu, H. Lu, R.J. Conzemius, Large-eddy simulation of atmospheric boundary layer flow through wind turbines and wind farms. J. Wind Eng. Ind. Aerodyn. **99**(4), 154–168 (2011). The Fifth International Symposium on Computational Wind Engineering
47. L. Prandtl, über die ausgebildeten turbulenz. Zeitschrift für angewandte Mathematik und Mechanik **5**, 136–139 (1925)
48. L. Prandtl, *Prandtl—Essentials of Fluid Mechanics*, 3rd edn., vol. 158. Applied Mathematical Sciences (Springer, New York, 2010). Translated from the 12th German edition by Katherine Asfaw and edited by Herbert Oertel, With contributions by P. Erhard, D. Etling, U. Müller, U. Riedel, K.R. Sreenivasan, J. Warnatz
49. O. Reynolds, An experimental investigation of the circumstances which determine whether the motion of water shall be direct or sinuous, and of the law of resistance in parallel channels. Philos. Trans. R. Soc. **174**, 935–982 (1883)
50. P. Sagaut, *Large Eddy Simulation for Incompressible Flows*, 3rd edn. Scientific Computation (Springer, Berlin, 2006). An introduction, Translated from the 1998 French original, With forewords by Marcel Lesieur and Massimo Germano, With a foreword by Charles Meneveau
51. J. Smagorinsky, On the application of numerical methods to the solution of systems of partial differential equations arising in meteorology, in *Frontiers of Numerical Mathematics* (University of Wisconsin Press, Madison, WI, 1960), pp. 107–125
52. J. Smagorinsky, General circulation experiments with the primitive equations. Mon. Weather Rev. **93**(3), 99 (1963)
53. G.G. Stokes, On the effect of the internal friction of fluids on the motion of pendulums. Trans. Cambridge Philos. Soc. **9**, 8–106 (1851)
54. G.I. Taylor, Statistical theory of turbulence. part i-iv. Proc. Roy. Soc. A **151**, 421–478 (1935)
55. R. Temam, *Navier-Stokes Equations* (AMS Chelsea Publishing, Providence, RI, 2001). Theory and numerical analysis, Reprint of the 1984 edition
56. V.M. Tikhomirov, in *Selected Works of A.N. Kolmogorov: Volume I: Mathematics and Mechanics*, ed. by V.M. Tikhomirov (Kluwer Academic Publishers, Dordrecht, Boston, London, 1992)
57. H.G. Weller, G. Tabor, H. Jasak, C. Fureby, A tensorial approach to computational continuum mechanics using object-oriented techniques. Comput. Phys. **12**(6), 620–631 (1998)
58. B. Zhou, F.K. Chow, Nested large-eddy simulations of the intermittently turbulent stable atmospheric boundary layer over real terrain. J. Atmos. Sci. **71**(3), 1021–1039 (2014)
59. B. Zhou, J.S. Simon, F.K. Chow, The convective boundary layer in the terra incognita. J. Atmos. Sci. **71**, 2545–2563 (2014)

Chapter 6
History of Chaos from a French Perspective

Pierre Coullet and Yves Pomeau

Abstract This review tries to explain how Chaos theory developed in France in the late seventies-early eighties, not as the result of a planned attempt to bolster a field but, as often in human matters, as a result of an unlikely convergence of various events, as well as of a long tradition in the study of nonlinear phenomena that can be traced back to Poincaré. Some general reflexions will be presented on the connection between the way Science and research are organized and the way things really work.

6.1 Introduction

Usually the history of Science is written by professional historians, just because it has to do mostly with Science made by people not present anymore. The case of Chaos theory is a bit exceptional in this respect because this Science was developed by people who, for many of them, are still alive and even remain active scientists. Several articles have been published already [1] on this subject (History of Chaos), but we hope that our point of view of (formerly) active players in this field could be of interest. Because it is centered on our own experience, there will be surely some distortion in our text, but we tried to limit it to a reasonable minimum. We believe also that there is some value in such a personal perspective as we shall focus on how and why new ideas concretely came out, something hard to find just by reading the written documents and/or comparing articles published in the literature. Our choice of a French perspective is also motivated by an attempt to explain how new ideas and new fields may find their way in a rigid system like the one of state-supported French Science, something which could have a broader significance for the way research is supported elsewhere.

P. Coullet
Université de Nice-Sophia Antipolis, Nice, France
e-mail: pcoullet@mac.com

Y. Pomeau (✉)
Department of Mathematics, University of Arizona, Tucson, AZ, USA
e-mail: pomeau@math.arizona.edu

C. Skiadas (ed.), *The Foundations of Chaos Revisited: From Poincaré to Recent Advancements*, Understanding Complex Systems,
DOI 10.1007/978-3-319-29701-9_6

In contrast perhaps to published articles or books on the history of Chaos, we shall not focus on particular events like scientific meetings, for instance, which played, from what we recall, a minor role or no role at all in the production of new ideas and concepts. Truly informal contacts, discussions and seminars were at the basis of most developments, together with hard thinking by the players. This is perhaps a lesson for the future: Chaos theory was innovative in many respects, using almost for the first time computers to explore mathematical models in an interactive way. Another important issue is that scientists in the field knew (and still know) often each other well and did not have to rely on official channels of scientific communication like grand and costly conferences or various bureaucratic schemas of concerted/planned action. The French system being formally heavily centralized cannot be efficient in promoting whatever scientific agenda it could have had, such an agenda being almost always limited to obvious extensions of existing things and ideas. Counterintuitively perhaps this French research system, because of its absurdity, was somehow well adapted to an outburst of new ideas and concepts because it left actually more freedom to individual scientists than a formally more efficient system with strong incentives for scientists to stay on well trodden tracks. In retrospect it could be a bit like the Soviet science (although on a minor mode), which was the brightest in Stalin's time where everything was formally planned but where actually many scientists (but of course not all of them) seemingly had enough freedom in their research, if not in their everyday life, to produce outstanding results.

6.2 Before Chaos: The French Tradition in Dynamical Systems

6.2.1 Poincaré

The history of Chaos begins with Poincaré. His PhD thesis [2] can be seen as the very beginning of dynamics as we know it. He invented powerful geometrical methods to understand "qualitatively" the behavior of solutions of ordinary differential equations. His message remains alive, because of the power of his methods. As a side remark it is curious to see his basic concepts rediscovered again and again. The saddle-node bifurcation (noeud-col in Poincaré thesis) is fairly popular in this respect and has got lately various fancy new names. Poincaré not only started qualitative method of analysis of differential equations, but he also began to study dissipative dynamical systems different of the (far more complex) Lagrangian dynamics (a topic where he brought also fundamental ideas). One of the things we shall emphasize is the link between Poincaré and modern theory of Chaos in France, a link between scientists from one generation to the next. It is also significant to point out that the notion of bifurcation can be traced back to much older times. Somehow it appeared first at the eve of modern science: Archimedes of Syracuse [3] did show that, as the center of gravity of a floating hull gets higher and higher, there is a bifurcation in the equilibrium position of the body, if it is

symmetrical with respect to a vertical plane: classically a loss of symmetry of the equilibrium position takes place and two new equilibrium positions appears, both stable although the symmetric position becomes unstable. The classical Elastica problem solved by Euler makes the next important step in the history of the concept of bifurcation. There the beautiful geometrical method of Archimedes is replaced by modern analytical methods.

The power of Poincaré approach was to link geometrical intuition with analytical problems. Of course this link between geometry and analysis did not begin with him: it can be traced back to Newton's Principia where the two-body problem is essentially solved as a consequence of (non trivial) properties of conics. As had been shown [4] by Jean-Marc Ginoux, Poincaré did more than lay the ground idea of bifurcation theory (he coined also the word bifurcation) but he also worked it out concretely for a particular case, relevant for the generation of self-oscillations in an electrical device. This explicit use of Poincaré method, supported by geometrical methods was at the basis of the book by Yves Rocard, "Dynamique des vibrations" [5], a book familiar to many scientists in France going to work on Chaos (Libchaber, Coullet, Pomeau and others). Having attended the 1933 meeting at IHP on nonlinear science (devoted mostly to the Van der Pol equation) Rocard made a link between the old time of Poincaré and modern times of Chaos theory. True, Rocard never referred to Poincaré in his lectures at Ecole Normale as far as one of us (YP) can recall, a lack of reference to mathematicians quite common among physicists in France at this time (think to German science and the role played by Hilbert and Sommerfeld in the birth of Quantum Mechanics). In his lectures Rocard said a few things about the response of the Van der Pol oscillator to external periodic forcing. He said that if more and more frequencies were added, the solutions remains quasi periodic with the composition of many base frequencies, something that was already known to be wrong at this time thanks to the deep results by Levinson [6].

This was (although Rocard never mentions it) the conception put down by Landau on the bifurcation to turbulence in flows: at every bifurcation a new frequency appears as well as its linear combination with integer coefficients with the already existing frequencies. In this (erroneous) view, turbulence/Chaos, seen as a continuous noise spectrum appear only after an infinite number of bifurcations, something requiring to reach infinite Reynolds number in a turbulent flow. This has been proved, by Ruelle and Takens [7], to be theoretically wrong and experiments later fully confirmed this point (see below).

6.3 Other Precursors and Foreign Influences

6.3.1 Michel Hénon

Michel Hénon, who passed away in 2013, was a French pioneer in the research on nonlinear phenomena and Chaos. This modest man was remarkable for many

reasons, As a student at Ecole Normale Supérieure (early fifties), at a time where no computer was available, he managed to build one with the purpose of solving the three-body problem, an item in the list of problems to be solved with computers as given by Fermi (who had not much time to do it before his early death). Incidentally Fermi chosen those topics with a very sure taste. Likely the most famous item there is the Fermi-Pasta-Ulam problem, namely the return to equilibrium of a chain of nonlinear oscillators. Corning back to Michel Hénon, he inspired a very active group of scientists in Nice, and has left two important legacies in nonlinear science: Hénon-Heiles differential equations [8] and Hénon attractor [9]. The second one is a good example of how things worked early in the science of Chaos: one of us, YP, gave a talk at the Nice Observatory on recent work he had done with Jose-Luis Ibanez on an attractor they had discovered in the Lorenz system for parameter values different of the one chosen originally by Lorenz. In this attractor, by following the trajectory in phase space one could find two well defined plane transformations along the trajectory: one of stretching and another one of folding (the so-called baker's transform), something impossible with the "classical" Lorenz attractor. The result was an attractor with a cross section looking like a folded object with infinitely many folds. In Nice the talk was given before lunch and Michel Hénon managed to find during lunch time a quadratic invertible map contracting areas and doing basically the same thing as was done by the continuous flow of the Lorenz system for the parameter values of Ibanez and YP [10]. Because of its easiness to be put in a pocket computer, Hénon's attractor became popular very quickly, although its mathematical status remains undecided: for instance one does not know yet what is its true topology, one only knows that it is not the product of a Cantor set and of a smooth manifold, as it appeared visually to be the case first.The mathematical difficulty there is that this attractor is not hyperbolic, which makes hard to prove things in a rigorous way. Later it turned that this kind of quadratic iteration had already a rather long mathematical history, belonging to the class of Cremona maps, although they do not seem to have been studied before as dynamical systems, by looking at long iterations.

Let us briefly mention another legacy of Poincaré on nonlinear dynamics, the "solution" of the three-body problem. As just said, this motivated Michel Hénon to begin his studies of Chaos in a model of non integrable Lagrangian system, the Hénon-Heiles system. It showed an unexpected coexistence of regular orbits and of a chaotic sea. This problem has been taken over since with far more powerful numerical methods and in more realistic situations. It has been shown by Laskar [11] that our solar system is unstable in the long run, contrary to expectations, including by Newton!

6.3.2 The Toulouse Group on Iterations

For the sake of completeness we mention the work of the research group of Mira and collaborators in Toulouse [12]. In an engineering school they made over the

years a systematic "experimental" study of rational iterations of non invertible (mostly 2D) maps, a topic started earlier at Los Alamos National Lab by Ulam and Metropolis. They focused their research on the geometric properties of the attractors and their basin of attraction. It is fair to say that this work had little influence on the developments of the French side of the science of Chaos. The authors developed their own terminology which remained quite unfamiliar to outside readers and the level of analysis involved was quite hard to fathom, since the papers seemed to be mostly descriptive. All those works had little or no influence on developments we shall mention later. The same can be said of a paper by May [13] in Nature in the early days of Chaos theory, which included a fairly complete list of references at the end.

6.3.3 Prigogine

There is also the question of the influence of Prigogine and the Brussels school on the development of the science of Chaos in France. Prigogine was a flamboyant person and an outstanding speaker. He steadfastly maintained that out-of equilibrium systems are interesting and should be studied, his ideas having been diffused in a number of books. His interest in dissipative structures brought somehow people to the field of non equilibrium systems. The goal was to understand non trivial things like how Bénard cells are created, how nonlinearity operates above the onset of stability, etc. The fundamental problem of physics, as seen by Prigogine, namely the microscopic origin of irreversibility was however not central to the field of research on Chaos as it unfolded. Most scientists did take for granted the macroscopic equations with chaotic solutions without worrying too much about their derivation from basic principles, ultimately from atomic physics. The Brussels school put a lot of insistence on the effect of thermal fluctuations on macroscopic dynamics, a very small effect hard to put in evidence. Summarizing Prigogine pointed in the right direction (study non equilibrium dynamics) but perhaps not with the most appropriate tools of study, because requiring to start from microscopic physics is somewhat too demanding. Moreover, we (YP and others) had a chance to spend some time in Prigogine's lab in Brussels in the late sixties early seventies, it was a great place of discussion on scientific subjects between young and bright people coming from all around the world. It is too bad that such a place does not exist anymore in Europe.

6.4 The Transition

The study of Chaos got a big jump start with the paper by Ruelle and Takens. There is no more than one or two papers of this class every 10 years: it introduced a new mathematical idea, namely that after a finite number of bifurcations to oscillations,

the generic behavior of a dynamical system is not quasi periodic with more and more independent frequencies and their combinations with integer coefficients, but chaotic with a finite correlation time and a continuous frequency spectrum. The transition to turbulence in flows had been studied by Landau in 1944 [14]. Landau saw the continuous spectrum of a turbulent system as a superposition of infinitely many frequency lines. The existence of this infinity of independent frequencies requires an infinity of bifurcations. Accordingly, turbulence can only set in at infinite Reynolds number, after infinitely many bifurcations. Ruelle and Takens, quoting explicitly Landau, showed that the implicit extension of the quasi periodic paradigm to more than three independent frequencies is not correct. If they are four independent frequencies, the phase space is a 4D torus and so the Poincaré map is of one 3D torus on itself. Such a map bifurcates generically toward a chaotic map where the distance along the large circle is multiplied by two at each iteration although the circular cross section of the torus is mapped in two small discs inside the disc one starts from. The iteration of this mapping yields a strange attractor where each trajectory is unstable along the large circle and contracting in the dimension of the cross section. The result in the cross section is a Cantor set of discs embedded in discs, etc, see for instance [15] on this structure. Such a bifurcation of the dynamics with four independent frequencies is structurally stable, which proves that four independent frequencies can do something which is not a quasi periodic dynamics but which is completely chaotic.

This deep result met some resistance on the side of the "classical fluid mechanics" community, without, it is true, trying to find a flaw in Ruelle-Takens. On the side of experimental physics, a few groups took the task of checking Ruelle-Takens in real experiments This was not such a simple job in the original formulation of the Ruelle-Takens scenario of transition to turbulence. Actually one must have a sequence of bifurcations to oscillations and after a finite number of bifurcations a direct transition to Chaos. This difficult job was taken over in the US by Swinney and Gollub [16] and in France by Maurer and Libchaber at Ecole Normale [17] and Bergé and Dubois at CEA-Saclay [18]. This emphasizes a geographical strength (dating back to many centuries) of the French system of research: almost all the people involved in the early stage of Chaos theory in France not only knew each other but also worked either in Paris or nearby (Bures-sur-Yvette and Saclay).

To summarize, the interest of physicists was raised not so much perhaps by the depth of the mathematics of Ruelle and Takens, but by the fact that it contradicted a statement in an universally admired set of textbooks, the Course of theoretical physics by Landau and Lifshitz. Furthermore the connection with experiments was also very important, experiments being done either in the same lab as the place where theory was done or in the lab next door.

It is worth pointing out that, there were rather frequent scientific meetings on "nonlinear science" at the time (seventies and early eighties), culminating with a Summer school at Les Houches in the French Alps, preceded by a Winter workshop at the same place. At this time nonlinear meetings had a mixed audience and lecturing. On one side people did soliton theory, integrability, etc. all purely mathematical things, motivated by the remarkable feat of Martin Kruskal and

collaborators who succeeded in solving the Korteweg-deVries (KdV) nonlinear partial differential equations thanks to a very innovative method of inverse scattering.The same meetings were also attended by pioneers in Chaos theory, motivated in part by attempts to continue on the path opened by Ruelle. One can still find a mixture of articles coming from those two branches of nonlinear science in Journals like Nonlinearity and Physica D-nonlinear physics. However, there was very little overlap between the two groups (integrable systems and Chaos), and the mixture demixed quite soon.

6.5 Why in France at This Time?

This brings to the fore a significant question: why did this field emerged at this time in France? And particularly why a small group of loosely connected scientists started doing research on Chaos? At the time, French theoretical physics was dominated by attempts to prove rigorously results in statistical physics and field theory by using a formal device called C-star algebra. This very abstract approach to theoretical physics did not fit the taste of everyone, precisely because it was too much on the side the farthest of physics (and remains so). Some felt dissatisfied with this state of affair. Somehow the old Poincaré spirit was almost completely gone, even though one of the fundamental item in this C-star field was the requirement of symmetry under the general Poincaré group, namely the Lorentz group with translations in space and time added. By the way, this requirement of symmetry is hard to satisfy if one wants also to get rid of the infinities in the field theory of interacting quantum fields. The last word is yet to be printed in this area of research.

A small subset of physicists continued however to do theory in a far less mathematized and formal way. The authors of this text shared an interest in problems, almost forgotten now, of the long time relaxation of time correlation functions in classical equilibrium systems. This point was raised by Alder and Wainwright who had discovered the slow power decay of certain time correlations [19], a result also consistent with a result by YP derived a little before from the so-called mode-mode coupling theory for the kinetic theory of a dense gas [20]. This kind of result, although very likely exact, was and still is far away from a formal proof by using methods of the C-star formalism. For our story however it has an interest because this slow decay of time-correlation was one of the first example of a qualitative and significant new result derived in part from computer studies, an example that inspired the analysis of the bifurcation to Chaos that were going to be discovered.

This goes beyond the intellectual motivation for studying fundamental questions with computers, but also because this followed the fast increase in the availability of powerful computers, all relying of the unbelievably efficient Californian computer industry.

6.6 Theoreticians and Experimentalists Talk to Each Other

In France, in contrast with other countries, the role of light experiments was emphasized, for a reason mainly related to the personal relationship between people (theoreticians and experimentalists), like Libchaber at ENS, Bergé and Dubois in Saclay, Coullet and Tresser and Pomeau and collaborators, Paul Manneville and Bernard Derrida. A (although quite remote) model for such a theory-experiment cooperation was the way de Gennes group worked. But this was its only influence. de Gennes stayed out of the Chaos business (but for a quick explanation of what is a strange attractor in his lectures on fluid mechanics at Collège de France). This direct connection with experimentalists was against the French tradition in theoretical physics. Traditionally most French theoreticians in Physics try to equal their mathematician colleagues, mathematics being the top ladder of the Auguste Comte scale. Any interest for applications bring them a few steps down on this ladder, without helping much in their professional trajectory.

Moreover this "light experiment (or corner table) philosophy" goes also against another ground tendency in French science, the ever-going and costly expansion of large facilities like Synchrotron radiation, neutron facilities, high energy devices, all types of fusion machines, etc. much liked by the French bureaucracy and politicians of all sides: big size means high visibility to outsiders without need to explain what new, useful and interesting results are obtained, if they ever are.

However things soon got far easier for experimentalists on Chaos because of two discoveries, one made simultaneously in France and in the US. Both discoveries, done at about the same time, showed that other scenarios of transition to turbulence existed than the one of Ruelle and Takens, and far easier to explain and so to find in experiments.

6.7 What New Results Have Been Obtained ?

After the dust has settled, it is time to see what remains, namely what scientific results remain as a legacy of all the work of scientists in the field of Chaos, if anything remains, and particularly what kind of result can be attributed to French science. Of course our choice is prejudiced by our own interest and our personal work. It is likely that others would emphasize different contributions as long lasting.

This is the place where we should give some insight on the way two routes to Chaos were discovered by the present authors with collaborators.

The transition by intermittency was discovered in systematic studies of the Lorenz set of equations. There was no obvious motivation for that, because, at the time it was unclear if there was other scenario for the transition to turbulence besides the one found by Ruelle and Takens, which was fairly complex already. In this respect the Lorenz system was perhaps not such a good system, because it was of rather low dimension (3) and so had no chance to show anything like a

Ruelle-Takens scenario. Nevertheless, Paul Manneville and YP started to run the Lorenz model on an analog computer. It is time to pause to explain what is (actually was) an analog computer. The idea, was to simulate a certain set of coupled ODE's (ordinary differential equations) by building an electrical network with linear and nonlinear elements designed in such a way that (for instance) the voltage between two nodes is precisely given by the solution of the equations one wished to study. At the time this idea was already a complete dead end, although it had been supported by the research division of the National French utility for electric power (EDF). A big analog computer had been built and improved over the years. It did more or less the job with many circuits. This device had been donated to the French Atomic Energy commission (CEA) where it was still in use. Its running required about ten dedicated people, engineers and technicians: because of its many electrical components, failures were happening all the time and had to be fixed. In this respect it was closer to the first vacuum-lamp computers in Los Alamos with the same problem of replacing failed components. The number of people necessary for the running was a bit large compared to the various (digital) computer centers of the time, but not by such a huge factor. Compared to the digital computers of the time, this analog computer had the big advantage to yield an immediate display (on a small video screen) of change of behaviour following a change of parameter value. By changing continuously a parameter value of the Lorenz system, it was possible to discover bifurcations seen as obvious changes in trajectories in phase space. Of course this had to be distinguished from a mere change of behaviour due to the failure of an electric element. The transition by intermittency did show itself by random bursting of the trajectory getting rarer and rarer as the transition was approached. The next step was to try to find a rational explanation of this remarkable phenomenon [21]. This was made possible by the familiarity gained by looking at iterations of one dimensional rational maps. Rather surprisingly such a simple idea had not been found before, although it could have been done without the help of a computer, because the final explanation relies a geometrical construction only, not on detailed analysis.

Another scenario of transition to turbulence was discovered in France, in Nice, the transition by accumulation of period doubling. Period doubling was discovered and explained at about the same time (1978–1980) by Mitch Feigenbaum in the US [22] and by Pierre Coullet, one of the authors of this paper, and Charles Tresser [23] in France. The history of Coullet-Tresser is almost a novel: Tresser had no position at the University of Nice and Coullet had just been recruited by CNRS, the French organisation for scientific research to do theoretical physics. The two (Coullet and Tresser) had been given a small office in an attic near the gate of the campus with a small computer.

Pierre Coullet began working on a model of population dynamics, called Lokta-Volterra. He discovered a rather unusual behaviour of one of those models, where three unstable states are visited at longer and longer intervals, something quite non generic for dynamical systems. His advisor, Jean Coste, discussed this curious dynamics with Michel Hénon at the Observatory of Nice who told him that even more spectacular behaviours of non linear dynamical systems were reported in

a review paper by May. This led Pierre to iterations of simple maps, something referred to in this review as example of non linear dynamics.

Pierre Coullet then discovered the accumulation of period doubling and explained it, with the help of Charles Tresser, with the non trivial idea of fixed point of the iteration process and its universal properties. The idea of scaling and of fixed point was borrowed then from Wilson theory of critical phenomena, Pierre having a PhD in theoretical physics knew renormalisation. They put together quickly the note [23] on their discovery and paid a visit to Michel Hénon at the Nice observatory who had just received a preprint by Feigenbaum reporting results related to theirs (but without the RNG part which came later) [22].

As a final note on the discovery of the two scenario of transition to turbulence (period doubling and intermittency), they were both put in evidence rather quickly in experiments on Rayleigh-Bénard thermal convection in fluids, by Maurer and Libchaber at Ecole Normale for period doubling and by Bergé and Dubois at Saclay for intermittency. A slightly later, a beautiful experiment at Bordeaux put in evidence the scenario of intermittency in non equilibrium chemical dynamics [24]. This experiment showed very nicely the opening of a channel in the iteration derived from the experimental data.

Summarizing one can see on those two examples that progress in the field owed a lot to chance and unlikely meeting of various people on a completely informal basis and that administrative planning of research did not play any role.

6.8 Lessons for the Future

In France, as in many countries, it is difficult for a new scientific domain like Chaos to emerge, if not to blossom. This has two obvious explanations: first there is a finite cake to share, and new customers are never welcome. Next French Science is (formally) well organized with each field and subfield developing in its own nest. Therefore there is a priori no nest for a new bird: it should find its place somewhere in the big tree of organized Science. The obvious drawback of such an organization is that it leaves little space for freedom and imagination so that it becomes harder and harder as time goes to attract bright young minds. Said otherwise, it is easy to attract people who will participate to incremental progress, another word for no progress, but much more difficult to help the imaginative ones needed to produce new Science and new results. By the way, this does not apply to pure Science only but also to applied science. The rigidity, not to say the absurdity, of the French system was so big that it has actually little power to control everything and so left enough freedom to young scientists to start their own successful research.

Surely Chaos theory and experiments did not suffer from lack of attractiveness. Nowadays it has morphed into a wider field, nonlinear science, with many bright young colleagues. We hope this tree will continue to blossom,

References

1. D. Aubin, A. Dahan Dalmonico, Writing the history of dynamical systems and chaos: longue durée and revolution, disciplines and culture. Hist. Math. **29**, 1 (2002) and references therein
2. H. Poincaré, Sur les courbes définies par une équation différentielle. Journal de mathématiques pures et appliquées, Série 1 **7**, 375 (1881); **8**, 251 (1882); Série 2 **1**, 167 (1885) and **2**, 151 (1886). Those four papers, based on Poincaré PhD thesis are a monument of the history of Mathematics
3. P. Coullet, Bifurcation at the dawn of Modern Science. CR Mecanique **340**, 777 (2012). We can only urge interested readers to read this beautiful piece on Science of classical times
4. J.M. Ginoux, History of Nonlinear Oscillations Theory (1880–1940, to appear)
5. Y. Rocard, Dynamique générale des vibrations (Dunod, Paris, 1971)
6. N. Levinson, Transformation theory of nonlinear differential equations of the second order. Ann. Math. **45**, 723 (1944)
7. D. Ruelle, F. Takens, On the nature of turbulence. Commun. Math. Phys. **20**, 167 (1971)
8. M. Hénon, C. Heiles, The applicability of the third integral of motion: some numerical experiments. Astrophys. J. **69**, 73 (1964)
9. M. Hénon, A two-dimensional mapping with a strange attractor. Commun. Math. Phys. **50**, 69 (1976)
10. J.L. Ibanez, Y. Pomeau, Simple case of non-periodic (strange) attractor. J. Non-Equilib. Thermodyn. **3**, 135 (1978)
11. J. Laskar, Large-scale Chaos in the solar system. Astron. Astrophys. **287**, L9 (1994)
12. C. Mira, Nonlinear maps from Toulouse colloquium (1973) to Noma'13, in *Nonlinear Maps and Their Applications*, edited by R. Lopez-Ruiz et al. Springer Proceedings in Mathematics and Statistics, vol. 112 (Springer, Heidelberg, 2014)
13. R. May, Simple mathematical models with complicated dynamics. Nature **261**, 459 (1976)
14. L.D. Landau, On the problem of turbulence. Dokl. Akad. Nauk SSSR **44**, 339 (1944)
15. P. Bergé, Y. Pomeau, C. Vidal, Order Within Chaos: Toward a Deterministic Approach to Turbulence (Wiley, New York, 1984)
16. J.P. Gollub, H.L. Swinney, Onset of turbulence in a rotating fluid. Phys. Rev. Lett. **35**, 927 (1975)
17. J. Maurer, A. Libchaber, Une expérience de Rayleigh-Bénard de geometrie réduite: multiplication, démultiplication et accrochage de fréquences. J. Phys.**41**, Colloque C3, 51 (1980)
18. P. Bergé, Intermittency in Rayleigh-Bénard convection. J. Phys. Lett. **41**, L341 (1980)
19. B.J. Alder, T.E. Wainwright, Decay of the velocity autocorrelation function. Phys. Rev. **A1**, 18 (1970)
20. Y. Pomeau, A new kinetic theory for a dense classical gas. Phys. Lett. A. **27A**, 601 (1968); A divergence free kinetic equation for a dense Boltzmann gas. Phys. Lett. A **26A**, 336 (1968)
21. Y. Pomeau, P. Manneville, Intermittent transition to turbulence in dissipative dynamical systems. Commun. Math. Phys. **74**, 189 (1980)
22. M.J. Feigenbaum, Quantitative universality for a class of nonlinear transformations. J. Stat. Phys. **19**, 25 (1978)
23. P. Coullet, C. Tresser, Iterations d'endomorphismes et groupe de renormalisation. CRAS Série A **287**, 577 (1978)
24. Y. Pomeau et al., Intermittent behaviour in the Belousov-Zhabotinsky reaction. J. Phys. Lett. **42**, L271 (1981)

Chapter 7
Quasiperiodicity: Rotation Numbers

Suddhasattwa Das, Yoshitaka Saiki, Evelyn Sander, and James A. Yorke

Abstract A map on a torus is called "quasiperiodic" if there is a change of variables which converts it into a pure rotation in each coordinate of the torus. We develop a numerical method for finding this change of variables, a method that can be used effectively to determine how smooth (i.e., differentiable) the change of variables is, even in cases with large nonlinearities. Our method relies on fast and accurate estimates of limits of ergodic averages. Instead of uniform averages that assign equal weights to points along the trajectory of N points, we consider averages with a non-uniform distribution of weights, weighing the early and late points of the trajectory much less than those near the midpoint $N/2$. We provide a one-dimensional quasiperiodic map as an example and show that our weighted averages converge far faster than the usual rate of $O(1/N)$, provided f is sufficiently differentiable. We use this method to efficiently numerically compute rotation numbers, invariant densities, conjugacies of quasiperiodic systems, and to provide evidence that the changes of variables are (real) analytic.

7.1 Introduction

Let X a topological space with a probability measure μ and $T : X \to X$ be a measure preserving map. Let $f : X \to E$ be an integrable function, where E is a finite-dimensional real vector space. Given a point x in X, we will refer to the

S. Das (✉)
Department of Mathematics, University of Maryland, College Park, MD, USA
e-mail: sdas11@umd.edu

Y. Saiki
Graduate School of Commerce and Management, Hitotsubashi University, Tokyo, Japan

E. Sander
Department of Mathematical Sciences, George Mason University, Fairfax, VA, USA

J.A. Yorke
Institute for Physical Science and Technology, University of Maryland, College Park, MD, USA

C. Skiadas (ed.), *The Foundations of Chaos Revisited: From Poincaré to Recent Advancements*, Understanding Complex Systems,
DOI 10.1007/978-3-319-29701-9_7

long-time average of the function f along the trajectory at x

$$\frac{1}{N}\sum_{n=0}^{N-1} f(T^n(x)), \tag{7.1}$$

as a **Birkhoff average**. The Birkhoff Ergodic Theorem (see Theorem 4.5.5. in [1]) states that if $f \in L^1(X,\mu)$, then (7.1) converges to the integral $\int_X f d\mu$ for μ-a.e. point $x \in X$. The Birkhoff average (7.1) can be interpreted as an approximation to an integral, but convergence is very slow, as given below.

$$\left|\frac{1}{N}\sum_{n=1}^{N} f(T^n(x)) - \int_X f d\mu\right| \leq CN^{-1},$$

and even this slow rate will occur only under special circumstances such as when $(T^n(x))$ is a quasiperiodic trajectory. In general, the rate of convergence of these sums can be arbitrarily slow, as shown in [2].

The speed of convergence is often important for numerical computations. Instead of weighing the terms $f(T^n(x))$ in the average equally, we weigh the early and late terms of the set $1, \cdots, N$ much less than the terms with $n \sim N/2$ in the middle. We insert a weighting function w into the Birkhoff average, which in our case is the following C^∞ function that we will call the **exponential weighting**

$$w(t) = \begin{cases} \exp\left(\frac{1}{t(t-1)}\right) & \text{for } t \in (0,1) \\ 0 & \text{for } t \notin (0,1). \end{cases} \tag{7.2}$$

Let $\mathbb{T}^d$ denote a d-dimensional torus. For $X = \mathbb{T}^d$ and a continuous f and for $\phi \in \mathbb{T}^d$, we define what we call a **Weighted Birkhoff ($\mathbf{WB}_N$) average**

$$\mathrm{WB}_N(f)(x) := \frac{1}{A_N}\sum_{n=0}^{N-1} w\left(\frac{n}{N}\right) f(T^n x), \text{ where } A_N := \sum_{n=0}^{N-1} w\left(\frac{n}{N}\right). \tag{7.3}$$

Note that the sum of the terms $w(n/N)/A_N$ is 1, that w and all of its derivatives are 0 at both 0 and 1, and that $\int_0^1 w(x)dx > 0$.

Quasiperiodicity Each $\vec{\rho} \in (0,1)^d$ defines a **rotation**, i.e. a map $T_{\vec{\rho}}$ on the d-dimensional torus $\mathbb{T}^d$, defined as

$$T_{\vec{\rho}} : \theta \mapsto \theta + \vec{\rho} \mod 1 \text{ in each coordinate.} \tag{7.4}$$

This map acts on each coordinate θ_j by rotating it by some angle ρ_j. We call the ρ_j values "**rotation numbers**."

A vector $\vec{\rho} = (\rho_1, \ldots, \rho_d) \in \mathbb{R}^d$ is said to be **irrational** if there are no integers k_j for which $k_1\rho_1 + \cdots + k_n\rho_n \in \mathbb{Z}$, except when all k_j are zero. In particular, this

implies that each ρ_j must be irrational. The rotation numbers depend on the choice of the coordinate system. In any other coordinates in which the system is also a rotation, the rotation vector $\vec{\rho}$ is $A\vec{\rho}$, for some matrix A whose entries are integers such that the determinant of A is ± 1. Conversely, any such matrix corresponds to a coordinate change which also changes $\vec{\rho}$ to $A\vec{\rho}$.

A map $T : X \to X$ is said to be **d-dimensionally C^m quasiperiodic** on a set $X_0 \subseteq X$ for some $d \in \mathbb{N}$ iff there is a C^m-diffeomorphism $h : \mathbb{T}^d \to X_0$, such that,

$$T(h(\theta)) = h(T_{\vec{\rho}}(\theta)). \tag{7.5}$$

where $T_{\vec{\rho}}$ is an irrational rotation. In this case, h is a conjugacy of T to $T_{\vec{\rho}}$. In particular, a (pure) **irrational rotation**, (a rotation by an irrational vector $\vec{\rho}$) is a quasiperiodic map.

Invariant Measure for Quasiperiodic Maps An irrational rotation $T_{\vec{\rho}} : \mathbb{T}^d \to \mathbb{T}^d$ on the torus has a unique invariant measure, which is the Lebesgue probability measure. This measure also turns out to be the unique ergodic measure. It follows that if a dynamical system $T : X_0 \to X_0$ is d-dimensionally C^1 quasiperiodic, there is a unique T-invariant measure on X_0 which, under change of variables, becomes the Lebesgue probability measure on $\mathbb{T}^d$.

Diophantine Rotations An irrational vector $\vec{\rho} \in \mathbb{R}^d$ is said to be **Diophantine** if for some $\beta > 0$ it is **Diophantine of class** β (see [3], Definition 3.1), which means there exists $C_\rho > 0$ such that for every $\vec{k} \in \mathbb{Z}^d$, $\vec{k} \neq 0$ and every $p \in \mathbb{Z}$,

$$|\vec{k} \cdot \vec{\rho} - p| \geq \frac{C_\rho}{\|k\|^{d+\beta}}. \tag{7.6}$$

For every $\beta > 0$ the set of Diophantine vectors of class β have full Lebesgue measure in $\mathbb{R}^d$ (see [3], 4.1). The Diophantine class is crucial in the study of quasiperiodic behavior, for example in [4, 5].

Continued Fractions Every irrational number $\alpha_0 \in (0, 1)$ has a representation known as its continued fraction expansion $[n_1, n_2, n_3, \ldots]$, where $n_1, n_2, n_3, \ldots$ are positive integers. It can be defined inductively as follows

$$n_1 = \lfloor \frac{1}{\alpha_0} \rfloor; \alpha_1 := \frac{1}{\alpha_0} - n_1;$$
$$n_{k+1} := \lfloor \frac{1}{\alpha_k} \rfloor; \alpha_{k+1} := \frac{1}{\alpha_k} - n_{k+1}.$$

Continued Fractions as Approximations The **k-th convergent** of an irrational $\alpha_0 \in (0, 1)$ is the number p_k/q_k defined as follows.

$$\frac{p_k}{q_k} = [n_1, \ldots, n_k] := \frac{1}{n_1 + \frac{1}{\ldots + \frac{1}{a_k}}}. \tag{7.7}$$

Then for every integers $q, k \geq 0$, integer p, if $q\alpha - p$ is strictly between $q_k\alpha - p_k$ and $q_{k+1}\alpha - p_{k+1}$, then either $q \geq q_k + q_{k+1}$ or both p, q must be zero. In other words, the best approximation of α by a fraction p/q with q not exceeding q_k, is the k-th convergent p_k/q_k. We rely on the continued fraction expansion of a number to decide whether it is rational or not. Every rational number has a finite number of terms in its continued fraction expansion. If α is irrational, then the sequence continues forever, while if it is rational, it stops when some α_k is zero.

The Diophantine class β of an irrational number is a measure of how closely it can be approximated by a rational number. The Diophantine class of an irrational number can be deduced from its continued fractions. This is because the k-th convergent p_k/q_k provides the best rational approximation among all rational numbers whose denominator is $\leq q_k$.

We will now state our main theorem about fast convergence of weighted Birkhoff sums (7.3). We will first define a notion of fast convergence called super-convergence.

Definition Let $(z_N)_{N=0}^{\infty}$ be a sequence in a normed vector space such that $z_N \to z$ as $N \to \infty$. We say (z_N) has **super-polynomial convergence** to z or **super converges** to z if for each integer $m > 0$ there is a constant $C_m > 0$ such that

$$|z_N - z| \leq C_m N^{-m} \text{ for all m.}$$

Theorem 7.1.1 *Let X be a C^∞ manifold and $T : X \to X$ be a d-dimensional C^∞ quasiperiodic map on $X_0 \subseteq X$, with invariant probability measure μ. Assume T has a Diophantine rotation vector. Let $f : X \to E$ be C^∞, where E is a finite-dimensional, real vector space. Assume w is the exponential weighting (see Eq. (7.2)). Then for each $x_0 \in X_0$, the weighted Birkhoff average $WB_N f(x_0)$ has super convergence to $\int_{X_0} f d\mu$.*

Other Studies on Weighted Averages The convergence of weighted ergodic sums has been discussed, for example, [6–8]), but without any conclusions on the rate of convergence. In [9], a convergence rate of $O(N^{-\alpha})$, $(0 < \alpha < 1)$, was obtained for functionals in $L^{2+\epsilon}$ for a certain choice of weights. A series of our applications of the method discussed in this paper appear in [10], and the details of the proof of our theorem appears in [11].

The use of a temporal weight in ergodic averages has been a subject of study for several decades, usually using more generic weighting sequences in the form of

$$T_N(f) := \sum_{n=0}^{\infty} \nu_N(n) U^n(f), \text{ where } \nu_N \text{ is a probability distribution on } \mathbb{N}. \quad (7.8)$$

In our theorem, the probability measure ν_N are the values of the weight function w sampled at the points $\{n/N : 0 \leq n < N\}$ and divided by the normalizing constant A_N, as defined in (7.3). In [6], sufficient conditions were derived for (7.8) to converge in weighting sequences of a similar kind. Equations (7.3) and (7.8) arise

from the study of functionals on the Hilbert Space L^2. On the other hand, Berkson and Gillespie [12] considered the convergence of (7.8) for invertible operators on Banach spaces. It was shown that for a particular choice for $(\nu_N)_{N\in\mathbb{N}}$, the operators converge in the strong operator topology to an idempotent operator.

Remark Our results apply to C^m or smooth functions, which are L^2, and carry the assumption that the underlying dynamics is quasiperiodic. We are interested in exploring the applicability of the theorem to other dynamical systems, while keeping in mind that various counter-examples exist in which weighted ergodic averages do not converge. For example, in [13], the authors derived a property called *strong sweeping property* for the operators in (7.8), under the assumption that each ν_N is a *dissipative probability measure* and certain other conditions on the underlying dynamical system (X, T). The strong sweeping out property implies that the limits do not converge but attain values over an interval of numbers. In [14] similar results are obtained to prove the lack of convergence of (7.8) for a dense set of L^1 characteristic functions, in the context of ergodic rotations of the unit circle.

7.2 Application I of Theorem 7.1.1: Rotation Numbers

To illustrate some applications of Theorem 7.1.1, we will work with the following dynamical system for the rest of the paper.

A Cylinder-Map Consider the infinitely long cylinder $\mathbb{R} \times S^1$, where S^1 is the standard topological circle. Consider the following map on this cylinder, first studied in [15].

$$\begin{aligned} x_{n+1} &= 3x_n + \sigma(x_n, y_n) \\ y_{n+1} &= y_n - \delta \sin(y_n) + \epsilon(1 - \cos(x_n)) \mod 2\pi. \end{aligned} \tag{7.9}$$

Here σ is a small perturbation term, δ and ϵ are parameters satisfying $0 < 2\delta < \epsilon$. It turns out that for every such parameter value, if σ is sufficiently small, then there exists an invariant topological circle. Note that if $\sigma \equiv 0$, then this is the circle whose points are $\{(\pi, y) : y \in S^1\}$. Though the map is C^∞, the invariant circle may not be smooth. We are however interested in demonstrating that the dynamics on it is C^∞-conjugate to a rotation. See Fig. 7.1 for some of these curves.

7.2.1 Rotation Number as a Weighted Birkhoff Sum

Rotation Number Let $\bar{F} : \mathbb{R}^d \to \mathbb{R}^d$ be the lift of a quasiperiodic map $F : \mathbb{T}^d \to \mathbb{T}^d$. It is well known (see for example, [16]) that the following limit exists and is a

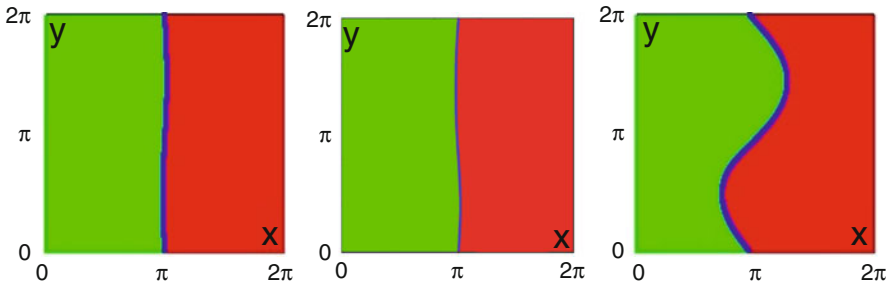

Fig. 7.1 Invariant circles in the cylinder map (7.9), for values of $(\sigma, \delta, \epsilon)$ equal to (**a**) (0.1, 0.1, 0.1), (**b**) (0.2, 0.8, 0.8) and (**c**) (1.0, 0.1, 0.1). Points in the region on the right of the *curves* diverge to $x = +\infty$, while points on the left diverge to $x = -\infty$. Therefore, these *circles* are quasiperiodic repellers and we are interested in the classification of the dynamics on these curves as periodic or quasiperiodic

constant independent of $\vec{z} \in \mathbb{R}^d$.

$$\vec{\rho}(F) := \lim_{n\to\infty} \frac{\bar{F}^n(z) - \vec{z}}{n}. \tag{7.10}$$

This limit is called the **rotation number** of F. The limit in (7.10) is a means of approximating ρ, but its convergence is bounded by the $O(1/N)$, where N is the number of iterates taken into account. We propose a better method based on the weighting factor w.

Note that in the example under discussion, X_0 is a one-dimensional quasiperiodic curve embedded in $X = \mathbb{R}^2$. Let X_0 be given the coordinates θ of a circle S^1 (in this case, θ could be the Y-coordinate of each point on the invariant curve divided by 2π). Given two angles $\theta_1, \theta_2 \in [0, 1)$, $\theta_2 - \theta_1$ denotes the positive angle difference between these two angles, i.e., with value in $[0, 1)$. We are interested in the limit $\rho := \lim_{N\to\infty} \frac{1}{N} \sum_{n=0}^{N-1} [\theta_{n+1} - \theta_n]$, which can be obtained as the super-convergent limit of

$$\mathrm{WB}_N((\theta_{n+1} - \theta_n)) := \frac{1}{A_N} \sum_{n=0}^{N-1} w\left(\frac{n}{N}\right) [\theta_{n+1} - \theta_n].$$

More generally, let X_0 be a quasiperiodic curve embedded in $X = \mathbb{R}^2$. Let $C := C_B \cup C_U$ be the complement of X_0 in $\mathbb{R}^2$, where C_B and C_U are the bounded and unbounded components of C respectively. For $p \in \mathbb{R}^2$, define $\phi(\theta) = (\theta - p)/\|\theta - p\|$. Therefore $\phi(\theta) \in S^1$. Let $\bar{\phi} : \mathbb{R} \to \mathbb{R}$ be the lift of ϕ. If $p \in C_B$, then $\bar{\phi}$ is of the form

$$\bar{\phi}(\bar{\theta}) = \pm\bar{\theta} + \bar{g}(\bar{\theta}),$$

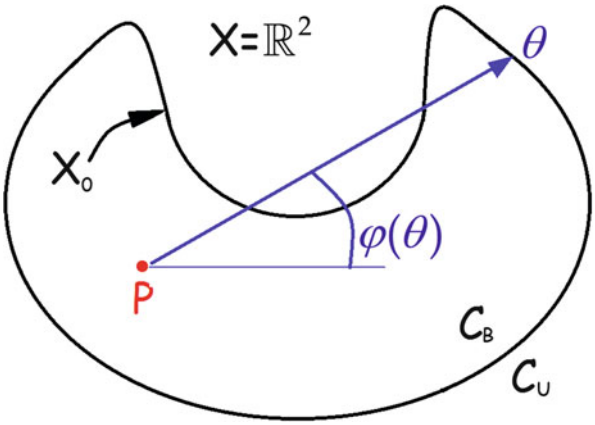

Fig. 7.2 Rotation number on a quasiperiodic curve. The numbers $\phi_n = \phi(\theta_n)$ can be used to calculate the rotation number, as stated in Application 1

where $\bar{\theta} \in \mathbb{R}$ is a lift of $\theta \in C$. Notice that the real valued function $\bar{g} : \mathbb{R} \to \mathbb{R}$ is period one and hence factors into a smooth function $g : X_0 \to \mathbb{R}$. Define a limit ρ_ϕ as follows.

$$\rho_\phi := \mathrm{WB}_N(g(\theta)) = \frac{1}{A_N} \sum_{n=0}^{N-1} w\left(\frac{n}{N}\right) [(\theta_{n+1} - \theta_n) + g(\theta_n)].$$

Then ρ_ϕ is ρ or $1 - \rho$, depending on the orientation of θ, both being legitimate representations of ρ. We have illustrated this construction in Fig. 7.2. If $p \in C_U$, then $\rho_\phi = 0$.

7.2.2 *Error Bound for the Unweighted Method*

Given a one-dimensional quasiperiodic trajectory (x_n) on the circle $S^1 = [0, 1)$, one can define a trajectory on the real line $\bar{x}_n$ for $n = 0, \cdots, N$, where $\bar{x}_0 = x_0$, $\bar{x}_n$ is a lift of x_n and $\bar{x}_{n+1} - \bar{x}_n \in (0, 1)$. It therefore follows that $\bar{x}_{n+1} = \bar{F}(\bar{x}_n)$. Let

$$k_n := \bar{x}_n - x_n \tag{7.11}$$

be the winding number of the n-th iterate. Let the (x_n) iterates be sorted in increasing order as

$$x_{n_0} = 0 < x_{n_1} < \ldots < x_{n_N} < 1.$$

If ρ is the true rotation number, then the iterates $\theta_n = n\rho \mod 1$, for $n = 0, \ldots, N$ have the same cyclic order as the x-orbit. In other words, $0 = \theta_{n_0} < \theta_{n_1} < \ldots < \theta_{n_N}$. We can determine the interval of ρ values for which that is true. First note that

$$0 < x_{n_1} \text{ so } \rho < k_{n_1}/n_1$$
$$x_{n_N} < 1 \text{ so } \rho > (k_{n_N} + 1)/n_N.$$

Suppose $n_i < n_{i+1}$, then $(n_{i+1} - n_i)\rho = k_{n_{i+1}} - k_{n_i} + \epsilon_{n_i}$, for some $\epsilon_{n_i} \in [0, 1)$. Similarly, if $n_i > n_{i+1}$, then $(n_i - n_{i+1})\rho = k_{n_i} - k_{n_{i+1}} - \epsilon_{n_i}$. These two identities give the following two inequalities respectively.

$$\rho > \frac{k_{n_{i+1}} - k_{n_i}}{n_{i+1} - n_i}, \tag{7.12}$$

$$\rho < \frac{k_{n_i} - k_{n_{i+1}}}{n_i - n_{i+1}}. \tag{7.13}$$

For each of the $N-1$ consecutive pairs $(x_{n_i}, x_{n_{i+1}})$, we get such an inequality and they combine to give the possible range of values of ρ. Note that instead of consecutive x-s from the sorted list, we could have taken distant x-s, but the following inequality shows that would not have yielded a sharper bound.

$$\text{If } a_1, a_2, b_1, b_2 > 0, \text{ then } \frac{a_1 + a_2}{b_1 + b_2} \text{ lies in-between } \frac{a_1}{b_1} \text{ and } \frac{a_2}{b_2}. \tag{7.14}$$

7.2.3 Another Calculation of the Rotation Number Using Unweighted Birkhoff Sums

Let $F : \mathbb{T}^d \to \mathbb{T}^d$ be a homeomorphism, where $\mathbb{T}^d$ is the n-torus, obtained from the n-cube $[0, 1)^d$ by taking each coordinate modulo 1. Using the weighting methods, an initial estimate $\vec{\rho}'$ of the rotation number $\vec{\rho}$ of F, by analysing a dense trajectory $\vec{z_0}, \ldots, \vec{z_{N-1}}$. This section describes how to obtain a better estimate $\vec{\rho}''$ of $\vec{\rho}$ from $\vec{\rho}'$.

Let $\vec{z}_{n_1}, \vec{z}_{n_2}, \ldots, \vec{z}_{n_{d+1}}$ be $d + 1$ points on the trajectory which are close to the origin O and whose convex hull contains O. Then there are constants $\alpha_i \in (0, 1)$, for $i = 1, \ldots, n + 1$ such that O is a convex combination of the points $\vec{z_{n_i}}$, i.e.,

$$\vec{0} = \sum_{i=1\ldots,d+1} \alpha_i \vec{z}_{n_i}. \tag{7.15}$$

Since the map is quasiperiodic, there is a homeomorphism $G : \mathbb{T}^d \to \mathbb{T}^d$ such that for every $k = 0, \ldots, d + 1$, $\vec{z_k} = G(k\vec{\rho} \mod 1)$. If the points $\vec{z}_{n_1}, \vec{z}_{n_2}, \ldots, \vec{z}_{n_{d+1}}$ are very close to the origin, G can be considered to be linear in a neighborhood

containing these points. for every $i = 1, \ldots, n+1$. Therefore, $\vec{z_{n_i}} = G(n_i\vec{\rho} \mod 1) \approx dG(0)(n_i\vec{\rho} \mod 1)$. If both sides are multiplied by $dG(0)^{-1}$ then, (7.15) becomes

$$\vec{0} \approx \sum_{i=1\ldots,d+1} \alpha_i dG(0)(n_i\vec{\rho} \mod 1). \tag{7.16}$$

Now let the integral part of $n_i\vec{\rho}$ be $\vec{k_i}$, i.e., $n_i\vec{\rho} = \vec{k_i} + \epsilon_i$, where $\vec{k_i}$ is a vector with integer entries and the entries of ϵ_i lie in $(-0.5, 0.5)^d$ and are very small. Therefore $n_i\vec{\rho} \mod (2\pi) = \epsilon_i$. Therefore (7.16) becomes

$$\vec{0} = \sum_{i=1\ldots,d+1} [\alpha_i(n_i\vec{\rho} - \vec{k_i})]. \tag{7.17}$$

Therefore, the equation can be solved to ρ as

$$\vec{\rho} = \frac{\sum_{i=1,\ldots,d+1} \alpha_i\vec{k_i}}{\sum_{i=1,\ldots,d+1} \alpha_i n_i}. \tag{7.18}$$

Note that for every $i = 1, \ldots, d+1$, $\vec{k_i}/n_i$ is a close approximation to ρ, so the sum (7.18) is an optimal combination of these optimizations.

7.2.4 Fine Tuning the Rotation Number

Let (x_n) be a quasiperiodic trajectory on a circle $S^1 = [0, 1)$. If we attempt to graph the conjugacy map $h(\theta)$ from (7.5), we have only N points and they are not equally spaced. We can compute the slopes between successive points and choose $\hat{\rho}$ so as to minimize the fluctuations in the derivatives of successive slopes. Define points $\theta_n = n\hat{\rho} \mod 1$. As before, let the (x_n) iterates be sorted in increasing order as

$$x_{n_0} = 0 < x_{n_1} < \ldots < x_{n_N} < 1.$$

This ordering will be the same (cyclically) as that of $\theta_0, \ldots, \theta_{N-1}$. Therefore, if consider the graph of h, the successive points of the graph are $p_j := (\theta_j, x_{n_j})$. The slope from p_j to p_{j+1} is:

$$S_i = \frac{\Delta x}{\Delta\theta} := \frac{x_{n_{i+1}} - x_{n_i}}{n_{i+1}\hat{\rho} \mod 1 - n_i\hat{\rho} \mod 1}.$$

From each estimate $\hat{\rho}$ of ρ, a circle map $h : S^1 \to S^1$ be constructed which maps $n\hat{\rho} \mapsto y_n$. From h, one can construct the map $h : S^1 \to S^1$ defined as $g(\theta) = h(\theta) - \theta$. When the function h is lifted to $\mathbb{R}$ it becomes a function with period one.

The closer $\hat{\rho}$ is to the true rotation number ρ, the smoother h is going to be. The following is used as a measure of smoothness of the h.

$$\sigma(\hat{\rho}) := \sum_{i=0,\ldots,N} \left[\left(\frac{\Delta x}{\Delta \theta} \right)_i - \left(\frac{\Delta x}{\Delta \theta} \right)_{i-1} \right]^2, \tag{7.19}$$

where the indices -1 refers to the index N. The sequence of quantities $(\Delta x/\Delta\theta)_i$ is defined as,

$$\left(\frac{\Delta x}{\Delta \theta} \right)_i := \frac{[x_{n_i} + k_{n_i} - n_i\hat{\rho}] - [x_{n_{i-1}} + k_{n_{i-1}} - n_{i-1}\hat{\rho}]}{[n_i\hat{\rho} \mod 1] - [n_{i-1}\hat{\rho} \mod 1]}, \tag{7.20}$$

where the sequence (k_n) is as in (7.11). Equation (7.19) is a measure of the smoothness of h in terms of the sum of the squares of the difference between successive slopes of the map h. If h is smooth, the slope changes slowly and the sum is expected to be small. We can change ρ to minimize the quantity $\sigma(\rho)/\rho$.

7.3 Other Applications of Theorem 7.1.1

We will now describe a computationally efficient method of determining whether invariant tori show quasiperiodic behavior, and we will numerically estimate the analyticity of the conjugacy to a pure rotation. There is a large volume of literature about determining invariant periodic or quasiperiodic sets, these being two of the three types of typical recurrent behavior. An algorithm was introduced in [17], which uses the Newton's method to determine all periodic orbits up to a fixed period along with their basins of attraction. Variants of the Newton's method have been employed to determine quasiperiodic trajectories in various other settings. For example, Becerra et al. [18] used the monodromy variant of Newton's method to locate periodic or quasi-periodic relative satellite motion. In [17], a quantity called local Lyapunov exponent distribution was defined and used to locate basins of small period/quasiperiodic trajectories which lie in the vicinity of larger quasiperiodic trajectories. This step is followed by an application of the Newton method. They used this method to locate co-existing quasiperiodic and periodic trajectories in the standard map. In [19], the authors defined an invariance equation involving partial derivatives. The invariant tori are then computed using finite element methods of PDE-s. See [19, Chap. 2] for more references on the numerical computation of invariant tori.

The analysis is based on the use of Theorem 7.1.1 for performing fast integration of smooth, periodic functions on the torus.

Application II, Computing the Integral of a Periodic C^∞ Function A C^∞ periodic map $f : \mathbb{R}^d \to E$ can be integrated with respect to the Lebesgue measure quickly and accurately in the following manner. We first rescale coordinates so that

its domain is a d-dimensional torus $\mathbb{T}^d = [0,1]^d \mod 1$. We next choose any $\vec{\rho} = (\rho_1, \cdots, \rho_d) \in (0,1)^d$ of Diophantine class $\beta \geq 0$. For example, a good choice for the case $d = 1$ is $\rho = \frac{\sqrt{5}-1}{2}$, the golden ratio, for which $\beta = 0$. Let $T = T_{\vec{\rho}}$ be the rotation by the Diophantine vector ρ on $\mathbb{T}^d$. Let w be the exponential weighting function Eq. (7.2). Then by Theorem 7.1.1, for every $\theta \in \mathbb{T}^d$, $\mathrm{WB}_N(f)(\theta)$ *has super convergence to* $\int_{\mathbb{T}^d} f d\mu$ *and convergence is uniform in* θ.

7.3.1 Application III, Fourier Series of the Embedding

After computing the rotation number ρ by the method explained in Application 1, we can construct the parameterization $\phi = h(\theta)$, where $h : S^1 \to \mathbb{R}$, for which $x_{n+1} = T(x_n)$ is conjugate to the pure rotation $\theta_{n+1} = \theta_n + \rho$. The map h is not known explicitly, but its values $(x_n := h(n\vec{\rho} \mod 1))_{n=0,1,2,\ldots}$ are known. Let $\bar{h} : \mathbb{R} \to \mathbb{R}$ be a lift of the map h. Consider the following function $g : \mathbb{R} \to \mathbb{R}$ defined as

$$g(\theta) := \bar{h}(\theta) - \theta. \tag{7.21}$$

The continuity and the degree of differentiability of h is the same as that of g, and the latter can be non-rigorously estimated by observing the rate of decay of the Fourier series coefficients of the function g. For every $k \in \mathbb{Z}$, the k-th Fourier coefficient of g is described below.

$$a_k(h) := \int_{S^1} h(\theta) e^{-i2\pi k\theta} d\theta.$$

For every $\theta \in S^1$, h has the Fourier series representation

$$h(\theta) = \sum_{k\in\mathbb{Z}} a_k e^{i2\pi k\theta}.$$

To study the decay rate of the coefficients a_k with $|k|$, we need to accurately calculate each term a_k. By Theorem 7.1.1 , $a_k(h)$ can be approximated by a weighted Birkhoff sum that has super convergence to $a_k(h)$,

$$a_k(h) = \lim_{N\to\infty} \mathrm{WB}_N[h(\theta)e^{-i2\pi k\theta}] = \lim_{N\to\infty} \sum_{n=0}^{N-1} w\left(\frac{n}{N}\right) x_n e^{-i2\pi nk\rho}.$$

Instead of computing the complex-valued Fourier coefficients, we will compute the Fourier sine and cosine series. Given a periodic map $f : S^1 \to \mathbb{R}$, the Fourier sine and cosine representation of f is the following. For every $t \in S^1$,

$$f(t) = \frac{a_0}{2} + \sum_{n=1,2,\ldots} a_n \cos(2n\pi t) + \sum_{n=0,1,2,\ldots} b_n \sin(2n\pi t), \tag{7.22}$$

where the coefficients a_n and b_n are given by the following formulas.

$$a_n = 2 \int_{\theta \in S^1} f(\theta) \cos(2n\pi\theta) d\theta, \tag{7.23}$$

$$b_n = 2 \int_{\theta \in S^1} f(\theta) \sin(2n\pi\theta) d\theta. \tag{7.24}$$

See Fig. 7.4 for the decay of the Fourier sine and cosine coefficients with k.

Role of Length of Trajectory Using a higher number of iterates enables a more accurate computation of the higher order Fourier terms (up to 400 terms), up to the accuracy limit which is possible with the precision being used. Figure 7.3 shows that the sine and cosine series decay exponentially, as expected in an analytic conjugation.

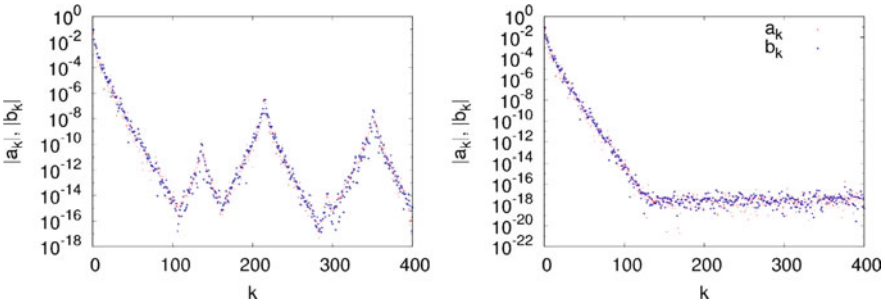

Fig. 7.3 Accuracy of Fourier series, orbit length and computer arithmetic. In all these figures, the Fourier sine and cosine terms of the map $h(\theta) - \theta$ were calculated up to 400 terms, with $\epsilon = 0.8$, $\delta = 0.8$, $\sigma = 0.2$. In (**a**) and (**b**), 10^4 and 2×10^5 iterates respectively were used along with double precision. The earlier Fig. 7.4 shows the highest accuracy, as it used 2×10^5 iterates and quadruple precision. From these results, it becomes apparent that increasing the number of iterates leads to an accurate calculation of higher order Fourier terms. Use of double precision limits the accuracy of the results to 10^{-16} while the accuracy limit for quadruple precision is around 10^{-32}, as seen is Fig. 7.4

7.3.2 Smoothness of Conjugacies

In [20], Denjoy proved that if a C^2, orientation-preserving circle diffeomorphism has an irrational rotation number α, then it is topologically conjugate to the pure rotation $T_\alpha : z \mapsto z + \alpha$, via some continuous map h. We are interested in inferring more about the smoothness class of h. The question of smoothness of conjugacy to a pure rotation is an old problem. While we have described here a non-rigorous method, the papers [3, 21–23] arrive at rigorous conclusions on the differentiability of f by making various assumptions on the smoothness of the quasiperiodic map T and the Diophantine class of its rotation number ρ. We will give a brief summary of some of the classical results before describing our approach.

The **Arnold family** is a commonly studied in the context of existence of quasiperiodic trajectories. In this seminal work [16], Arnold studied the following 2-parameter family of circle diffeomorphisms where ϕ is a T-periodic real analytic function with period one, meaning $\phi(y+1) \equiv \phi(y)$:

$$A_{\omega,\epsilon} : y \mapsto y + \omega + \epsilon\phi(y) \mod 1 \text{ for } y \in [0,1] \text{ and } \epsilon \text{ in } [0,1). \tag{7.25}$$

One of the main theorems about this generic family of maps is that was that for ω belonging to a certain, full-measure set of irrational numbers, for all small values of the parameter ϵ, the map (7.25) will be analytically conjugate to the pure rotation T_ρ (7.4). By "small" ϵ, we mean all ϵ which are less in magnitude than a positive constant ϵ_0 which depends on ω. Subsequently, several other conjugacy results have been established. They differ in their claims on the degree of smoothness of the conjugacy ($C^0, C^1, C^2, \ldots$, or C^∞ or C^ω); as well as in their assumptions on f.

Consider the following four assumptions on the circle map F which will serve as the hypothesis of some of the known results we are going to cite. The subscripted variables, namely r and ν denote parameters which are a part of their respective assumptions.

(A1) ${}_r$ F is C^r.

(A2) ${}_\nu$ $\rho(F)$ is irrational and there is some $\nu > 0$ such that the continued fraction expansion $k_1, k_2, \ldots$ of the rotation number satisfies : $\{k_n n^{-\nu} : n \in \mathbb{N}\}$ is bounded.

(A3) ${}_\beta$ There is $\beta \geq 0$ and a $c > 0$ such that for every $n \in \mathbb{Z} - \{0\}$, $|e^{2\pi\iota n\rho} - 1| > c|n|^{-\beta-1}$. Equivalently, ρ is Diophantine with Diophantine class β.

(A4) $\lim\limits_{B\to\infty} \limsup\limits_{N\to\infty} \left[\sum\limits_{\substack{1 \leq i \leq N \\ a_i \geq B}} \ln(1+a_i) \Big/ \sum\limits_{1\leq i\leq N} \ln(1+a_i) \right] = 0$. A4 is a full-measure condition.

In [3], Herman proves that F is C^1-conjugate to a pure rotation if it satisfies $(A1)_r$ for some $r > 2$. By Katznelson and Ornstein [21], if F satisfies $(A1)_r$ for some $r > 2$ and $(A3)_0$, then h is absolutely continuous. According to [22] if F satisfies more generally $(A1)_r$ for some $r > 2$ and $(A3)_\tau$, then h is $C^{r-1-\tau-\epsilon}$ for every $\epsilon > 0$.

In [24], the following smoothness result is derived for rotation numbers belonging to a full measure subset of $\mathbb{R}$. There exists $\epsilon > 0$ and $C > 0$ such that for $\forall \beta > 0$, if F satisfies $(A1)_5$, $(A3)_\beta$ and if $\|f - R_\alpha\|_{C^5} \leq \epsilon\gamma$, then h is C^3 and satisfies

$$\|D^3 h\|_{L^2} \leq \frac{C}{\gamma}\|f - R_\alpha\|_{C^5}.$$

In [23], it is shown that if F satisfies $(A3)_\beta$ for some $\beta \geq 0$ and $(A1)_r$, for $r \geq 3$ and $r > 2\beta + 1$. Then h is $C^{r-1-\beta-\epsilon}$ for every $\epsilon > 0$. As a corollary, it follows that under the same hypothesis, if F is C^∞, then so is h.

In [25], the following conclusions are made about h:

- If F satisfies $(A1)_r$ for some $r \geq 3$ and α satisfies (A4), then h is $C^{r-1-\epsilon}$, for every $\epsilon > 0$.
- F is conjugate to a rotation if and only if the sequence $(F^n)_{n\in\mathbb{N}}$ is bounded in the C^1-topology.

In our case, we conclude that h is real analytic if $\|a_k\|$ decreases exponentially fast, i.e.,

$$\log \|a_k\| \leq A + B|k| \tag{7.26}$$

for some A and B, to the extent checkable by compute precision (see Fig. 7.4). In this section, $F : S^1 \to S^1$ is a circle diffeomorphism and $\alpha := \rho(F)$ is its rotation number.

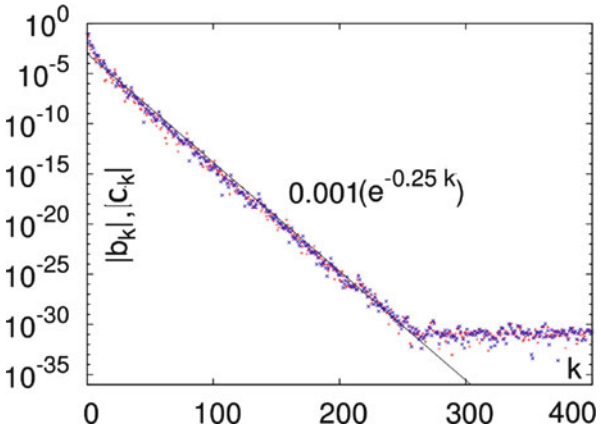

Fig. 7.4 Exponential decay of Fourier coefficients for the cylinder-map (7.9). The figure shows the magnitude of the Fourier coefficients of the periodic function g in (7.21). The first 400 Fourier sine and cosine terms were calculated and the magnitude of the n-th sine and cosine terms was plotted as a function of n, in a log(base 10)-linear scale. All calculations were carried out in quadruple precision computer arithmetic. The graph shows that the Fourier coefficients decay according to the law in (7.26), with $c = -0.25$. The tail of the graph appears flat because the higher order Fourier coefficients could not be calculated to values with magnitude less than the limits of quadruple precision

References

1. M. Brin, G. Stuck, *Introduction to Dynamical Systems* (Cambridge University Press, Cambridge, 2002)
2. U. Krengel, On the speed of convergence in the ergodic theorem. Monatsh. Math. **86**(1), 3–6 (1978)
3. M.R. Herman, Sur la conjugaison différentiable des difféomorphismes due cercle à des rotations. Publications Mathématiques de l'Institut des Hautes Études Scientifiques **49**(1), 5–233 (1979)
4. C. Simó, *Averaging Under Fast Quasiperiodic Forcing* (Plenum Pub. Co., New York, 1994)
5. C. Simó, P. Sousa-Silva, M. Terra, Practical stability domains near $L_{4,5}$ in the restricted three-body problem: some preliminary facts. Prog. Chall. Dyn. Syst. **54**, 367–382 (2013)
6. M. Lin, M. Weber, Weighted ergodic theorems and strong laws of large numbers. Ergod. Theory Dyn. Syst. **27**(02), 511–543 (2007)
7. A. Bellow, R. Jones, J. Rosenblatt, Almost everywhere convergence of convolution powers. Ergod. Theory Dyn. Syst. **14**(03), 415–432 (1994)
8. A. Bellow, V. Losert, The weighted pointwise ergodic theorem and the individual ergodic theorem along subsequences. Ann. l'Inst. Fourier **52**(2), 561–583 (2002)
9. F. Durand, D. Shneider, Ergodic averages with deterministic weights. Trans. Am. Math. Soc. **288**(1), 307–345 (1985)
10. S. Das, E. Sander, Y. Saiki, J.A. Yorke, Quantitative quasiperiodicity. Preprint: arXiv:1508.00062 [math.DS] (2015)
11. S. Das, J.A. Yorke, Super convergence of ergodic averages for quasiperiodic orbits. Preprint: arXiv:1506.06810 [math.DS] (2015)
12. E. Berkson, T.A. Gillespie, Spectral decompositions, ergodic averages, and the Hilbert transform. Stud. Math. **144**, 39–61 (2001)
13. M. Akcoglu et al., The strong sweeping out property for lacunary sequences, Riemann sums, convolution powers, and related matters. Ergod. Theory Dyn. Syst. **16**(02), 207–253 (1996)
14. M.D. Ha, Weighted ergodic averages. Turk. J. Math. **22**(1), 61–68 (1998)
15. E.J. Kostelich, I. Kan, C. Grebogi, E. Ott, J.A. Yorke, Unstable dimension variability: a source of nonhyperbolicity in chaotic systems. Phys. D **109**(1–2), 81–90 (1997)
16. V. Arnold, Small denominators. I. Mapping of the circumference onto itself. Am. Math. Soc. Transl. (2) **46**, 213–284 (1965)
17. J.R. Miller, J.A. Yorke, Finding all periodic orbits of maps using Newton methods: sizes of basins. Phys. D: Nonlinear Phenom. **135**(3), 195–211 (2000)
18. V.M. Becerra, J.D. Biggs, S.J. Nasuto, V.F. Ruiz, W. Holderbaum, D. Izzo, Using Newton's method to search for quasi-periodic relative satellite motion based on nonlinear Hamiltonian models, in *7th International Conference on Dynamics and Control of Systems and Structures in Space*, vol. 7 (2006)
19. F. Schilder, H.M. Osinga, W. Vogt, Continuation of quasi-periodic invariant tori. SIAM J. Appl. Dyn. Syst. **4**(3), 459–488 (2005)
20. A. Denjoy, Sur les courbes definies par les equations differentielles a la surface du tore. J. Math. Pures et Appl. **11**, 333–375 (1932)
21. Y. Katznelson, D. Ornstein, The absolute continuity of the conjugation of certain diffeomorphisms of the circle. Ergod. Theory Dyn. Syst. **9**, 681–690 (1989)
22. Y. Katznelson, D. Ornstein, The differentiability of the conjugation of certain diffeomorphisms of the circle. Ergod. Theory Dyn. Syst. **9**, 643–680 (1989)

23. J.C. Yoccoz, Conjugaison differentiable des diffeomorphismes du cercle dont le nombre de rotation verifie une condition diophantine. Ann. Sci. l'École Norm. Supér. **17**(3), 333-359 (1984)
24. M. Herman, Simple proofs of local conjugacy theorems for diffeomorphisms of the circle with almost every rotation number. Boletim da Sociedade Brasileira de Matemática **16**(1), 45–83 (1985)
25. M.R. Herman, Resultats recents sur la conjugaison differentiable, in *Proceedings of the International Congress of Mathematicians, Helsinki*, vol. 2 (American Mathematical Society, Providence, 1978), pp. 811–820

Chapter 8
Heat Transfer in a Complex Medium

A.G. Ramm

Abstract The heat equation is considered in the complex medium consisting of many small bodies (particles) embedded in a given material. On the surfaces of the small bodies an impedance boundary condition is imposed. An equation for the limiting field is derived when the characteristic size a of the small bodies tends to zero, their total number $\mathcal{N}(a)$ tends to infinity at a suitable rate, and the distance $d = d(a)$ between neighboring small bodies tends to zero: $a << d$, $\lim_{a\to 0} \frac{a}{d(a)} = 0$. No periodicity is assumed about the distribution of the small bodies. These results are basic for a method of creating a medium in which heat signals are transmitted along a given line. The technical part for this method is based on an inverse problem of finding potential with prescribed eigenvalues.

MSC 80M40; 80A20, 35B99; 35K20; 35Q41; 35R30;74A30; 74G75

PACS 65.80.-g

8.1 Introduction and Results

In this paper the problem of heat transfer in a complex medium consisting of many small impedance particles of an arbitrary shape is solved. Equation for the effective limiting temperature is derived when the characteristic size a of the particles tends to zero while their number tends to infinity at a suitable rate while the distance d between closest neighboring particles is much larger than a, $d >> a$.

These results are used for developing a method for creating materials in which heat is transmitted along a line. Thus, the information can be transmitted by a heat signals.

A.G. Ramm (✉)
Department of Mathematics, Kansas State University, Manhattan, KS 66506-2602, USA
e-mail: ramm@math.ksu.edu

C. Skiadas (ed.), *The Foundations of Chaos Revisited: From Poincaré to Recent Advancements*, Understanding Complex Systems,
DOI 10.1007/978-3-319-29701-9_8

The contents of this paper is based on the earlier papers of the author cited in the bibliography, especially [13, 16, 17].

Let many small bodies (particles) D_m, $1 \leq m \leq M$, of an arbitrary shape be distributed in a bounded domain $D \subset \mathbb{R}^3$, $\text{diam}D_m = 2a$, and the boundary of D_m is denoted by $\mathcal{S}_m$ and is assumed twice continuously differentiable. The small bodies are distributed according to the law

$$\mathcal{N}(\Delta) = \frac{1}{a^{2-\kappa}} \int_{\Delta} N(x)dx[1 + o(1)], \quad a \to 0. \tag{8.1}$$

Here $\Delta \subset D$ is an arbitrary open subdomain of D, $\kappa \in [0, 1)$ is a constant, $N(x) \geq 0$ is a continuous function, and $\mathcal{N}(\Delta)$ is the number of the small bodies D_m in Δ. The heat equation can be stated as follows:

$$u_t = \nabla^2 u + f(x) \text{ in } \mathbb{R}^3 \setminus \bigcup_{m=1}^{M} D_m, := \Omega, \quad u|_{t=0} = 0, \tag{8.2}$$

$$u_N = \zeta_m u \text{ on } \mathcal{S}_m, \quad 1 \leq m \leq M, \qquad Re\zeta_m \geq 0. \tag{8.3}$$

Here N is the outer unit normal to $\mathcal{S}$,

$$\mathcal{S} := \bigcup_{m=1}^{M} \mathcal{S}_m, \quad \zeta_m = \frac{h(x_m)}{a^{\kappa}}, \quad x_m \in D_m, \quad 1 \leq m \leq M,$$

and $h(x)$ is a continuous function in D, $\text{Re}h \geq 0$.

Denote

$$\mathcal{U} := \mathcal{U}(x, \lambda) = \int_0^{\infty} e^{-\lambda t} u(x, t)dt.$$

Then, taking the Laplace transform of Eqs. (8.2)–(8.3) one gets:

$$-\nabla^2 \mathcal{U} + \lambda \mathcal{U} = \lambda^{-1} f(x) \text{ in } \Omega, \tag{8.4}$$

$$\mathcal{U}_N = \zeta_m \mathcal{U} \text{ on } \mathcal{S}_m, 1 \leq m \leq M. \tag{8.5}$$

Let

$$g(x, y) := g(x, y, \lambda) := \frac{e^{-\sqrt{\lambda}|x-y|}}{4\pi|x - y|}, \tag{8.6}$$

$$F(x, \lambda) := \frac{1}{\lambda} \int_{\mathbb{R}^3} g(x, y) f(y)dy. \tag{8.7}$$

Look for the solution to (8.4)–(8.5) of the form

$$\mathcal{U}(x,\lambda) = F(x,\lambda) + \sum_{m=1}^{M} \int_{\mathcal{S}_m} g(x,s)\sigma_m(s)ds, \tag{8.8}$$

where

$$\mathcal{U}(x,\lambda) := \mathcal{U}(x) := \mathcal{U}, \tag{8.9}$$

and $\mathcal{U}(x)$ depends on λ.

The functions σ_m are unknown and should be found from the boundary conditions (8.5). Equation (8.4) is satisfied by $\mathcal{U}$ of the form (8.8) with arbitrary continuous σ_m. To satisfy the boundary condition (8.5) one has to solve the following equation obtained from the boundary condition (8.5):

$$\frac{\partial \mathcal{U}_e(x)}{\partial N} + \frac{A_m\sigma_m - \sigma_m}{2} - \zeta_m\mathcal{U}_e - \zeta_m T_m\sigma_m = 0 \text{ on } \mathcal{S}_m, \quad 1 \le m \le M, \tag{8.10}$$

where the effective field $\mathcal{U}_e(x)$ is defined by the formula:

$$\mathcal{U}_e(x) := \mathcal{U}_{e,m}(x) := \mathcal{U}(x) - \int_{\mathcal{S}_m} g(x,s)\sigma_m(s)ds, \tag{8.11}$$

the operator T_m is defined by the formula:

$$T_m\sigma_m = \int_{\mathcal{S}_m} g(s,s')\sigma_m(s')ds', \tag{8.12}$$

and A_m is:

$$A_m\sigma_m = 2\int_{\mathcal{S}_m} \frac{\partial g(s,s')}{\partial N_s}\sigma_m(s')ds'. \tag{8.13}$$

In deriving Eq. (8.10) we have used the known formula for the outer limiting value on $\mathcal{S}_m$ of the normal derivative of a simple layer potential.

We now apply the ideas and methods for solving many-body scattering problems developed in [12–15].

Let us call $\mathcal{U}_{e,m}$ the effective (self-consistent) value of $\mathcal{U}$, acting on the m-th body. As $a \to 0$, the dependence on m disappears, since

$$\int_{\mathcal{S}_m} g(x,s)\sigma_m(s)ds \to 0 \text{ as } a \to 0.$$

One has

$$\mathcal{U}(x,\lambda) = F(x,\lambda) + \sum_{m=1}^{M} g(x,x_m)Q_m + \mathcal{J}_2, \quad x_m \in D_m, \tag{8.14}$$

where

$$Q_m := \int_{\mathcal{S}_m} \sigma_m(s)ds,$$

$$\mathcal{J}_2 := \sum_{m=1}^{M} \int_{\mathcal{S}_m} [g(x,s') - g(x,x_m)]\sigma_m(s')ds'. \tag{8.15}$$

Define

$$\mathcal{J}_1 := \sum_{m=1}^{M} g(x,x_m)Q_m. \tag{8.16}$$

We prove in Lemma 3, Sect. 8.4 (see also [13, 16]) that

$$|\mathcal{J}_2| << |\mathcal{J}_1| \text{ as } a \to 0 \tag{8.17}$$

provided that

$$\lim_{a\to 0} \frac{a}{d(a)} = 0, \tag{8.18}$$

where $d(a) = d$ is the minimal distance between neighboring particles.

If (8.17) holds, then problem (8.4)–(8.5) is solved asymptotically by the formula

$$\mathcal{U}(x,\lambda) = F(x,\lambda) + \sum_{m=1}^{M} g(x,x_m)Q_m, \quad a \to 0, \tag{8.19}$$

provided that asymptotic formulas for Q_m, as $a \to 0$, are found.

To find formulas for Q_m, let us integrate (8.10) over $\mathcal{S}_m$, estimate the order of the terms in the resulting equation as $a \to 0$, and keep the main terms, that is, neglect the terms of higher order of smallness as $a \to 0$.

We get

$$\int_{\mathcal{S}_m} \frac{\partial \mathcal{U}_e}{\partial N} ds = \int_{D_m} \nabla^2 \mathcal{U}_e dx = O(a^3). \tag{8.20}$$

Here we assumed that $|\nabla^2 \mathcal{U}_e| = O(1), a \to 0$. This assumption is valid since $\mathcal{U} = \lim_{a\to 0} \mathcal{U}_e$ is smooth as a solution to an elliptic equation. One has

$$\int_{\mathcal{S}_m} \frac{A_m \sigma_m - \sigma_m}{2} ds = -Q_m[1 + o(1)], \; a \to 0. \tag{8.21}$$

This relation is proved in Lemma 2, Sect. 8.4, see also [13]. Furthermore,

$$-\zeta_m \int_{\mathcal{S}_m} \mathcal{U}_e ds = -\zeta_m |\mathcal{S}_m| \mathcal{U}_e(x_m) = O(a^{2-\kappa}), \quad a \to 0, \tag{8.22}$$

where $|\mathcal{S}_m| = O(a^2)$ is the surface area of $\mathcal{S}_m$. Finally,

$$\begin{aligned} -\zeta_m \int_{\mathcal{S}_m} ds \int_{\mathcal{S}_m} g(s, s')\sigma_m(s')ds' &= -\zeta_m \int_{\mathcal{S}_m} ds' \sigma_m(s') \int_{\mathcal{S}_m} ds g(s, s') \\ &= Q_m O(a^{1-\kappa}), \qquad a \to 0. \end{aligned} \tag{8.23}$$

Thus, the main term of the asymptotic of Q_m, as $a \to 0$, is

$$Q_m = -\zeta_m |\mathcal{S}_m| \mathcal{U}_e(x_m). \tag{8.24}$$

Formulas (8.24) and (8.19) yield

$$\mathcal{U}(x, \lambda) = F(x, \lambda) - \sum_{m=1}^{M} g(x, x_m)\zeta_m |\mathcal{S}_m| \mathcal{U}_e(x_m, \lambda), \tag{8.25}$$

and

$$\mathcal{U}_e(x_m, \lambda) = F(x_m, \lambda) - \sum_{m' \neq m, m'=1}^{M} g(x_m, x_{m'})\zeta_{m'} |\mathcal{S}_{m'}| \mathcal{U}_e(x_{m'}, \lambda). \tag{8.26}$$

Denote

$$\mathcal{U}_e(x_m, \lambda) := \mathcal{U}_m, \quad F(x_m, \lambda) := F_m, \quad g(x_m, x_{m'}) := g_{mm'},$$

and write (8.26) as a linear algebraic system for $\mathcal{U}_m$:

$$\mathcal{U}_m = F_m - a^{2-\kappa} \sum_{m' \neq m} g_{mm'} h_{m'} c_{m'} \mathcal{U}_{m'}, \quad 1 \leq m \leq M, \tag{8.27}$$

where $h_{m'} = h(x_{m'})$, $\zeta_{m'} = \frac{h_{m'}}{a^\kappa}$, $c_{m'} := |S_{m'}| a^{-2}$.

Consider a partition of the bounded domain D, in which the small bodies are distributed, into a union of $P << M$ small nonintersecting cubes Δ_p, $1 \leq p \leq P$,

of side b,

$$b >> d, \quad b = b(a) \to 0 \quad \text{as } a \to 0 \quad \lim_{a\to 0} \frac{d(a)}{b(a)} = 0.$$

Let $x_p \in \Delta_p$, $|\Delta_p|$ = volume of Δ_p. One has

$$a^{2-\kappa} \sum_{m'=1, m' \neq m}^{M} g_{mm'} h_{m'} c_{m'} \mathcal{U}_{m'} = a^{2-\kappa} \sum_{p'=1, p' \neq p}^{P} g_{pp'} h_{p'} c_{p'} \mathcal{U}_{p'} \sum_{x_{m'} \in \Delta_{p'}} 1 =$$

$$= \sum_{p' \neq p} g_{pp'} h_{p'} c_{p'} \mathcal{U}_{p'} N(x_{p'}) |\Delta_{p'}| [1 + o(1)], \quad a \to 0. \tag{8.28}$$

Thus, (8.27) yields a linear algebraic system (LAS) of order $P << M$ for the unknowns $\mathcal{U}_p$:

$$\mathcal{U}_p = F_p - \sum_{p' \neq p, p'=1}^{P} g_{pp'} h_{p'} c_{p'} N_{p'} \mathcal{U}_{p'} |\Delta_{p'}|, \quad 1 \leq p \leq P. \tag{8.29}$$

Since $P << M$, the order of the original LAS (8.27) is drastically reduced. This is crucial when the number of particles tends to infinity and their size a tends to zero. We have assumed that

$$h_{m'} = h_{p'}[1 + o(1)], \quad c_{m'} = c_{p'}[1 + o(1)], \quad \mathcal{U}_{m'} = \mathcal{U}_{p'}[1 + o(1)], \ a \to 0, \tag{8.30}$$

for $x_{m'} \in \Delta_{p'}$. This assumption is justified, for example, if the functions $h(x)$, $\mathcal{U}(x, \lambda)$,

$$c(x) = \lim_{x_{m'} \in \Delta_x, a \to 0} \frac{|S_{m'}|}{a^2},$$

and $N(x)$ are continuous, but these assumptions can be relaxed.

The continuity of the $\mathcal{U}(x, \lambda)$ is a consequence of the fact that this function satisfies elliptic equation, and the continuity of $c(x)$ is assumed. If all the small bodies are identical, then $c(x) = c = const$, so in this case the function $c(x)$ is certainly continuous.

The sum in the right-hand side of (8.29) is the Riemannian sum for the integral

$$lim_{a\to 0} \sum_{p'=1, p' \neq p}^{P} g_{pp'} h_{p'} c_{p'} N(x_{p'}) \mathcal{U}_{p'} |\Delta'_p| =$$

$$\int_D g(x, y) h(y) c(y) N(y) \mathcal{U}(y, \lambda) dy$$

Therefore, linear algebraic system (8.29) is a collocation method for solving integral equation

$$\mathcal{U}(x,\lambda) = F(x,\lambda) - \int_D g(x,y)c(y)h(y)N(y)\mathcal{U}(y,\lambda)dy. \tag{8.31}$$

Convergence of this method for solving equations with weakly singular kernels is proved in [10], see also [11, 20].

Applying the operator $-\nabla^2 + \lambda$ to Eq. (8.31) one gets an elliptic differential equation:

$$(-\Delta + \lambda)\mathcal{U}(x,\lambda) = \frac{f(x)}{\lambda} - c(x)h(x)N(x)\mathcal{U}(x,\lambda). \tag{8.32}$$

Taking the inverse Laplace transform of this equation yields

$$u_t = \Delta u + f(x) - q(x)u, \quad q(x) := c(x)h(x)N(x). \tag{8.33}$$

Therefore, the limiting equation for the temperature contains the term $q(x)u$. Thus, the embedding of many small particles creates a distribution of source and sink terms in the medium, the distribution of which is described by the term $q(x)u$.

If one solves Eq. (8.31) for $\mathcal{U}(x,\lambda)$, or linear algebraic system (8.29) for $\mathcal{U}_p(\lambda)$, then one can Laplace-invert $\mathcal{U}(x,\lambda)$ for $\mathcal{U}(x,t)$. Numerical methods for Laplace inversion from the real axis are discussed in [4, 19].

If one is interested only in the average temperature, one can use the relation

$$\lim_{T\to\infty} \frac{1}{T}\int_0^T u(x,t)dt = \lim_{\lambda\to 0} \lambda\mathcal{U}(x,\lambda). \tag{8.34}$$

Relation (8.34) is proved in Lemma 1, Sect. 8.4. It holds if the limit on one of its sides exists. The limit on the right-hand side of (8.34) let us denote by $\psi(x)$. From Eqs. (8.7) and (8.31) it follows that ψ satisfies the equation

$$\psi = \varphi - B\varphi,$$

where

$$\varphi := \int_\Omega g_0(x,y)f(y)dy,$$

$$g_0(x,y) := \frac{1}{4\pi|x-y|},$$

$$B\psi := \int_\Omega g_0(x,y)q(y)\psi(y)dy,$$

and

$$q(x) := c(x)h(x)N(x).$$

The function ψ can be calculated by the formula

$$\psi(x) = (I + B)^{-1}\varphi. \tag{8.35}$$

From the physical point of view the function $h(x)$ is non-negative because the flux $-\nabla u$ of the heat flow is proportional to the temperature u and is directed along the outer normal N: $-u_N = h_1 u$, where $h_1 = -h < 0$. Thus, $q \geq 0$.

It is proved in [5, 6] that zero is not an eigenvalue of the operator $-\nabla^2 + q(x)$ provided that $q(x) \geq 0$ and

$$q = O\Big(\frac{1}{|x|^{2+\epsilon}}\Big), \quad |x| \to \infty,$$

and $\epsilon > 0$.

In our case, $q(x) = 0$ outside of the bounded region D, so the operator $(I + B)^{-1}$ exists and is bounded in $C(D)$.

Let us formulate our basic result.

Theorem 1 *Assume (8.1), (8.18), and $h \geq 0$. Then, there exists the limit $\mathcal{U}(x, \lambda)$ of $\mathcal{U}_e(x, \lambda)$ as $a \to 0$, $\mathcal{U}(x, \lambda)$ solves Eq. (8.31), and there exists the limit (8.34), where $\psi(x)$ is given by formula (8.35).*

Methods of our proof of Theorem 1 are quite different from the proof of homogenization theory results in [1, 3].

The author's plenary talk at Chaos-2015 Conference was published in [18].

8.2 Creating Materials Which Allows One to Transmit Heat Signals Along a Line

In applications it is of interest to have materials in which heat propagates along a line and decays fast in all the directions orthogonal to this line.

In this section a construction of such material is given. We follow [17] with some simplifications.

The idea is to create first the medium in which the heat transfer is governed by the equation

$$u_t = \Delta u - q(x)u \quad \text{in } D, \quad u|_S = 0, \quad u|_{t=0} = f(x), \tag{8.36}$$

where D is a bounded domain with a piece-wise smooth boundary S, $D = D_0 \times [0, L]$, $D_0 \subset \mathbb{R}^2$ is a smooth domain orthogonal to the axis x_1, $x = (x_1, x_2, x_3)$, $x_2, x_3 \in D_0$, $0 \leq x_1 \leq L$.

Such a medium is created by embedding many small impedance particles into a given domain D filled with a homogeneous material. A detailed argument, given in Sect. 8.1 (see also [13, 16]), yields the following result.

Assume that in every open subset Δ of D the number of small particles is defined by the formula:

$$\mathcal{N}(\Delta) = \frac{1}{a^{2-\kappa}} \int_{\Delta} N(x)dx[1 + o(1)], \quad a \to 0, \tag{8.37}$$

where $a > 0$ is the characteristic size of a small particle, $\kappa \in [0, 1)$ is a given number and $N(x) \geq 0$ is a continuous in D function.

Assume also that on the surface S_m of the m-th particle D_m the impedance boundary condition holds. Here

$$1 \leq m \leq M = \mathcal{N}(D) = O\left(\frac{1}{a^{2-\kappa}}\right), \quad a \to 0,$$

and the impedance boundary conditions are:

$$u_N = \zeta_m u \quad \text{on } S_m, \quad \text{Re}\zeta_m \geq 0, \tag{8.38}$$

where

$$\zeta_m := \frac{h(x_m)}{a^{\kappa}}$$

is the boundary impedance, $x_m \in D_m$ is an arbitrary point (since D_m is small the position of x_m in D_m is not important), κ is the same parameter as in (8.37) and $h(x)$ is a continuous in D function, $\text{Re}h \geq 0$, N is the unit normal to S_m pointing out of D_m. The functions $h(x)$, $N(x)$ and the number κ can be chosen as the experimenter wishes.

It is proved in Sect. 8.1 (see also [13, 16]) that, as $a \to 0$, the solution of the problem

$$u_t = \Delta u \quad \text{in} D \setminus \bigcup_{m=1}^{M} D_m, \; u_N = \zeta_m u \quad \text{on } S_m, \; 1 \leq m \leq M, \tag{8.39}$$

$$u|_S = 0, \tag{8.40}$$

and

$$u|_{t=0} = f(x), \tag{8.41}$$

has a limit $u(x, t)$. This limit solves problem (8.36) with

$$q(x) = c_S N(x)h(x), \tag{8.42}$$

where

$$c_S := \frac{|S_m|}{a^2} = const, \tag{8.43}$$

and $|S_m|$ is the surface area of S_m. By assuming that c_S is a constant, we assume, for simplicity only, that the small particles are identical in shape, see [13].

Since $N(x) \geq 0$ is an arbitrary continuous function and $h(x)$, $Reh \geq 0$, is an arbitrary continuous function, and both functions can be chosen by experimenter as he/she wishes, it is clear that an arbitrary real-valued potential q can be obtained by formula (8.42).

Suppose that

$$(-\Delta + q(x))\phi(x) = \lambda_n \phi_n, \quad \phi_n|_S = 0, \quad ||\phi_n||_{L^2(D)} = ||\phi_n|| = 1, \tag{8.44}$$

where $\{\phi_n\}$ is an orthonormal basis of $L^2(D) := H$. Then the unique solution to (8.36) is

$$u(x,t) = \sum_{n=1}^{\infty} e^{-\lambda_n t}(f, \phi_n)\phi_n(x). \tag{8.45}$$

If $q(x)$ is such that $\lambda_1 = 0$, $\lambda_2 \gg 1$, and $\lambda_2 \leq \lambda_3 \leq \dots$, then, as $t \to \infty$, the series (8.45) is well approximated by its first term

$$u(x,t) = (f, \phi_1)\phi_1 + O(e^{-10t}), \quad t \to \infty. \tag{8.46}$$

If $\lambda_1 > 0$ is very small, then the main term of the solution is

$$u(x,t) = (f, \phi_1)\phi_1 e^{-\lambda_1 t} + O(e^{-10t})$$

as $t \to \infty$. The term $e^{-\lambda_1 t} \sim 1$ if $t << \frac{1}{\lambda_1}$.

Thus, our problem is solved if $q(x)$ has the following property:

$$|\phi_1(x)| \text{decays as } \rho \text{ grows}, \quad \rho = (x_2^2 + x_3^2)^{1/2}. \tag{8.47}$$

Since the eigenfunction is normalized, $||\phi_1|| = 1$, this function will not tend to zero in a neighborhood of the line $\rho = 0$, so information can be transformed by the heat signals along the line $\rho = 0$, that is, along $s-$axis. Here we use the cylindrical coordinates:

$$x = (x_1, x_2, x_3) = (s, \rho, \theta), \quad s = x_1, \quad \rho = (x_2^2 + x_3^2)^{1/2}.$$

In Sect. 8.3 the domain D_0 is a disc and the potential $q(x)$ does not depend on θ.

The technical part of solving our problem consists of the construction of $q(x) = c_S N(x)h(x)$ such that

$$\lambda_1 = 0, \quad \lambda_2 \gg 1; \quad |\phi_1(x)| \text{ decays as } \rho \text{ grows.} \tag{8.48}$$

Since the function $N(x) \geq 0$ and $h(x), \mathrm{Re}h \geq 0$, are at our disposal, any desirable $q, \mathrm{Re}\, q \geq 0$, can be obtained by embedding many small impedance particles in a given domain D. In Sect. 8.3, a potential q with the desired properties is constructed. This construction allows one to transform information along a straight line using heat signals.

8.3 Construction of $q(x)$

Let

$$q(x) = p(\rho) + Q(s),$$

where $s := x_1$, $\rho := (x_2^2 + x_3^2)^{1/2}$. Then the solution to problem (8.44) is $u = v(\rho)w(s)$, where

$$-v_m'' - \rho^{-1}v_m' + p(\rho)v_m = \mu_m v_m, \quad 0 \leq \rho \leq R,$$
$$|v_m(0)| < \infty, \quad v_m(R) = 0, \tag{8.49}$$

and

$$-w_l'' + Q(s)w_l = \nu_l w_l, \quad 0 \leq s \leq L,$$
$$w_l(0) = 0, \quad w_l(L) = 0. \tag{8.50}$$

One has

$$\lambda_n = \mu_m + \nu_l, \quad n = n(m, l). \tag{8.51}$$

Our task is to find a potential $Q(s)$ such that $\nu_1 = 0$, $\nu_2 \gg 1$ and a potential $p(\rho)$ such that $\mu_1 = 0$, $\mu_2 \gg 1$ and $|v_m(\rho)|$ decays as ρ grows.

It is known how to construct $q(s)$ with the desired properties: the Gel'fand-Levitan method allows one to do this, see [7]. Let us recall this construction. One has $\nu_{l0} = l^2$, where we set $L = \pi$ and denote by ν_{l0} the eigenvalues of the problem (8.50) with $Q(s) = 0$. Let the eigenvalues of the operator (8.50) with $Q \neq 0$ be $\nu_1 = 0, \nu_2 = 11, \nu_3 = 14, \nu_l = \nu_{l0}$ for $l \geq 4$.

The kernel $L(x,y)$ in the Gel'fand-Levitan theory is defined as follows:

$$L(x,y)=\int_{-\infty}^{\infty}\frac{\sin(\sqrt{\lambda}x)}{\sqrt{\lambda}}\frac{\sin(\sqrt{\lambda}y)}{\sqrt{\lambda}}d(\varrho(\lambda)-\varrho_0(\lambda)),$$

where $\varrho(\lambda)$ is the spectral function of the operator (8.50) with the potential $Q=Q(s)$, and $\varrho_0(\lambda)$ is the spectral function of the operator (8.50) with the potential $Q=0$ and the same boundary conditions as for the operator with $Q\neq 0$.

Due to our choice of ν_l and the normalizing constants α_j, namely: $\alpha_j=\frac{\pi}{2}$ for $j\geq 2$ and $\alpha_1=\frac{\pi^3}{3}$, the kernel $L(x,y)$ is given explicitly by the formula:

$$L(x,y)=\frac{3xy}{\pi^3}+\frac{2}{\pi}\Big(\frac{\sin(\sqrt{\nu_2}x)}{\sqrt{\nu_2}}\frac{\sin(\sqrt{\nu_2}y)}{\sqrt{\nu_2}}+\frac{\sin(\sqrt{\nu_3}x)}{\sqrt{\nu_3}}\frac{\sin(\sqrt{\nu_3}y)}{\sqrt{\nu_3}}\Big)-$$
$$-\frac{2}{\pi}\Big(\sin x\sin y+\sin(2x)\sin(2y)+\sin(3x)\sin(3y)\Big),\quad (8.52)$$

where $\nu_1=0$, $\nu_2=11$ and $\nu_3=14$. This is a finite rank kernel. The term xy is the value of the function $\frac{\sin\nu x}{\nu}\frac{\sin\nu y}{\nu}$ at $\nu=0$, and the corresponding normalizing constant is $\frac{\pi^3}{3}=||x||^2=\int_0^\pi x^2dx$.

Solve the Gel'fand-Levitan equation:

$$K(s,\tau)+\int_0^s K(s,s')L(s',\tau)ds'=-L(s,\tau),\quad 0\leq\tau\leq s,\qquad (8.53)$$

which is uniquely solvable (see [7]). Since Eq. (8.53) has finite-rank kernel it can be solved analytically being equivalent to a linear algebraic system.

If the function $K(s,\tau)$ is found, then the potential $Q(s)$ is computed by the formula [2, 7]:

$$Q(s)=2\frac{dK(s,s)}{ds},\qquad (8.54)$$

and this $Q(s)$ has the required properties: $\nu_1=0,\nu_2\gg 1,\nu_l\leq\nu_{l+1}$.

Consider now the operator (8.49) for $v(\rho)$. Our problem is to calculate $p(\rho)$ which has the required properties:

$$\mu_1=0,\quad \mu_2\gg 1,\quad \mu_m\leq\mu_{m+1},$$

and $|\phi_m(\rho)|$ decays as ρ grows.

We reduce this problem to the previous one that was solved above. To do this, set $v=\frac{\psi}{\sqrt{\rho}}$. Then equation

$$-v''-\frac{1}{\rho}v'+p(\rho)v=\mu v,$$

is transformed to the equation

$$-\psi'' - \frac{1}{4\rho^2}\psi + p(\rho)\psi = \mu\psi. \tag{8.55}$$

Let

$$p(\rho) = \frac{1}{4\rho^2} + Q(\rho), \tag{8.56}$$

where $Q(\rho)$ is constructed above. Then Eq. (8.55) becomes

$$-\psi'' + Q(\rho)\psi = \mu\psi, \tag{8.57}$$

and the boundary conditions are:

$$\psi(R) = 0, \quad \psi(0) = 0. \tag{8.58}$$

The problem (8.57)–(8.58) has the desired eigenvalues $\mu_1 = 0, \mu_2 \gg 1, \mu_m \leq \mu_{m+1}$.

The eigenfunction

$$\phi_1(x) = v_1(\rho)w_1(s),$$

where $v_1(\rho) = \frac{\psi_1(\rho)}{\sqrt{\rho}}$, decays as ρ grows, and the eigenvalues λ_n can be calculated by the formula:

$$\lambda_n = \mu_m + \nu_l, \quad m, l \geq 1, \quad n = n(m, l).$$

Since $\mu_1 = \nu_1 = 0$ one has $\lambda_1 = 0$. Since $\nu_2 = 11$ and $\mu_2 = 11$, one has $\lambda_2 = 11 \gg 1$.

Thus, the desired potential is constructed:

$$q(x) = Q(s) + (\frac{1}{4\rho^2} + Q(\rho)),$$

where $Q(s)$ is given by formula (8.54).

This concludes the description of our procedure for the construction of q.

Remark 1 It is known (see, for example, [2]) that the normalizing constants

$$\alpha_j := \int_0^\pi \varphi_j^2(s)ds$$

and the eigenvalues λ_j, defined by the differential equation

$$-\frac{d^2\varphi_j}{ds^2} + Q(s)\varphi_j = \lambda_j\varphi_j,$$

the boundary conditions

$$\varphi_j'(0) = 0, \quad \varphi_j'(\pi) = 0,$$

and the normalizing condition $\varphi_j(0) = 1$, have the following asymptotic:

$$\alpha_j = \frac{\pi}{2} + O(\frac{1}{j^2}) \quad \text{as } j \to \infty,$$

and

$$\sqrt{\lambda_j} = j + O(\frac{1}{j}) \quad \text{as } j \to \infty.$$

The differential equation

$$-\Psi_j'' + Q(s)\Psi_j = \nu_j\Psi_j,$$

the boundary condition

$$\Psi_j(0) = 0, \quad \Psi_j(\pi) = 0,$$

and the normalizing condition $\Psi_j'(0) = 1$ imply

$$\sqrt{\lambda_j} = j + O(\frac{1}{j}) \quad \text{as} \quad j \to \infty,$$

$$\Psi_j(s) \sim \frac{\sin(js)}{j} \quad \text{as} \quad j \to \infty.$$

The main term of the normalized eigenfunction is:

$$\frac{\Psi_j}{||\Psi_j||} \sim \sqrt{2/\pi}\sin(js) \quad \text{as} \quad j \to \infty,$$

and the main term of the normalizing constant is:

$$\alpha_j \sim \frac{\pi}{2j^2} \quad \text{as} \quad j \to \infty.$$

8.4 Auxiliary Results

Lemma 1 *If one of the limits* $\lim_{t\to\infty} \frac{1}{t}\int_0^t u(s)ds$ *or* $\lim_{\lambda\to 0} \lambda\mathcal{U}(\lambda)$ *exists, then the other also exists and they are equal to each other:*

$$\lim_{t\to\infty} \frac{1}{t}\int_0^t u(s)ds = \lim_{\lambda\to 0} \lambda\mathcal{U}(\lambda),$$

where

$$\mathcal{U}(\lambda) := \int_0^\infty e^{-\lambda t}u(t)dt := \bar{u}(\lambda).$$

Proof Denote

$$\frac{1}{t}\int_0^t u(t)dt := v(t), \quad \bar{u}(\sigma) := \int_0^\infty e^{-\sigma t}u(t)dt.$$

Then

$$\bar{v}(\lambda) = \int_\lambda^\infty \frac{\bar{u}(\sigma)}{\sigma}d\sigma$$

by the properties of the Laplace transform.

Assume that the limit $v(\infty) := v_\infty$ exists:

$$\lim_{t\to\infty} v(t) = v_\infty. \tag{8.59}$$

Then,

$$v_\infty = \lim_{\lambda\to 0} \lambda\int_0^\infty e^{-\lambda t}v(t)dt = \lim_{\lambda\to 0} \lambda\bar{v}(\lambda).$$

Indeed $\lambda\int_0^\infty e^{-\lambda t}dt = 1$, so

$$\lim_{\lambda\to 0} \lambda\int_0^\infty e^{-\lambda t}(v(t) - v_\infty)dt = 0,$$

and (8.59) is verified.

One has

$$\lim_{\lambda\to 0} \lambda\bar{v}(\lambda) = \lim_{\lambda\to 0}\int_\lambda^\infty \frac{\lambda}{\sigma}\bar{u}(\sigma)d\sigma = \lim_{\lambda\to 0} \lambda\bar{u}(\lambda), \tag{8.60}$$

as follows from a simple calculation:

$$\lim_{\lambda\to 0}\int_\lambda^\infty \frac{\lambda}{\sigma}\bar{u}(\sigma)d\sigma = \lim_{\lambda\to 0}\int_\lambda^\infty \frac{\lambda}{\sigma^2}\sigma\bar{u}(\sigma)d\sigma = \lim_{\sigma\to 0}\sigma\bar{u}(\sigma), \tag{8.61}$$

where we have used the relation $\int_\lambda^\infty \frac{\lambda}{\sigma^2}d\sigma = 1$.

Alternatively, let $\sigma^{-1} = \gamma$. Then,

$$\int_\lambda^\infty \frac{\lambda}{\sigma^2}\sigma\bar{u}(\sigma)d\sigma = \frac{1}{1/\lambda}\int_0^{1/\lambda}\frac{1}{\gamma}\bar{u}(\frac{1}{\gamma})d\gamma = \frac{1}{\omega}\int_0^\omega \frac{1}{\gamma}\bar{u}(\frac{1}{\gamma})d\gamma. \tag{8.62}$$

If $\lambda \to 0$, then $\omega = \lambda^{-1} \to \infty$, and if

$$\psi := \gamma^{-1}\bar{u}(\gamma^{-1}),$$

then

$$\lim_{\omega\to\infty}\frac{1}{\omega}\int_0^\omega \psi d\gamma = \psi(\infty) = \lim_{\gamma\to 0}\gamma^{-1}\bar{u}(\gamma^{-1}) = \lim_{\sigma\to\infty}\sigma\bar{u}(\sigma). \tag{8.63}$$

Lemma 1 is proved. □

Lemma 2 *Equation (8.21) holds.*

Proof As $a \to 0$, one has

$$\frac{\partial}{\partial N_s}\frac{e^{-\sqrt{\lambda}|s-s'|}}{4\pi|s-s'|} = \frac{\partial}{\partial N_s}\frac{1}{4\pi|s-s'|} + \frac{\partial}{\partial N_s}\frac{e^{-\sqrt{\lambda}|s-s'|}-1}{4\pi|s-s'|}. \tag{8.64}$$

It is known (see [8]) that

$$\int_{\mathcal{S}_m} ds\int_{\mathcal{S}_m}\frac{\partial}{\partial N_s}\frac{1}{4\pi|s-s'|}\sigma_m(s')ds' = -\frac{1}{2}\int_{\mathcal{S}_m}\sigma_m(s')ds' = -\frac{1}{2}Q_m. \tag{8.65}$$

On the other hand, as $a \to 0$, one has

$$\left|\int_{\mathcal{S}_m} ds\int_{\mathcal{S}_m}\frac{e^{-\sqrt{\lambda}|s-s'|}-1}{4\pi|s-s'|}\sigma_m(s')ds'\right| \le |Q_m|\int_{\mathcal{S}_m} ds\frac{1-e^{-\sqrt{\lambda}|s-s'|}}{4\pi|s-s'|} = o(Q_m). \tag{8.66}$$

The relations (8.65) and (8.66) justify (8.21).

Lemma 2 is proved. □

Lemma 3 *If assumption (8.18) holds, then inequality (8.17) holds.*

Proof One has

$$\mathcal{J}_{1,m} := |g(x, x_m)Q| = \frac{|Q_m|e^{-\sqrt{\lambda}|x-x_m|}}{4\pi|x-x_m|}, \tag{8.67}$$

and

$$\mathcal{J}_{2,m} \leq \frac{e^{-\sqrt{\lambda}|x-x_m|}}{4\pi|x-x_m|} \max\left(\sqrt{\lambda}a, \frac{a}{|x-x_m|}\right) \int_{\mathcal{S}_m} |\sigma_m(s')|ds' \tag{8.68}$$

where $|x - x_m| \geq d$, and $d > 0$ is the smallest distance between two neighboring particles. One may consider only those values of λ for which $\lambda^{1/4}a < \frac{a}{d}$, because for the large values of λ, such that $\lambda^{1/4} \geq \frac{1}{d}$ the value of $e^{-\sqrt{\lambda}|x-x_m|}$ is negligibly small. The average temperature depends on the behavior of $\mathcal{U}$ for small λ, see Lemma 1.

One has $|Q_m| = \int_{\mathcal{S}_m} |\sigma_m(s')|ds' > 0$ because σ_m keeps sign on $\mathcal{S}_m$, as follows from Eq. (8.24) as $a \to 0$.

It follows from (8.67)–(8.68) that

$$\left|\frac{\mathcal{J}_{2,m}}{\mathcal{J}_{1,m}}\right| \leq O\left(\left|\frac{a}{x-x_m}\right|\right) \leq O\left(\frac{a}{d}\right) << 1. \tag{8.69}$$

From (8.69) by the arguments similar to the given in [9] one obtains (8.17).

Lemma 3 is proved. □

References

1. V. Jikov, S. Kozlov, O. Oleinik, *Homogenization of Differential Operators and Integral Functionals* (Springer, Berlin, 1994)
2. B.M. Levitan, *Inverse Sturm-Liouville Problems* (VNU Press, Utrecht, 1987)
3. V.A. Marchenko, E.Ya. Khruslov, *Homogenization of Partial Differential Equations* (Birkhäuser, Boston, 2006)
4. A.G. Ramm, Inversion of the Laplace transform from the real axis. Inverse Prob. **2**, L55–L59 (1986)
5. A.G. Ramm, Sufficient conditions for zero not to be an eigenvalue of the Schrödinger operator. J. Math. Phys. **28**, 1341–1343 (1987)
6. A.G. Ramm, Conditions for zero not to be an eigenvalue of the Schrödinger operator. J. Math. Phys. **29**, 1431–1432 (1988)
7. A.G. Ramm, *Inverse Problems* (Springer, New York, 2005)
8. A.G. Ramm, *Wave Scattering by Small Bodies of Arbitrary Shapes* (World Scientific Publishers, Singapore, 2005)
9. A.G. Ramm, Many-body wave scattering by small bodies and applications. J. Math. Phys. **48**(N10), 103511 (2007)
10. A.G. Ramm, A collocation method for solving integral equations. Int. J. Comput. Sci. Math. **3**(N2), 222–228 (2009)

11. A.G. Ramm, Collocation method for solving some integral equations of estimation theory. Int. J. Pure Appl. Math. **62**(N1), 57–65 (2010)
12. A.G. Ramm, Wave scattering by many small bodies and creating materials with a desired refraction coefficient. Afr. Mat. **22**(N1), 33–55 (2011)
13. A.G. Ramm, *Scattering of Acoustic and Electromagnetic Waves by Small Bodies of Arbitrary Shapes. Applications To Creating New Engineered Materials* (Momentum Press, New York, 2013)
14. A.G. Ramm, Many-body wave scattering problems in the case of small scatterers. J. Appl. Math. Comput. **41**(N1), 473–500 (2013). doi:10.1007/s12190-012-0609-1
15. A.G. Ramm, Wave scattering by many small bodies: transmission boundary conditions. Rep. Math. Phys. **71**(N3), 279–290 (2013)
16. A.G. Ramm, Heat transfer in a medium in which many small particles are embedded. Math. Model. Nat. Phenom. **8**(N1), 193–199 (2013)
17. A.G. Ramm, Creating materials in which heat propagates along a line. Boll Union. Math. Ital. **8**(N3), 165–168 (2015). doi:10.1007/s40574-015-0033-1 (Published 8 Sept. 2015)
18. A.G. Ramm, Scattering of EM waves by many small perfectly conducting or impedance bodies. J. Math. Phys. **56**(N9), 091901 (2015)
19. A.G. Ramm, S. Indratno, Inversion of the Laplace transform from the real axis using an adaptive iterative method. Int. J. Math. Math. Sci. **2009**(Article 898195), 38 (2009)
20. A.G. Ramm, S. Indratno, A collocation method for solving some integral equations in distributions. J. Comput. Appl. Math. **236**, 1296–1313 (2011)

Chapter 9
Plasma Hysteresis and Instability: A Memory Perspective

V.J. Law, W.G. Graham, and D.P. Dowling

Abstract This paper presents a historical review of the significance of Duddell 'Singing-arc' in the context of its application of deleterious effects in the control of both hysteresis and spatial-temporal stability as the two-electrode valve evolved into the three-electrode triode vacuum tube. The use of oscillograph Lissajous figure in I-V plane, Q-V plane and harmonic plane in investigating of these deleterious effects within modern low-pressure parallel-plate systems and atmospheric pressure plasma system are illustrated and compared the hysteresis and stability within the 'Singing arc'. The development from the original oscillograph measurement today's analog, digital, and software methods of measurement is considered. The question, whether the 'Signing-arc' and other plasma systems fall in the category of a memory element is discussed.

9.1 Historical Introduction

The understanding of the electric, optical and acoustic performance of modern plasma systems has its origins well before Sir Humphry Davy's direct current carbon-arc light that replaced the gas street lighting systems in major European cities. Arguably, the investigative work on complex harmonic motion by Nathaniel Bowditch (1773–1838) and later by Jules-Antoine Lissajous (1822–1880) provided the mathematical and the graphical tools [1] for the measurement of periodic waveforms and harmonics. This viewpoint is supported by considering in the development of electrical, optical and acoustic measurements of the early carbon electric arc that had the annoying drawback of generating an audible hissing sounding and changing luminosity. Over a century later, this hissing sound is thought to be one of the first chaotic processes to be reported [2].

V.J. Law (✉) • D.P. Dowling
School of Mechanical and Materials Engineering, University College Dublin, Belfield, Dublin, Ireland
e-mail: viclaw66@gmail.com

W.G. Graham
Centre for Plasma Physics, Queen's University Belfast, Belfast BT7 1NN, UK

C. Skiadas (ed.), *The Foundations of Chaos Revisited: From Poincaré to Recent Advancements*, Understanding Complex Systems,
DOI 10.1007/978-3-319-29701-9_9

The aim of this paper is to reviews the early work on the 'Singing-arc' and is development into the triode vacuum tube. The use of Lissajous figures to understand instabilities, hysteresis, power dissipation within modern atmospheric plasma sources is then discussed, leading to the generation of Lissajous figures from the original 'Singing-arc' data.

9.2 Historical Perspective

In 1899 the English scientist William Edward Ayrton asked Hertha Ayrton and William Du Bois Duddell to solve these problems. Their experimental investigations used an inductor and capacitor circuit shunted across the arc and a resistor in series with the arc, they also used a newly invented cinematic film recording oscillograph and thermo-galvanometer for recording time-vary electrical waveforms and optical intensities [3]. Duddell found that by applying a shunt circuit to the arc, the audible sound is transformed from a hissing sound to a hum with musical tones ranging between 500 and 15,000 Hz [4]. Additionally their oscillograph records revealed that the time dependent current, voltage and optical intensities changed from a deterministic signature for the hissing mode to a near-smooth sinusoidal waveform for the hum mode where a by-product of the hum mode is that it extended working life of the carbon electrodes. Within this work [4], Duddell also acknowledges Alexander Pelham Trotter's study that showed the rotational velocity of the ace is synchronised to the acoustic emission frequency when the arc is in the humming mode [5]. Moreover, telephony experiments by Hermann Theodor Simon revealed that a microphone and a receiver can be coupled to the resonant circuit using a second inductor coil [6]. Earlier, Duddell used this experimental approach to play 'God Save the Queen' at a meeting of the London Institution of Electrical Engineers in 1899 [7]. In 1902 Paul Jennet (1863–1937) published a mathematical treatment of the electrical circuit and arrived at a conclusion that agreed with those of Duddell [8]. André Blondel (1863–1938) made improvement of the Lord Kelvin resonant frequency formula by introducing an internal resistive loss within the inductor to account for the observed damped oscillations [9].

Figure 9.1 shows the basic topology of Duddell's 'Singing-arc' circuit with Simon's transformer telephony circuit, where L_2 is the secondary coil, m is the mutual inductance and M and R are the microphone, or antenna, resistivity. The arc may be in an open air or in a glass globe. The carbon rods are approximately 10 mm in diameter with their opposing end gas-gap separation is of the order of 0.2 to 1 mm. Also shown are the components values based on [10] for a fixed resonant frequency, $f_o = 15$ kHz, where the undamped resonant frequency formula is used

$$f_0 = \frac{1}{2\pi\sqrt{LC}} \tag{9.1}$$

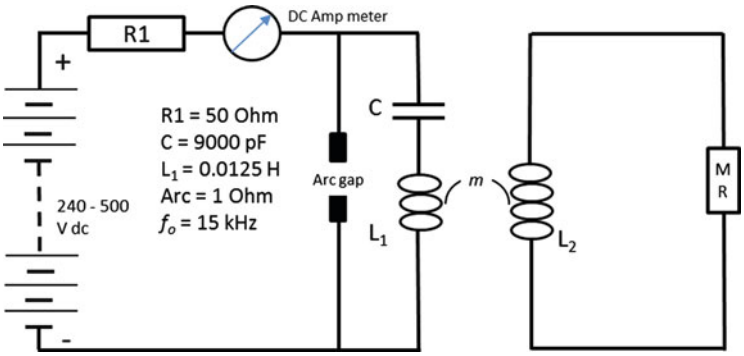

Fig. 9.1 Circuit topology of Duddell's 'Singing-arc' (*left*) and Simon's telephony coupling circuit (*right*)

where L_1, the inductance, and C the, capacitance and have the values given in Fig. 9.1.

An important omission from the circuit is the transformation of the dc input into two components, one flowing through shunt circuit and the other flowing through the arc [6]. Hence, the arc's I-V characteristic changes from a static characteristic (no shunt circuit applied) to a dynamic characteristic (shunt circuit applied).

Using a Lissajous representation of the current and voltage (I-V) waveforms Simon was also able to demonstrate that the rising voltage curve is different from the falling voltage curve so inducing 'Lichtbogenhysteresis' (arc hysteresis) [6]. The hysteresis effect is thought to be due to the arc's gas-gap being sufficiently ionized to allow two parallel currents: one flowing through arc and the other flowing through the shunt circuit. In the case of the shunt circuit, the capacitor determines the characteristic charging and discharging time which is much slower than the arc since the electrons in ionized gas (plasma) follow the instantaneous electric field within the arc almost instantaneously: so the current waveforms becomes harmonically distorted. By 1912, the development of the electric oscilloscope allowed J.E. Hoyt to publish an oscilloscope study of the dynamic acoustic and electrical dynamic characteristics of the 'Singing-arc' [11]. In this work Hoyt reveals that the dynamic characteristic of the 'Singing-arc' has a distorted limit cycle with no double pinched hysteresis loop in the I-V plane both for the current flowing through the arc and through the shunt circuit. Thus indicating that the cinematic film recording of the oscillograph did not compromise the earlier work of Duddell [4] and Simon [6]. Although, Duddell, Simon, and Hoyt did not report a loop pinching in the I-V hysteresis loop [2], Ginoux and Rossetto have conjectured that the 'Singing-arc' may be one of the oldest memristor [12]; in Sect. 9.5 this conjecture is discussed. Modern (1994–2016) experiments and theoretic analysis have shown that power coupling into plasma is the driving force of the observed hysteresis [13–17]. Nevertheless, the Lissajous figure has become one of the main diagnostic standards for measuring the electric performance of plasma systems. By 1903 Valdemar

Poulsen (1869–1942) had isolated the arc's two electrodes in a glass envelope so that experiments using different; gases, electrode material and magnetic fields could be studied. Using a copper anode within the glass envelope containing hydrogen gas plus the addition of a transverse magnetic field, he found the arc produced an undamped or continuous wave (CW) frequency up to 200 kHz with considerably more power (1 MW) developed in the antenna circuit with respect to the arc burning in air. This configuration became known as the 'arc-convertor' and patented as a CW radio transmitter [18] and was used commercially in high-power long-distance radiotelegraphy until superseded by the triode vacuum tube in the 1920s.

The triode vacuum tube became a practical device only after a number of development stages; for example from the Ambrose Fleming's thermionic valve (subsequently owned by Guglielmo Marconi) through the Poulsen's arc-converter, and then to the Lee De Forest's partially evacuated (now termed soft valve) Audion. The (U.S. Patent 841387) version of Audion had a third electrode placed within the glass envelope between the emitter and plate used to amplitude-modulate the detected electrical signal: thus making a new receiver for wireless telegraphy. Due to residual gas within the soft vacuum, of the Audion, the valve however still had many unpredictable amplitude modulation problems. Harold D Arnold (AT&T's Western Electric research branch) saw how these problems could be overcome, however valve could still be useful as an amplifier in long distance telephony. By 1914 the Audion valve was evacuated to a high vacuum standard of approximately 7.6×10^{-7} Torr allowing the modulation stage to work properly and was renamed the 'Kenotron' from the Greek word keno (empty, as in a vacuum) and tron (device, or instrument). Lee De Forest believed the residual gas was essential to its operation and maybe perhaps that is why he contracted the Latin verb 'aud' (derived from the verb to mean hear) and the Greek noun 'ion' to create the word Audion to describe his valve.

Irving Langmuir was first the person to propose that the mutual repulsion of electrons (space-charge effect) is the basic mechanism that controls electronic conduction in a high (hard) vacuum [19]. Moreover, his experimental analysis revealed that molecular gas impurities (N_2, O_2, H_2O and CO) when ionised or dissociated caused a reduction in the current flow, thus giving us the understanding of the root cause of the erratic behaviour of the Audion valve.

Through happenstance at the outbreak of World War 1 (WW1) the Audion and Kenotron valve fell in to the hands of the Marconi Company in London by Paul Pichon [20] and from there in 1916 a production line model was produced in France as the TM triode and in England as the R valve.

In the 1920s B. Van de Pol, J. Van de Mark and V.E. Appleton published a series of paper on experimental studies on the relaxation oscillations and hysteresis within the triode vacuum tube. This led to a mathematical model for the production of harmonics and sub harmonics at the extreme limit of the vacuum tube's external circuit [21–23]. Reference [24] provides a good historical review of the relaxation oscillation model, too.

A recent re-evaluation of the work of Joules Henri Poincaré [25] has revealed that he too played a significant role in the mathematical understanding of the arc's stable

regime using limit cycles and their deviation that regime. Even though Poincaré did not study the triode vacuum tube, the review claims that the two-electrode 'Singing-arc' is analogous to the three-electrode triode vacuum tube. Given the extended triode development time-line it would seem unlikely that, at Poincaré's wireless telegraphy conference in 1908 or at the time close to his death in 1912, he was able to deduce or describe the behaviour of early triode vacuum tubes that operated under soft or hard vacuum conditions. Nevertheless, Poincaré's closed limit cycles do predate the work of Van de Pol, and J. Van de Mark [22] along with Andronov self-oscillations [26].

Beyond this period, the electric arc continues to be used as an intense light source for searchlights and lighthouses, as a source of UV radiation in gas discharge lamps [2] and plasma welding of metal components [27]. In bringing the electric arc in to the twentieth and twenty-first century, a redesign of the discharge electrode configuration so that the ionized gas is directed onto a target surface has brought new technological plasma processing importance. From Duddell's, and Pioncaré's, point of view the atmospheric pressure cathode-cavity torch design may be a recognisable design [28, 29]. However low gas kinetic temperature plasma jets [30–34] and the parallel-plate dielectric barrier discharge (DBD) may not be so recognisable [13–15, 35–38]. Nevertheless, in each case closed limit cycles and their deviation from the cycle are employed to visualise the electrical, optical and acoustic and parameters.

9.3 Lissajous Figure as a Plasma Diagnostic

We have mentioned that the Lissajous figure has provided a means of understanding the electrical performance of electric discharge. It continues to have a role as modern plasma diagnostic for both atmospheric- and low-pressure plasma systems. The following paragraphs provide a few examples of how Lissajous figures in three different planes (current–voltage (I-V), charge–voltage (Q-V) plane and the harmonic plane) that are currently used in the characterisation of atmospheric pressure jets, DBD and low-pressure parallel-plate plasma system operating in the MHz range.

9.3.1 I-V Plane

In this section, the I-V-plane of two pilot scale atmospheric pressure plasma systems are presented Sect. 9.3.1.1 deals with a helium-based plasma jet (specially the PlasmaStream [17, 32]) and Sect. 9.3.1.2 looks at the I-V of helium-based atmospheric pressure parallel-plate reel-to-reel plasma system [16]. These two plasma systems were developed for low temperature plasma treatment of polymers and biological materials.

9.3.1.1 Plasma Jet

The atmospheric pressure plasma jet discussed here uses a high voltage flyback transformer producing a non-sinusoidal voltage waveform in the 11–20 kHz range [17, 30]. The jet uses helium gas (99.999 % purity) which when ionised nitrogen, oxygen species are generated. A typical triplet of Lissajous figures is shown in Fig. 9.2a–c in the I-V plane as a function of helium gas flow rate ($a = 1$, $b = 4$ and $c = 10$) standard litre per minute (slm) and drive frequency 18, 14 and 11 kHz, respectively. Shown to the right of each plot is its time average digital image.

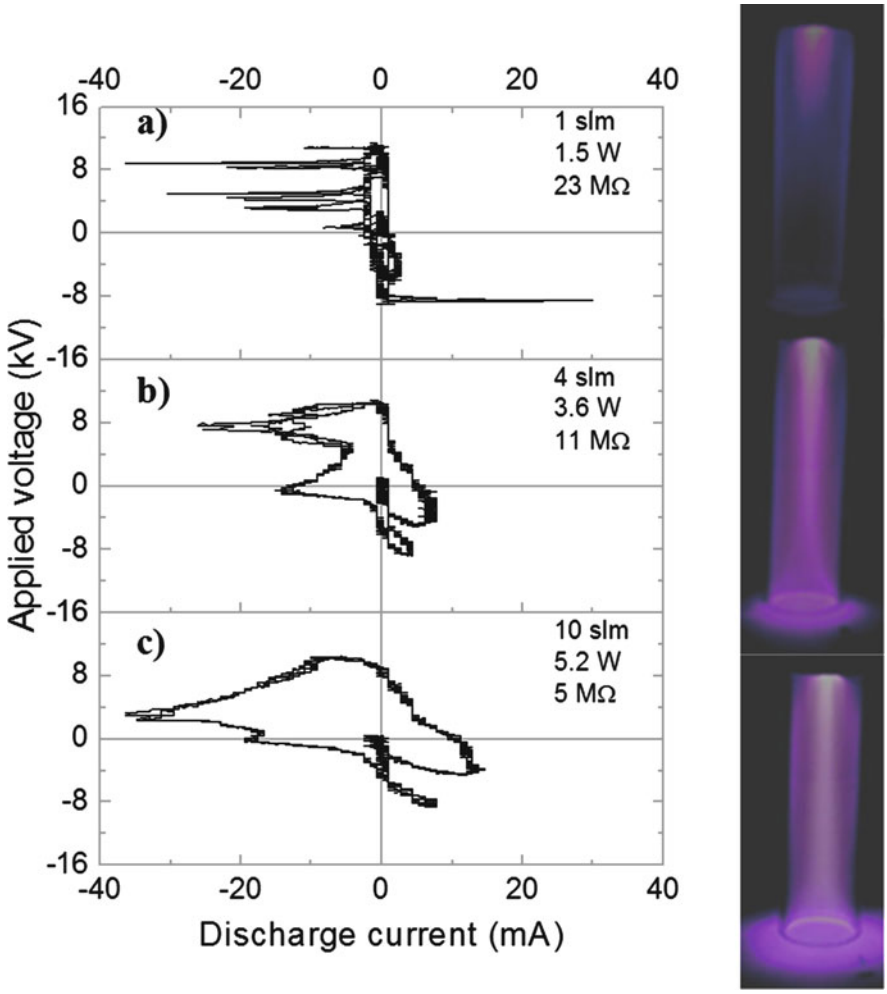

Fig. 9.2 An I-V plane plot of discharge current and voltage as a function of the gas flow rate. To the right of each I-V plane is the associated discharge time average digital image [17]

In Fig. 9.2a it can be seen that the 1 slm the I-V plane exhibits a chaotic attractor. For example in the bottom right quadrant the attractor exhibits three positive current spikes overlaying each other at the maximum negative voltage point. This is due to the collapse of the magnetic field associated with the flyback transformer and the resultant release of the stored energy. In the top left quadrant of Fig. 9.2a the attractor has three sets of two negative voltage spikes of different amplitudes and time delays. The six current spikes are approximately 1 μs long and falling within a 15 μs envelope. These current spikes are due to the discharge having irregular temporal and spatial electrical properties.

With increasing helium flow (Fig. 9.2b, c) the I-V plane attractor becomes quasi-periodic, or a closed limit cycle, with two spikes of negative current of approximately 15 μs per period. The time delay of these current spikes is similar to that at the low helium flow rate. A feature to note in Fig. 9.2b and c is the single negative going voltage loop in the lower right quadrant. The correct interpretation of this single loop is a zero-crossing point of the flyback transformer rather than the behaviour of a memristor that requires a double pinch hysteresis loop in the I-V plane [2, 12].

9.3.1.2 Parallel-Plate DBD Reel-to-Reel Plasma

One of the simplest nonthermal atmospheric plasma is the DBD. A large system based on the Dow Corning SE-1100 LabLine™ reel-to-reel system is discussed [16]. This plasma system uses flowing helium gas to produce an atmospheric pressure glow discharge (APGD) where there are two plasma current pulses of opposite polarity per cycle. The APGD is powered by a bipolar variable frequency (16–25 kHz) matching power supply with, powers of up to 1000 W per chamber, where each chambers measures 320 mm × 320 mm with a 5 mm gas-gap. Within the gas-gap, a web handling system allows rolls of polymer material to be passed through the plasma, while 99.999 % pure helium is flowing through the gas-gap. The current and voltage measurements captured using 1000-to-1 voltage probe and a current monitor, and acquired using a 100 MS/s National Instrument data logger and processed using LabVIEW 2010 software.

Figure 9.3 is an I-V plane snapshot of the system operating in pure helium at 18.92 kHz over 20 periods (1 ms). It is shown that each period produces a unique limit cycle, where the bipolar power supply produces a symmetric characteristic at each polarity with the breakdown occurring at close to (±3000 V). Within each period, specific phase regions have different period-to-period stability profiles. The regions that show the most marked phase instability are the region of glow discharge. The onset of each glow region starts at the breakdown voltage (±3000 V) from where the glow current rapidly increases. The two highlighted blue lines depict the first in the sequence of glow periods and the two arrows mark the region of collapse of the glow. Note how each consecutive glow advances in phase space by approximately +0.3 μs per period to produces a total phase shift of some +6 μs, while the glow collapse is compressed to approximately +3 μs.

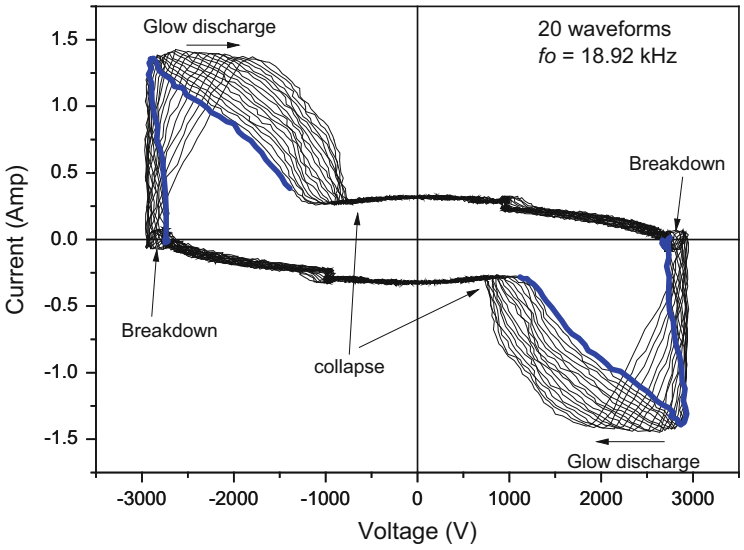

Fig. 9.3 A 1-ms snapshot of the I-V plane of a helium glow discharge within the LabLine plasma system. The *highlighted bold blue lines* represent the initial two (±) glow ignition cycles

To illustrate a key electrical behaviour of the uniform APGD. The two dielectric layers each chamber behaves as capacitances where the charges of the opposite polarities accumulate on the dielectrics during the previous discharge pulse. Thus, during the glow mode, the glow voltage (V_g) is equal to the applied voltage (V_a) minus a memory voltage (V_m), see Eq. (9.2).

$$V_g(t) = V_a(t) - V_m(t) \tag{9.2}$$

If drive frequency (18.9 kHz) and voltage memory (±1000 V) is sufficiently high (as in Fig. 9.3) then as the I-V behaviours the proceeding glow discharge pulse influences the next one.

9.3.1.3 Q-V Plane

In his publication in 1943 Manley [13] demonstrated that Lissajous figures provide a measurement of the electrical power coupled into plasma, if the integrated charge–voltage (Q-V) plane for one voltage cycle is used. He showed that area within this V-Q plot equates to the dissipated power for that cycle. The mean power is obtained by multiplying this by the frequency of applied voltage. By the year, 1993 Okazaki et al. [35] found that silent electrical discharges in filamentary mode contain multiple current spikes per each half cycle that causes the characteristic parallelogram of the V-Q plot to change voltage level within the time constant of

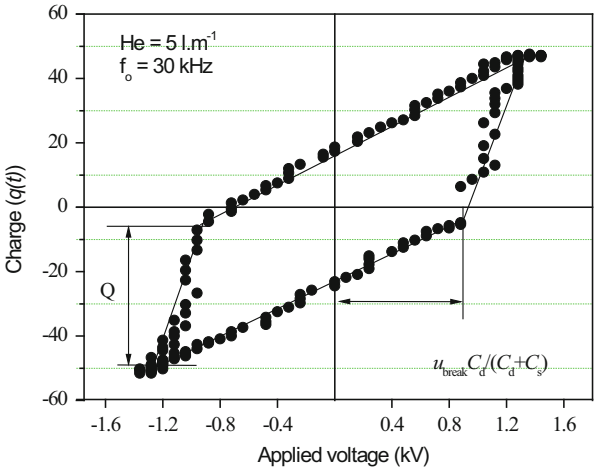

Fig. 9.4 A typical Lissajous figure for the DBD: $U_{appl} = 2.6$ kV (peak–peak)

the individual current spike. More recently, Falkenstein and Coogan (1997) [36] found that gas impurities (H_2O, 3.2 % absolute humidity) injected in to an dry air discharge causes the V-Q parallelogram morphology to change.

Figure 9.4 shows the result one such measurement where the plasma is created between two steel mesh metal electrodes in contact with two 4 mm thick, glass-ceramic plates separated by 5 mm [14]. The helium flow rate is 5 L min^{-1} at atmospheric pressure and the drive frequency of 30 kHz applied to one electrode and the other is grounded. The applied voltage, $u_{appl}(t)$ is measured using a high voltage probe, the discharge current, $i_d(t)$, from the voltage drop, $u_R(t)$, across a resistor which is connected in series with the electrodes. The voltage drop, $u_T(t)$, across a capacitor, C, connected in series with the resistor, is used to calculate the charge, $q(t)$, transferred across the electrode gap using the expression

$$u_T(t) = \frac{1}{C}\int_{t_0}^{t} i_d\,(t')\,dt' = q(t)/C \tag{9.3}$$

The main characteristics of the discharge such as the total charge and breakdown voltage are found from the slopes and intersections of these plots The energy deposited into the discharge during one cycle of the applied voltage is $A = 2Qu_{break}$, where Q is the charge moved through the discharge cell during a half cycle and u_{break} is the breakdown voltage. The mean power density is the order of a 100 mW cm^{-3}. However, the stray capacitance of the reactor does not influence the area enclosed by the V-Q plot: therefore detailed linear equivalent electrical model of the system must be used to derive the stray capacitance value [14, 36–38].

9.3.2 *Harmonic Plane*

The Lissajous figure has also be used in the harmonic phase plane by operating an oscilloscope in the X-Y plot display mode and then displaying two harmonically related frequency (usually the fundamental drive frequency and its second, or third, harmonic and where the harmonic ratio determines the number of visual "loops" per cycle). This approach has the advantage of locating a specific plasma mode of operation [39] and instability coupling regions between the external drive circuit and the internal plasma impedance [40, 41].

Figure 9.5a shows an example of an impedance matching-network-induced bi-stable (on–off) plasma instability within a chlorine inductively coupled low-pressure parallel-plate system operating at $f_o = 13.56$ MHz. Full details of the induced plasma instability is reported in reference [41]. In the figure, the analogue oscilloscope screen display is set as follows: the fundamental radio frequency (RF: $f_o = 13.56$ MHz) is plotted on X-axis and it second harmonic (27.12 MHz) is plotted on the Y-axis, and the inputs are set to 50 mV/div and 1 V/div, respectively. The oscilloscope sampling time is of the order of 5 μs and therefore is able to capture

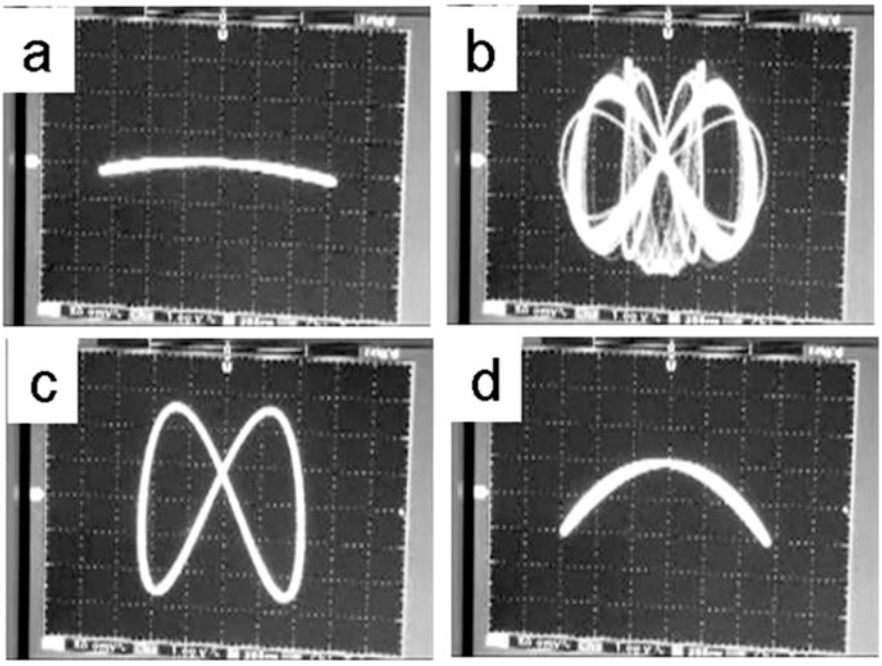

Fig. 9.5 Lissajous figure (harmonic plane) snapshots of plasma on-off instability. Screen display settings: $f_o = 13.56$ MHz plotted on the horizontal axis and; second harmonic (27.12 MHz) plotted on the vertical axis; the major divisions are set to 50 mV/div on the X-axis and 1 V/div on the Y-axis, respectively

approximately 20 loops, but is to slow to capture the spiral trajectory (non-stable state) between each loop.

This type of harmonic image snapshot shown in Fig. 9.5b has been termed a "butterfly" image due to the time modulation of the loops where the amplitude of the fundamental is rapidly changing and the harmonic amplitude and its time-delay are relatively constant. The physical interpretation of the harmonic modulation is twofold. Firstly, the forward power is reflected back from the plasma to the RF generator output where the over-power protection circuit shuts down output stage of the generator thus turning of the plasma (Fig. 9.5b). Secondly, when the reflected power has reduced to a predetermined safe level where the power is automatically turned-on so igniting the plasma (Fig. 9.5c).

In terms of real-time monitoring each Poincaré limit cycle or Andronov self-oscillation [26] represents a stable impedance condition per RF cycle. The large jump between the grouped loops indicates the point in time of the impedance transition. As in reference [36], the harmonic plane becomes useful in locating a mode change and instabilities induced by the external circuit.

9.4 Reconstruction of the 'Singing-arc' Lissajous Figure I-V Plane

This section the "current and voltage waveforms of the Singing-arc" first published in 1900 [4] is re-examined. In addition, the arc's optical output synchronised to the electrical waveforms is studied [5]. The optical output is due to the oscillograph mirror focused on to the positive carbon electrode and recording the light intensity onto the photographic film. [*N.B*. Off cause today the arc's optical output would be studied using a photodiode [17, 18]]. Sections 9.4.1, 9.4.2 and 9.4.3 report on the 'Singing-arc' under three different modes: hum, Continuous hissing intermittent hissing modes, respectively. In each, the electrical drive frequency is 6.4 kHz and the I-V planes are constructed using a digitation process employing Origin software. To preserve the current and voltage phase relationship in the digitation process the same equally spaced x-axis time stamped sequence is used. Finally, the I-V plane constructions use direct one-to-one mapping, rather to calibrate the current and voltage amplitudes, therefore the amplitudes are presented in arbitrary units (a.u.), so preserving the topology of each original waveform.

9.4.1 Hum Mode

Figure 9.6 shows the hum mode current and voltage waveforms for a mean current of 15.3 A flowing through the arc and an electrical drive frequency of 6.4 kHz. The selected time region is approximately two periods, or 0.32 ms. In this figure

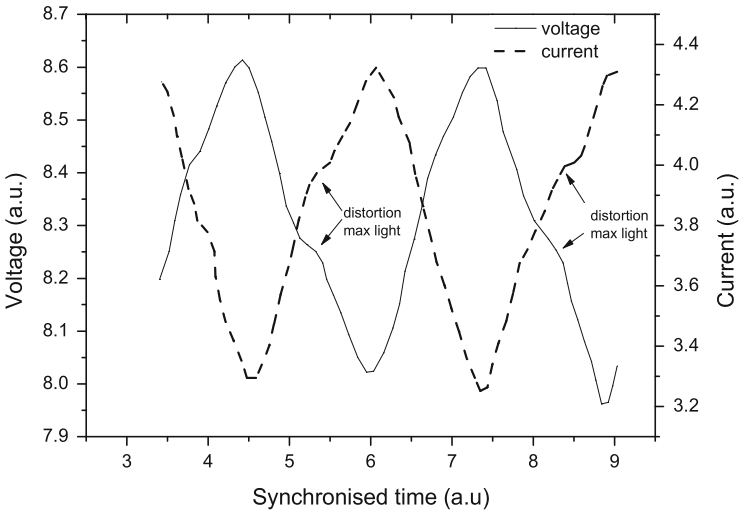

Fig. 9.6 Hum mode current and voltage waveforms with arrows pointing towards the distortion and maximum light intensity regions. The mean voltage = 50.5 V and the mean current = 15.2 A

there are three features of note. Firstly, the current and voltage have smooth periodic waveform, with their main peaks in anti-phase (180°) to each other. Secondly, the light density varies in a similar manner with maximum light output occurring close to maximum in current. Duddell attributes this motion to the axial rotation of the arc between the carbon electrodes. Thirdly, electrical distortion is the present (see arrows) in the falling edge of the voltage waveform and vice versa for the current waveform. The distortion is also in phase with the maximum light output. Simple harmonic analysis of the distortion reveals it is due to the presence synchronised second harmonic with magnitude approximately 50 % of the fundamental.

Figure 9.7 shows the Lissajous figure of the two waveforms $v(t)$ and $i(t)$ from Fig. 9.6 in the I-V plane. The Lissajous figure reveals the period-to-period phase noise of the voltage and current signals in the form of two closed limit cycles. The second harmonic distortion is seen as kink in the I-V loop. Note there is no evidence of a double pinched hysteresis loop. The vertical dash lines depict the selected time region (approximately two periods, or 0.32 ms).

9.4.2 Continuous Hissing Mode

Duddell found by keeping the electrical drive frequency through the arc constant and increasing mean current to 22.3 Amperes where an audible hissing along with a varying luminosity output occurs. For this reason, we have chosen to present the original oscillograph that purports the hissing mode [4]. The oscillograph hissing

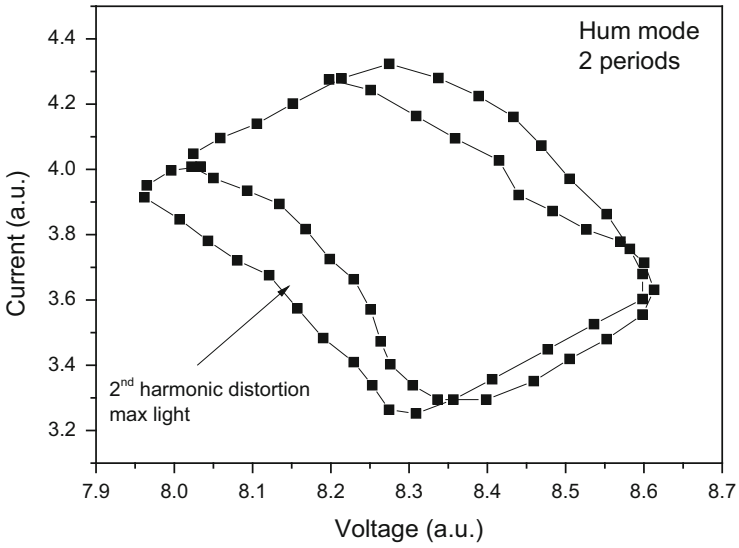

Fig. 9.7 Hum mode construed Lissajous I-V plane with arrows pointing towards the distortion and maximum light intensity region

mode is depicted in Fig. 9.8a is shown. To add the readers eye, we have annotated the oscillograph to highlight the bright (a-b and c-d) and dull (c-d) luminosity regions. For the Lissajous I-V plane investigation, we have selected the bright (a-b) and dull (b-c) time-periods. Directly below Fig. 9.8a is the constructed I-V planes of the bight and dull regions, combined in to Fig. 9.8b.

Within the current and voltage (PD) waveforms, there is a slow variation with a more rapid response superimposed and the majority of the small current peaks follow the voltage peaks. Both Duddell and Ayrton have provided a explanation which is as follows; The slow variation is due to the continuing axial rotation of the arc as in the hum mode. However, the unstable mode allows the surrounding air to access the carbon electrodes where oxygen reacts freely with the carbon surface. This causes the following sequence of events: a rise in temperature, an increase in light emission and a drop in voltage followed shortly by a rise in the current. They also explain this effect is opposite to what happens when deliberately changing the current in the external circuit, for in the latter case maximum current occurs before maximum light output.

As for the Lissajous figure I-V plane representation of the bright (open circles) and dull (closed circles) time-periods, in general it is observed that as the current falls and the light voltage increase as one would expect. However, for the bright data points their phase grouping is more compact with respect to the dull data points. This is because the current and light voltage has in general a lower amplitude and smaller variation within the bright periods.

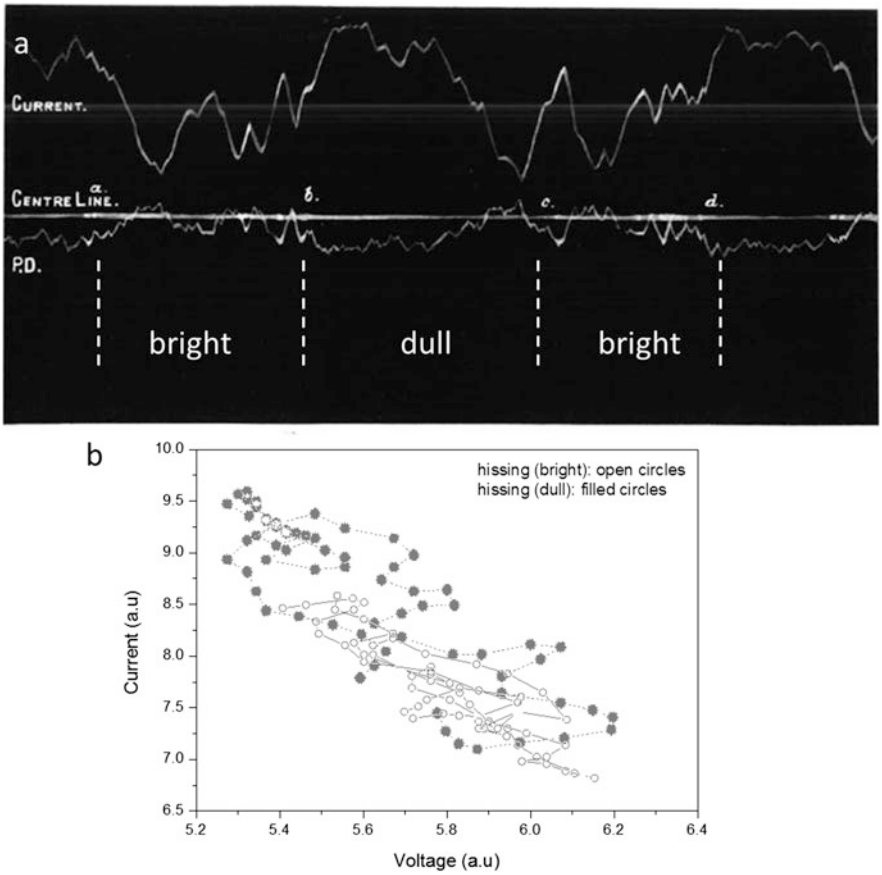

Fig. 9.8 (**a**) Current and voltage waveforms for continuous hissing mode [4] annotated with our selected bright and dull regions for Lissajous figures. The mean voltage = 38 V and the mean current = 22.3 A. (**b**) Represents the current–voltage plane for the selected bright and dull regions

9.4.3 Intermittent Hissing Modes

Using a short gas-gap a hissing (whistling) mode no light is emitted from the gas-gap. Figure 9.9 shows a current and voltage oscillograph [4] that has been inverted in colour (black to white) of this mode. The oscillograph trace reveals that there are two distinct pulse phases, these are: a short voltages pulse (24 V) where the current falls to a minimum valve (22.3 A) and an extended voltage pulse, again with the current reduce to the same minimum value. Duddell [4] has described the production of this mode being due to a temporary short circuit of the arc (maximum voltage minimum current) when a loose piece of carbon falls across the gas-gap and air burns until completely removed. A schematic of this process is also given by Prodromakis et al. [2]. In this mode, a Lissajous I-V pot produces two main clusters of data points (one

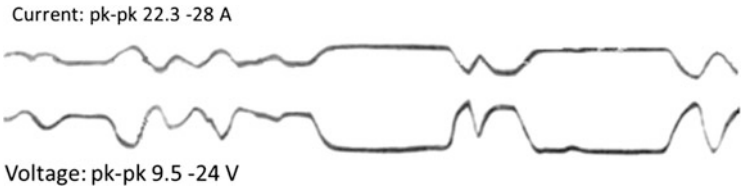

Fig. 9.9 Current and voltage waveforms for short air gap hissing mode. The voltage peak-to-peak varies between 9.5 and 24 V and the current peak-to-peak varies between 22.3 and 28 A

at maximum voltage and minimum current, and the other at minimum voltage and maximum current) similar to that of embedded state-space representation of square waveform with a phase delay of 180° [46].

The intermittent (or musical) mode as first discovered by Elihu Thomson in 1892 ([4], p. 247) and discussed by Duddell [4], Blondel [9] and Ginoux and Letellier [24] is of interest. This mode is found by increasing the shunt capacitor value to an extent that the circuit resonant frequency is too low to sustain a stable arc discharge. Moreover removing extraneous inductance in series with the capacitor (increasing circuit resonance) the arc discharge it ignited again. The frequency range of this mode is in the audible range (5 and 10 kHz). Thomson, Duddell and Blondel have described the production of this mode as due to the transformation of the direct current flowing through circuit into two oscillatory currents which have different time constants, one flowing shunt LC circuit and the other flowing through the resistance of the arc.

9.5 Memory Element Perspective

In 1971 L.O. Chua proposed a theoretical description of certain nonlinear two-terminal devices which have the ability to remember the charge that has previously flowed through them. From this early definition, the term ‘ideal memristor’ became established; however, by 1977 a more generalised definition was developed that included subclasses. By 2012 high-pressure and low-pressure mercury-vapour lamps and fluoresce tubes where included into the generalised definition under the classification of volatile memory [2]. The term ‘volatile memory’ is used since when the plasma excitation energy is removed the ionized gas reverts to the neutral state, i.e., the current and voltage levels move to the origin in the I-V plane. More recently (2014) two further papers have provided a detailed theoretical and experimental explanation of mercury and sodium discharge lamps, the T8 Florence tube and the Davy’s direct-current carbon arc; all of which fall within the volatile memory memristor classification [42, 43].

For the memristor and its two analogues’ (memcapacitor and meminductor), there are three generalised graphical fingerprints: two found in the Lissajous representation and the third in the time-domain. The first two are: (a) a double

Table 9.1 Physical parameters of modern plasma discharges described in this work

Gas (eV)	Pressure	Frequency	Electrode gap	Plasma-discharge	Memory	Reference
He (24.5)	Atmospheric	11–18 kHz	4 mm	Corona-filamentary	No	[17]
He (24.5)	Atmospheric	18.92 kHz	5 mm	APGD DBD	Yes	[16]
He (24.5)	Atmospheric	3–30 kHz	5 mm	Parallel-plate DBD	Yes	[14]
Cl_2 (12.9)	2 mTorr	13.56 MHz	90 mm	Parallel-plate	No	[40, 41]

pinched hysteresis loop in the I-V (Q-V, or L-V plane) and; (b) the shape of the hysteresis curve tends to a single straight line as the drive frequency increases to infinity. For example in the mercury and sodium lamps and the T8 fluorescence lamp the I-V plane collapses to a straight when the frequency degenerates to a straight line exceeds 30 kHz [42, 43]. The third working definition involves identical zero-crossing points in the waveform time-domain. As we are concerned with a phase delay between current and voltage waveforms (damped and undamped) here the definition it highlighted but not considered further.

To place the plasma discharges considered here into context of the volatile memory it is useful to compare and contrast the physical parameters (gas type, ionization potential, pressure, driving frequency, electrode gas-gap, type of discharge). These parameters are listed in Table 9.1.

We first considered the I-V and Q-V planes measurements for the helium-based atmospheric plasma systems as described in Sects. 9.3.1.1, 9.3.1.2 and 9.3.1.3, all of which operate below or near the memristor frequency limit (∼30 kHz).

For the PlasmaStream corona/filamentary plasma jet the Lissajous I-V plane evolves with increasing helium gas flow, from signature that is dominated by corona/filamentary current spikes to that a distorted limit cycle without a double pinched loop hysteresis at increased helium flow.

In the case of the helium-based parallel-plate DBD reel-to-reel system (LabLine), the Lissajous I-V plane reveals distorted limit cycles. Over a 20-cycle period, no doubled pinched loop hysteresis is observed. However, the limit cycles does provide reactor dielectric voltage memory information and the procession of each plasma glow period. Under high current conditions, or when polymer deposition (carbon) forms on the dielectric, glow-to-arc formation may occur leading to carbon tracking [44, 45] which can lead to power supply damage. Under these temporary and deleterious conditions a double pinched hysteresis loop in the I-V plane may occur. Whether these DBD systems fall under the notion of a volatile memory memristor, or, more probably a voltage-controlled mem-capacitive system due to the charge on the dielectric surfaces is uncertain.

The Q-V plane of the for the parallel-plate DBD provides a classical parallelogram limit cycle with no double pinched hysteresis loop, and again the dielectric provides information on the dielectric voltage memory. The morphology of the constructed parallelogram also provides information on gas impurities and the discharge mode of operation.

Finally, concerning the low-pressure (2 mTorr) chlorine parallel-plate plasma system operating at 13.56 MHz (some 100 time faster than memristor frequency limit for mercury). With the knowledge of the second 'Fingerprint' of the generalised memristor we would not expected to see hysteresis. Indeed, it is shown that real-time monitoring of the Lissajous harmonic-plane captures the butterfly time-dependent instabilities without any observable hysteresis.

Now considering the conjecture that the 'Singing arc' could be considered as the oldest memristor [12]. This viewpoint can now be seen as erroneous on a number of counts. Firstly, acknowledging Langmuir's strongly worded warning that gas impurities is a major source of experimental variability in documented work published prior to 1913 [19] it is reasonable to state that the hum mode is associated with frequencies of around tens of Hz and hissing mode within frequency band of between 300 Hz and 10 kHz. These frequencies arise from acoustic effects and so involve the movement of gas which is generated by localised gas heating [47]. Given this observation, Lin's [42] and Chua's [43] theoretical and experimental work published in 2014 places the Davy's carbon arc before the 'Singing-arc'. Secondly, Duddell [4] and Hoyt [11] both report a hysteresis effect in Lissajous I-V plane, but their data does not support a double pinched hysteresis loop in the V-I plane for the hum mode, continuous hissing mode, or in the intermittent hissing mode. Thirdly, the lack of the memristor fingerprint Ginoux and Rossetto [12] ascribe to the 'imperfection' of the oscillograph and the wide experimental conditions used. With regard to the 'imperfection of instruments' conjecture, we have seen that early oscillograph [4] and oscilloscope [11] measurement present no concern to the measurement.

9.6 Harmonic Reconstruction of the Davy Reactor

Lin's [42] and Chua's [43] experimental study used, a 50 % duty-cycle undamped square waveform voltage source that produced a near sinusoidal current waveform. In the case of the voltage waveform the time dependent voltage level alternates (within a finite discontinuity) between two voltages levels around an average voltage (V/2). Under these conditions the two waveforms ($v(t)$, $i(t)$) reconstructed in a Lissajous I-V plane contained pinched loops at the extremities of the voltage and current amplitudes and not near or through the zero origin of the I-V plane, see reference Fig. 9.1e of [43].

It is reasonable hypotheses that the Lissajous I-V plane Fingerprint is a result of harmonic distortion rather than a memory effect. Thus ignoring the Gibbs phenomenon, which describes the ringing at the rising and falling edges [48], the Davy's reactor Lissajous I-V Fingerprint is modelled as follows.

For the voltage square waveform, the periodic amplitude (A_v) is synthesised by adding a limited series of odd harmonic (with every other even harmonic is

suppressed). Equation (9.4), mathematically expresses this process as a function of phase.

$$A_v = v_o.\sin n_o\phi\frac{\pi}{180} + v_3.\sin n_3\frac{\pi}{180} + v_5.\sin n_5\phi\frac{\pi}{180} + \ldots. \tag{9.4}$$

where $v_{0,3,5}$ is the amplitude of each sine wave in which the harmonic amplitude initially falls by a factor of 2 per octave from the fundamental frequency for $n = 3$ and $n = 5$, $n_{0,3,5}\ldots$ is the integer of the fundamental frequency and its odd harmonic and ϕ is piecewise phase number.

In the case of distorted sinusoidal current waveform the amplitude (A_I), the distortion is synthesis using even harmonics as in Eq. (9.5).

$$A_i = i_o.\frac{sin\ n_o\phi\pi}{180} + i_2.sin\ n_2\ \phi\frac{\pi}{180} + i_4.\frac{sin\ n_4\phi\pi}{180} + \ldots. \tag{9.5}$$

where $i_{0,3,5}$ is the amplitude of each sine wave in which the even harmonic amplitude initially falls by a factor of 2 per octave from the fundamental frequency for $n = 2$ and $n = 4$, $n_{0,2,4\ldots}$. is the integer fundamental frequency and its odd harmonic and ϕ is piecewise phase number.

To illustrate the effect of harmonic distortion within both the voltage and current waveforms Fig. 9.10a–d represents four Lissajous I-V planes of the harmonic

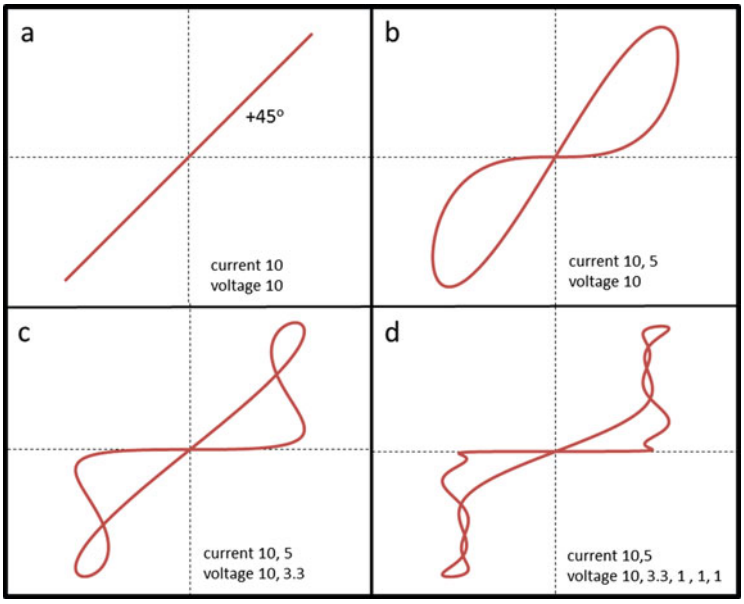

Fig. 9.10 Quartet of Lissajous I-V plane produced by harmonic synthesis. The fundamental voltage and current amplitudes are set to 10 V and 10 A, and the harmonic distortion amplitudes are selected to produces the pinched loops in (**d**)

distortion. For comparative purposes Fig. 9.10a shows the fundamental voltage (10 V) waveform and the current (10 A) waveform. As both sinusoidal waveforms have the same amplitude a straight line at positive angle of 45°. Figure 9.10b illustrates the effect of adding second harmonic (5 A) distortion to the current waveform. In this case, the Lissajous figure forms two pinched loops with their origin at the zero voltage and current. In Fig. 9.10c, the addition of third harmonic distortion (3.3 V) to the fundamental voltage waveform (thereby synthesising a simple square waveform) is presented. This procedure reveals an additional pinched loop at each of the voltage maxima. Finally adding $n = 5$ and $n = 7$ harmonic distortion to the voltage waveform (thereby generating a square waveform with a near finite discontinuity) reveals a further two pinched loops at each of the voltage maxima.

The I-V plane in Fig. 9.10d mimics the Davy's reactor results as publisher in [42, 43]. However to achieve a good match the higher order voltage odd harmonics ($n = 5$, 7 and 9) have a amplitude of 1 and therefore do not follow the factor of 2 fall per octave rule. The outcome of this simple model reflects the difficulty inherent in approximating a discontinuous function by a finite series of continuous sine waves. Nevertheless, the model outcome does provide sufficient reason to justify a harmonic distortion origin within Lin's and Chua's results.

9.7 Conclusion

This work has reviewed the 'Signing-arc' and its development into a functioning triode vacuum tube that is suitable for long-distance radiotelegraphy. The review not only provides a historical perspective, but also the required development, and understanding, for both material engineering and plasma physics of the discharge: in particular, the way that gas impurities and harmonic content effect the discharge current and voltage waveforms. From the early stages, the Lissajous figure representation of I-V plane played an important role in providing a means of understanding of plasma stability without prior knowledge of the plasma physics that drives, and hence defines the electrical characteristic of the device. In later years, the addition of the Lissajous figure Q-V and Harmonic plane helped the development of plasma jets, the DBD, and our understanding of plasma mode change. Limit cycles, self-oscillations and the more recent memory element 'Fingerprint' of the Lissajous figure (in all three planes) provide classification, or description, of the plasma discharge, and can inform the fundamental plasma physics of the device. Modern analogue, and digital, oscilloscopes and computer software enable these discharge mode change to be readily identify and thereby controlled.

Acknowledgement This research is partially support by the Irish Centre for Composites Research (IComp).

References

1. Patterns produced by intersection of two sinusoidal curves the axes of which are at right angles to each other were first studied by Nathaniel Bowditch in 1815, and later by Jules-Antoine Lissajous in 1857–1858.
2. T. Prodromakis, C. Toumazou, L.O. Chua, Two centuries of memristor. Nat. Mater. **11**, 478–481 (2012)
3. N. Hawkins, Wave form measurement, in *Hawkins Electrical Guide*, vol. 6, 2nd edn. (Theo. Audel and Co., New York, 1917), p. 1866, Figs. 2621–2623
4. W. Duddell, On rapid variations in the current through the direct current arc. J. Instit. Electr. Eng. **30**(148), 232–267 (1900)
5. A.P. Trottor, in *The Rotation of the Electric Arc. Proceedings of the Royal Society of London* (Philosophical Transactions of the Royal Society, London, 1st January 1894), pp. 262–261
6. H.T. Simon, Über die Dynamik der LichtbogenVorgänge und über Lichtbogenhysteresis. Phys. Z. **6**, 297–319 (1905)
7. L. Michael, 1900: nature reports on William Duddell 'musical arcs'. APS News **19**(11), 2 (2010)
8. P. Janet, Quelques remarques sur la théorie de l'arc chantant de *Duddell*. C. R. **134**, 821–823 (1902)
9. A. Blondel, Sur les phénomenes de l'arc chantant. Éclairage Électrique **44**(28), 41–58, 81–104 (1905)
10. L.W. Austin, The production of high frequency from the electric arc. Bull. Bur. Stand. **3**(2), 325–340 (1907)
11. J.E. Hoyt, Oscillographic study of the singing arc. Phys. Rev. (Series I) **35**, 387–399 (1912)
12. J.-M. Ginoux, B. Rossetto, The singing arc: the oldest memristor?, in *Chaos CNN Memristors and Beyond: A Festschrift for Leon Chua*, chap. 40, ed. by A. Adamatzky, G. Chen (World Scientific Publishing, Singapore, 2013), pp. 495–505. ISBN 978-981-4434-79-9. arXiv:1408.5103 [physics.hist-ph]
13. T.C. Manley, The electric characteristics of the ozonator discharge. Trans. Electrochem. Soc. **84**(1), 83–96 (1943)
14. G. Nersisyan, W.G. Graham, Characterization of a dielectric barrier discharge operating in an open reactor with flowing helium. Plasma Sources Sci. Technol. **13**, 582–587 (2004)
15. M.M. Turner, M.A. Lieberman, Hysteresis and the E-to-H transition in radio frequency inductive discharges. Plasma Sources Sci. Technol. **8**, 313–324 (1999)
16. V.J. Law, N. O'Connor, B. Twomey, D.P. Dowling, S. Daniels, in *Visualization of Atmospheric Pressure Plasma Plectrical Parameters*, ed. by C.H. Skiadas, I. Dimotikalis, C. Skiadas. Topics of Chaotic Systems: Selected Papers of Chaos 2008 International Conference (World Scientific Publishing, Singapore, 2009), pp. 204–213. ISBN: 978-981-4271-33-2
17. C.E. Nwankire, V.J. Law, A. Nindrayog, B. Twomey, K. Niemi, V. Milosavljević, W.G. Graham, D.P. Dowling, Electrical, thermal and optical diagnostics of an atmospheric plasma jet system. Plasma Chem. Plasma Process. **30**(5), 537–552 (2010)
18. V. Poulsen, in *System for Producing Continuous Electric Oscillations*. Transactions of the International Electrical Congress (J. R. Lyon Co., St. Louis, 1904), pp. 963–971
19. I. Langmuir, The effect of space charge and residual gases on thermionic currents in high vacuum. Phys. Rev. **2**(6), 450–486 (1913)
20. G.F.J. Tyne, in *Saga of the Vacuum Tube* (Howard W Sams & Co., Indianapolis, 1977), pp. 192–198
21. B. Van de Pol, A theory of amplitude of free and forced triode vibrations. Radio Rev. (Lond.) **1** (1920). 710–710 and 754–762
22. B. Van de Pol, J. Van de Mark, Frequency demultiplication. Nature **120**, 164–164 (1927)
23. V.E. Appleton, B. Van de Pol, On a type of oscillation-hysteresis in a simple triode generator. Philos. Mag. **43**, 177–193 (1922)
24. J.-M. Ginoux, C. Letellier, Van der Pol and the history of relaxation oscillations: toward the emergence of a concept. Chaos **22**, 023120 (2012)

25. J.-M. Ginoux, L. Petitgirard, Poincar´e's forgotten conferences on wireless telegraphy. Int. J. Bifurcat. Chaos **20**(11), 3617 (2010)
26. A. Andronov, Poincare's limit cycles and the theory of self-oscillations. C. R. Acad. Sci. **189**, 559–561 (1929)
27. Z. Szymański, J. Hoffman, J. Kurzyna, Plasma plume oscillations during welding of thin metal sheets with a CW CO_2 laser. J. Phys. D Appl. Phys. **34**, 189–199 (2001)
28. D.P. Dowling, F.T. O'Neill, S.J. Langlais, V.J. Law, Influence of dc pulsed atmospheric pressure plasma jet processing conditions on polymer activation. Plasma Process. Polym. **8**(8), 718–727 (2011)
29. D.P. Dowling, F.T. O'Neill, V. Milosavljević, V.J. Law, DC pulsed atmospheric pressure plasma jet image information. IEEE Trans. Plasma Sci. **39**(11), 2326–2327 (2011)
30. V.J. Law, V. Milosavljevic, N. O'Connor, J.F. Lalor, S. Daniels, Handheld flyback driven coaxial dielectric barrier discharge: development and characterization. Rev. Sci. Instrum. **79**(9), 094707 (2008)
31. V.J. Law, S.D. Anghel, Compact atmospheric pressure plasma self-resonant drive circuits. J. Phys. D Appl. Phys. **45**(7), 075202, 14 (2012)
32. F.T. O'Neill, B. Twomey, V.J. Law, V. Milosavljević, M.G. Kong, S.D. Anghel, D.P. Dowling, Generation of active species in a large atmospheric pressure plasma jet. IEEE Plasma Sci. **40**(11), 2994–3004 (2012)
33. J.L. Walsh, F. Iza, N.B. Janson, V.J. Law, M.G. Kong, Three distinct modes in a cold atmospheric pressure plasma jet. J. Phys. D Appl. Phys. **43**(7), 075201, 14 (2010)
34. J.L. Walsh, F. Iza, N.B. Janson, M.G. Kong, Chaos in atmospheric-pressure plasma jets. Plasma Sources Sci. Technol. **21**(3), 034008 (2012)
35. S. Okazaki, M. Kogoma, M. Uehara, Y. Kimura, Appearance of stable glow discharge in air, argon, oxygen and nitrogen at atmospheric pressure using a 50 Hz source. J. Phys. D Appl. Phys. **26**(5), 889–892 (1993)
36. Z. Falkenstein, J.J. Coogan, Microdischarge behaviour in the silent discharge of nitrogen-oxygen and water-air mixtures. J. Phys. D Appl. Phys. **30**(19), 817–825 (1997)
37. F. Massine, A. Rabehi, P. Decomps, R. Gadri, P. Sègur, C. Mayoux, Experimental and theoretical study of a glow discharge at atmospheric pressure controlled by dielectric barrier. J. Appl. Phys. **83**, 2950–2957 (1998)
38. F. Tochikubo, T. Chiba, T. Watanabe, Structure of low-frequency helium glow discharge at atmospheric pressure between parallel plate dielectric electrodes. Jpn. J. Appl. Phys. **38**, 5244–5250 (1999)
39. V.J. Law, A. Kenyon, N.F. Thornhill, A. Seeds, I. Batty, Rf probe technology for the next generation of technological plasmas. J. Phys. D Appl. Phys. **34**(18), 2726–2733 (2001)
40. A.R. Ellingboe, V.J. Law, F. Soberón, F. Garcia, W.G. Graham, External circuit system effects on Cl_2 plasma instabilities. Electr. Lett. **41**(9), 525–526 (2005)
41. F. Soberón, F.G. Marro, W.G. Graham, A.R. Ellingboe, V.J. Law, Chlorine plasma system instabilities within an ICP driven at a frequency of 13.56 MHz. Plasma Source Sci. Technol. **15**(2), 193–203 (2006)
42. D. Lin, S.Y.R. Hui, L.O. Chua, Gas discharge lamps are volatile memristor. IEEE Trans. Circuits Syst. **61**(7), 2066–2073 (2014)
43. L.O. Chua, If it's pinched it's a memristor. Semicond. Sci. Technol. **29**, 104001, 42 (2014)
44. J.J. Shi, D.W. Liu, M.G. Kong, Plasma stability control using dielectric barriers in radio-frequency atmospheric pressure glow discharges. Appl. Phys. Lett. **89**, 081502 (2004)
45. V.J. Law, A. Ramamoorthy, D.P. Dowling, Real-time process monitoring during the plasma treatment of carbon weave composite materials. JMSE **1**(2B), 164–169 (2011)
46. V.J. Law, D.P. Dowling, in *Embedded Delay Time-Series Analysis of Atmospheric Pressure Plasma Jet Treatment of Composite Surfaces*. Chaos 2015, Paris, 27th May 2015
47. V.J. Law, Plasma Harmonic and Overtone Coupling, in *Handbook of Applications of Chaos Theory*, ed. by C.H. Skiadas, C. Skiadas (Chapman and Hall/CRC Press, Taylor & Francis, 2016), chap. 20, pp. 405–422. ISBN: 9781466590434
48. J.W. Gibbs, Fourier's Series. Nature **59**, 200, 606 (1899)

Chapter 10
Stochastic Anti-Resonance in Polarization Phenomena

Vladimir L. Kalashnikov and Sergey V. Sergeyev

Abstract The phenomenon of resonant stochastization, so-called stochastic anti-resonance, is considered on an example of Raman fibre amplifier with randomly varying birefringence. Despite a well-known effect of noise suppression and global regularization of dynamics due to resonant interaction of noise and regular external periodic perturbation, as it takes a place in the case of stochastic resonance, here we report about reverse situation when regular perturbation assists a noise-induced escape of a system from metastable state. Such an escape reveals itself by different signatures like growth of dispersion, dropping of Hurst parameter and Kramers length characterizing behavior of physically relevant parameters (e.g. average gain and projection of signal state of polarization to pump one). This phenomenon is analyzed by the means of two techniques: direct numerical simulations of underlying stochastic differential equations and multi-scale averaging method reducing a problem to a set of deterministic ordinary differential equations for average values characterizing the states of polarization. It is shown, that taking into account a relevant set of scales characterizing a system results in excellent agreement between results of direct numerical simulations and average model. It is very challenging outcome because allows replacing the cumbersome numerical simulations and revealing the system-relevant signatures for many important real-world systems.

10.1 Introduction

Existence of different, frequently incommensurate scales is a common phenomenon in nature. An interactions between processes characterized by different scales can result in multitude of emergent phenomena when a system cannot be described as a scale-separated hierarchy of underlying processes but presents a substantially new entity with qualitatively new properties and behavior ("The emergent is unlike its components insofar as these are incommensurable, and it cannot be reduced to their sum or their difference" [1]). Striking examples are life, fractals and chaos

V.L. Kalashnikov (✉) • S.V. Sergeyev
Aston Institute of Photonic Technologies, Aston University, Birmingham B4 7ET, UK
e-mail: kalashnikov@aston.ac.uk

C. Skiadas (ed.), *The Foundations of Chaos Revisited: From Poincaré to Recent Advancements*, Understanding Complex Systems,
DOI 10.1007/978-3-319-29701-9_10

[2]. No wonder that multi-scaling processes and methods for their investigation are attracting much attention during last 100 years [3–6].

For instance, in a fibre transmission system there are several substantially different scales encompassing a light wavelength ($\sim 1\,\mu$m), a fibre core diameter ($\sim 10\,\mu$m), a pulse duration ($\sim 10 \div 100$ mm), fibre beat and correlation lengths ($\sim 10 \div 100$ m), an attenuation length (~ 10 km), nonlinear and dispersion lengths (> 100 km), and, at last, a propagation length (Southern Cross Cable Network, whose length is about 30 mm), i.e. more than 13 orders [7]. Each scale defines a quite specific physics: from effects of electronic nonlinearities at the shortest time edge, through frequency comb formation in the middle to auto- and relaxation oscillations, long-living pattern formation etc. at the slowest time edge. In fibre Raman amplifiers [8] (see next Section), the longest scale is associated with the attenuation length and characteristics lengths of *Kerr nonlinearity* (L_{nl}) and *dispersion* (L_D). It is of approximately several kilometers. On other hand, fibre *mode beat-length* (L_b) induced by birefringence varies from several to hundreds of meters. But a birefringence of commercial telecommunication fibres is inherently *stochastic* (see next Section) with typical *correlation length* (L_c) overlapping with mode beat-length range. Hence, using the traditional averaging techniques in this case [9, 10] can be disputed because they describe precisely only asymptotical cases $L_{nl}, L_D \gg L_b \gg L_c$ (Manakov's limit) or $L_{nl}, L_D \gg L_c \gg L_b$ (diffusion limit) [11, 12]. Therefore, development of multi-scale techniques taking into account carefully contributions and interrelations of processes with different scales is of interest from both practical and theoretical points of view. As relevant examples concerning Raman fibre amplifiers, one may point to [13–15]. These multi-scale approaches allow in principle to cover all range of parameters by using sophisticated averaging techniques and, thereby to avoid a very cumbersome numerical simulations of underlying stochastic differential equations (SDEs). Nevertheless, the validity of such techniques has to be proved just numerically.

Here we shall demonstrate as a cooperation between analytical multi-scale techniques and direct numerical simulations of SDEs reveals a quite non-trivial phenomenon, *stochastic anti-resonance* (SAR), which can be characterized by different signatures including Hurst parameter, Kramers length, standard deviation, etc. This phenomenon can be treated as a noise-driven escape from metastable state which is inherent in diffusion in crystals, protein folding, activated chemical reactions and many others [16–20]. As a test-bed, we consider a fibre Raman amplifier with random birefringence that is a device with direct practical impact on development of the high-transmission-rates optical networks.

10.2 Physical Background

We will consider a Raman fibre amplifier as a test-bed model for analysis of SAR. Such an amplifier is based on using the stimulated Raman scattering (SRS), that is a process by which energy is transferred from the pump wavelength to a longer signal

wavelength (∼100 nm shift in silica) through nonlinear inelastic photon scattering on an optical phonon [8]. The advantage of Raman amplifiers is that they provide a relatively smooth and high gain over a broad spectral range (Fig. 10.1). The inherent property of SRS is that it is polarization dependent [21]. Gain is maximum for co-polarized pump and signal but minimum for their mutually transverse polarizations. Since the birefringence is inherent in fibres (see Fig. 10.2), such a dependence cannot be ignored. Birefringence can be illustrated by the birefringence vector $\boldsymbol{W} = b(\omega)(1,0,0)^T$ on the Poincaré sphere (see Fig. 10.3a). Here $b = 2\pi/L_b$ is a "rate" of mode beating induced by birefringence ($L_b = \lambda/\Delta n$ is a beat-length).

Besides influence on SRS, this inherent birefringence changes *state of polarization* (SOP) of arbitrary polarized light due to difference of effective refraction coefficients Δn along the birefringence axes. Pulses with SOPs oriented along these axes will propagate with different group delays $\Delta\tau$. This difference can

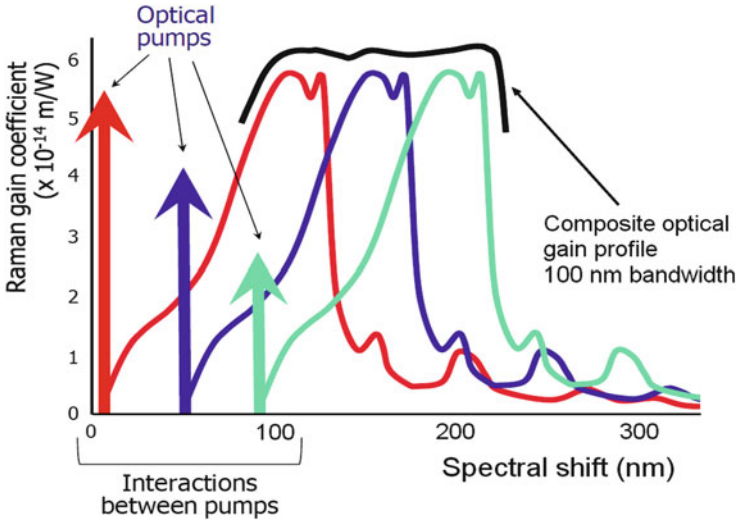

Fig. 10.1 Illustration of broadband Raman amplification. Narrowband pumps (*arrows*) at different wavelengths produce broadband overlapping Raman gain bands shifted into infra-red spectral domain. As a result, a relatively smooth effective gain profile covering a broad spectral range can be created

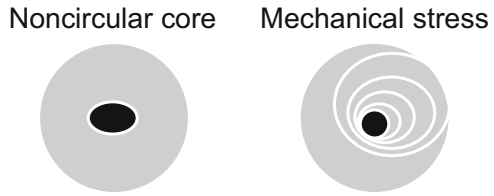

Fig. 10.2 Fibre cross-sections with cylindrical symmetry broken by manufacturing process. As a result, a fibre becomes birefringent

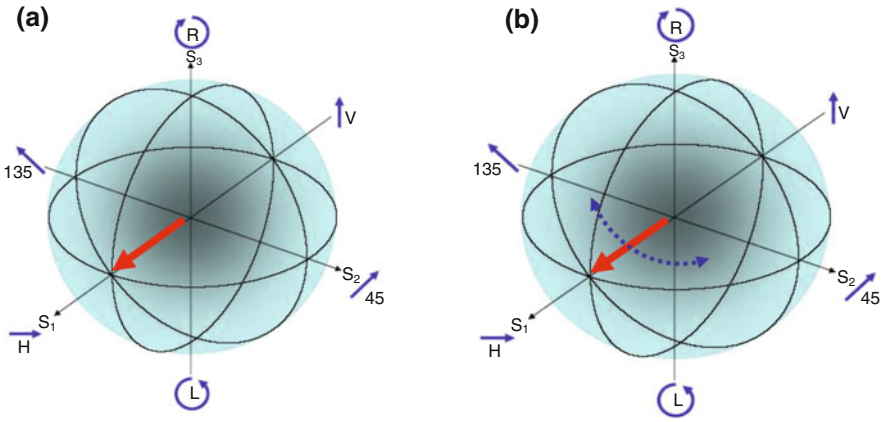

Fig. 10.3 (**a**): Birefringence vector $\boldsymbol{W}$ (*red*) on the Poincaré sphere. (**b**): Birefringence vector walks randomly in equatorial plane (in the chosen reference frame) due to stochastic birefringence (Color figure online)

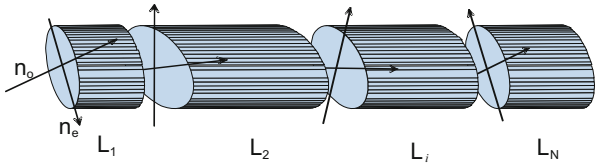

Fig. 10.4 Fixed modulus model of stochastic birefringence: polarization maintaining fibre sectors with fixed lengths L_N differ by random rotation of polarization axes

be characterized by the parameter called *polarization mode dispersion* (PMD) $\Delta\tau/L = d(\Delta n\omega/c)/d\omega$ [7]. Since it is very hard technologically to provide identical physical conditions along a fiber, birefringence (i.e. direction of $\boldsymbol{W}$) will change stochastically with the length z. There are different ways to emulate the stochastic birefringence [7]. In particular, one may consider a concatenation of polarization maintaining fibre sections of fixed lengths with random rotation of polarization vector from section to section (the fixed modulus model [10], see Fig. 10.4).

An appropriate transformation of reference frame [14] allows expressing an evolution of normalized signal ($\hat{\boldsymbol{s}}$) and pump ($\hat{\boldsymbol{p}}$) Stokes vectors in such a fibre as their rotation in the plane transverse to the equatorial one on the Poincaré sphere around the corresponding birefringence vectors $\boldsymbol{W}_{s,p}$ with the different rates b_s (for a signal) and b_p (for a pump) (Fig. 10.5). Due to $b_s \neq b_p$, vector $\hat{\boldsymbol{s}}$ rotates around $\hat{\boldsymbol{p}}$ at the rate $b_p - b_s$. Simultaneously, the birefringence vectors will wander randomly in equatorial plane (Figs. 10.3b and 10.5).

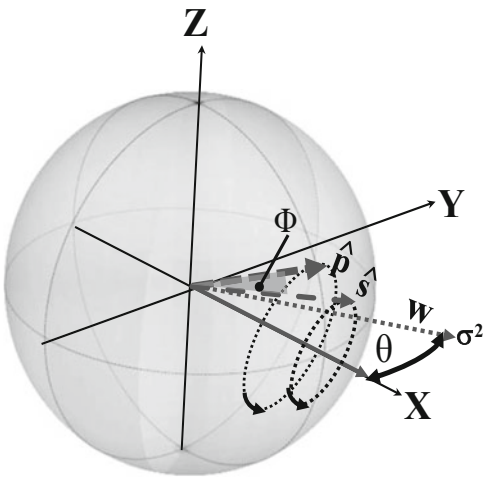

Fig. 10.5 Poincaré sphere with signal ($\hat{\boldsymbol{s}}$) and pump ($\hat{\boldsymbol{p}}$) SOP vectors (Φ is their mutual angle) rotating around birefringence vector $\boldsymbol{W}$ (only one is shown for simplicity) which wanders randomly in horizontal plane (θ is a randomly changing angle defining this wandering and σ is a volatility of corresponding random process, see Eqs. (10.1)–(10.3))

10.3 Model

Extended vector theory of SRS within the context of fibre Raman amplifiers is presented in [8, 13]. In terms of unit vectors $\hat{\boldsymbol{s}} = (s_1, s_2, s_3)$ and $\hat{\boldsymbol{p}} = (p_1, p_2, p_3)$ pointing SOPs on the Poincaré sphere and $\boldsymbol{W}_{p,s} = \left(2b_{p,s}\cos\theta, 2b_{p,s}\sin\theta, 0\right)^T$ (Fig. 10.5), the system of SDEs describing an evolution of co-propagating pump and signal SOPs under action of random birefringence can be written in the following form:

$$\frac{d\hat{\boldsymbol{S}}}{dz} = \frac{g_R}{2}\left(\left|\hat{\boldsymbol{P}}\right|\hat{\boldsymbol{S}} + \left|\hat{\boldsymbol{S}}\right|\hat{\boldsymbol{P}}\right) - \alpha_s\hat{\boldsymbol{S}} + \beta\begin{pmatrix} S_2 \\ -S_1 \\ 0 \end{pmatrix} + 2b_s\begin{pmatrix} 0 \\ -S_3 \\ S_2 \end{pmatrix}, \quad (10.1)$$

$$\frac{d\hat{\boldsymbol{P}}}{dz} = -\frac{\omega_p}{\omega_s}\frac{g_R}{2}\left(\left|\hat{\boldsymbol{P}}\right|\hat{\boldsymbol{S}} + \left|\hat{\boldsymbol{S}}\right|\hat{\boldsymbol{P}}\right) - \alpha_p\hat{\boldsymbol{P}} + \beta\begin{pmatrix} P_2 \\ -P_1 \\ 0 \end{pmatrix} + 2b_p\begin{pmatrix} 0 \\ -P_3 \\ P_2 \end{pmatrix}, \quad (10.2)$$

where $\hat{\boldsymbol{S}} = S_0\hat{\boldsymbol{s}}$ and $\hat{\boldsymbol{P}} = P_0\hat{\boldsymbol{p}}$ ($S_0 = \left|\hat{\boldsymbol{S}}\right|$ and $P_0 = \left|\hat{\boldsymbol{P}}\right|$ are signal and pump powers, respectively), g_R is a Raman gain coefficient, ω_p and ω_s are pump and power optical frequencies, respectively. SDEs (10.1) and (10.2) have to be understood in the Stratonovich's sense with a noise source $\beta(z)$ defined as the Wiener process with zero drift and volatility σ:

$$\frac{d\theta}{dz} = \beta(z), \ \langle\beta(z)\rangle = 0, \ \left\langle\beta(z), \beta\left(z'\right)\right\rangle = \sigma^2\delta\left(z - z'\right), \quad (10.3)$$

where $\langle \ldots \rangle$ means averaging of birefringence fluctuations along a propagation coordinate z and $\sigma^2 = 1/L_c$.

Equations (10.1) and (10.2) allow some further simplifications. The first one is neglect of the pump depletion, i.e. the decrease of pump power due to energy transfer to a signal (first term at r.h.s. of Eq. (10.2)). Due to nonlinear nature of SRS, this effect is defined by both pump and signal powers ($P_0 \sim 1$ W and $S_0 \sim 10$ mW, respectively). As $P_0 \gg S_0$, it is reasonable assumption for propagation lengths of few kilometers. Then, it is possible to exclude the scalar gain and loss effects by simple normalization [14]:

$$\hat{\boldsymbol{S}} = \hat{\boldsymbol{S}}' \exp\left[\int_0^L \left(\frac{g_R}{2} P_0\left(z'\right) - \alpha_s z'\right) dz'\right], \tag{10.4}$$

where $P_0(z) = P_0^{in} \exp\left(-\alpha_p z\right)$, L is a full propagation length and P_0^{in} is an input pump power.

Let's $\hat{\boldsymbol{S}}' = s_0 \hat{\boldsymbol{s}}$, $s_0 = \left|\hat{\boldsymbol{S}}'\right|$, then Eqs. (10.1) and (10.2) can be rewritten in the following form:

$$\frac{d\hat{\boldsymbol{S}}'}{dz} = \frac{g_R}{2} P_0(z) \hat{\boldsymbol{p}} + \beta \begin{pmatrix} S_2' \\ -S_1' \\ 0 \end{pmatrix} + 2b_s \begin{pmatrix} 0 \\ -S_3' \\ S_2' \end{pmatrix}, \tag{10.5}$$

$$\frac{d\hat{\boldsymbol{p}}}{dz} = \beta \begin{pmatrix} p_2 \\ -p_1 \\ 0 \end{pmatrix} + 2b_p \begin{pmatrix} 0 \\ -p_3 \\ p_2 \end{pmatrix}. \tag{10.6}$$

The next step is transition to a reference frame, where $\widetilde{\boldsymbol{W}}_{p,s} = (2b_{p,s}, 0, 0)$ [14]:

$$\widetilde{\boldsymbol{W}}_{p,s} = \begin{pmatrix} \cos\theta & \sin\theta & 0 \\ -\sin\theta & \cos\theta & 0 \\ 0 & 0 & 1 \end{pmatrix} \boldsymbol{W}_{p,s}. \tag{10.7}$$

Applying this transformation results in the following system of SDEs:

$$\frac{ds_0}{dz} = \frac{g_R}{2} P_0(z)\, x, \tag{10.8}$$

$$\frac{dx}{dz} = \frac{g_R}{2} P_0(z)\, s_0 - 2\left(b_p - b_s\right)\left(\tilde{p}_3 \tilde{s}_2 - \tilde{p}_2 \tilde{s}_3\right), \tag{10.9}$$

$$\frac{d\tilde{\hat{\boldsymbol{s}}}}{dz} = \frac{g_R}{2} P_0(z)\, s_0 \tilde{\hat{\boldsymbol{p}}} + 2b_s \begin{pmatrix} 0 \\ -\tilde{s}_3 \\ \tilde{s}_2 \end{pmatrix} + \beta \begin{pmatrix} \tilde{s}_2 \\ -\tilde{s}_1 \\ 0 \end{pmatrix}, \tag{10.10}$$

$$\frac{d\tilde{\hat{p}}}{dz} = 2b_p \begin{pmatrix} 0 \\ -\tilde{p}_3 \\ \tilde{p}_2 \end{pmatrix} + \beta \begin{pmatrix} \tilde{p}_2 \\ -\tilde{p}_1 \\ 0 \end{pmatrix}, \tag{10.11}$$

$$\frac{d\theta}{dz} = \beta\,(z)\,. \tag{10.12}$$

Here tildes denote the corresponding vectors and their components in new reference frame and $x = \tilde{\hat{\boldsymbol{p}}} \cdot \tilde{\hat{\boldsymbol{s}}} = \hat{\boldsymbol{p}} \cdot \hat{\boldsymbol{s}}$ is scalar product of pump and signal SOPs. Numerical analysis of Eqs. (10.8)–(10.12) will be presented in the next Section.

Now, let's apply the averaging technique of [10, 14] to the system of SDEs (10.8)–(10.12). In agreement with the theorem of theory of SDEs [22], any continuous and sufficiently smooth function $\psi(\hat{\boldsymbol{\Omega}})$ obeys the following equation (Dynkin's formula [23]):

$$\frac{\partial \langle \psi \rangle}{\partial z} = \langle \Gamma\,(\psi) \rangle\,, \tag{10.13}$$

where components of $\hat{\boldsymbol{\Omega}}$ obey SDE:

$$\frac{d\Omega_i}{dz} = \sum_{k=1}^{m} Q_{ik}\beta_k + U_i, \tag{10.14}$$

which can be treated, in particular, as a matrix representation of Eqs. (10.8)–(10.12). In Eq. (10.14), Ω_i and U_i are $n-$dimensional vectors and $Q_{ik}(\Omega_i, z)$ is $n \times m$-dimensional matrix. Noise terms β_k corresponds to a Wiener process with $\langle \beta_k(z) \rangle = 0$ and $\langle \beta_k(z)\beta_l(z') \rangle = \sigma_k^2 \delta_{kl} \delta(z - z')$. $\Gamma(\psi)$ in Eq. (10.13) is a Stratonovich generator [22, 24]:

$$\Gamma = \sum_{j=1}^{n} U_j \frac{\partial}{\partial \Omega_j} + \frac{\sigma_l^2}{2} \sum_{j=1}^{n} \sum_{k=1}^{n} \sum_{l=1}^{n} \left(Q_{jl} Q_{kl} \frac{\partial^2}{\partial \Omega_j \partial \Omega_k} + Q_{kl} \frac{\partial Q_{jl}}{\partial \Omega_k} \frac{\partial}{\partial \Omega_j} \right). \tag{10.15}$$

Returning to Eqs. (10.8)–(10.12), the non-zero components of Eq. (10.15) can be written as [14]:

$$\Omega_1 = s_0,\ \Omega_2 = \tilde{s}_1,\ \Omega_3 = \tilde{s}_2,\ \Omega_4 = \tilde{s}_3,$$

$$\Omega_5 = \tilde{p}_1,\ \Omega_6 = \tilde{p}_2,\ \Omega_7 = \tilde{p}_3,\ \Omega_8 = \theta,$$

$$Q_{21} = \Omega_3,\ Q_{31} = -\Omega_2,\ Q_{51} = \Omega_6,\ Q_{61} = -\Omega_5,\ Q_{81} = 1,$$

$$U_1 = \frac{g_R}{2} P_0\,(z)\,(\tilde{p}_1\tilde{s}_1 + \tilde{p}_2\tilde{s}_2 + \tilde{p}_3\tilde{s}_3)\,,\ U_2 = \frac{g_R}{2} P_0\,(z)\,s_0\tilde{p}_1,$$

$$U_3 = \frac{g_R}{2} P_0(z)\, s_0 \tilde{p}_2 - 2b_s \tilde{s}_3,\ U_4 = \frac{g_R}{2} P_0(z)\, s_0 \tilde{p}_3 + 2b_s \tilde{s}_2,$$
$$U_6 = -2b_p \tilde{p}_3,\ U_7 = 2b_p \tilde{p}_2. \tag{10.16}$$

Applying this procedure leads to the following equations for different momenta of Eqs. (10.8)–(10.12) [15, 25]:

$$\frac{d\langle s_0\rangle}{dz'} = \varepsilon_1 \exp\left(-\varepsilon_2 z'\right)\langle x\rangle,\ \frac{d\langle x\rangle}{dz'} = \varepsilon_1 \exp\left(-\varepsilon_2 z'\right)\langle s_0\rangle - \varepsilon_3\langle y\rangle,$$
$$\frac{d\langle y\rangle}{dz'} = \varepsilon_3\left[\langle x\rangle - \langle \tilde{p}_1\tilde{s}_1\rangle\right] - \frac{L}{2L_c}\langle y\rangle,\ \frac{d\langle s_0^2\rangle}{dz'} = 2\varepsilon_1 \exp\left(-\varepsilon_2 z'\right)\langle s_0 x\rangle,$$
$$\frac{d\langle s_0 y\rangle}{dz'} = \varepsilon_1 \exp\left(-\varepsilon_2 z'\right)\langle xy\rangle + \varepsilon_3\left[\langle s_0 x\rangle - \langle y^2\rangle - \langle s_0\rangle\langle \tilde{p}_1\tilde{s}_1\rangle\right] - \frac{L}{2L_c}\langle s_0 y\rangle,$$
$$\frac{d\langle s_0 x\rangle}{dz'} = \varepsilon_1 \exp\left(-\varepsilon_2 z'\right)\left(\langle s_0^2\rangle + \langle x_0^2\rangle\right) - \varepsilon_3\langle y s_0\rangle,$$
$$\frac{d\langle x^2\rangle}{dz'} = 2\varepsilon_1 \exp\left(-\varepsilon_2 z'\right)\langle s_0 x\rangle - 2\varepsilon_3\langle xy\rangle,\ \frac{d\langle u^2\rangle}{dz'} = \frac{L}{L_c}\left(\langle y^2\rangle - \langle u^2\rangle\right),$$
$$\frac{d\langle xy\rangle}{dz'} = \varepsilon_1 \exp\left(-\varepsilon_2 z'\right)\langle s_0 y\rangle + \varepsilon_3\left[\langle x^2\rangle - \langle x\rangle\langle \tilde{p}_1\tilde{s}_1\rangle\right] - \frac{L}{2L_c}\langle xy\rangle,$$
$$\frac{d\langle y^2\rangle}{dz'} = 2\varepsilon_3\left[\langle xy\rangle - \langle y\rangle\langle \tilde{p}_1\tilde{s}_1\rangle\right] - \frac{L}{L_c}\left(\langle y^2\rangle - \langle u^2\rangle\right), \tag{10.17}$$

where $z' = z/L$, $\langle x\rangle = \left\langle \tilde{\vec{s}}\cdot\tilde{\vec{p}}\right\rangle$, $\langle \tilde{p}_1\tilde{s}_1\rangle = \tilde{p}_1(0)\,\tilde{s}_1(0)\exp(-z'L/L_c)$, $\langle y\rangle = \langle \tilde{p}_3\tilde{s}_2 - \tilde{p}_2\tilde{s}_3\rangle$, $\epsilon_1 = g_R P_{in} L/2$, $\epsilon_2 = \alpha_s L$, and $\epsilon_3 = 2\pi L(\omega_p/\omega_s - 1)/L_{bp}$. The averaging procedure here has to be understood as averaging over an ensemble of stochastic trajectories at the fixed z, i.e. we do not apply the ergodic theorem.

Thus, we arrived at a reach set of momenta defined by deterministic ordinary differential equations. We will analyze the results obtained from numerical simulations of Eqs. (10.8)–(10.12) and (10.17) in the next section.

Now we will demonstrate that a direct application of procedure described in [10] to only random birefringence in the coupled Manakov-PMD equations gives result which is valid in only limit of large PMDs (Manakov's limit) despite of Eq. (10.17) which are valid within a whole range of PMDs as it will shown in the next Section.

It is convenient to use the bra-ket formalism that is the Jones-matrix notations [13]. The coupled Manakov-PMD equations without taking into account the group-

delay dispersion and the nonlinear effects (i.e. $L \ll 100\,\text{km}$) have a form [26, 27]:

$$i\frac{\partial |A_s\rangle}{\partial z} + b_s\left(\sigma_3\cos(\theta) + \sigma_1\sin(\theta)\right)|A_s\rangle + \frac{i\alpha_s}{2}|A_s\rangle + \tag{10.18}$$

$$ib_s\left(\sigma_3\cos(\theta) + \sigma_1\sin(\theta)\right)\frac{\partial |A_s\rangle}{\partial t} - \frac{ig_R}{2}|A_p\rangle\langle A_p|A_s\rangle = 0,$$

$$i\frac{\partial |A_p\rangle}{\partial z} + b_p\left(\sigma_3\cos(\theta) + \sigma_1\sin(\theta)\right)|A_p\rangle + \frac{i\alpha_p}{2}|A_p\rangle + \tag{10.19}$$

$$ib_p\left(\sigma_3\cos(\theta) + \sigma_1\sin(\theta)\right)\frac{\partial |A_p\rangle}{\partial t} + \frac{ig_R}{2}\frac{\omega_p}{\omega s}|A_s\rangle\langle A_s|A_p\rangle = 0,$$

where

$$\sigma_1 = \begin{pmatrix} 0 & 1 \\ 1 & 0 \end{pmatrix},\ \sigma_2 = \begin{pmatrix} 0 & -i \\ i & 0 \end{pmatrix},\ \sigma_3 = \begin{pmatrix} 1 & 0 \\ 0 & -1 \end{pmatrix},$$

$$|A_{s,p}\rangle = \left(A_{(s,p),x}, A_{(s,p),y}\right)^T,\ \langle A_{s,p}| = |A_{s,p}\rangle^+ = \left(A^*_{(s,p),x}, A^*_{(s,p),y}\right) \tag{10.20}$$

and transformation to the Stokes representation can be made by transformation:

$$\hat{\boldsymbol{S}} = \langle A_s|\hat{\boldsymbol{\sigma}}|A_s\rangle,\ \hat{\boldsymbol{P}} = \langle A_p|\hat{\boldsymbol{\sigma}}|A_p\rangle,\ \hat{\boldsymbol{\sigma}} = \hat{\boldsymbol{i}}\sigma_1 + \hat{\boldsymbol{j}}\sigma_2 + \hat{\boldsymbol{k}}\sigma_3 \tag{10.21}$$

($\hat{\boldsymbol{i}}, \hat{\boldsymbol{j}}, \hat{\boldsymbol{k}}$ are unit vectors; don't confuse the Pauli matrixes $\hat{\boldsymbol{\sigma}}$ with a Wiener process volatility σ!). The time-derivatives in Eqs. (10.18) and (10.19) describe group-delays of signal and pump.

Rotation:

$$|A_{s,p}\rangle = \begin{pmatrix} \cos\left(\theta/2\right) & \sin\left(\theta/2\right) \\ -\sin\left(\theta/2\right) & \cos\left(\theta/2\right) \end{pmatrix}|a_{s,p}\rangle \tag{10.22}$$

results in:

$$i\frac{\partial |a_s\rangle}{\partial z} + \Sigma_s|a_s\rangle + \frac{i\alpha_s}{2}|a_s\rangle + ib_s\sigma_3\frac{\partial |a_s\rangle}{\partial t} - \frac{ig_R}{2}|a_p\rangle\langle a_p|a_s\rangle = 0, \tag{10.23}$$

$$i\frac{\partial |a_p\rangle}{\partial z} + \Sigma_p|a_p\rangle + \frac{i\alpha_p}{2}|a_p\rangle + ib_p\sigma_3\frac{\partial |a_p\rangle}{\partial t} + \frac{ig_R}{2}\frac{\omega_p}{\omega_s}|a_s\rangle\langle a_s|a_p\rangle = 0, \tag{10.24}$$

where

$$\Sigma_{s,p} = \begin{pmatrix} b_{s,p} & -\theta_z \\ \theta_z & -b_{s,p} \end{pmatrix},$$

$$\theta_z \equiv \frac{\partial \theta}{\partial z} = \beta(z), \ \langle \beta(z) \rangle = 0, \ \left\langle \beta(z)\beta\left(z'\right)\right\rangle = \sigma^2 \delta\left(z - z'\right). \tag{10.25}$$

An unitary transformation T:

$$\mathrm{T} = \begin{pmatrix} \tau_1 & \tau_2 \\ -\tau_2^* & \tau_1^* \end{pmatrix}, \ |\tau_1|^2 + |\tau_2|^2 = 1, \ \tau_1(0) = 1, \ \tau_2(0) = 0,$$

leads to a new set of equations:

$$i\frac{\partial |U\rangle}{\partial z} + \left(b_s - b_p\right)\tilde{\sigma}_3 |U\rangle + i\frac{\alpha_s}{2}|U\rangle + ib_s\tilde{\sigma}_3\frac{\partial |U\rangle}{\partial t} - i\frac{g_R}{2}|V\rangle\langle V|U\rangle = 0,$$

$$i\frac{\partial |V\rangle}{\partial z} + i\frac{\alpha_p}{2}|V\rangle + ib_p\tilde{\sigma}_3\frac{\partial |V\rangle}{\partial t} + i\frac{g_R}{2}\frac{\omega_p}{\omega_s}|U\rangle\langle U|V\rangle = 0,$$

$$\tilde{\sigma}_3 = \mathrm{T}^+\sigma_3\mathrm{T} = \begin{pmatrix} \Omega_1 & \Omega_4^* \\ \Omega_4 & -\Omega_1 \end{pmatrix}. \tag{10.27}$$

The six-component vector $\hat{\boldsymbol{\Omega}}$ describes an action of random birefringence and obeys the following SDE:

$$\frac{d\hat{\boldsymbol{\Omega}}}{dz} = \hat{\boldsymbol{Q}}\beta(z) + \hat{\boldsymbol{\Lambda}},$$

$$\Omega_1 = |\tau_1|^2 - |\tau_2|^2, \ \Omega_2 = -\left(\tau_1\tau_2 + \tau_1^*\tau_2^*\right), \ \Omega_3 = i\left(\tau_1\tau_2 - \tau_1^*\tau_2^*\right),$$

$$\Omega_4 = 2\tau_1^*\tau_2^*, \ \Omega_5 = \tau_1^2 - \left(\tau_2^*\right)^2, \ \Omega_6 = -i\left[\tau_1^2 + \left(\tau_2^*\right)^2\right],$$

$$Q_1 = 2\Omega_2, \ Q_2 = -2\Omega_1, \ Q_3 = 0, \ Q_4 = 2\Omega_5, \ Q_5 = -2\Omega_4, \ Q_6 = 0,$$

$$\Lambda_1 = 0, \ \Lambda_2 = -2b_p\Omega_3, \ \Lambda_3 = 2b_p\Omega_2, \ \Lambda_4 = 0, \ \Lambda_5 = -2b_p\Omega_6, \ \Lambda_6 = 2b_p\Omega_5, \tag{10.28}$$

where the components obey the following constraints and initial conditions:

$$\begin{gathered}\Omega_1^2+\Omega_2^2+\Omega_3^2=1,\ \Omega_4^2+\Omega_5^2+\Omega_6^2=0,\\ \Omega_1(0)=1,\ \Omega_2(0)=0,\ \Omega_3(0)=0,\\ \Omega_4(0)=0,\ \Omega_5(0)=0,\ \Omega_6(0)=-i.\end{gathered} \tag{10.29}$$

Equations (10.27) and (10.28) can be analyzed numerically, but we average Eq. (10.27) using a rule (10.13)–(10.15). Applying the Stratonovich's generator:

$$\begin{gathered}\frac{d\langle\psi(\Omega_i)\rangle}{dz}=\langle\Gamma[\psi(\Omega_i)]\rangle,\\ \Gamma=\sum_{i=1}^{6}\Lambda_i\frac{\partial}{\partial\Omega_i}+\frac{\sigma^2}{2}\sum_{i=1}^{6}\sum_{j=1}^{6}\left(Q_iQ_j+Q_j\frac{\partial Q_i}{\partial\Omega_j}\frac{\partial}{\partial\Omega_i}\right)\end{gathered} \tag{10.30}$$

results in:

$$\begin{gathered}\frac{d\langle\Omega_1\rangle}{dz}=-2\sigma^2\langle\Omega_1\rangle,\ \frac{d\langle\Omega_2\rangle}{dz}=-2b_p\langle\Omega_3\rangle-2\sigma^2\langle\Omega_2\rangle,\ \frac{d\langle\Omega_3\rangle}{dz}=2b_p\langle\Omega_2\rangle,\\ \frac{d\langle\Omega_4\rangle}{dz}=-2\sigma^2\langle\Omega_4\rangle,\ \frac{d\langle\Omega_5\rangle}{dz}=-2b_p\langle\Omega_6\rangle-2\sigma^2\langle\Omega_5\rangle,\ \frac{d\langle\Omega_6\rangle}{dz}=2b_p\langle\Omega_5\rangle\end{gathered} \tag{10.31}$$

with an initial condition $\langle(\Omega_1,\Omega_2,\Omega_3,\Omega_4,\Omega_5,\Omega_6)\rangle|_{z=0}=(1,0,0,0,0,0)$. Trivially $\langle\Omega_1(z)\rangle=\exp\left(-2\sigma^2z\right)$, $\langle\Omega_4(z)\rangle=\exp\left(-2\sigma^2z\right)$.

We have another groups of coupled equations for Ω_m-variables, as well (the argument z is omitted):

$$\begin{gathered}\frac{d\left\langle\Omega_1^2\right\rangle}{dz}=4\sigma^2\left(\left\langle\Omega_2^2\right\rangle-\left\langle\Omega_1^2\right\rangle\right),\ \frac{d\left\langle\Omega_2^2\right\rangle}{dz}=4\sigma^2\left(\left\langle\Omega_1^2\right\rangle-\left\langle\Omega_2^2\right\rangle\right)-4b_p\langle\Omega_2\Omega_3\rangle,\\ \frac{d\left\langle\Omega_3^2\right\rangle}{dz}=4b_p\langle\Omega_2\Omega_3\rangle,\ \frac{d\langle\Omega_2\Omega_3\rangle}{dz}=2b_p\left(\left\langle\Omega_2^2\right\rangle-\left\langle\Omega_3^2\right\rangle\right)-2\sigma^2\langle\Omega_2\Omega_3\rangle,\\ \left\langle\left(\Omega_1^2,\Omega_2^2,\Omega_3^2,\Omega_2\Omega_3\right)\right\rangle\Big|_{z=0}=(1,0,0,0),\end{gathered} \tag{10.32}$$

$$\frac{d\left\langle\Omega_4^2\right\rangle}{dz}=4\sigma^2\left(\left\langle\Omega_5^2\right\rangle-\left\langle\Omega_4^2\right\rangle\right),\ \frac{d\left\langle\Omega_5^2\right\rangle}{dz}=4\sigma^2\left(\left\langle\Omega_4^2\right\rangle-\left\langle\Omega_5^2\right\rangle\right)-4b_p\left\langle\Omega_5\Omega_6\right\rangle,$$
$$\frac{d\left\langle\Omega_6^2\right\rangle}{dz}=4b_p\left\langle\Omega_5\Omega_6\right\rangle,\ \frac{d\left\langle\Omega_5\Omega_6\right\rangle}{dz}=2b_p\left(\left\langle\Omega_5^2\right\rangle-\left\langle\Omega_6^2\right\rangle\right)-2\sigma^2\left\langle\Omega_5\Omega_6\right\rangle,$$
$$\left\langle\left(\Omega_4^2,\Omega_5^2,\Omega_6^2,\Omega_5\Omega_6\right)\right\rangle\Big|_{z=0}=(0,1,-1,-i),\tag{10.33}$$

$$\frac{d\left\langle|\Omega_4|^2\right\rangle}{dz}=4\sigma^2\left(\left\langle|\Omega_5|^2\right\rangle-\left\langle|\Omega_4|^2\right\rangle\right),$$
$$\frac{d\left\langle|\Omega_5|^2\right\rangle}{dz}=4\sigma^2\left(\left\langle|\Omega_4|^2\right\rangle-\left\langle|\Omega_5|^2\right\rangle\right)-2b_p\left(\left\langle\Omega_5\Omega_6^*\right\rangle+\left\langle\Omega_6\Omega_5^*\right\rangle\right),$$
$$\frac{d\left\langle|\Omega_6|^2\right\rangle}{dz}=2b_p\left(\left\langle\Omega_5\Omega_6^*\right\rangle+\left\langle\Omega_6\Omega_5^*\right\rangle\right),$$
$$\frac{d}{dz}\left(\left\langle\Omega_5\Omega_6^*\right\rangle+\left\langle\Omega_6\Omega_5^*\right\rangle\right)=4b_p\left(\left\langle|\Omega_5|^2\right\rangle-\left\langle|\Omega_6|^2\right\rangle\right)-2\sigma^2\left(\left\langle\Omega_5\Omega_6^*\right\rangle+\left\langle\Omega_6\Omega_5^*\right\rangle\right),$$
$$\left\langle\left(|\Omega_4|^2,|\Omega_5|^2,|\Omega_6|^2,\Omega_5\Omega_6,\Omega_5\Omega_6^*+\Omega_6\Omega_5^*\right)\right\rangle\Big|_{z=0}=(0,1,1,0),\tag{10.34}$$

$$\frac{d\left\langle\Omega_3\Omega_6\right\rangle}{dz}=2b_p\left(\left\langle\Omega_2\Omega_6\right\rangle+\left\langle\Omega_3\Omega_5\right\rangle\right),$$
$$\frac{d\left\langle\Omega_2\Omega_5\right\rangle}{dz}=-2b_p\left(\left\langle\Omega_2\Omega_6\right\rangle+\left\langle\Omega_3\Omega_5\right\rangle\right)-4\sigma^2\left(\left\langle\Omega_2\Omega_5\right\rangle-\left\langle\Omega_1\Omega_4\right\rangle\right),$$
$$\frac{d\left\langle\Omega_1\Omega_4\right\rangle}{dz}=4\sigma^2\left(\left\langle\Omega_2\Omega_5\right\rangle-\left\langle\Omega_1\Omega_4\right\rangle\right)$$
$$\frac{d}{dz}\left(\left\langle\Omega_2\Omega_6\right\rangle+\left\langle\Omega_3\Omega_5\right\rangle\right)=4b_p\left(\left\langle\Omega_2\Omega_5\right\rangle-\left\langle\Omega_3\Omega_6\right\rangle\right)-2\sigma^2\left(\left\langle\Omega_2\Omega_6\right\rangle+\left\langle\Omega_3\Omega_5\right\rangle\right),$$
$$\left\langle\left(\Omega_3\Omega_6,\Omega_2\Omega_6+\Omega_3\Omega_5,\Omega_2\Omega_5,\Omega_1\Omega_4\right)\right\rangle\Big|_{z=0}=(0,0,0,0),\tag{10.35}$$

and

$$\frac{d\left\langle \Omega_3\Omega_6^*\right\rangle}{dz} = 2b_p\left(\left\langle \Omega_2\Omega_6^*\right\rangle + \left\langle \Omega_3\Omega_5^*\right\rangle\right),$$

$$\frac{d\left\langle \Omega_2\Omega_6^*\right\rangle}{dz} 2b_p\left(\left\langle \Omega_2\Omega_5^*\right\rangle - \left\langle \Omega_3\Omega_6^*\right\rangle\right) - 2\sigma^2\left\langle \Omega_2\Omega_6^*\right\rangle,$$

$$\frac{d\left\langle \Omega_1\Omega_4^*\right\rangle}{dz} = 4\sigma^2\left(\left\langle \Omega_2\Omega_5^*\right\rangle - \left\langle \Omega_1\Omega_4^*\right\rangle\right),$$

$$\frac{d\left\langle \Omega_3\Omega_5^*\right\rangle}{dz} = 2b_p\left(\left\langle \Omega_2\Omega_5^*\right\rangle - \left\langle \Omega_3\Omega_6^*\right\rangle\right) - 2\sigma^2\left\langle \Omega_3\Omega_5^*\right\rangle$$

$$\left\langle\left(\Omega_3\Omega_6^*, \Omega_2\Omega_6^*, \Omega_2\Omega_5^*, \Omega_1\Omega_4^*, \Omega_3\Omega_5^*\right)\right\rangle\Big|_{z=0} = (0,0,0,0). \tag{10.36}$$

Returning to the Stokes representation, one has:

$$\frac{d\hat{\boldsymbol{S}}}{dz} = \frac{g_R}{2}\left(\hat{\boldsymbol{P}}\left|\hat{\boldsymbol{S}}\right| + \left|\hat{\boldsymbol{P}}\right|\hat{\boldsymbol{S}}\right) - \alpha_s\hat{\boldsymbol{S}} + \left(b_s - b_p\right)\exp\left(-2\sigma^2 z\right)\begin{pmatrix}0\\ -S_3\\ S_2\end{pmatrix},$$

$$\frac{d\hat{\boldsymbol{P}}}{dz} = -\frac{g_R\omega_p}{2\omega_s}\left(\hat{\boldsymbol{P}}\left|\hat{\boldsymbol{S}}\right| + \left|\hat{\boldsymbol{P}}\right|\hat{\boldsymbol{S}}\right) - \alpha_p\hat{\boldsymbol{P}}. \tag{10.37}$$

Equation (10.37) demonstrates that polarization effects are exponentially suppressed by the term $\propto \exp\left(-2\sigma^2 z\right)$ as $L_c \ll L$ (i.e. $\sigma^2 L \gg 1$). It is the so-called Manakov's limit corresponding to asymptotically large PMD [28] and it cannot describe polarization phenomena within a whole range of parameters.

10.4 Stochastic Anti-Resonance

System (10.17) allows analytical consideration in the framework of linear stability analysis [15]. Let's introduce new variables $\langle y'\rangle = \langle y\rangle/\langle s_0\rangle$, $\langle x'\rangle = \langle x\rangle/\langle s_0\rangle$, where $\langle x'\rangle \to 1$ describes a phenomenon of *polarization pulling* or trapping [11, 15, 26, 28–40]. The physical sense of this phenomenon is clearly visible from Eq. (10.1). Since SRS is polarization-dependent, the identical SOPs of pump and signal produce a maximum Raman gain. It means that the pump SOP will pull signal so that a Raman gain medium acts as effective polarizer. Inverse situation of $\langle x'\rangle \to 0$ corresponds to escape from a pulling state and can be treated as "*escape from metastable state*" [16, 17, 20].

Let's try to characterize this phenomenon. Figure 10.6 shows evolution of a "particle" (signal SOP in our case) within a *potential well* (which is created by

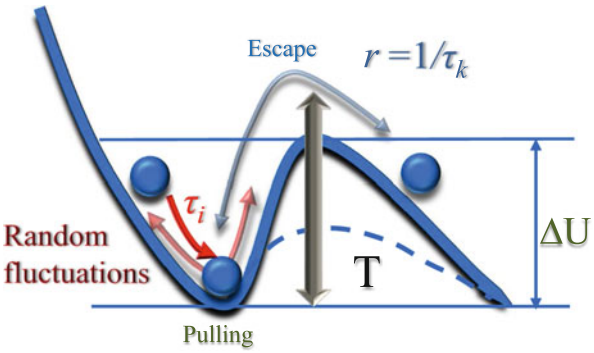

Fig. 10.6 Noise-induced escape from a metastable state (pulling state) controlled by an external periodic force with the period of potential barrier modulation T. ΔU is a potential barrier, $r = 1/\tau_k$ is an escape rate, τ_k is a Kramers (residence) time, and τ_i is an intra-well relaxation time

signal-pump SOP pulling) under influence of external *periodic perturbation* (beatings caused by birefringence) and *noise* (random birefringence). From Eq. (10.17), the steady-state (i.e. z−independent) solutions $\langle x_0' \rangle$ and $\langle y_0' \rangle$ corresponding to the pulling state for $\exp(-\varepsilon_2 z') \ll 1$ can be found from [15]:

$$\Delta^2 \langle x_0' \rangle^3 + \Delta \langle x_0' \rangle^2 + \left(\Delta_1^2 - \Delta^2\right) \langle x_0' \rangle - \Delta = 0,$$

$$\langle y_0' \rangle = \frac{\Delta_1 \langle x_0' \rangle}{\Delta \langle x_0' \rangle + 1}, \tag{10.38}$$

where $\Delta = 2L_c\varepsilon_1 \exp(-\varepsilon_2 z')/L$ and $\Delta_1 = 2L_c\varepsilon_3/L$. Linear stability analysis of the steady-state (10.38) gives the perturbation eigenvalues:

$$\Lambda_{1,2} = -\frac{3\Delta \langle x_0' \rangle + 1}{4L_c} \pm \frac{1}{4L_c}\sqrt{(1 - \Delta \langle x_0' \rangle)^2 + \Delta_1 (\Delta \langle y_0' \rangle - 4\Delta_1)}. \tag{10.39}$$

Let's introduce the intra-well relaxation length ("intra-well relaxation time" τ_i in Fig. 10.6) as $\tau_i = 1/|\mathrm{Re}(\Lambda_{1,2})|$. Brownian movement of a "particle" (i.e. SOP) in the vicinity of $\langle x_0' \rangle, \langle y' \rangle$ can cause escape from the pulling state [16–20] if $\mathrm{Im}(\Lambda_{1,2}) \neq 0$. The corresponding escape rate $r = 1/\tau_k$ is defined by the Kramers length ("Kramers time" in Fig. 10.6): $\tau_k = 1/r = 2\pi L/|\mathrm{Im}(\Lambda_{1,2})|$. Since $r \propto \exp(-\Delta U/D)$ [18], the noise strength D is defined by $\mathrm{Im}(\Lambda_{1,2})$ so that growth of imaginary part of perturbation increment corresponds to increase of the noise strength, i.e. to growth of effective "temperature", initiating an escape from the potential well.

Figure 10.7, *a* demonstrates dependencies of Kramers and relaxation lengths as well as $\langle x_0' \rangle$ and $\langle y_0' \rangle$ on the PMD parameter D_p. One can see, that abrupt decrease of the Kramers length (black solid curve) occur in the vicinity of $D_p \approx 0.02\, ps/\sqrt{km}$. This is evidence of growth of escape rate $r = 1/\tau_k$ from a potential well (i.e. from polarization pulling $\langle x_0' \rangle \to 1$). Such an escape is accompanied by threshold-like decrease of $\langle x_0' \rangle$ that means decorrelation of pump and signal SOPs. The fact of $\tau_k \approx \tau_i$ for $D_p > 0.02\, ps/\sqrt{km}$ can be interpreted as a strong stochastization of

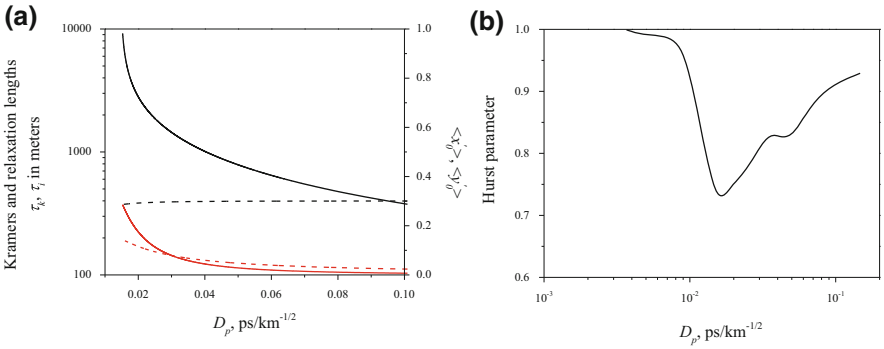

Fig. 10.7 (**a**): Dependencies of Kramers (*black solid curve*) and intra-well relaxation lengths (*black dashed curve*) as well as $\langle x_0' \rangle$ (*red solid curve*) and $\langle y_0' \rangle$ (*red dashed curve*) on the PMD coefficient D_p. (**b**): Analogous dependence of the Hurst parameter. The input SOPs are: $\tilde{\hat{\boldsymbol{s}}} = (1, 0, 0)$ and $\tilde{\hat{\boldsymbol{p}}} = (1, 0, 0)$, $s_0 = 10\,\text{mW}$, $P_0^{in} = 1\,\text{W}$, $L = 5\,\text{km}$ (Color figure online)

SOP evolution. The approximate equality $\tau_k \approx \tau_i$ means that the SOP excitation probability is characterized by a single rate as it takes a place for excitable systems [19]. Moreover, an enhancement of stochastization (see below) distinguishes this phenomenon from the *stochastic resonance* (SR) when the correlation between input and output signals increases and the signal-to-noise ratio passes through maximum [17, 19]. Therefore our phenomenon can be named "stochastic *anti*-resonance" (SAR). Also, one has to note that SAR develops in even linear system (10.8)–(10.12) unlike SR [41].

Another signature of such stochastization is provided by the Hurst parameter $0 < H < 1$ (Fig. 10.7b) [5]. This parameter is useful for characterizing of long memory processes and can be defined from an asymptotic behavior of corresponding correlation function $F(k) \sim k^{2H-2},\ k \to \infty$. If $0 < H < 1/2$, the process has anti-persistent correlation. If $1/2 < H < 1$, the process has persistent correlation (i.e. there are long range dependencies). If $H = 1/2$, the process is like to Brownian motion, i.e. it is memoryless or short-range-dependent. The Hurst parameter can be defined by the following method. Let's $\{x_k, k = 1, 2, \ldots, n\}$ is a sampled set of $x(z)$ with a mean value $\langle x(n) \rangle$ and a variance $\sigma_x^2(n)$. Then a so-called R/S-statistics [5] is defined by:

$$\frac{R(n)}{S(n)} = \frac{1}{\sigma_x(n)} \left[\max(0, W_1, W_2, \ldots, W_n) - \min(0, W_1, W_2, \ldots, W_n)\right],$$

$$W_k = \sum_{i=1}^{k} [x_i - \langle x(n) \rangle]. \tag{10.40}$$

The Hurst parameter can be found from

$$\left\langle \frac{R(n)}{S(n)} \right\rangle \propto n^H, \ n \to \infty. \tag{10.41}$$

The dependence of the Hurst parameter on the PMD parameter D_p was obtained from numerical simulations of Eqs. (10.8)–(10.12) (see below) and is shown in Fig. 10.7b. One can see, that $H \to 1$ for small PMDs (polarization pulling) but drops abruptly in the vicinity of $D_p \approx 0.02\ ps/\sqrt{km}$ when an escape from pulling state is intensified. The minimum value of $H \approx 0.7$ approaches the Brownian limit and such a dropping of persistent statistic distinguishes SAR from SR [19]. Nevertheless, H remains within the persistent statistic range (i.e. turbulence does not appear in our system). A further growth of PMD increases H. The physical interpretation of these phenomena will be presented below based on the result of numerical simulations of (10.8)–(10.12).

To analyze details of SAR phenomenon, we investigated Eqs. (10.8)–(10.12) numerically on the basis of the Wolfram Mathematica 9/10 computer algebra system. We have tested different numerical methods provided by both Mathematica and Matlab. Figure 10.8 demonstrates sets of stochastic trajectories obtained by Milstein, Stochastic Runge-Kutta, Stochastic Runge-Kutta Scalar Noise and Kloeden-Platen-Schurz algorithms built-in Mathematica. Only two latter methods provide a long-range convergence for all stochastic trajectories. These two algorithms were used for numerical simulations. Variation of step-size shown the optimal value of $\Delta z = 10^{-4} \min(L_c, L_b)$.

It is interesting to analyze dependencies of the averaged gain $\langle G \rangle$

$$\langle G \rangle = 10 \log \left(\frac{\langle s(L) \rangle}{s_0(0)} \right), \tag{10.42}$$

and the normalized variance of gain σ_G

$$\sigma_G = \sqrt{\frac{\langle s_0^2(L) \rangle}{\langle s_0(L) \rangle^2} - 1} \tag{10.43}$$

on PMD (Fig. 10.9a). One can see a kink-like behavior of $\langle G \rangle$ which maximum value is defined by polarization pulling (small D_p, nonnormalized gain $G \approx \exp(gPL - \ln 2)$ [28]) and minimum value defined by averaging over SOPs caused by their fast rotation for large D_p (solid black curve in Fig. 10.9). Owing such an averaging in the latter (scalar) limit, a fibre acts like a medium with effectively scalar Raman gain so that the nonnormalized gain is $G = g_R/2$ [28] and a correlation between pump and signal SOPs disappears (i.e. $\langle x \rangle \to 0$, black solid curve in Fig. 10.9b). The opposite case of small PMDs corresponds to almost isotropic medium with small "birefringence noise". In this case, the vector nature of Raman gain prevail so that the pump SOP attracts the signal one.

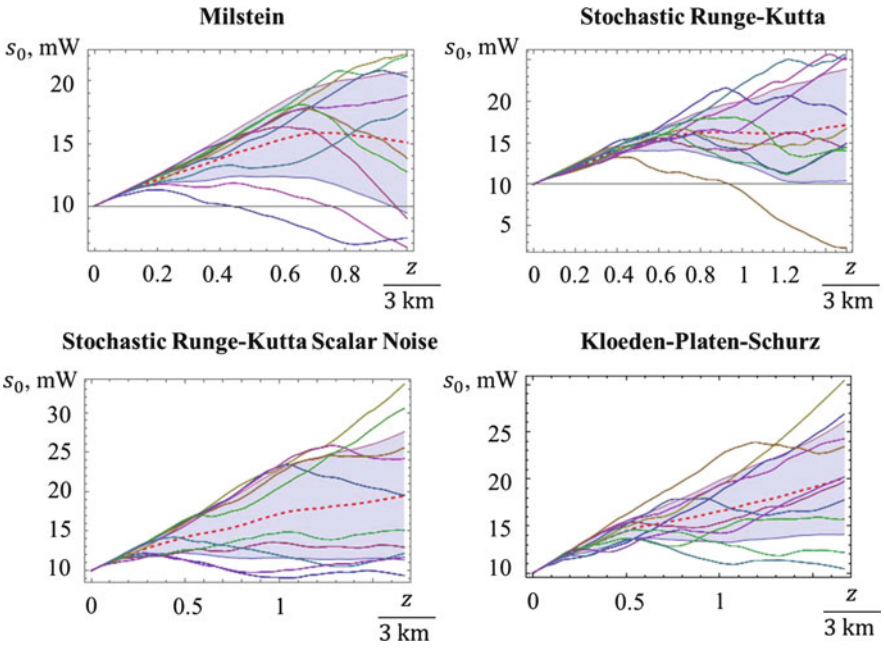

Fig. 10.8 Groups of ten stochastic trajectories of the signal power s_0 for the different numerical algorithms. Algorithms corresponding to bottom row congregate for all trajectories. *Dashed curves* show $\langle s_0 \rangle$ and filled regions correspond to ranges of the s_0 standard deviation. The input SOPs are: $\tilde{\hat{s}} = (1, 0, 0)$ and $\tilde{\hat{p}} = (1, 0, 0)$, $P_0^{in} = 1$ W

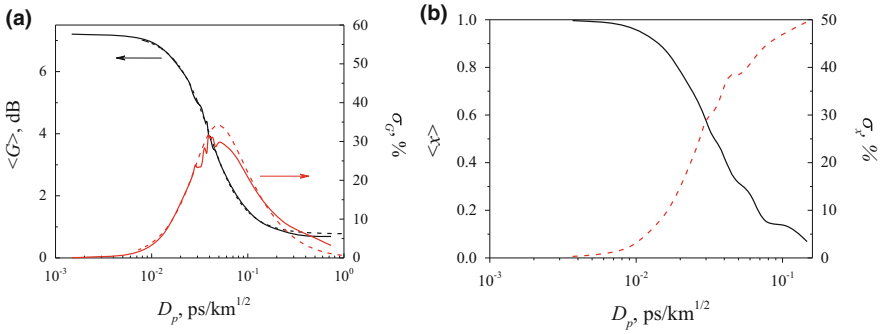

Fig. 10.9 (**a**): The average gain $\langle G \rangle$ (*black curves*) and the gain variance σ_G (*red curves*) obtained by the direct numerical simulations of SDEs (10.8)–(10.12) (*solid curves*) and from the averaged model (10.17) (*dashed curves*). (**b**) The analogous dependencies for $\langle x \rangle$ (*solid black curve*) and σ_x (*dashed red curve*) obtained from (10.8)–(10.12). The input SOPs are: $\tilde{\hat{s}} = (1, 0, 0)$ and $\tilde{\hat{p}} = (1, 0, 0)$, $s_0 = 10$ mW, $P_0^{in} = 1$ W, $L = 5$ km (Color figure online)

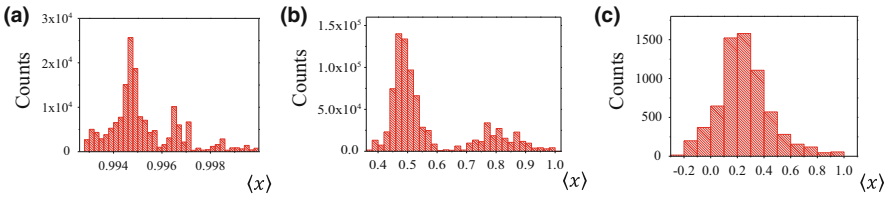

Fig. 10.10 Histograms of $\langle x(L)\rangle$ corresponding to Fig. 10.9. $D_p = 0.3 \times 10^{-2}$ (**a**), 3×10^{-2} (**b**) and 10^{-1} (**c**) $ps/\sqrt{km}$

Notable phenomenon is an existence of maximum of the gain variance at $D_p \approx (3 \div 4) \times 10^{-2}$ ($L_b \approx L_c/4$, solid red curve in Fig. 10.9a). This demonstrates the above described SAR when resonant interaction between periodic perturbations (polarization beatings) and noise (random birefringence) enhances randomness in a system unlike SR which enhances a regularity. As histogram in Fig. 10.10b demonstrates, a complete chaotization does not develop in the vicinity of σ_G maximum ($H \approx 0.7$, see above). Instead of that, there are two peaks corresponding to the states with maximum averaged residence times [19]. Further growth of D_p, although σ_G decreases due to averaging over SOPs (solid red curve in Fig. 10.9a), increases σ_x (dashed curve in Fig. 10.9b) due to decorrelation of pump and signal SOPs induced by fast polarization beatings. In particular, such a decorrelation reveals itself as substantial broadening of histogram peak in Fig. 10.10c. Random birefringence plays a role of rare "kicks" for fast rotating $\hat{\boldsymbol{s}}$ and $\hat{\boldsymbol{p}}$ so that H tends to 0.9 with further PMD growth. Despite decorrelation of SOPs, some residual correlation remains that is demonstrated by $\langle G\rangle \neq 0$ (Fig. 10.9a) and shift of histogram maximum in $\langle x\rangle \neq 0$ (Fig. 10.10c).

The very interesting and challenging result is a perfect agreement between the numerical data (Eqs. (10.8)–(10.12); solid curves in Fig. 10.9a) and the data obtained from the multi-scale averaging procedure (Eq. (10.17); dashed curves in Fig. 10.9a). It means that the averaging procedure has to take into account both birefringence beating and random birefringence scales unlike the classical Manakov's averaging over only random fluctuations (Eqs. (10.30)–(10.37)). Since the averaged equations are deterministic ODEs, they are easily solvable as opposed to SDEs (10.8)–(10.12). It can be very useful for simulations of long communication lines ($L \gg 1$ km). The important steps in this direction are taking into account pump depletion, group delay and group-delay dispersion, self-phase and cross-phase modulation.

10.5 Conclusion

Multi-scaling is a widespread property of both inanimate and animate nature. If multi-scaling is closely interwoven with interaction between deterministic and random processes, a multitude of interesting phenomena develop. For instance,

new steady-states can appear (*coherent resonance*), low-intensity and slow regular oscillations can be amplified by noise (*stochastic resonance*) or vise versus randomness can be resonantly increased by regular oscillations (*stochastic anti-resonance*). The last phenomenon was analyzed above on an example of fibre Raman oscillator. As was demonstrated lately, photonics opens a broad road for analog modeling of phenomenon ranging from gravity and cosmology [42] to neuroscience and informatics [41, 43–45]. Here, we used a fibre Raman amplifier with random birefringence as a test-bed for modeling multi-scale phenomena. Two main approaches were considered: direct numerical simulations of SDEs describing the evolution of signal and pump SOPs, and averaging techniques. For the lasts, we used averaging over only random birefringence or multi-scale averaging technique. It was demonstrated that the last method agrees perfectly with the results of direct numerical simulations. This can accelerate substantially simulations of long ($\gg$ 1 km) communication systems because the underlying deterministic ODEs are fast solvable in contrast with SDEs. Moreover, such an approach provides with a rich set of signatures characterizing the statistical properties of system. For instance, we considered averaged gain and SOP projection, their variances, autocorrelations, spectra, Kramers length and Hurst parameter, etc.

Our analysis demonstrated that variation of control parameter (PMD) leads to resonant enhancement of fluctuations in a system: *stochastic anti-resonance*. This enhancement can be interpreted as a noise-induced escape from metastable state. Such a state (potential well) is created by the polarization pulling that is attraction of signal SOP to pump SOP due to vectorial nature of the Raman gain. A fibre behaves like isotropic medium and the Raman gain works as an effective polarizer in this case. When the polarization beat-length defining a period of potential barrier modulation becomes lesser than the birefringence correlation length, the rate of escape from meta-stable state (which is inversely proportional to the Kramers length) grows abruptly that initiates an escape from potential well. As a result, randomness of dynamics enhances that is demonstrated by growth of the gain variance and by abrupt decrease of the Hurst parameter. Nevertheless, dynamics remains partially correlated due to $H \geq 0.7$. Further decrease of L_b (i.e., PMD-growth) results in so fast rotation of SOP that pump and signal become almost de-correlated. As a result, only polarization-averaged (i.e. scalar) Raman gain contributes to dynamics. Randomness decreases and plays a role of rare "kicks" disturbing SOP. The Hurst parameter approaches 0.9 and the gain variance decreases.

We guess that the described methods and phenomena are of great importance not only for photonics but also for study of complex coupled systems, nanostructures, biology and medicine, neuroscience, finance, etc.

Acknowledgements Support of the FP7-PEOPLE-2012-IAPP (project GRIFFON, No. 324391) is acknowledged. The computational results have been achieved using the Vienna Scientific Cluster (VSC).

References

1. A. Beckermann (ed.), *Emergence or Reduction? Esseys on the Prospects of Nonreductive Physicalism* (de Gruyter, Berlin, 1992), p. 28
2. R. Lewin, Complexity. *Life at the Edge of Chaos* (Macmillan Publishing Company, New York, 1992)
3. H. Poincaré, *Les méthodes nouvelles de la mécanique céleste*, tome I (Gauthier-Villars, Paris, 1892)
4. A. Nayfeh, *Perturbation Methods* (Wiley, New York, 1973)
5. J. Gao, Y. Cao, W. Tung, J. Hu, *Multiscale Analysis of Complex Time Series: Integration of Chaos and Random Fractal Theory, and Beyond* (Wiley-Blackwell, New Jersey, 2007)
6. E. Weinan, *Principles of Multiscale Modeling* (Cambridge University Press, Cambridge, 2011)
7. A. Galtarossa, C.R. Menyuk, *Polarization Mode Dispersion* (Springer, New-York, 2005)
8. C. Headley, G.P. Agrawal (eds.), *Raman Amplification in Fiber Optical Communication Systems* (Elsevier, Amsterdam, 2005)
9. S.V. Manakov, On the theory of two-dimensional stationary self-focusing of electromagnetic waves. Sov. Phys. J. Exp. Theor. Phys. **38**, 248–253 (1974)
10. P.K.A. Wai, C.R. Menyuk, Polarization mode dispersion, decorrelation, and diffusion in optical fibers with randomly varying birefringence. J. Lightwave Technol. **14**, 148–157 (1996)
11. V.V. Kozlov, J. Nuño, J.D. Ania-Castañón, S. Wabnitz, Trapping polarization of light in nonlinear optical fibers: an ideal Raman polarizer, in *Spontaneous Symmetry Breaking, Self-Trapping, and Josephson Oscillations*, ed. by B.A. Malomed. Progress in Optical Science and Photonics, vol. 1 (Springer, Berlin, 2013), pp. 227–246
12. V. Kalashnikov, S.V. Sergeyev, G. Jacobsen, S. Popov, S.K. Turitsyn, Multi-scale polarisation phenomena. Light Sci Appl **5**, e16011 (2016)
13. Q. Lin, G.P. Agrawal, Vector theory of stimulated Raman scattering and its application to fiber-based Raman amplifiers. J. Opt. Soc. Am. B **20**, 1616–1631 (2003)
14. S. Sergeyev, S. Popov, A.T. Friberg, Modeling polarization-dependent gain in fiber Raman amplifiers with randomly varying birefringence. Opt. Commun. **262**, 114–119 (2006)
15. S. Sergeyev, Activated polarization pulling and de-correlation of signal and pump states of polarization in fiber raman amplifier. Opt. Express **19**, 24268–24279 (2011)
16. P. Hanggi, Escape from a metastable state. J. Stat. Phys. **42**, 105–148 (1986)
17. B. Lindner, J. Garsia-Ojalvo, A. Neiman, L. Schimansky-Greif, Effects of noise in excitable systems. Phys. Rep. **392**, 321–424 (2004)
18. L. Gammaitoni, P. Hänggi, P. Jung, F. Marchesoni, Stochastic resonance. Rev. Mod. Phys. **70**, 223–287 (1998)
19. Th. Wellens, V. Shatochin, A. Buchleitner, Stochastic resonance. Rep. Prog. Phys. **67**, 45–105 (2004)
20. M.I. Dykman, B. Golding, L.I. McCann, V.N. Smelyanskiy, D.G. Luchinsky, R. Mannella, P.V.E. McClintock, Activated escape of periodically driven systems. Chaos **11**, 587–594 (2001)
21. R.H. Stolen, Polarization effects in fiber Raman and Brillouin Lasers. IEEE J. Quantum Electron. **QE-15**, 1157–1160 (1979)
22. L. Arnold, *Stochastic Differential Equations: Theory and Applications* (Wiley, New York, 1974)
23. B. Øksendal, *Stochastic Differential Equations* (Springer, Berlin, 2007)
24. G.A. Pavliotis, *Stochastic Processes and Applications: Diffusion Process, the Fokker-Planck and Langevin Equations* (Springer, New York, 2014)
25. S. Sergeyev, S. Popov, A.T. Friberg, Virtually isotropic transmission media with fiber raman amplifier. IEEE J. Quantum Electron. **QE-46**, 1492–1497 (2010)
26. V.V. Kozlov, J. Nuño, J.D. Ania-Castañón, S. Wabnitz, Theory of fiber optic Raman polarizers. Opt. Lett. **35**, 3970–3972 (2010)

27. V.V. Kozlov, J. Nuño, J.D. Ania-Castañón, S. Wabnitz, Multichannel Raman polarizer with suppressed relative intensity noise for wavelength division multiplexing transmission lines. Opt. Lett. **37**, 2073–2075 (2012)
28. V.V. Kozlov, J. Nuño, J.D. Ania-Castañón, S. Wabnitz, Trapping polarization of light in nonlinear optical fibers: an ideal Raman polarizer, in *Progress in Optical Science and Photonics. Spontaneous Symmetry Breaking, Self-Trapping, and Josephson Oscillations*, ed. by B.A. Malomed (Springer, Berlin, 2012), pp. 227–246
29. V.V. Kozlov, J. Nuño, J.D. Ania-Castañón, S. Wabnitz, Theoretical study of optical fiber Raman polarizers with counterpropagating beams. J. Lightwave Technol. **29**, 341–347 (2011)
30. V.V. Kozlov, J. Nuño, J.D. Ania-Castañón, S. Wabnitz, Analytic theory of fiber-optic Raman polarizers. Opt. Express **20**,27242–27247 (2012)
31. S. Sergeyev, S. Popov, Two-section fiber optic Raman polarizer. IEEE J. Quantum Electron. **QE-48**, 56–60 (2012)
32. S. Sergeyev, S. Popov, A.T. Friberg, Spun fiber Raman amplifiers with reduced polarization impairments. Opt. Express **16**, 14380–14389 (2008)
33. S. Sergeyev, Fiber Raman amplification in a two-scale spun fiber. Opt. Mater. Express **2**, 1683–1689 (2012)
34. L. Ursini, M. Santagiustina, L. Palmieri, Raman nonlinear polarization pulling in the pump depleted regime in randomly birefringent fibers. IEEE Photon. Technol. Lett. **23**, 254–256 (2011)
35. F. Chiarello, L. Ursini, L. Palmieri, M. Santagiustina, Polarization attraction in counterpropagating fiber Raman amplifiers. IEEE Photon. Technol. Lett. **23**, 1457–1459 (2011)
36. M. Martinelli, M. Cirigliano, M. Ferrario, L. Marazzi, P. Martelli, Evidence of Raman-induced polarization pulling. Opt. Express **17**, 947–955 (2009)
37. S. Popov, S. Sergeyev, A.T. Friberg, Impact of pump polarization on the polarization dependence of Raman gain due to the break of fiber circular symmetry. J. Opt. A Pure Appl. Opt. **6**, S72–S76 (2004)
38. N.J. Muga, M.F.S. Ferreira, A.N. Pinto, Broadband polarization pulling using Raman amplification. Opt. Express **19**, 18707–18712 (2011)
39. P. Morin, S. Pitois, J. Fatome, Simultaneous polarization attraction and Raman amplification of a light beam in optical fibers. J. Opt. Soc. Am. B **29**, 2046–2052 (2012)
40. F. Chiarello, L. Palmieri, M. Santagiustina, R. Gamatham, A. Galtarossa, Experimental characterization of the counter-propagating Raman polarization attraction. Opt. Express **20**, 26050–26055 (2012)
41. M.D. McDonnell, D. Abbott, What is stochastic resonance? Definitions, misconceptions, debates, and its relevance to biology. PLoS Comput. Biol. **5**, e1000348 (2009)
42. D. Faccio, F. Belgiorno, S. Cacciatori, V. Gorini, S. Liberati, U. Moschella (eds.), *Analogue Gravity Phenomenology. Analogue Spacetimes and Horizons, from Theory to Experiment* (Springer, Cham, 2013)
43. M. Naruse (ed.), *Nanophotonic Information Physics* (Springer, Berlin, 2014)
44. F. Moss, L.M. Ward, W.G. Sannita, Stochastic resonance and sensory information processing: a tutorial and review of application. Clin. Neurophysiol. **115**, 267–281 (2004)
45. P. Hänggi, Stochastic resonance in biology. ChemPhysChem **3**, 285–290 (2002)

Chapter 11
A Simple Plankton Model with Complex Behaviour

Irene M. Moroz, Roger Cropp, and John Norbury

Abstract In this paper we extend the P_1P_2ZN model, introduced by Cropp and Norbury (J Plankton Res 31:939–963, 2009) to investigate the effects of specialist (or discriminate) and generalist (or indiscriminate) grazing (as parameterised by ρ) on a prey-prey-predator model for plankton, in the presence of a limiting nutrient. We also examine the influence of facultative and obligate omnivory on the survival of Z as a generalist predator, as we vary the linear mortality parameter σ_Z. This leads to bifurcation transition diagrams, which also include steady state stability branches for certain critical points. For specialist grazing ($\rho = 0$) the bifurcation transition diagram shows steady states, periodic and chaotic dynamics, with very small windows of periodic behaviour, as σ_Z varies, while for generalist grazing ($\rho = 1$), we only find periodic or steady state behaviours. The dynamics is interpretable in terms of facultative/obligate omnivory of Z. Results suggest that green ocean plankton code in global climate change modelling might run more stably with generalist grazing terms and careful control of grazer mortality.

11.1 Introduction

Plankton are organisms that cannot swim faster than ocean currents. They comprise single-cell microscopic plants called phytoplankton (diatoms and dinoflagellates) and smaller and larger grazers called zooplankton (e.g. from ciliates and copepods to krill and jelly fish), found in the upper 50 m sunlit layers of marine ecosystems.

I.M. Moroz (✉) • J. Norbury
Mathematical Institute, University of Oxford, Andrew Wiles Building, ROQ, Oxford, OX2 6GG,UK
e-mail: moroz@maths.ox.ac.uk; john.norbury@lincoln.ox.ac.uk

R. Cropp
Griffith School of Environment, Griffith University, Nathan, QLD 4111, Australia
e-mail: r.cropp@griffith.edu.au

C. Skiadas (ed.), *The Foundations of Chaos Revisited: From Poincaré to Recent Advancements*, Understanding Complex Systems,
DOI 10.1007/978-3-319-29701-9_11

Using sunlight and dissolved nutrients (e.g. nitrates, phosphates, etc, carried by rivers into oceans) phytoplankton convert CO_2 from the atmosphere during photosynthesis in the upper mixed ocean surface layer, eventually drawing it down into the deep ocean. Decomposers (viruses, bacteria and fungi) capture and recycle waste products, remineralising organic nutrients into inorganic dissolved nutrients, and thus completing the nutrient recycling loop. Phytoplankton account for about half of global synthesis of organic compounds and CO_2 [7], as well as producing half of the world's oxygen in the atmosphere via photosynthesis [3]. They are the primary food source for zooplankton. Together, these plankton form the base of the ocean's food chain, without which sharks, tuna, mackerel and other small fish would not survive. In turn, fish provide nearly 20 % of total protein for humans.

Plankton may be key indicators of climate change as production depends upon water temperature and acidity, and nutrient availability. Coccolithophore phytoplankton produce dimethylsulphide and other volatile compounds, affecting cloud formation over the oceans [4]. Long term climate change could alter the plankton community structure, affecting seasonal plankton blooms, and so affect the marine food chain. Collapse or extinction of a plankton population may push the climate system across a tipping point. Indeed Falkowski [7] writes regarding the crucial role played by phytoplankton in offsetting the effects of burning fossil fuels:

> ... if the phytoplankton in the upper ocean stopped pumping carbon down to the deep sea tomorrow, atmospheric levels of carbon dioxide would eventually rise by another 200 $p.p.m.$ and global warming would accelerate further.

PlankTOM5 [13], PlankTOM10 [12], and MAREMIP (MARine Ecosystem Model Inter-comparison Project [16]. See also [1]) are examples of global marine models, representing ecosystems with many different plankton functional types, developed to quantify the interactions between climate and ocean biogeochemistry, especially through CO_2. The merits of incorporating such complex ecological models into operational global climate models is questionable in the absence of a thorough understanding of the behaviours supported by such models in their own right. Our approach is to gain understanding from a study of much simpler models.

In this paper we consider a simple model of two different prey populations of phytoplankton P_1, P_2, being eaten by a population of predator zooplankton Z, where the interacting plankton populations are connected by a single limiting nutrient N. We focus on behaviour that is possible in this P_1P_2ZN model for plankton population dynamics as we vary the zooplankton mortality parameter, and as we change the zooplankton grazing function from discriminate ($\rho = 1$) to indiscriminate ($\rho = 0$) prey hunting behaviour.

11.2 The Plankton Model

We study the P_1P_2ZN model for plankton dynamics:

$$\dot{P}_1 = P_1[\frac{\mu_1 N}{N+\kappa_1} - \frac{\phi_1 Z}{1+\epsilon_1 P_1 + \rho\epsilon_2 P_2} - \sigma_1], \tag{11.1}$$

$$\dot{P}_2 = P_2[\frac{\mu_2 N}{N+\kappa_2} - \frac{\phi_2 Z}{1+\rho\epsilon_1 P_1 + \epsilon_2 P_2} - \sigma_2], \tag{11.2}$$

$$\dot{Z} = Z[\frac{\phi_1(1-\psi_1)P_1}{1+\epsilon_1 P_1 + \rho\epsilon_2 P_2} + \frac{\phi_2(1-\psi_2)P_2}{1+\rho\epsilon_1 P_1 + \epsilon_2 P_2} - \sigma_Z], \tag{11.3}$$

together with the nutrient N mass conservation condition:

$$\dot{N} = -\dot{P}_1 - \dot{P}_2 - \dot{Z}, \tag{11.4}$$

for two phytoplankton prey populations P_1 and P_2 and one zooplankton predator Z, where $P_1 + P_2 + Z + N = 1$. See [5, 6] for further details.

The various parameters appearing in Eqs. (11.1)–(11.3) (except for ρ) are explained in Table 11.1.

Table 11.1 Measured parameter values for Eqs. (11.1)–(11.3) and their physical interpretations

Par.	Process	Value	Reference
μ_1	Maximum rate of N uptake by P_1	1.00	Gabric et al. [9]
μ_2	Maximum rate of N uptake by P_2	1.15	Muller-Niklas and Herndl [15]
κ_1	Half-saturation constant for N uptake by P_1	0.25	Slagstad and Stole-Hansen [17]
κ_2	Half-saturation constant for N uptake by P_2	0.07	Billen and Becquevort [2]
ϕ_1	Z grazing rate on P_1	6.18	Hansen et al. [11]
ϕ_2	Z grazing rate on P_2	1.85	Gabric et al. [9]
ϵ_1	Half-saturation constant for Z uptake of P_1	5.50	Fenchel [8]
ϵ_2	Half-saturation constant for Z uptake of P_2	5.50	Fenchel [8]
σ_1	P_1 specific mortality rate	0.00	Gabric et al. [10]
σ_2	P_2 specific mortality rate	0.26	Moloney et al. [14]
σ_Z	Z specific mortality rate	0.19	Moloney et al. [14]
ψ_1	Proportion of P_1 uptake excreted by Z	0.40	Moloney et al. [14]
ψ_2	Proportion of P_2 uptake excreted by Z	0.40	Moloney et al. [14]

11.2.1 The Four Cases of Interest

There are four combinations of cases that are of interest:

- specialist (or discriminate) vs generalist (or indiscriminate) grazing;
- facultative vs obligate omnivory by Z.

The **specialist** predator ($\rho = 0$) feeds on multiple prey resources, but on each independently of the other, and in a discriminating manner. The feeding of the **generalist** predator ($\rho = 1$) on each prey resource is indiscriminate. See Cropp et al. [6] for a more detailed explanation of these grazing functions, which are used in the green ocean components of several climate change programs (for example by Sailley et al. [16]).

We define Z to be a **facultative omnivore** if it can survive on either P_1 or P_2 independently:

$$0 < \sigma_Z < \min\left(\frac{\phi_1(1-\psi_1)}{1+\epsilon_1}, \frac{\phi_2(1-\psi_2)}{1+\epsilon_2}\right) = \sigma_{Zmin}, \tag{11.5}$$

while Z is an **obligate omnivore** if it must have P_1 present (this choice comes from the parameter values given in Table 11.1) in order to survive; we order P_1 and P_2 to get:

$$\sigma_{Zmin} < \sigma_Z < \max\left(\frac{\phi_1(1-\psi_1)}{1+\epsilon_1}, \frac{\phi_2(1-\psi_2)}{1+\epsilon_2}\right) = \sigma_{Zmax}. \tag{11.6}$$

Using the parameter values in Table 11.1,

$$\left(\frac{\phi_1(1-\psi_1)}{1+\epsilon_1}, \frac{\phi_2(1-\psi_2)}{1+\epsilon_2}\right) = (0.5705, 0.1708), \tag{11.7}$$

so that Z is a facultative omnivore if

$$0 < \sigma_Z < \sigma_{Zmin} = 0.1708, \tag{11.8}$$

and an obligate omnivore, (requiring the presence of P_1 to survive) if:

$$0.1708 < \sigma_Z < \sigma_{Zmax} = 0.5705. \tag{11.9}$$

If $\sigma_Z > 0.5705$, Z is no longer a viable population and dies out.

We shall therefore describe the dynamics in terms of bifurcation transition diagrams as σ_Z varies, for both $\rho = 0$ and $\rho = 1$.

11.2.2 Critical Points

Our analysis of the critical (or equilibrium) points of (11.1)–(11.4) and their linear stabilities uses the same notation and labelling as [5]. Indeed the analyses for the origin and prey-only critical points are identical to that in [5]. Also, there is no predator-only critical point nor a pure prey-prey critical point for $\sigma_Z > 0$.

11.3 Generalist Predation $\rho = 1$, Indiscriminate Grazing

When $\rho = 1$, we have generalist predation. By evaluating the Jacobian of the rhs of Eqs. (11.1)–(11.3) at each of the critical points listed in Table 11.2, we determined the eigenvalues and so the linear stability of each critical point in terms of the predator mortality σ_Z. We then combined these results with numerical integrations of Eqs. (11.1)–(11.3) to produce a bifurcation transition diagram in terms of the maximum and minimum values of prey P_2 as σ_Z varies.

To produce the transition diagram, we fixed σ_Z and integrated the system numerically for 20,000 time units, ignoring transients. We plotted the maximum and minimum values of prey P_2 over each oscillation; for steady states, these reduce to the steady state value of P_2 for the relevant critical point. We then took the final variable values as the initial conditions for the next value of σ_Z and repeated the procedure. The results are summarised in Fig. 11.1.

Table 11.2 Critical points of Eqs. (11.1)–(11.3), and their labels as in [5]

Critical point	Label (P_1, P_2, Z, N)
Origin	$(0, 0, 0, 1)$
Prey A	$(P_{1A}, 0, 0, N_A)$
Prey C	$(0, P_{2C}, 0, N_C)$
Predator-Prey D	$(P_{1D}, 0, Z_D, N_D)$
Predator-Prey F	$(0, P_{2F}, Z_F, N_F)$
Predator-Prey-Prey E	$(P_{1E}, P_{2E}, Z_E, N_E)$

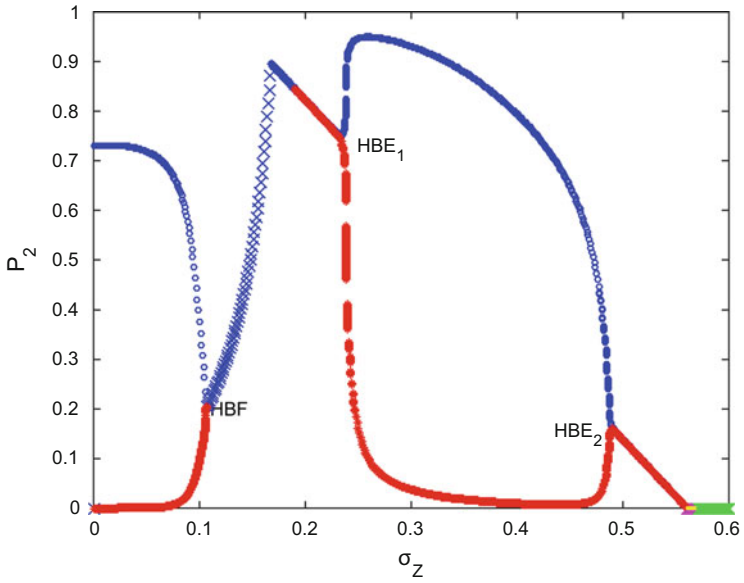

Fig. 11.1 Bifurcation transition diagram for generalist grazing ($\rho = 1$) for $0 \leq \sigma_Z \leq 0.6$. '*blue circle*' indicate maximum and '*red star*' minimum values of the amplitude of P_2 over each cycle. The 'x' denotes the stable critical point F steady state, the *yellow* denotes the stable critical point D steady state, and the *green* the stable critical point A state. *HBn* denotes Hopf bifurcation for critical point n. There are two branches of stable critical point E steady states, one joining the end of the steady critical point F steady state to HBE_1, the other joining HBE_2 to the stable critical point D steady state (Color figure online)

For $0 < \sigma_Z < 0.11$, we obtain stable (P_2, Z, N) limit cycle oscillations. This predator-prey state then undergoes a supercritical Hopf Bifurcation at $\sigma_Z = 0.11$ (labelled as *HBF* in Fig. 11.1), following which we have stable critical point $(0, P_{2F}, Z_F, N_F)$ steady states for $0.11 < \sigma_Z < 0.17$. $(0, P_{2F}, Z_F, N_F)$ then loses stability to stable critical point $(P_{1E}, P_{2E}, Z_E, N_E)$ steady states, which exist in the region $0.17 < \sigma_Z < 0.225$. Stable (P_1, P_2, Z, N) oscillations then appear via a supercritical Hopf bifurcation (labelled as HBE_1 in Fig. 11.1). These oscillations persist until a second supercritical Hopf bifurcation (HBE_2) at $\sigma_Z = 0.49$ gives rise once more to stable $(P_{1E}, P_{2E}, Z_E, N_E)$ steady states for $0.49 < \sigma_Z < 0.56$, before $P_2 \to 0$ and this prey-prey-predator state loses stability to a stable $(P_{1D}, 0, Z_D, N_D)$

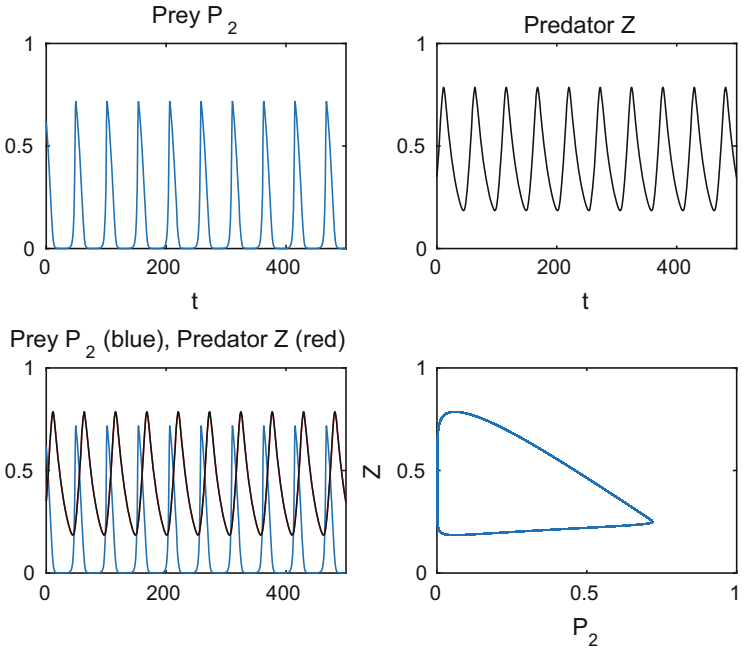

Fig. 11.2 P_2 and Z time series, and the (P_2, Z) phase portrait for the facultative omnivore predator-prey F for $\rho = 1$ and $\sigma_Z = 0.05$

steady state at $\sigma_Z = 0.56$. This critical point D steady state has a very small window of stability: $0.56 < \sigma_Z < 0.57$. For $\sigma_Z > 0.57$, Z is no longer viable as $Z \to 0$ and we are left with only a stable A prey steady state thereafter.

We found no evidence of chaotic states for $\rho = 1$.

Figure 11.2 shows the time series and phase portrait for the facultative omnivore (P_2, Z, N) when $\sigma_Z = 0.05$. The time scale is such that 3650 time units $\approx$ 1 year. Figure 11.3 shows time series and a three-dimensional phase portrait for the obligate omnivore (P_1, P_2, Z, N) for $\sigma_Z = 0.45$.

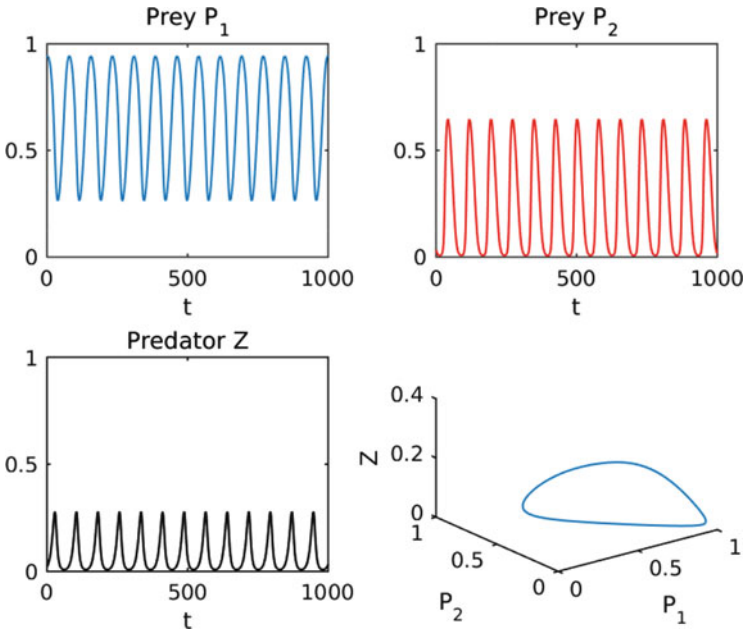

Fig. 11.3 P_1, P_2 and Z time series, and a 3-D phase portrait for the obligate omnivore $\rho = 1$ and $\sigma_Z = 0.45$

11.4 Specialist Predation ($\rho = 0$, Discriminate Grazing)

When $\rho = 0$, we have specialist predation. Following the procedure outlined in the previous section, we produced a bifurcation transition diagram in terms of the maximum and minimum values of prey P_2 as σ_Z varies. The results are summarised in Fig. 11.4.

For $0 \leq \sigma_Z < 0.11$, we again obtain stable (P_2, Z, N) limit cycle oscillations. This F predator-prey state then undergoes a supercritical Hopf Bifurcation (labelled as *HBF* in Fig. 11.4) at $\sigma_Z = 0.11$, following which we have a stable F steady state for $0.11 < \sigma_Z < 0.17$. $(0, P_{2F}, Z_F, N_F)$ then loses stability to $(P_{1E}, P_{2E}, Z_E, N_E)$ oscillations at $\sigma_Z \approx 0.168$. In view of (11.8), Z is a facultative omnivore in this region.

For $0.168 < \sigma_Z < 0.533$, P_1 is no longer zero and we find predominantly chaotic (P_1, P_2, Z, N) oscillations, before $P_2 \to 0$, resulting in this prey-prey-predator state losing stability to a stable (P_{1D}, Z_D, N_D) steady state at $\sigma_Z = 0.533$. This critical point D steady state is stable in a larger window of $0.533 < \sigma_Z < 0.57$ than for the generalist case. From (11.9), Z is now an obligate omnivore, requiring the presence of P_1 to exist.

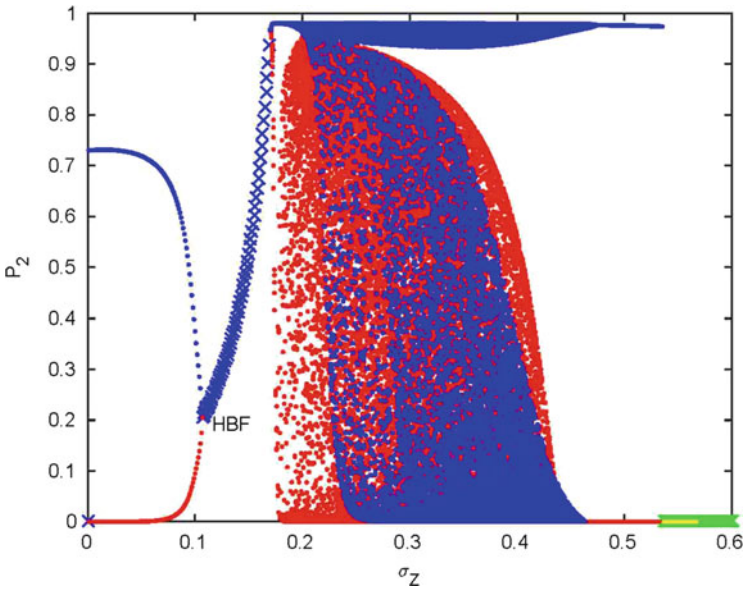

Fig. 11.4 Bifurcation transition diagram for specialist grazing ($\rho = 0$) for $0 \leq \sigma_Z \leq 0.6$. The maximum (*blue 'circle'*) and minimum (*red 'star'*) values of the amplitude of P_2 over each cycle as σ_Z varies. Also shown are regions of stability of critical point F steady states (*blue 'times'*), critical point D steady states (*yellow 'circle'*) and critical point A steady states (*green 'circle'*). *HBF* denotes the supercritical Hopf Bifurcation for critical point F (Color figure online)

The prey-only critical point A is unstable for $\sigma_Z < 0.57$. For $\sigma_Z > 0.57$, Z is no longer viable as $Z \to 0$ and we are left with only a stable critical point prey A steady state thereafter.

We now show plots of time series and phase portraits for selected values of σ_Z in the range $0.17 < \sigma_Z < 0.53$, chosen from Fig. 11.4.

For $\sigma_Z = 0.2$, we are just inside the chaotic regime for the obligate omnivore (P_1, P_2, Z, N). Since Z requires the presence of P_1 to exist, Fig. 11.5 shows that P_1 and Z are synchronised, with Z leading P_1, but both are out of phase with P_2. The (P_1, P_2, Z) phase portrait shows that the system never visits the interior of the (P_1, P_2) plane, in contrast to the example shown in Fig. 11.6.

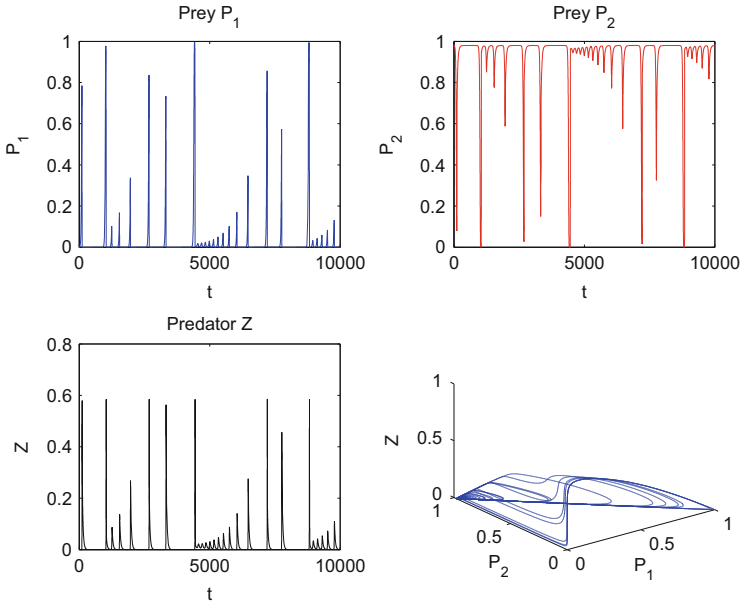

Fig. 11.5 Time series for P_1, P_2 and Z, and a 3-D (P_1, P_2, Z) phase portrait for $\rho = 0$ and $\sigma_Z = 0.2$

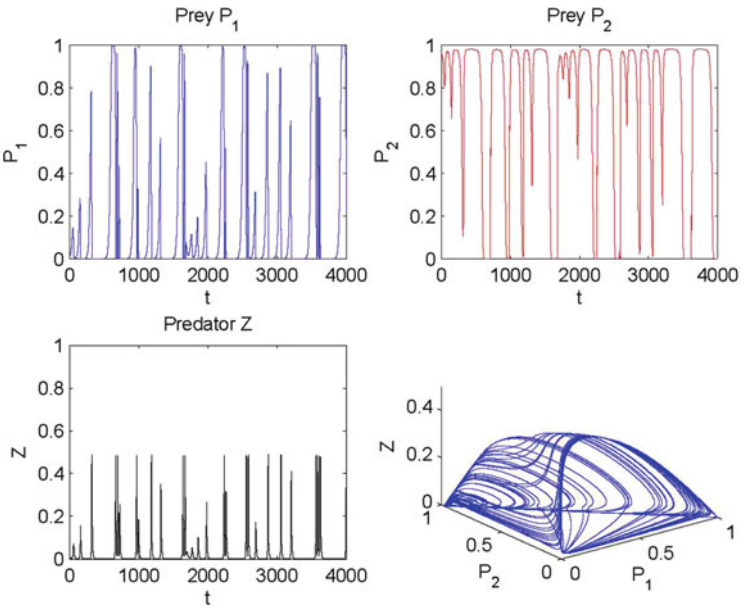

Fig. 11.6 As in Fig. 11.5 but for $\sigma_Z = 0.3$

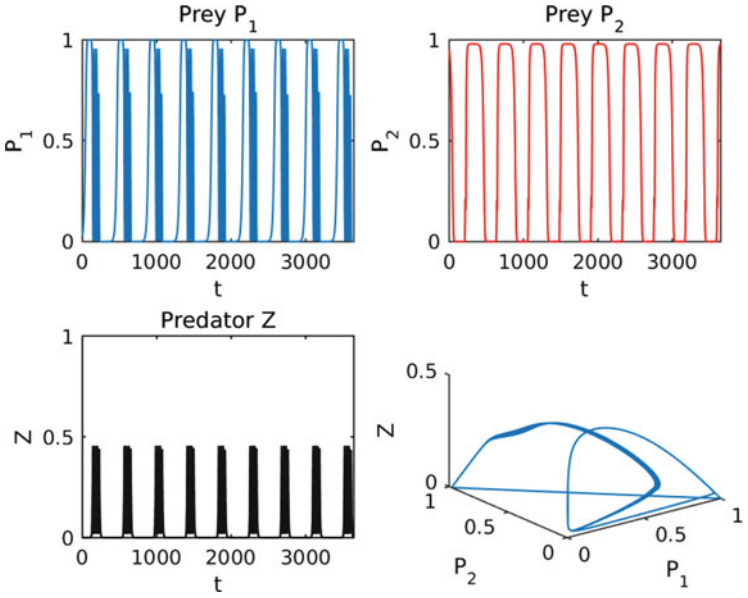

Fig. 11.7 Periodic E solutions for $\rho = 0$ and $\sigma_Z = 0.33$

When $\sigma_Z = 0.3$, we are in the middle of the chaotic regime for E. Figure 11.6 shows P_1 and Z are still synchronised, with $min(Z) \approx 8.10^{-15}$, but out of phase with P_2. Now the trajectory visits the interior of the (P_1, P_2) plane.

Intermingled with the chaotic behaviour, there are small windows of periodicity. Figure 11.7 shows the behaviour in one such window (which extends from $0.329 < \sigma_Z < 0.331$) for $\sigma_Z = 0.33$. Figure 11.8 shows chaotic 'pinball' dynamics: P_1 and P_2 alternate in dominance; Z is still linked with P_1. Rapid oscillations in P_1 and Z are interleaved with long slow oscillations, each irregular. In comparison with Figs. 11.5 and 11.6, counter-intuitively, an increase in Z mortality σ_Z, has rendered Z more robust. Again note the trajectories do not visit the interior of the (P_1, P_2) plane.

Just prior to loss of stability of the E state, Fig. 11.9 shows a periodic (P_1, P_2, Z, N) cycle. Here $min(P_2) \approx 6.10^{-42}$. Since 20,000 time units $\approx$ 6 years, the very low values for P_2 between sudden growth spurts, could be misconstrued as possible extinction of P_2. This is an example of a 'breather': in dynamical systems language, this is where a solution arises out of exponentially small terms.

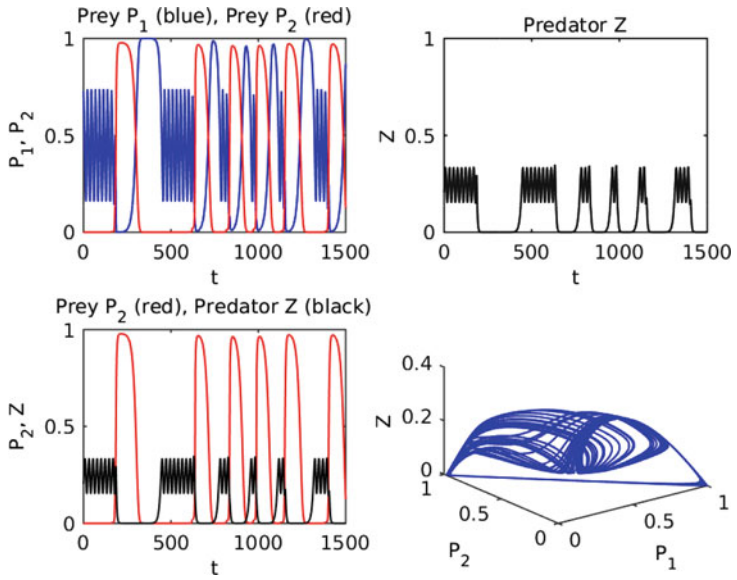

Fig. 11.8 Chaotic 'pinball' dynamics: rapid oscillations, with long slow oscillations interspersed for $\rho = 0$ and $\sigma_Z = 0.45$

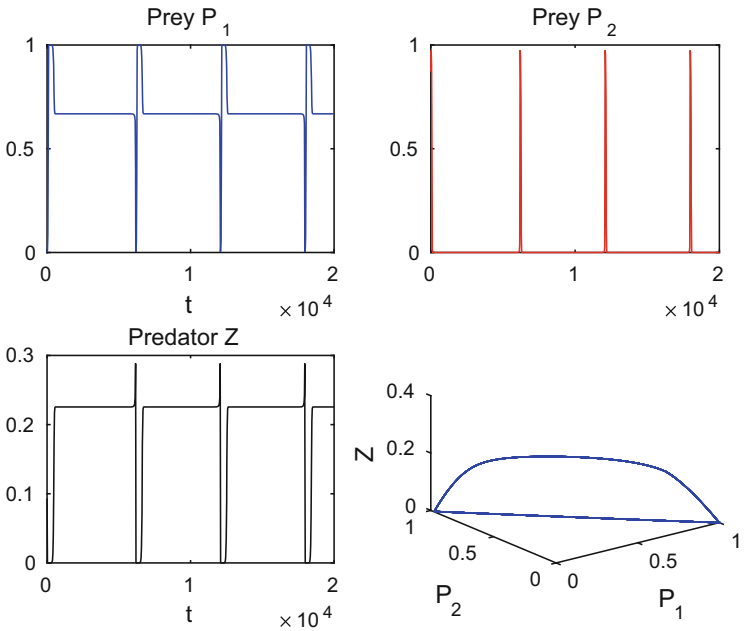

Fig. 11.9 Long periodic oscillations of E for $\rho = 0$ and $\sigma_Z = 0.53$

11.5 Discussion

In this paper we reported on our investigations of a system of four coupled nonlinear ordinary differential equations for plankton predator-prey-prey interactions, comprising two phytoplankton P_1, P_2 populations, one zooplankton Z population, and one limiting nutrient N. Because of the constraint $P_1 + P_2 + Z + N = 1$, this system reduces to three coupled nonlinear differential equations for P_1, P_2, Z.

We considered four different types of grazing using measured parameter values:

- specialist (or discriminate) and facultative: $\rho = 0$, $0 < \sigma_Z < 0.1708$;
- specialist and obligate (Z requires the presence of P_1 to exist): $\rho = 0$, $0.1708 < \sigma_Z < 0.5705$;
- generalist (or indiscriminate) and facultative: $\rho = 1$, $0 < \sigma_Z < 0.1708$;
- generalist and obligate: $\rho = 1$, $0.1708 < \sigma_Z < 0.5705$.

These different grazing strategies create very different system behaviours. For specialist grazing, the system exhibits periodic (P_2, Z, N) limit cycle behaviour as well as stable critical point F steady states for $\sigma_Z < 0.1708$, before losing stability to chaotic (P_1, P_2, Z, N) behaviour, interspersed with thin periodic windows. Numerical integrations show long periods when P_2 takes very small values, but then recovers. Such behaviour could have significant implications in both climate change studies and fisheries management.

For generalist grazing, the model exhibits only simple oscillations or stable steady states, regardless of Z being a facultative or an obligate omnivore.

Less complex than operational models such as PlankTOM5 [13] or PlankTOM10 [12], our model has interesting and complicated limit cycle behaviour for measured parameter values that correspond to plankton blooms in the Earth's oceans. For operational models, obligate generalist grazers appear to provide the most desirable outcomes of stability and predictability, thereby giving more reproducible results under changes in environmental forcings.

References

1. T.R. Anderson, W. Gentleman, B. Sinha, Influence of grazing formulations on the emergent properties of a complex ecosystem model in a global ocean general circulation model. Prog. Oceanogr. **87**, 201–213 (2010)
2. G. Billen, S. Becquevort, Phytoplankton: bacteria relationships in the Antarctic marine ecosystem. Pol. Res **10**, 245–253 (1991)
3. P. Bork, C. Bowler, C. de Vargas, G. Gorsky, E. Karsenti, P. Wincker, Tara Oceans studies plankton at planetary scale. Science **348**, 873 (2015)
4. R.J. Charlson, J.E. Lovelock, M.O. Andreae, S.G. Warren, Oceanic phytoplankton, atmospheric sulphur, cloud albedo and climate. Nature **326**, 655–661 (1987)
5. R.A. Cropp, J. Norbury, Parameterizing plankton functional type models: insights from a dynamical systems perspective. J. Plankton Res. **31**, 939–963 (2009)

6. R.A. Cropp, I.M. Moroz, J. Norbury, The role of grazer predation choices in the dynamics of consumer-resource based ecologies (2015 submitted to Marine Systems)
7. P. Falkowski, The power of plankton. Nature **483**, 817–820 (2012)
8. T. Fenchel, Ecology of heterotrophic microflagellates. IV. Quantitative occurrence and importance as bacterial consumers. Mar. Ecol. Prog. Ser. **9**, 35–42 (1982)
9. A.J. Gabric, P.A. Matrai, M. Vernet, Modelling the production and cycling of dimethylsulphide during the vernal bloom in the Barents Sea. Tellus **51B**, 919–937 (1999)
10. A.J. Gabric, P.H. Whetton, R.A. Cropp, Dimethylsulphide production in the sub-Antarctic southern ocean under enhanced greenhouse conditions. Tellus **53**, 273–287 (2001)
11. B. Hansen, S. Christiansen, G. Pedersen, Plankton dynamics in the marginal ice zone of the central Barents Sea during spring: carbon flow and the structure of the grazer food chain. Polar Biol. **16**, 115–128 (1996)
12. L. Kwiatkowski, A. Yool, J.I. Allen, T.R. Anderson, R. Barciela, E.T. Buitenhuis, M. Butenschön, C. Enright, P.R. Halloran, C. Le Quéré, L. de Mora, M.F. Racault, B. Sinha, I.J. Totterdell, P.M. Cox, iMarNet: an ocean biogeochemistry model intercomparison project within a common physical ocean modelling framework. Biogeosciences **11**, 7291–7304 (2014)
13. C. Le Quéré, S.P. Harrison, I.C. Prentice, E.T. Buitenhuis, O. Aumont, L. Bopp, H. Claustre, L.C. Da Cunha, R. Geider, X. Giraud, C. Klaas, K.E. Kohfeld, L. Legendre, M. Manizza, T. Platt, R.B. Rivkin, S. Sathyendranath, J. Uitz, A.J. Watson, D. Wolf-Gladrow, Ecosystem dynamics based on plankton functional types for global ocean biogeochemistry models. Glob. Chang. Biol. **11**, 2016–2040 (2005)
14. C.L. Moloney, M.O. Bergh, J.G. Field, R.C. Newell, The effect of sedimentation and microbial nitrogen regeneration in a plankton community: a simulation investigation. J. Plankton Res. **8**, 427–445 (1986)
15. G. Muller-Niklas, G.J. Herndl, Dynamics of bacterio-plankton during a phytoplankton bloom in the high Arctic waters of the Franz-Joseph Land archipelago. Aquat. Microb. Ecol. **11**, 111–118 (1996)
16. S.F. Sailley, M. Vogt, S.C. Doney, M.N. Aita, L. Bopp, E.T. Buitenhuis, T. Hashioka, I. Lima, C. Le Quéré, Y. Yamanaka, Comparing food web structures and dynamics across a suite of global marine ecosystem models. Ecol. Model. **261–262**, 43–57 (2013)
17. D. Slagstad, K. Stole-Hansen, Dynamics of plankton growth in the Barents Sea. Polar Res. **10**, 173–186 (1991)

Chapter 12
Chaos Theory, Fractals and Scaling in the Radar: A Look from 2015

Alexander A. Potapov

Abstract Results of application of theory of fractal and chaos, scaling effects and fractional operators in the fundamental issues of the radio location and radio physic are presented in this report. The key point is detection and processing of super weak signals against the background of non-Gaussian intensive noises and strays. An alternative—the radar range is increased dramatically. The results of researches of spectrum fractal dimensions of lightning discharge in the middle atmosphere at attitudes from 20 to 100 km which are above the majority of clouds are presented. The author has been investigating these issues for exactly 35 years and has obtained results of the big scientific and practical worth. The reader is invited to look at the fundamental problems with the synergetic point of view of non-Markovian micro- and macro systems.

12.1 Introduction

The entire current radio engineering is based on the classical theory of an integer measure and an integer calculation. Thus an extensive area of mathematical analysis which name is the fractional calculation and which deals with derivatives and integrals of a random (real or complex) order as well as the fractal theory has been historically turned out "outboard" (!). At the moment the integer measures (integrals and derivatives with integer order), Gaussian statistics, Markov processes etc., are mainly and habitually used everywhere in the radio physics, radio electronics and processing of multidimensional signals. It is worth noting that the Markov processes theory has already reached its satiation and researches are conducted at the level of abrupt complication of synthesized algorithms. Radar systems should be considered with relation to open dynamical systems. Improvement of classical radar detectors

A.A. Potapov (✉)
V.A. Kotel'nikov Institute of Radio Engineering and Electronics, Russian Academy of Sciences, Moscow 125009, Russia

President of Cooperative Chinese-Russian Laboratory of Informational Technologies and Signals Fractal Processing, Jinan University, Guangzhou, China
e-mail: potapov@cplire.ru

C. Skiadas (ed.), *The Foundations of Chaos Revisited: From Poincaré to Recent Advancements*, Understanding Complex Systems,
DOI 10.1007/978-3-319-29701-9_12

of signals and its mathematical support basically reached its saturation and limit. It forces to look for fundamentally new ways of solving of problem of increasing of sensitivity or range of coverage for various radio systems.

At the same time I'd like to point out that it often occurs in science that the mathematical apparatus play a part of "Procrustean bed" for an idea. The complicated mathematical symbolism and its meanings may conceal an absolutely simple idea. In particular the author put forward one of such ideas *for the first time in the world* in the end of seventies of twentieth century. To be exact he suggested to introduce fractals, scaling and fractional calculation into the wide practice of radio physics, radio engineering and radio location. Now after long intellectual battles my idea has shown its advantages and has been positively perceived by the majority of the thoughtful scientific community. For the moment the list of the author's and pupils works counts more than 750 papers including 20 monographs on the given fundamental direction. Nowadays it is absolutely clear that the application of ideas of scale invariance—"scaling" along with the set theory, fractional measure theory, general topology, measure geometrical theory and dynamical systems theory reveals big opportunities and new prospects in processing of multidimensional signals in related scientific and engineering fields. In other words a full description of processes of modern signal and fields processing is impossible basing on formulas of the classical mathematics [1–11].

The work objective is to consider the use of the fractal theory and effects of physical scaling in development of new informational technologies using examples of solving of up-to-date basic radar problems. The author has been investigating these issues in V.A. Kotel'nikov IREE RAS for exactly 35 years.

12.2 On the Theory of Fractional Measure and Nonintegral Dimension

The main feature of fractals is the nonintegral value of its dimension. A development of the dimension theory began with the Poincare, Lebesgue, Brauer, Urysohn and Menger works. The sets which are negligibly small and indistinguishable in one way or another in the sense of Lebesgue measure arise in different fields of mathematics. To distinguish such sets with a pathologically complicated structure one should use unconventional characteristics of smallness—for example Hausdorff's capacity, potential, measures and dimension and so on. Application of the fractional Hausdorff's dimension which is associated with entropy conceptions, fractals and strange attractors has turned out to be most fruitful in the dynamical systems theory [1, 3–7, 9–11]. This fractional dimension is determined by the p—dimensional measure with an arbitrary real positive number p proposed by Hausdorff in 1919. Generally the measure conception is related neither to metric nor to topology. However the Hausdorff measure can be built in an arbitrary metric space basing on its metric and the Hausdorff measure itself is related to the topological dimension. The Hausdorff–Besicovitch dimension is a metrical conception but

there is its fundamental association with topological dimension dim E, which was established by L.S. Pontryagin and L.G. Shnirelman who introduced a conception of the metrical order in 1932: the greatest lower bound of the Hausdorff–Besicovitch dimension for all the metrics of compact E is equal to its topological dimension $\dim E \leq \alpha(E)$. One of much used methods for estimation of sets Hausdorff dimension known as the mass distribution principle was proposed by Frostman in 1935.

Sets whose Hausdorff–Besicovitch dimension is a fractional number are called fractal sets or fractals. More strictly, set E is called fractal (a fractal) in the wide sense (in the B. Mandelbrot sense) if its topological dimension is not equal to the Hausdorff–Besicovitch dimension, to be exact $\alpha_0(E) > \dim E$. For example, set E of all the surd points [0; 1] is fractal in the wide sense since $\alpha_0(E) = 1$, $\dim E = 0$. Set E is called fractal (a fractal) in the narrow sense if $\alpha_0(E)$ is not integer. A fractal set in the narrow sense is also fractal in the wide sense.

12.3 Measuring of Fractal Dimension and Fractal Signatures

Fractal methods can function on all signal levels: amplitude, frequency, phase and polarized. The absolute worth of Hausdorff–Besicovitch dimension is the possibility of experimental determining [3–10]. Let's consider some set of points N_0 in d—dimensional space. If there are $N(\varepsilon)$—dimensional sample bodies (cube, sphere) needed to cover that set with typical size ε, at that

$$N(\varepsilon) \approx 1/\varepsilon^D, \quad \varepsilon \to 0 \tag{12.1}$$

is determined by the self-similarity law.

The practical implementation of the method described above faces the difficulties related to the big volume of calculations. It is due to the fact that one must measure not just the ratio but the upper bound of that ratio to calculate the Hausdorff–Besicovitch dimension. Indeed, by choosing a finite scale which is larger than two discretes of the temporal series or one image element we make it possible to "miss" some peculiarities of the fractal. Building of *the fractal signature* [4–7] or estimates dependence (1) on the observation scale helps to solve this problem. Also the fractal signature describes the spatial *fractal cestrum* of the image. In IREE RAS we developed various original methods of measuring the fractal dimension including methods: dispersing, singularities accounting, on functionals, triad, basing on the Hausdorff metric, samplings subtraction, basing on the operation "Exclusive OR" and so on [4–7]. During the process of adjustment and algorithms mathematical modeling our own data were used: air photography (AP) and radar images (RI) on millimeter waves [9]. Season measurements of scattering characteristics of the earth coverings were already naturally conducted on wavelength 8.6 mm by the author in co-operation with representatives of Central Design Bureau "Almaz" from a helicopter MI-8 in the 1980s of twentieth century.

A significant advantage of dispersing dimension is its implementation simplicity, processing speed and calculations efficiency. In 2000 it was proposed to calculate a fractal dimension using the locally dispersing method (reference for example [4–7, 9–11]). In the developed algorithms they use two typical windows: scale and measuring. The scale window defines the necessary scale of measurements which the scaling is observed in. That is why the scale window serves for selection of the object to be recognized and its following description in the framework of fractal theory. An image brightness or image intensity local variance is determined by the measuring window. The locally dispersing method of the fractal dimension D measurements is based on measuring a variance of the image fragments intensity/brightness for two spatial scales:

$$D \approx \frac{\ln \sigma_2^2 - \ln \sigma_1^2}{\ln \delta_2 - \ln \delta_1}. \tag{12.2}$$

In formula (2) σ_1, σ_2—root-mean-squares on the first δ_1 and second δ_2 scales of image fragment, respectively. Accuracy characteristics of the locally dispersing method were investigated in [4, 5, 7]. It is proved [7] that in the Gaussian case the dispersing dimension of a random sequence converges to the Hausdorff dimension of corresponding stochastic process. The essential problem is that any numerical method includes a discretization (or a discrete approximation) of the process or object under analysis and the discretization destroys fractal features. The development of special theory based on the methods of fractal interpolation and approximation is needed to fix this contradiction. Various topological and dimensional effects during the process of fractal and scaling detecting and multidimensional signals processing were studied in [4–11].

12.4 Textural and Fractal Measures in Radio Location

During the process of radio location the useful signal from target is a part of the general wave field which is created by all reflecting elements of observed fragments of the target surrounding background, that is why in practice signals from these elements form the interfering component.

It is worthwhile to use the texture conception to create radio systems for the landscape real inhomogeneous images automatic detecting [4–6, 9]. A texture describes spatial properties of earth covering images regions with locally homogenous statistical characteristics. Target detecting and identification occurs in the case when the target shades the background region at that changing integral parameters of the texture. Many natural objects such as a soil, flora, clouds and so on reveal fractal properties in certain scales [4–6].

The fractal dimension D or its signature $D(t, f, \overrightarrow{r})$ in different regions of the surface image is a measure of texture, i.e., properties of spatial correlation of radio waves scattering from the corresponding surface regions. At already far first

steps the author initiated a detailed research of the texture conception during the process of radio location of the earth coverings and objects against its background. Further on a particular attention was paid to development of textural methods of objects detecting against the earth coverings background with low ratios of signal/background [4].

12.5 Fractal Signal and Image Processing in the Interference

The author was the first who shows that the fractal processing excellently does for solving modern problems when processing the low-contrast images and detecting super weak signals in high-intensity noise while the modern radars does not practically function [4–7, 9–11]. The author's developed fractal classification was approved by B. Mandelbrot during the personal meeting in USA in 2005. It is presented on Fig. 12.1 where the fractal properties are described, D_0—is a topological dimension of the space of embeddings.

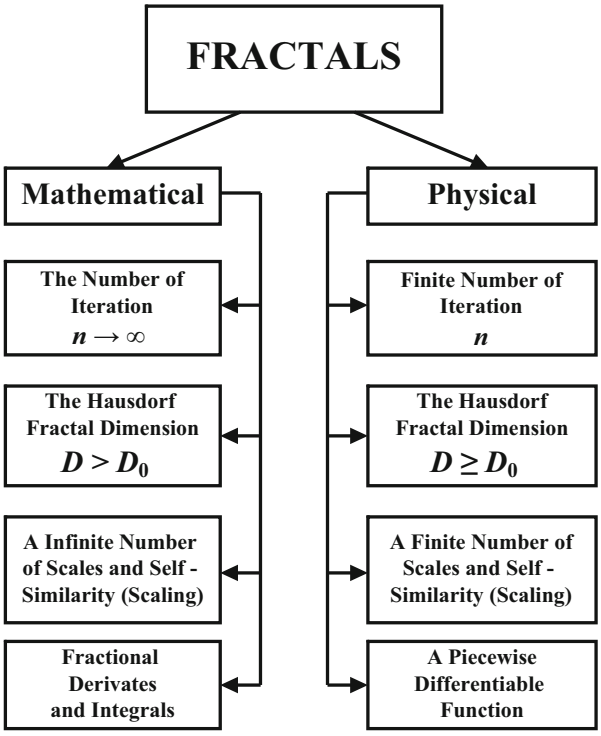

Fig. 12.1 The author's classification of fractal sets and signatures

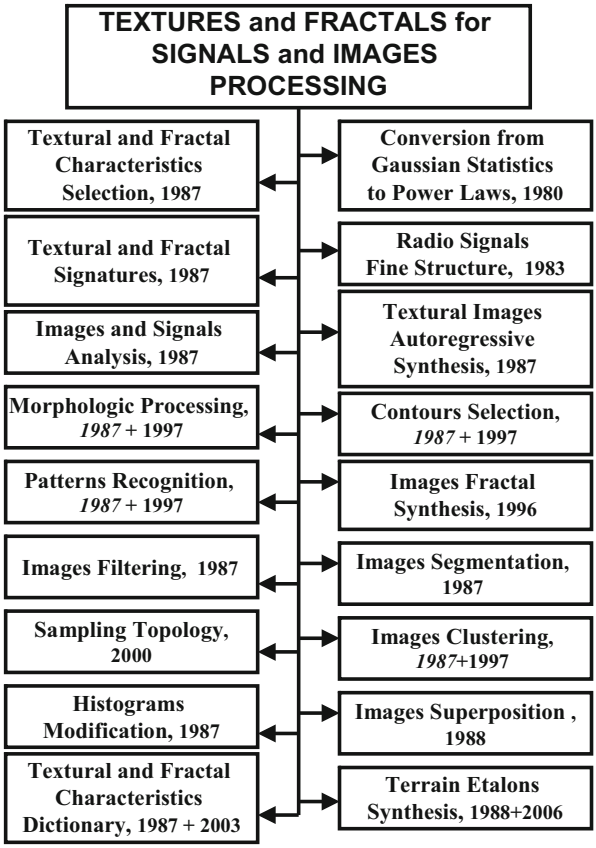

Fig. 12.2 Textural and fractal methods of processing low-contrast images and super weak signals in high-intensity non-Gaussian noise

The textural and fractal digital methods under author's development (Fig. 12.2) allow to overcome a prior uncertainty in radar problems using *the sampling geometry or topology* (one- or multidimensional). At that topological peculiarities of the sampling and also the scaling hypothesis and stable laws with heavy "tails" get important as opposed to the average realizations which frequently have different behavior [4–7, 9–11].

12.6 Development of "Fractal Ideology" in Radio Physics

A critical distinction between the author's proposed fractal methods and classical ones is due to fundamentally different approach to the main components of a signal and a field. It allowed to switch over the new level of informational structure of the real non-Markov signals and fields. Thus this is *the fundamentally new* radio engineering. For 35 years of scientific researches my global fractal scaling method

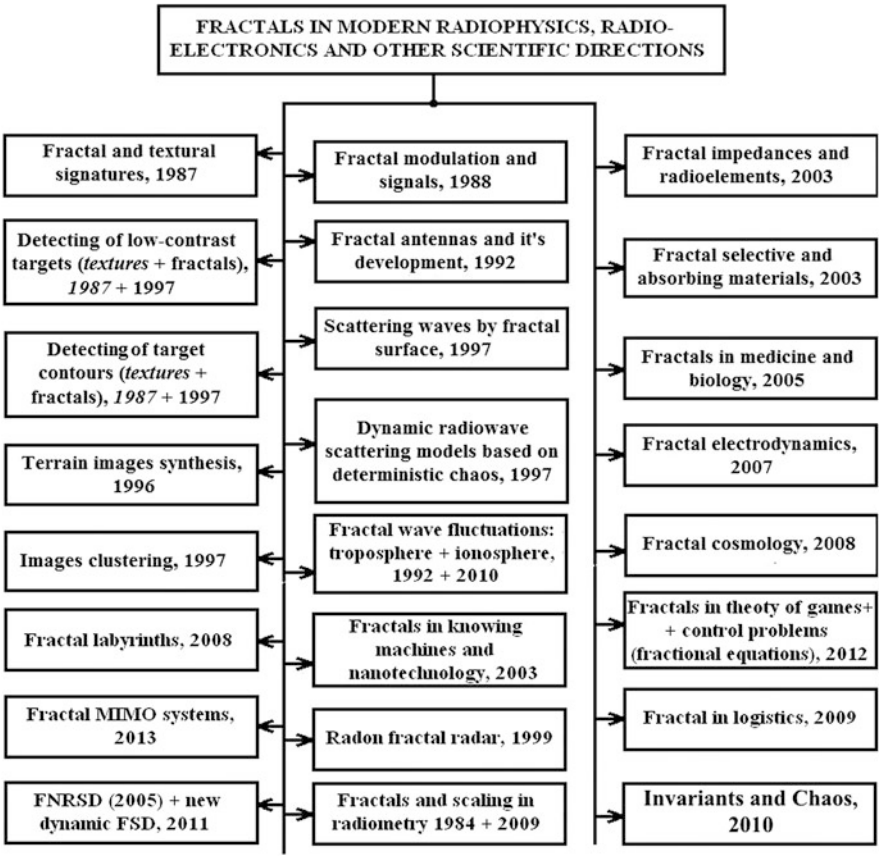

Fig. 12.3 A sketch of author's new informational technologies development basing on fractals, fractional operators and scaling effects for nonlinear physics and radio electronics

has justified itself in many applications—Fig. 12.3. This is *a challenge to time* in a way. Here only the facts say! Slightly exaggerating one can say that the fractals formed a thin amalgam on the powerful framework of science of the end of twentieth century. In the modern situation attempts of underestimating its significance and basing only on the classical knowledge came to grief in an intellectual sense.

In fractal researches I always rest upon my three global theses:

1. Processing of information distorted by non-Gaussian noise in the fractional measure space using scaling and stable non-Gaussian probabilistic distributions (1981)—Figs. 12.1, 12.2, and 12.3.
2. Application of continuous nondifferentiable functions (1990)—Fig. 12.1.
3. Fractal radio systems (2005)—Figs. 12.3 and 12.4 [4–7, 9–11].

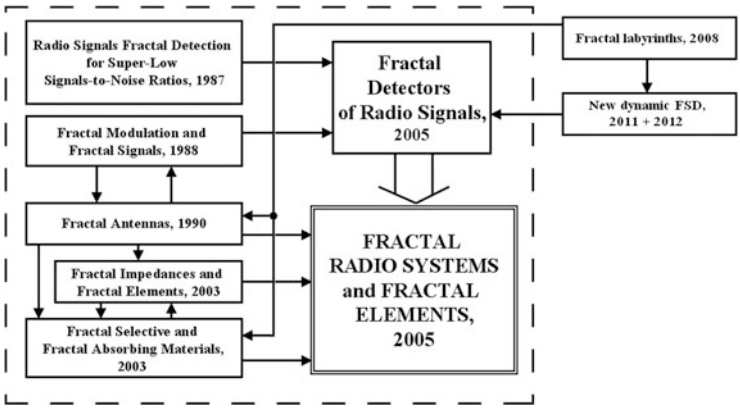

Fig. 12.4 The author's conception of fractal radio systems, devices and radio elements

A logic aggregation of the problems triad described above into the general "fractal analysis and synthesis" creates a basis of *fractal scaling method* (2006) and a unified global idea of the fractal natural science and *fractal paradigm* (2011) which were proposed and are investigated by the author now [4–7, 9–11]. Basing on the matter reviewed above next we will proceed to description of *the fractal radar* conception and also issues of its scale-invariant principles application in other systems of radio monitoring. In fact the question is about a fundamentally new type of radio location: *fractal scale or scale-invariant radio location*.

12.7 Principles of Scale-Invariant or Fractal Scaling Radio Location and Its Applications

At the moment world investigations on fractal radio location are exclusively conducted in V.A. Kotel'nikov IREE RAS. Almost all the application points of hypothetic or currently projectable fractal algorithms, elements, nodes and processes which can be integrated into the classical radar scheme are represented on Fig. 12.5. The ideology of proceeding to the fractal radar is based on the fractal radio systems conception—Fig. 12.4.

In particular a multifrequency work mode is typical for the fractal MIMO-system [11–13] proposed by the author earlier since fractal antennas can radiate several waves lengths at the same time. Building of a tiny fractal radar with fractal elements and modern parametrons is possible for unmanned aerial vehicles (UAV).

At the same time the fractal processing at the point of control of UAV transmitted information will allow to improve sharply and automatize the processes of detecting, clustering and identification of targets and objects. Moreover UAV fractal coating will sharply reduce the probability of its detecting in flight.

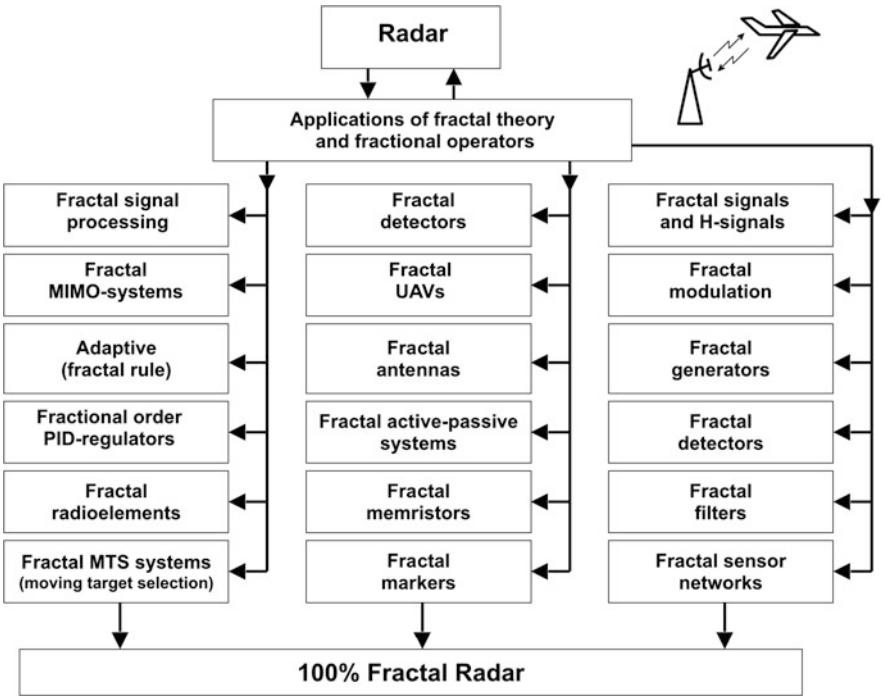

Fig. 12.5 The points of application of fractals, scaling and fractional operators for proceeding to the fractal radar

12.8 Fractal Detection of Objects on Images from SAR and UAV

The base data for digital fractal processing of radar images were obtained by satellite radar with the synthetic aperture (SAR) PALSAR of *L*-range (Japan). PALSAR is a space SAR at wavelength 23 cm with spatial resolution of about 7 m which is developed by Japanese agency JAXA and which was successfully working on orbit from 2006 till 2011.

A radar image of Selenga estuary in Transbaikalia obtained in the FBS high resolution mode on the coherent horizontal polarization on 7 August 2006 is presented on Fig. 12.6 as an example.

The shooting zone of about 60×50 km includes the forest covered mountainous area Hamar-Daban (at the bottom, it is reproduced by a brighter tone with the typical "crumpled" structure), the flat area of Selenga estuary (in the middle of the top image part, it is reproduced by darker tones) and the smooth water surface of the lake Baikal (the black segment in the left upper corner of the image). The banded structures are seen in the flat part of the image, these are the bounds of agricultural fields. Also the clusters of bright objects are seen, these are the strongly reflecting

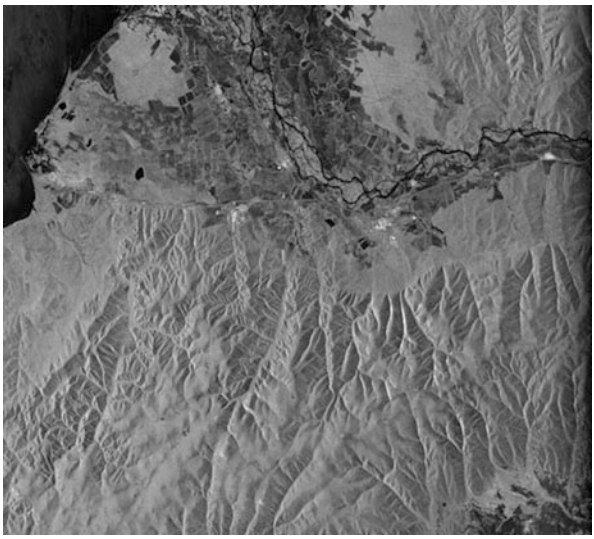

Fig. 12.6 Selenga estuary on the PCA PALSAR photo from 7 August 2006

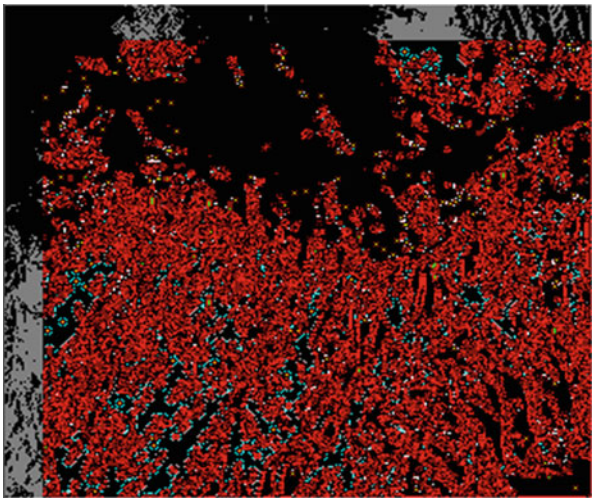

Fig. 12.7 The result of fractal processing of the PCA PALSAR

elements of buildings and other constructions in the range of settlements. The long twisting dark lines on the plain are the multiple arms of Selenga.

The fields of local values of dispersing fractal dimension D were measured at the first stage of radar images fractal processing by a SAR (Fig. 12.7). Next the empiric distribution of values of the instant fractal dimension D was obtained Fig. 12.8.

Below the examples of fractal clustering over D are presented (Figs. 12.9 and 12.10). The selected image fragment with fractal dimension $D \approx 2.2$ nearby the first big peak (Fig. 12.8) is presented on Fig. 12.9. The selected image fragment with fractal dimension $D \approx 2.5$ ($\approx$ Brownian surface) nearby the third and fourth big peak (Fig. 12.8) is shown on Fig. 12.10.

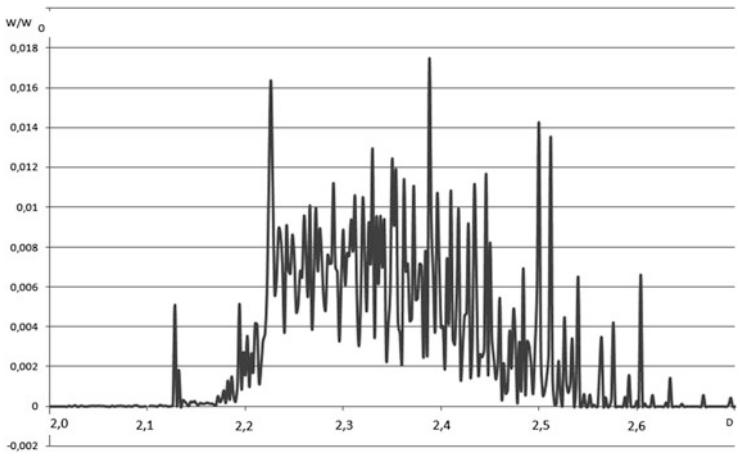

Fig. 12.8 An empiric distribution of values of the instant fractal dimension D

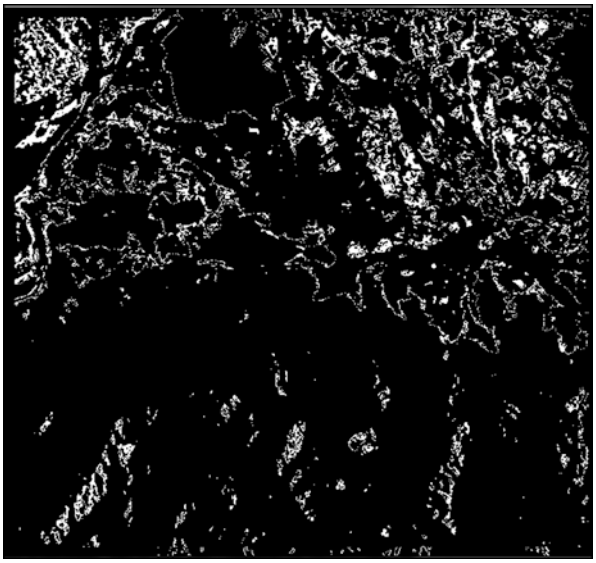

Fig. 12.9 A fragment with $D \approx 2.2$

Previously *invisible* (*hidden*) peculiarities (for example earth coverings distant probing clustering data [4–6]) along with a stable distribution by earth coverings types are registered after fractal processing of surface images. It allows speaking of application of fractal recognition methods for the identification of image parts which are "invisible" when using classical methods of clusterization over the brightness field.

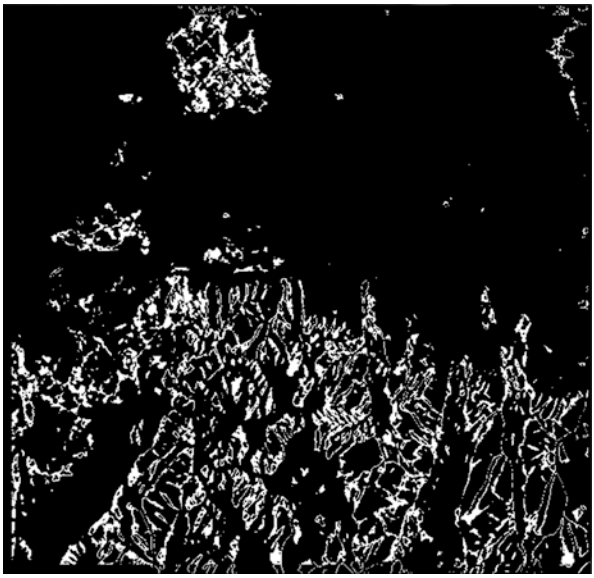

Fig. 12.10 A fragment with $D \approx 2.5$

12.9 Fractal Characteristics of the High-Altitude Discharges in Ionosphere

Four million lightnings draw the sky every 24 h and about 50 lightnings draw the sky every second. And over the lead thunderheads, a light show of "unreal lightnings" is developing in the upper atmosphere: azure jets, red-purple sprites, red rings of highly soaring elves. These are discharges of very high energy which do strike the ionosphere and not the ground! Thus high-altitude electrical discharges (20–100 km) subdivide into several basic types: elves, jets, sprites, halo and so on—Fig. 12.11 (This is the first colour image captured of one by NASA aircraft in 1994). A history brief: a significant event occurred in the Earth study history in the night of 5 to 6 July 1989. Retired professor and 73 years old NASA veteran John Randolph Winkler pointed an extremely sensitive camera recorder to thunderstorm clouds and then he detected two bright blazes during inspecting the record frame by frame. The blazes go up to the ionosphere in contrast to lightning's which should go down to the ground. This way the sprites were discovered. The sprites are the biggest high-altitude discharges in the Earth atmosphere. After these publications NASA had not already been able to disregard the potential threat to space vehicles and they started a comprehensive research of high-altitude discharges.

The most short-lived high-altitude discharges are *elves*. They arise in the lower ionosphere at altitudes 80–100 km. The luminescence arise in the center and expands to 300–400 km for less than a millisecond and then it goes out. The elves are born in 300 μs after a strong lightning stroke from a thunderstorm cloud to the ground. It gets altitude 100 km for 300 μs where it "arouse" a red

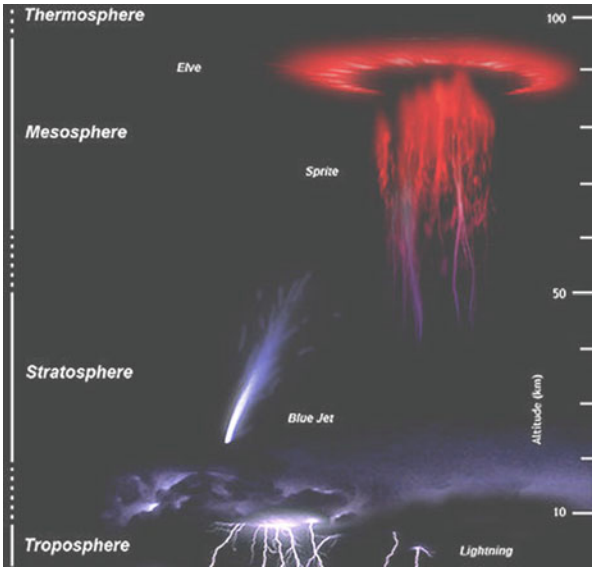

Fig. 12.11 Dynamical fractal structures in the atmosphere (copyright: Abestrobi (Wikipedia))

luminescence of nitrogen molecules. The most enigmatic high-altitude discharges are azure *jets*. These are also a luminescence of nitrogen molecules in the ultraviolet-blue band. They look like an azure narrow inverse cone which "starts" from the upper edge of a thunderstorm cloud. Sometimes jets reach altitude 40 km. Their propagation speed varies from 10 up to 100 km/s. Their occurrence is not always due to lightning discharges. Besides azure jets they mark out "azure starters" (they propagate up to altitudes $\leq$25 km) and "giant jets" (they propagate up to altitudes of the lower ionosphere about 70 km). *Sprites* are very bright three-dimensional blazes with duration around milliseconds. They arise at altitude 70–90 km and descend down 30–40 km. Their width reaches tens of kilometers in the upper part. Sprites blaze up in the mesosphere in about 100th part of a second after the discharge of powerful lightnings "cloud–ground." Sometimes it occurs at a distance of several tens kilometers horizontally from the lightning channel. The red-purple colour of sprites as well as elves is due to the atmosphere nitrogen. The frequency of sprites occurrence is about several 1000 events per 24 h over the entire globe. The fine structure of the lower sprites part is characterized by dozens of luminous channels with cross sectional dimensions from tens to hundreds meters. Sprites occurrence is related with formation of high electrical dipole moment of uncompensated charge after especially powerful lightning discharges cloud–ground with usually positive polarity.

Dynamical spatial-temporal singularities and morphology of sprites can be particularly explained by the discharges fractal geometry and percolation [14]. Here we have one more example of a self-organized criticality when the system (a high-altitude discharge in this case) dynamics is determined by reaching the threshold of the so called directed percolation which characterizes a formation of branchy

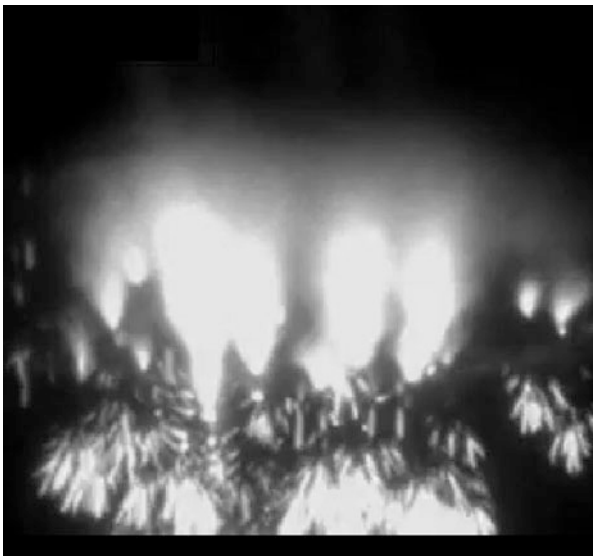

Fig. 12.12 The original sprite image (USA, NASA http://science.compulenta.ru/701264/)

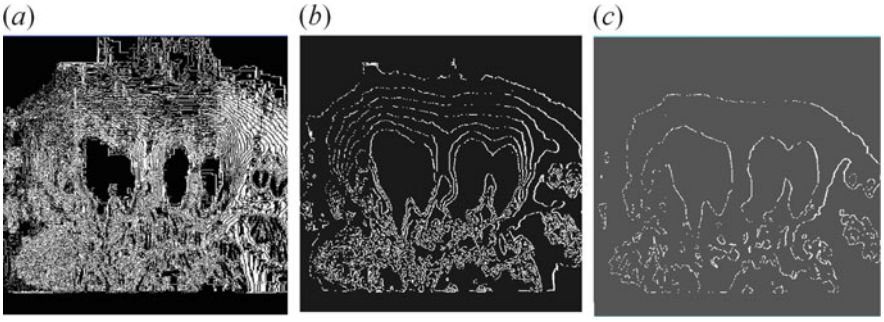

Fig. 12.13 Results of fractal filtering of a sprite image: (**a**) a pattern of fractal dimension with the mean value $D = 2.3$; (**b**) 2.8; (**c**) 3.0

(fractal) conductive channels overlapping all the sprite length. A different situation arises with issues of data statistical processing.

Here the classical methods are used by tradition. It does not allow to extract all the information about such newest atmospherically structures. Selected examples of our fractal processing of sprite profiles (Fig. 12.12) are presented on Fig. 12.13a–c. Examples of fractal processing of a jet (Fig. 12.14a) are presented on Fig. 12.14b, c.

The fractal-scaling methodology which was used for describing the morphology of jets, sprites and elves can be successfully used to estimate their parameters and dynamics of their evolution [14]. Then the mathematical physics problems are solved.

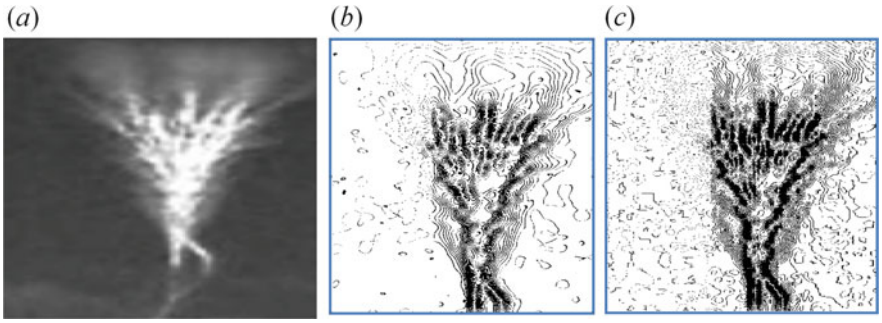

Fig. 12.14 Results of fractal filtering of a giant jet image (the photos were taken in China August 12, 2010) (**a**) the jet image [15], (**b**) and (**c**) profiles of D estimates

12.10 Fractal Signal Detectors in Radiolocation

Classical detectors and their mathematical supply have virtually reached its saturation and limit. It causes searching principally new ways of solving the problem. Principally, fractals and fractional operators are not possible one without the other. We showed for the first time that fractal processing is suitable as well as possible for solving modern problems of the low-contrast images identification and ultra weak signal detection in the presence of intensive non-Gaussian noises, when modern radars can not operate. One of our main conclusions is that working on the pointed evaluation of the fractal dimension D leads to absurd results. At the same time almost all the authors who begins using the fractal signal processing give absolutely accurate meanings even with the RMS deviation! In our works we introduced fractal signatures and fractal kepsters [4–7, 9, 16]. Therefore the accuracy problems in digital fractal processing in real-time mode are solved.

The series of principally new fractal signal detectors (FSD) not mentioned by me in press is shown below as an example of effective operation of the global fractal methodology and the conception of radio systems and devices created by the author. The main principles of fractal detection were proposed by us for the first time as early as in 1989 works. At the same time a working model of the fractal non-parametric radar signals detector (FNRSD—Fig. 12.3) was created. The high accuracy of fractal detecting was proved. The main kinds of FSD proposed by us during 2011–2012 are shown at Fig. 12.15.

Figures 12.16, 12.17, and 12.18 show selected results of fractal nonparametric filtering of low-contrast objects. Aircraft images were masked by an additive Gaussian noise. In this case, the signal/noise ratio (SNR) $q_0^2 = -3$ dB. It is seen in the figures that all desired information is hidden in the noise.

The optimum mode of filtering of necessary contours or objects is chosen by the operator using the spatial distribution of fractal dimensions D of a scene. This distribution is determined automatically and is shown in the right panel of the computer display [4–7, 9].

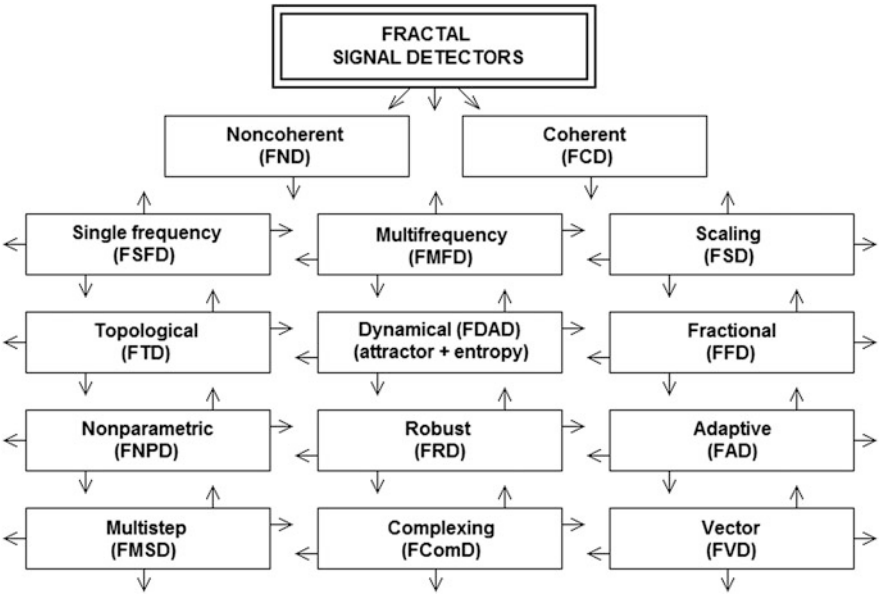

Fig. 12.15 The main kinds of new dynamical FSD proposed by author

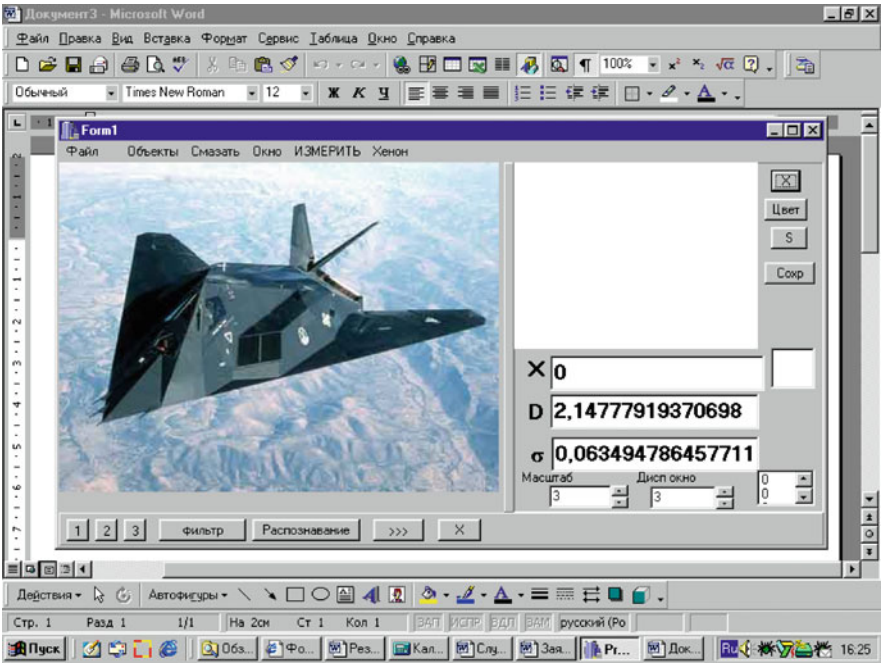

Fig. 12.16 Real image

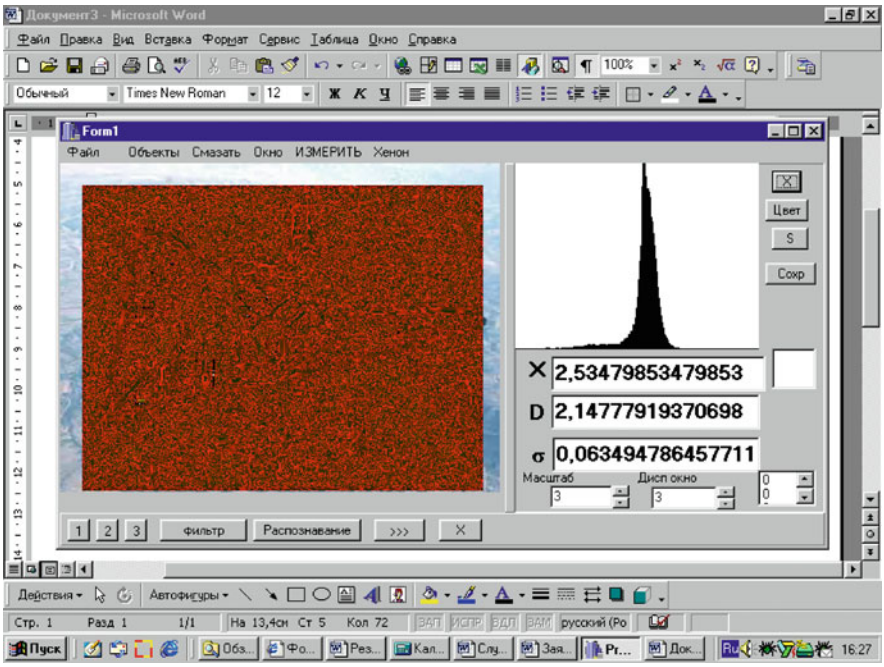

Fig. 12.17 Source image and noise q_0^2–3 dB

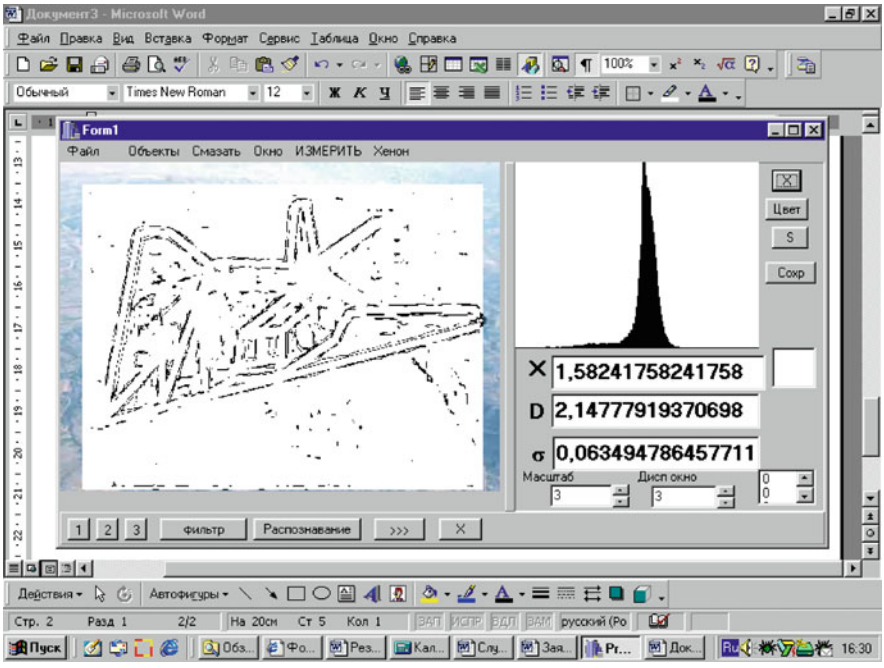

Fig. 12.18 Results of fractal filtration Fig. 12.17

12.11 Wave Scattering by Fractal Surface

In many works it has been shown that diffraction by fractal surfaces fundamentally differs from diffraction by conventional random surfaces and some of classical statistical parameters like correlation length and root-mean-square deviation go to infinity. This fact is result of self-similarity of fractal surface. In our work band-limited Weierstrass function was used. For the scattered field analysis we use Kirchhoff approach [17].

The most convenient function which both describes fractals well and is easy for using in calculations is the modified 2D band-limited Weierstrass function. It has a view:

$$W(x,y) = c_w \sum_{n=0}^{N-1} q^{(D-3)n} \sum_{m=1}^{M} \sin\left\{ Kq^n \left[x \cdot \cos\left(\frac{2\pi m}{M}\right) + \; y \cdot \sin\left(\frac{2\pi m}{M}\right)\right] + \varphi_{nm}\right\} \tag{12.3}$$

where c_w—the constant, that provides unit normalization; $q > 1$—the fundamental spatial frequency; D—the fractal dimension $(2 < D < 3)$; K—is the fundamental wave number; N and M—number of tones; φ_{nm}—an arbitrary phase that has a uniform distribution over the interval $[-\pi, \; \pi]$.

Since the natural surfaces are neither purely random nor periodical and are often anisotropic [2, 4] then function that was proposed above is a good candidate for characterizing of natural surfaces. Figure 12.19 shows us examples of band-limited Weierstrass function for different scales. It is also important that function (12.3) describes the mathematical fractals only if M and N go to infinity. It is clear from Fig. 12.19 that the function proposed possesses the self-similarity and multi-scale.

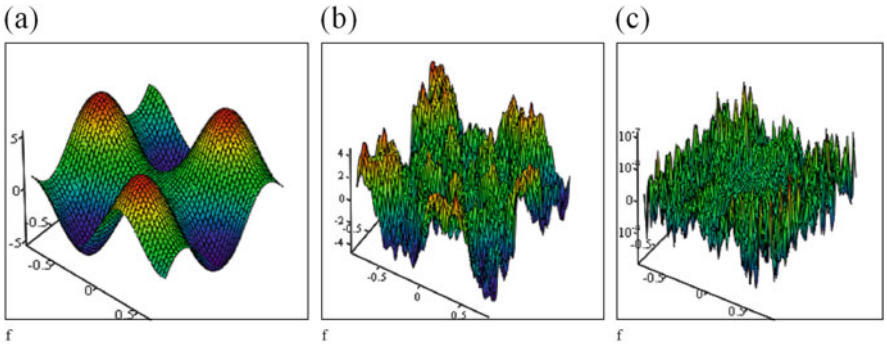

Fig. 12.19 $W(x,y)$ for (a)—$N = 2$, $M = 3$, $D = 2.01$, $q = 1.01$; (b)—$N = 5$, $M = 5$, $D = 2.5$, $q = 3$; (*c*)—$N = 10$, $M = 10$, $D = 2.99$, $q = 7$

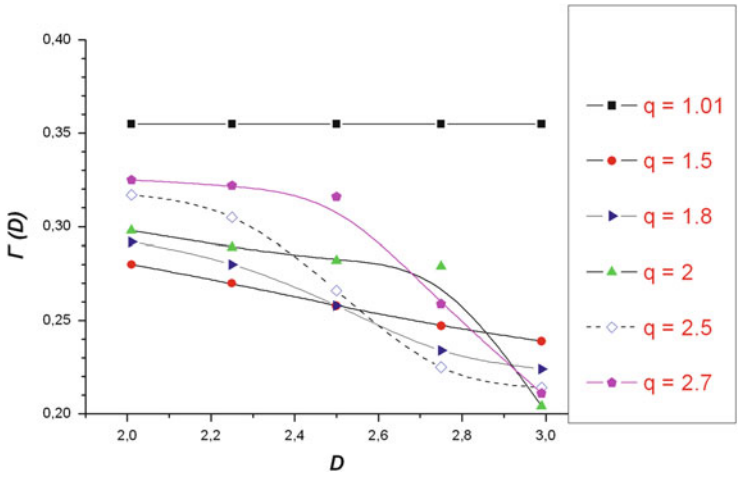

Fig. 12.20 Function $\tilde{\Gamma}$ dependence on D for various values of q

In this section of our work a statistical parameter is introduced for estimation of the fractal dimension D influence and other fractal parameters influence on the surface roughness. Such parameter as the correlation length Γ is conventionally used for numerical characterization of rough surface [4, 18, 19]:

$$\tilde{\Gamma}(\tau) = \langle \rho(\tau) \rangle_s = \left[\frac{\left(1 - q^{2(D-3)}\right)}{\left(1 - q^{2(D-3)N}\right)} \right] \sum_{n=0}^{N-1} q^{2(D-3)n} J_0\left(K q^n \tau\right) \tag{12.4}$$

There are $\tilde{\Gamma}$ dependences on q and D in Fig. 12.20 and Fig. 12.21 respectively. It is shown that with increased value of D, $\tilde{\Gamma}$ decreases more rapidly for the same variation of q. It is shown in Fig. 12.20 that value of $\tilde{\Gamma}$ reduces steadily with the increase of D value. However $\tilde{\Gamma}$ does not change when $q = 1.01$.

As mentioned above the Kirchhoff approach has been already used for analysis of wave scattering by fractal surfaces [18, 19]. Conventional conditions of the Kirchhoff approach applicability are the following: irregularities are large-scale; irregularities are smooth and flat. In the following calculations we assume that observation is carried out from Fraunhofer zone, an incident wave is plane and monochromatic, there are no points with infinite gradient on the surface, the Fresnel coefficient V_0 is constant for this surface, surface large scales are much greater than incident wave length. Shading effects will be taken into account in the following our investigations and studies.

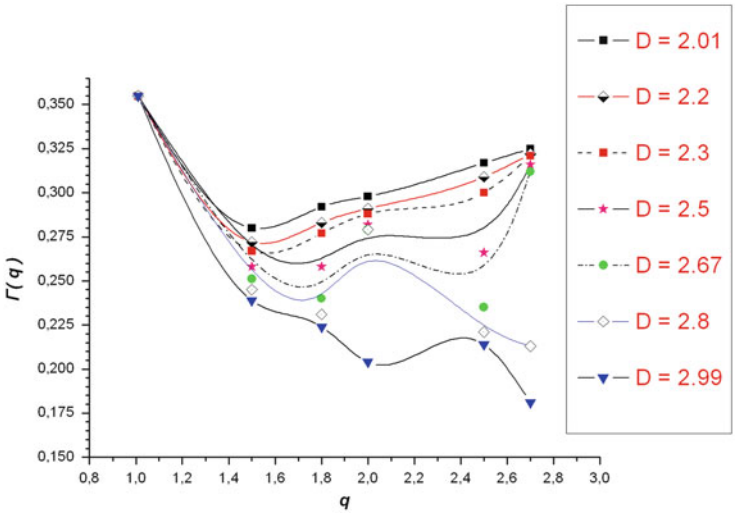

Fig. 12.21 Function $\tilde{\Gamma}$ dependence on q for various values of D

Scattering indicatrix for average field intensity and two-dimensional surface [18, 19]:

$$g \approx \frac{F^2(\theta_1,\theta_2,\theta_3)}{\cos^2\theta_1}\left\{\left[1-\frac{1}{2}(kC\sigma)^2\right]\cdot \operatorname{sinc}^2(kAL_x)\cdot \operatorname{sinc}^2(kBL_y)+\frac{1}{4}C_f^2\sum_{n=0}^{N-1}\sum_{m=1}^{M} q^{2(D-3)n}\cdot\right.$$
$$\left.\cdot \operatorname{sinc}^2\left[\left(kA+Kq^n\cos\frac{2\pi\cdot m}{M}\right)L_x\right]\cdot \operatorname{sinc}^2\left[\left(kB+Kq^n\sin\frac{2\pi\cdot m}{M}\right)L_y\right]\right\} \tag{12.5}$$

We have got a data base of scattering indicatrixes for various fractal scattering surfaces [19–21]. Also in terms of Weierstrass function (12.1) for one-dimensional fractal scattering surface we obtained scattering field absolute value dependences on incident angle and surface fractal dimension D. In subsequent computer calculations, we used the above expression for the coherence function

$$\Psi_k = \langle E_s(k_1)E_s(k_2)\rangle \tag{12.6}$$

of the fields scattered by the fractal surface [19–21].

We can show that the tail intensity of signals reflected by a fractal surface is described by power functions:

$$I(t) \sim 1/\left(t'\right)^{3-D} \tag{12.7}$$

Result (12.7) is very important because, for standard cases, the intensity of a reflected quasi-monochromatic signal decreases exponentially. Thus, the shape of a signal scattered by a fractal statistically rough surface substantially differs from the shape of a scattered signal obtained with allowance for classical effects of diffraction by smoothed surfaces [20, 22].

The results obtained can be widely applied for designing various modern radio systems in the microwave, optical, and acoustic bands.

12.12 Personal Meetings with Benois Mandelbrot

As it's seen from above the author uses the "fractal" term almost everywhere. In conclusion I'd like to share my impressions about the meeting with B. Mandelbrot with readers. The meeting occurred in his house near New York in December 2005. At that time I was responsible for the international project. I had to visit America frequently. My personal meeting with the founder of the fractal geometry B. Mandelbrot occurred on Friday 16 December 2005. Before this the intensive correspondence was going on both when I was still in Moscow and when I flew across USA from south to north with my lectures on the results of 5 years international project. Mandelbrot himself was in an extensive trip but his secretary phoned and told that the maitre would come back home ad hoc. He was extremely interested to meet at home and talk with the Russian physicist who dealt with various "fractal" experiments and applications of the fractal theory in radio physics and radio electronics.

I and my translator got to the New York Central railroad terminal by taxi and then we got to an electric train leaving at 9.30 local time. After a while we went down on a small station and went to the B. Mandelbrot's house by taxi. As approaching to the house we saw a silhouette of a high strong grayish man with glasses on a lace appeared behind the door. He dressed in home clothing. While we are getting off the car he's already opened the front glassed-in door. Mandelbrot's looking at me, smiling, holding out a hand first. Then he's suggesting us to undress and all of us are going to his room. He's asking me to seat down in front of him explaining that this way is better for him to talk and there is a more comfortable arm chair for me. There is his world-famous fundamental book "*Mandelbrot B.B.* The Fractal Geometry of Nature" on the table. I am taking out my monograph on fractals and presenting to Mandelbrot. At that I am telling about scientific work and my results on fractal applications in radio physics, answering his questions. Mandelbrot is listening with a keen interest and very attentively. It is a surprise for him that there is such a success on fractals' applications in Russia and there is already the direct approach to the fractal technologies. He became very interested in my proposed conception of fractal radio systems and in designing an essentially new fractal elemental base.

Hi is well familiar with fractal antennas. Suddenly he's spoken that sometime the matter would be in producing a fractal capacitor! I reply with enthusiasm that I am already "caught" with this idea for a lot of years and a big paper about physical modeling of fractal impedances, fractional operators and production of fractal capacitors is ready for the press. This is incredibly: we are thinking about realizing the same idea on the opposite sides of the world! Mathematical questions are less interesting for Mandelbrot. He is getting more and more interested in disciplines created in IREE RAS: the fractal radio physics and the fractal radio electronics, its development.

Human simplicity, openness, interest in the surrounding world and wisdom—these particular properties are peculiar to B. Mandelbrot. Sometime they tell about B. Mandelbrot's arrogance. I can assert only the reverse. He did not make me feel the difference between our statuses during all the conversation. He first inquired about all fractal developments.

Forty minutes later Mandelbrot stands up and after apologizing and going out to other room he comes back with a pile of his books. He asks me if I already have some of these books. Mandelbrot says that he likes my works. He inquires when and how my book was written. I reply that I prepared the first version as early as in the beginning of nineties of XX. Then the search for publishers began and at the same time improving and significant rework of the monograph text was going on. Mandelbrot says that now he has two books on the go: the one is in Italy and the other is in America. With a smile he admits that he writes slowly, thoroughly using all his old works. Our conversation's been lasting for almost 2 h. Tempus fugit. At a certain moment he is called by the phone. He suggests to give us a lift to the railway station on his car. Mandelbrot drives the car on his own. We are at the railway terminal already at noon. I tell goodbye to B. Mandelbrot and we are waving to each other. This is the unforgettable meeting. There are all the minutest details of the meeting with the great scientist in my memory.

12.13 Conclusions

The fractal problem in radio location, radio physics and radio engineering is indeed immense. Here I illustrate only fundamental initial issues. It is always hard and even impossible to recede from habitual standards... But the author has good reasons to think that the extensive and valuable material he already obtained and the results of further researches will be used in advanced radio systems. The fractal radio physics, fractal radio engineering and fractal radio location are peculiar radio sciences. They are suffused with a spirit and ideas of the classical radio physics and radio engineering but at the same time they are fundamentally new areas of focus. The results of conducted researches oriented to enhancing the interference immunity of work of radio systems on a radio channel with high-intensity noise and distortion showed opportunities of the approach on the basis of using textural and fractal-scaling methods of detecting and processing random signals and fields.

The author raised these questions back in 1980, and for 35 years has been successfully working on their resolution [4–6]. Fractal methods similar to ones presented in this work can be applied when considering wave and oscillatory processes in optics, acoustics and mechanics. Results and conclusions obtained by the author and his pupils have great innovative potential. We think that its realization will resolve a number of current problems of radio physics, radio engineering, radio location, communication and operation and also will allow to provide a new quality for detecting and recognition systems and also development of the new informational technologies.

Many important stages in fractal directions development including the stage of this science field formation have been already passed. However many problems are still to be solved. Results and specific solutions are not of so greatest value like *the solution method* and its approach are. The method is created by the author [4–14, 16, 19–21, 23–25]. It is necessary to put it all into practice!

References

1. C.A. Rogers, *Hausdorff Measures* (Cambridge University Press, London, 1970), 179 pp
2. K.B. Oldham, J. Spanier, *The Fractional Calculus* (Academic, New York, 1974), 234 pp
3. B. Mandelbrot, *The Fractal Geometry of Nature* (W.H. Freeman and Co., San Francisco, 1983), 460 pp
4. A.A. Potapov, *Fractals in Radiophysics and Radar* (Logos, Moscow, 2002), 664 pp
5. A.A. Potapov, *Fractals in Radiophysics and Radar: Topology of a Sample* (Universitetskaya Kniga, Moscow, 2005), 848 pp
6. A.A. Potapov, R.M. Crownover, *Introduction to Fractals and Chaos* (Tekhnosfera, Moscow, 2006), pp. 374–479
7. A.A. Potapov, Y.V. Gulyaev, S.A. Nikitov, A.A. Pakhomov, V.A. German, in *Newest Images Processing Methods*, ed. by A.A. Potapov (FIZMATLIT, Moscow, 2008), 496 pp
8. A.A. Potapov, V.A. Chernykh, A. Letnikov, *Fractional Calculus in the Physics of Fractals* (LAMBERT Academic Publishing, Saarbrücken, 2012), 688 pp

9. A.A. Potapov, in *The Textures, Fractal, Scaling Effects and Fractional Operators as a Basis of New Methods of Information Processing and Fractal Radio Systems Designing. Proceedings of SPIE*, vol. 7374 (Society of Photo-optical Instrumentation Engineers, Bellingham, 2009), pp. 73740E-1–73740E-14
10. A.A. Potapov, *Fractal Method and Fractal Paradigm in Modern Natural Science* (Nauchnaya Kniga, Voronezh, 2012), 108 pp
11. S.A. Podosenov, A.A. Potapov, J. Foukzon, E.R. Menkova, in *Nonholonomic, Fractal and Linked Structures in Relativistic Continuous Medium, Electrodynamics, Quantum Mechanics and Cosmology,* 3 vols., ed. by A.A. Potapov (ENAND, Moscow, 2015), 1128 pp
12. A.A. Potapov, in *Fractals and Scaling in the Radar: A Look from 2015, Book of Abstracts 8nd International Conference (CHAOS' 2015) on Chaotic Modeling, Simulation and Applications*, Henri Poincaré Institute, Paris, 26–29 May 2015, p. 102
13. A.A. Potapov, in *New Conception of Fractal Radio Device with Fractal Antennas and Fractal Detectors in the MIMO—Systems. Book of Abstracts Third International Scientific Symposium "The Modeling of Nonlinear Processes and Systems (MNPS-2015)*", Moscow, 22–26 June 2015, p. 33
14. A.A. Potapov, in *Features of Multi-Fractal Structure of the High-Attitude Lightning Discharges in the Ionosphere: Elves, Jets, Sprites, Book of Abstracts 8nd International Conference (CHAOS' 2015) on Chaotic Modeling, Simulation and Applications*, Henri Poincaré Institute, Paris, 26–29 May 2015, pp. 101–102
15. J. Yang, F. GuiLi, A gigantic jet event observed over a thunderstorm in mainland China. Chin. Sci. Bull. **57**(36), 4791–4800 (2012)
16. A.A. Potapov, V.A. German, Detection of artificial objects with fractal signatures. Pattern Recognit. Image Anal. **8**(2), 226–229 (1998)
17. F.G. Bass, I.M. Fuks, *Wave Scattering from Statistically Rough Surfaces* (Pergamon Press, Oxford, 1978)
18. N. Lin, H.P. Lee, S.P. Lim, K.S. Lee, Wave scattering from fractal surfaces. J. Mod. Opt. **42**, 225–241 (1995)
19. A.A. Potapov, A.V. Laktyunkin, Theory of the wave scattering by anisotropic fractal surface. Nonlinear World **6**(1), 3–35 (2008)
20. A.A. Potapov, The theory of functionals of stochastic backscattered fields. J. Commun. Technol. Electron. **52**, 245–292 (2007)
21. A.A. Potapov, A.V. Laktyun'kin, Frequency coherence function of a space–time radar channel forming images of an anisotropic fractal surface and fractal objects. J. Commun. Technol. Electron. **60**, 962–969 (2015)
22. M.V. Berry, Z.V. Blackwell, Diffractal echoes. J. Phys. A: Math. Gen. **14**, 3101–3110 (1981)
23. A.A. Potapov, The base of fractal antenna theory and applications: utilizing in electronic devices, in *Proceedings of the 2013 IX International Conference on Antenna Theory and Techniques* (16–20 September 2013, Odessa, Ukraine). Odessa National A.S. Popov Academy of Telecommunications, Odessa, 2013, p. 62–67
24. A.A. Potapov, The global fractal method and the fractal paradigm in fundamental radar problems, in *Book of Abstracts International Conference on Dynamics, Bifurcations and Strange Attractors*. Dedicated to the Memory of L.P. Shil'nikov (1934–2011) (1–5 July 2013, Nizhni Novgorod, Russia). Lobachevsky State University of Nizhni Novgorod, Nizhni Novgorod, 2013, p. 98
25. A.A. Potapov, Oscillator with fractional differential positive feedback as model of fractal dynamics. J. Comput. Intell. Electron. Syst. **3**, 236–237 (2014)

Chapter 13
Simulation of Multidimensional Nonlinear Dynamics by One-Dimensional Maps with Many Parameters

Irina N. Pankratova and Pavel A. Inchin

Abstract We propose a concrete class of discrete dynamical systems as nonlinear matrix models to describe the multidimensional multiparameter nonlinear dynamics. In this article we simulate the system asymptotic behavior. A two-step algorithm for the computation of ω-limit sets of the dynamical systems is presented. In accordance with the qualitative theory which we develop for this class of systems, we allocate invariant subspaces of the system matrix containing cycles of rays on which ω-limit sets of the dynamical systems are situated and introduce the dynamical parameters by which the system behavior is described in the invariant subspaces. As the first step of the algorithm, a cycle of rays which contains the ω-limit set of the system trajectory, is allocated using system matrix. As the second step, the ω-limit set of the system trajectory is computed using the analytical form of one-dimensional nonlinear Poincare map dependent on the dynamical parameters. The proposed algorithm simplifies calculations of ω-limit sets and therefore reduces computing time. A graphic visualization of ω-limit sets of n-dimensional dynamical systems, $n > 3$ is shown.

13.1 Introduction

To understand and analyse nonlinear multidimensional dynamics simple one-dimensional semi-dynamical systems with complicated dynamics and fairly complete qualitative description are used. These are, first of all, one-dimensional discrete dynamical systems, i.e. iterations of real one-dimensional maps. The first systematic results on one-dimensional discrete dynamical systems appeared in the early 60s and are linked to Sharkovskii [1]. Many properties of the dynamical systems are the direct result of the theories developed by Sharkovskii [2] and Feigenbaum [3].

I.N. Pankratova (✉) • P.A. Inchin
Department of Differential Equations, Institute of Mathematics and Mathematical Modeling, 050010 Pushkin str., 125, Almaty, Kazakhstan
e-mail: inpankratova@gmail.com; paul.inchin@yahoo.com

C. Skiadas (ed.), *The Foundations of Chaos Revisited: From Poincaré to Recent Advancements*, Understanding Complex Systems,
DOI 10.1007/978-3-319-29701-9_13

A representative of this class of systems is the dynamical system generated by the one-dimensional logistic map [4]. It was the first example of a complicated, chaotic behaviour of the system given by a simple nonlinear equation. Even though the properties of the one-dimensional logistic map are well studied, researchers continue referring to it as standard to check the many nonlinear phenomena [5–7]. However, up until now there is no well-developed qualitative theory available, which could be successfully applied in order to conduct a complete study of the multidimensional dynamical systems dependent on parameters. Therefore, it is appropriate to select concrete classes of the dynamical systems and to develop qualitative theories so as to be able to describe the properties and movements of the systems within these theories.

We focus our research on a concrete class of dynamical systems which represent a variant of generalization of one-dimensional discrete dynamical systems to the multidimensional multiparameter case. The systems are generated by a map in the form of the product of scalar and vector linear functions on compact sets of the real vector space. We propose the systems as nonlinear matrix models with limiting factors to describe the macro system dynamics, for example the dynamics of many group biological population in the presence of limited resources. In these models the scalar function plays a role of a limiting factor.

In recent years, the methods of computer simulation have become an essential tool in the study of the dynamical systems [8, 9]. The modern computer capabilities make it possible to include in the system complicated nonlinear relationships between its variables and a large number of parameters. The presence of nonlinear relationships and multiparameter dependence reproduces in the model the phenomena which can be observed in actual experiments and which cannot be produced by splitting the system into separate components or reducing the number of parameters or variables. Thus, the improvement of current methods and the development of new ones for the dynamical system research are necessary and relevant [10, 11]. In this case the quantitative research provides a theoretical basis for the algorithm constructions, and hence is particularly important.

We develop a qualitative theory for the class of the dynamical systems considered (see e.g. [12] and references there in). The systems possess the obvious properties which are determined by the linear vector function (the system matrix) and which do not depend on the scalar function. In particular, in vector space we allocate invariant subspaces containing cycles of rays of the system matrix, on which ω-limit sets of dynamical systems are situated. On the other hand, the complicated nonlinear dynamics of the systems can occur due to the scalar function. We study the system dynamics in the invariant subspaces containing cycles of rays using one-dimensional nonlinear Poincare maps and introduce the dynamical parameters by which the system behavior is described in the invariant subspaces. In this article we show the results of the simulation of the system asymptotic behavior and present an algorithm for the computation of ω-limit sets of the class of the dynamical systems considered. The algorithm consists of two steps of calculations in accordance with the qualitative theory. As the first step, a cycle of rays which contains the ω-limit set of the system trajectory is allocated using system matrix. The period of the cycle

of rays, the number and values of the dynamical parameters by which the system dynamics is described on the cycle of rays, are calculated as well. As the second step, the ω-limit set of the system trajectory is computed using one-dimensional nonlinear Poincare map dependent on the dynamical parameters. As a rule, these parameters differ from the system parameters and are unknown or not directly defined or computable [13]. The novelty of our research lies in the determination of the dynamical parameters and in the analytical form of one-dimensional nonlinear Poincare maps dependent on the dynamical parameters. We shall see below that the number of the dynamical parameters cannot be reduced without the loss of accuracy of the system behavior description, even when this number is greater than the number of the system parameters, i.e. entries of the system matrix.

13.2 Class of the Dynamical Systems

Let F be a map of the form [12]

$$F : \mathbb{R}^n \to \mathbb{R}^n, \quad Fy = \Phi(y)Ay \tag{13.1}$$

where $\mathbb{R}^n$ is n-dimensional real vector-space, $\Phi(y)$ is a scalar function, A is a linear operator (a matrix of n-th order). Allocate set $\mathrm{X} \subseteq \mathbb{R}^n$ invariant under F i.e., $F : \mathrm{X} \to \mathrm{X}$. Map F in general is non invertible and generates in X a cyclic semi-group of maps $\{F^m\}$, $m \in Z_+$, which is called the dynamical system and is denoted by $\{F^m, \mathrm{X}, Z_+\}$. Set X is called phase space of the dynamical systems and specifies a set of valid states of the dynamical system, $Z_+ = \mathbb{N} \bigcup \{0\}$ is the set of nonnegative integers. Set $\{F^m y\}$ where y is fixed and m runs over Z_+, is called a trajectory of the point y. The dynamics of the system $\{F^m, \mathrm{X}, Z_+\}$ is understood as the process of transition from one state to another.

The dynamics of the system $\{F^m, \mathrm{X}, Z_+\}$ generally varies for different $\Phi(y)$. So, the systems $\{F^m, \mathrm{X}, Z_+\}$ are different too. But the systems possess similar properties which are determined by the linear operator A and do not depend on the function $\Phi(y)$. Therefore, the systems $\{F^m, \mathrm{X}, Z_+\}$ form one class of the dynamical systems.The elements of this class are, in particular, linear dynamical systems with $\Phi(y) = const$ and the dynamical system $\{f^m, \mathrm{X}, Z_+\}$ generated by the map f of the form [14]

$$f : \mathbb{R}^n \to \mathbb{R}^n, \quad f\, y = (1 - \|y\|)Ay. \tag{13.2}$$

Here $\|\cdot\|$ is a vector norm in $\mathbb{R}^n$. If $n = 1$ then $A = \mu$ and we arrive at the well-known logistic map mentioned above

$$\psi_\mu : \mathbb{R}^1 \to \mathbb{R}^1, \quad \psi_\mu x = \mu(1 - x)x. \tag{13.3}$$

13.3 Mathematical Models with Limiting Factors

We propose the class of the dynamical systems $\{F^m, \mathrm{X}, Z_+\}$ as mathematical models for describing the dynamics of model and real macro systems in the presence of limiting factors.

Let

n be a number of macro system's components,
$y \in \mathrm{X}$ be a vector of components' characteristics,
A be a matrix of components' interrelations and
$\Phi(y)$ be a limiting function (limiting factor).

Let X be a compact of the form

$$\mathrm{X} = \{y \in \mathbb{R}^n \mid y \geq 0, \ \ \|y\| \leq a\}, \quad a < \infty. \tag{13.4}$$

Here $y = (y_1, \ldots, y_n)' \geq 0$ means $y_i \geq 0$, $i = \overline{1,n}$ and is called a nonnegative vector. Note that X is invariant under F i.e., $F : \mathrm{X} \to \mathrm{X}$ if and only if [12]

1) $\Phi(y) \geq 0$ is continuous function on X,
2) $A = (a_{ij}) \geq 0$ $(a_{ij} \geq 0, i, j = \overline{1,n})$,
3) $\|A\| \leq aC^{-1}$ where $C = \max\limits_{y \in \mathrm{X}} \Phi(y)\|y\|$ and $\|A\|$ is a subordinate matrix norm for a matrix A based on the vector norm in $\mathbb{R}^n$.

Then the dynamical system $\{F^m, \mathrm{X}, Z_+\}$ describes the macro system's state changes over time m. For any nontrivial $\{F^m y\}$ we introduce a unit vector

$$e_m(y) = \|F^m y\|^{-1} F^m y \tag{13.5}$$

which is called a macro system structure and defines the ratio between components' characteristics at the time m. The state of macro system governed by the dynamical system $\{F^m, \mathrm{X}, Z_+\}$ (at the time m) we characterize by

$$S^m(y) = \{F^m y, e_m(y)\}. \tag{13.6}$$

The limiting factor concept was first coined in biology by Libig J. and generally, means a factor that restricts or constrains the dynamics of the system, process or phenomena. By using limiting factors, the state of the system is regulated.

On one hand, models given by the systems $\{F^m, \mathrm{X}, Z_+\}$ generalize in n-dimensional case many nonlinear one- and two-dimensional models widely used in practice. In particular, for describing the dynamics of n-group biological population with discrete generations in the presence of limited resources we propose the dynamical system generated by the map f of the form (13.2). In this representation y is a vector of densities of population age groups so, $\|y\| \leq 1$. If $n = 1$ then y is the total population density, $A \equiv \mu$ is the reproductive coefficient. The

dynamical system $\{\psi_\mu^m, \mathrm{I}, Z_+\}$ in the interval $\mathrm{I} = [0, 1]$ describes a mechanism of self-regulation of one-species biological population with limited resources [2].

On the other hand, models given by the systems $\{F^m, \mathrm{X}, Z_+\}$ generalize many matrix models, in particular, Leslie models both linear and nonlinear [15, 16]. The last ones contain matrices A of the special form (Leslie matrix and its generalizations) and concrete limiting functions $\Phi(y)$.

13.4 Qualitative Theory

We develop a qualitative theory for the class of the dynamical systems $\{F^m, \mathrm{X}, Z_+\}$ and apply the results of the theory in computer simulation of their dynamics.

Denote by $\omega_F y$ ω-limit set of the trajectory $\{F^m y\}$ (the set which attracts $\{F^m y\}$ when $m \to +\infty$). A ray passing through $y \in \mathbb{R}^n$, $y \neq 0$ is the set $\mathrm{cone}(y) = \{\alpha y \mid \alpha \geq 0\}$. By a system of p elements we mean a sequence of these elements, $p \in \mathbb{N}$. Then the system of distinct rays $l_1, \ldots, l_p$ is called a cycle of rays of a linear operator A of period $p \in \mathbb{N}$ and is denoted by $\mathrm{L}_p = (l_1, \ldots, l_p)$ if

$$Al_k = l_{k+1}, \quad k = 1, \ldots, p-1, \quad Al_p = l_1.$$

As easy to see, that invariant sets of the system $\{F^m, \mathrm{X}, Z_+\}$ are contained in invariant subspaces of A. Denote $\ker A = \{y \in \mathbb{R}^n \mid Ay = 0\}$ and let

$$\mathcal{P}(A; p, \mu) = A^p - \mu^p E, \quad \mu \in \mathbb{C}.$$

We call the intersection $l \cap \mathrm{X}$ as a segment of ray l (ray segment). Denote by ϕ_μ map F when $n = 1$,

$$\phi_\mu x = \mu \Phi(x) x \tag{13.7}$$

where $x \in \mathrm{I_a} = [0, a]$. According to the qualitative theory there exist $p, q \in \mathbb{N}$, $\mu \in \sigma(A)$ such that any nontrivial ($\neq \{0\}$) $\omega_F y$ is located in some invariant subspace

$$\ker \mathcal{P}(A; p, \mu), \quad \mu^p > 0,$$

on a cycle of rays L_q where $\sigma(A)$ is a spectrum of A and q is a divisor of p, $1 \leq q \leq p$ [17]. More precisely, $\omega_F y \subseteq \mathrm{J_q} = \mathrm{L}_q \cap \mathrm{X} \subset \ker \mathcal{P}(A; p, \mu) \cap \mathrm{X}$ and $\mathrm{J_q}$ consists of q ray segments invariant under F^q. Without losing generality we agree $q = p$ and $\omega_F y \subseteq \mathrm{J}_p$. Then for the map F with $\Phi(\|y\|)$ map F^p represents in $\mathrm{J_p}$ as a superposition

$$F^p = \phi_{\mu_p} \circ \phi_{\mu_{p-1}} \circ \ldots \circ \phi_{\mu_1} \tag{13.8}$$

with some numbers $\mu_1 > 0, \ldots, \mu_p > 0$.

If to consider the system $\{F^m, \ker \mathcal{P}(A;p,\mu) \cap \mathrm{X}, Z_+\}$, then $\mu_1, \ldots, \mu_p$ turns into parameters. We call them dynamical parameters in contrast to the system parameters i.e. entries of the matrix A. Thus, in the whole X, the system dynamics is defined by the trajectory behavior in the sets $\ker \mathcal{P}(A;p,\mu) \cap \mathrm{X}$. So, by the parameters μ_1, $\ldots, \mu_p$ the system dynamics is described in the whole X. Every ray segment of $\mathrm{J_p}$ is the one-dimensional Poincare section for the trajectories located in $\mathrm{J_p}$ and F^p is the one-dimensional first return (Poincare) map for the map F in each ray segment of $\mathrm{J_p}$. For the special form $\Phi(\|y\|)$ map F^p has analytical representation (13.8).

Denote by $e_1, \ldots, e_p$ the unit vectors directed along the ray segments of $\mathrm{J_p}$. We define $e_1, \ldots, e_p$ and $\mu_1, \ldots, \mu_p$ by the recurrent formulas. Let $p = 1$. Then $e_1 \geq 0$ is an eigen vector of the matrix $A \geq 0$ and there exists an eigen value $\mu > 0$ such as $Ae_1 = \mu e_1$. So, (13.8) takes the form

$$F = \phi_\mu. \tag{13.9}$$

Let $p > 1$ then $e_1 \geq 0$ is not an eigen vector of A, $\|e_1\| = 1$ and $e_2, \ldots, e_p$ are defined by the sequence

$$e_j = \|Ae_{j-1}\|^{-1} Ae_{j-1}, \quad j = \overline{2,p}. \tag{13.10}$$

Denote

$$\mu_j = \|Ae_j\|, \quad j = \overline{1,p}. \tag{13.11}$$

For the map F with different $\Phi(\|y\|)$, parameters $\mu_1, \ldots, \mu_p$ and vectors e_1, $\ldots, e_p$ are the same and their computation by the formulas (13.10) and (13.11) does not cause difficulties.

It should be noted that the dynamical parameters, their number and values depend on the location of the sets $\ker \mathcal{P}(A;p,\mu) \cap \mathrm{X}$ in X and J_p in $\ker \mathcal{P}(A;p,\mu) \cap \mathrm{X}$ and vary, as a rule, at the fixed entries of the matrix A. So, the dynamical parameters differ from the system parameters and identify the regions with different dynamics. Their number is less than or equal to p and may be very large, in particular, when $p > n^2$ at $n \geq 19$ [17]. According to (13.8) all parameters are involved in the representation of the map F^p so, their number cannot be reduced.

13.5 Computer Simulation

We present computer simulation of multidimensional dynamics by the numerical realization of the models for the dynamics of biological population governed by the system $\{f^m, \mathrm{X}, Z_+\}$.

In the population model:

f is a map of the form (13.2): $fy = (1 - \|y\|)Ay$,
n is a number of population age groups,
y is a vector of densities of the age groups, $y \in \mathrm{X}$,
X is of the form (13.4) if $a = 1$ i.e.,

$$\mathrm{X} = \{y \in \mathbb{R}^n \mid y \geq 0,\ \|y\| \leq 1\},$$

A is a matrix of intergroup relations,

$\Phi(\|y\|) = 1 - \|y\|$ is a population size limiting function corresponding to the assumption of limited resources or available living space.

Let $\|y\| = \sum_1^n y_i$ then the condition 3) for the invariance of X is as follows: $\|A\| = \max_j \sum_{i=1}^n a_{ij} \leq 4$. For any nontrivial $\{f^m y\}$ a unit vector $e_m(y) = \|f^m y\|^{-1} f^m y$ is an age structure of many-group population and defines the ratio between densities of age groups in total population density (at the time m). The state of the population governed by the dynamical system $\{f^m, \mathrm{X}, Z_+\}$ (at the time m) is $S^m(y) = \{f^m y, e_m(y)\}$.

According to the Sect. 13.4, for any nonzero initial state $S^0(y)$, the structure of many-group population is asymptotically stabilized as p-periodic and is characterized by p vectors $e_1, \ldots, e_p$ defined by (13.10).

As to the population dynamics, we get that the many-group population model given by the dynamical system $\{f^m, \mathrm{X}, Z_+\}$ asymptotically has the same behavior as a family of one-species population models given by the one-dimensional systems $\{(\psi_{\mu_p} \circ \psi_{\mu_{p-1}} \circ \ldots \circ \psi_{\mu_1})^m, \mathrm{I}, Z_+\}$ where $\psi_{\mu_p} \circ \psi_{\mu_{p-1}} \circ \ldots \circ \psi_{\mu_1}$ is a superposition (13.8) with the map ψ_μ of the form (13.3) and $\mu_1, \ldots, \mu_p$ defined by (13.11).

Therefore, the population governed by the system $\{f^m, \mathrm{X}, Z_+\}$, has stabilized p-periodic structure at its final state, $p < \infty$ and densities of its age groups that change periodically or not. The same asymptotic behavior has the macro system governed by the system $\{F^m, \mathrm{X}, Z_+\}$ i.e., exactly p-periodic structure, $p < \infty$ and periodic or nonperiodic changes of its components' characteristics.

13.6 Method of One-Dimensional Superpositions

For correct determining cyclic ω-limit sets of large periods or chaotic ω-limit sets of the system $\{F^m, \mathrm{X}, Z_+\}$, we propose a computer method which we call as a method of one-dimensional superpositions. Let F be the map with a function $\Phi(\|y\|)$. The method implies calculations in two steps.

As the first step, a stable set J_p is determined for any nonzero $y \in \mathrm{X}$ using n-dimensional linear dynamical system $\{A^m, \mathbb{R}^n, Z_+\}$. At this step, period p is obtained

and the unit vectors $\{e_1, \ldots, e_p\}$ along the rays of a cycle of rays L_p in which $\omega_F y$ is located, are computed by the matrix A. The number $1 \leq t \leq p$ and values of the dynamical parameters by which the trajectory dynamics in J_p is described, are computed as well. Here t is a divisor of p.

As the second step, set $\omega_F y$ is determined using the one-dimensional dynamical system $\{(\phi_{\mu_p} \circ \phi_{\mu_{p-1}} \circ \ldots \circ \phi_{\mu_1})^m, \mathrm{I}, Z_+\}$. At this step, the norm x of the projection of the vector y in the set J_p is obtained and a one-dimensional ω-limit set of the trajectory $\{(\phi_{\mu_p} \circ \phi_{\mu_{p-1}} \circ \ldots \circ \phi_{\mu_1})^m x\}$ is computed by the one-dimensional nonlinear Poincare map F^p with t parameters $\mu_1 > 0, \ldots, \mu_t > 0$. The points of this ω-limit set are coordinates of vectors which compose the part of $\omega_F y$ along the vector e_1.

The parts of $\omega_F y$ along the other vectors $e_2, \ldots, e_p$ are of the same type and structure and the vectors which compose these parts, are computed as well.

The method proposed simplifies calculations for large n and p for instance, $p > n^2$, $p > n^3$ and so on. Indeed, at first we detect the stable cyclic set J_p and later on we describe the trajectory dynamics in it. Using the method we compute any nontrivial set $\omega_F y$, in particular, we obtain the final state of many-group population for any nonzero initial state $S^0(y)$. The method also provides graphic visualization of ω-limit sets of n-dimensional dynamical systems $\{F^m, \mathrm{X}, Z_+\}$ at $n > 3$ and for large p.

The calculation algorithm for the computation of the set $\omega_F y$ and the final macro system state by the method of one-dimensional superpositions is as follows:

1. enter initial vector $y \geq 0$ and matrix $A \geq 0$ ($\|y\| < 1$, $\|A\| \leq 4$);
1′. calculate eigen values and eigen vectors of matrix A;
2. calculate period p, vectors $e_1, \ldots, e_p$ of the set J_p and t distinct parameters $\mu_1, \ldots, \mu_t$ of the set $\{\mu_1, \ldots, \mu_p\}$ using (13.10), (13.11);
3. determine projection y' of vector y in the set $\mathrm{J_p}$ and calculate its norm $x = \|y'\|$;
4. obtain ω-limit set of the trajectory $\{\phi_{\mu_p} \circ \phi_{\mu_{p-1}} \circ \ldots \circ \phi_{\mu_1})^m x\}$ as some trajectory i.e.,

$$\omega_{\phi_{\mu_p} \circ \phi_{\mu_{p-1}} \circ \ldots \circ \phi_{\mu_1}} x = \{x_i^*\}_{i \geq 0}$$

where $x_i^* = (\phi_{\mu_p} \circ \phi_{\mu_{p-1}} \circ \ldots \circ \phi_{\mu_1})^i x^*$. After these calculations the iteration process stops;
5. The set $\omega_F y$ is a result of calculations done in step 4 and is the following set

$$\omega_F y = \{x^* e_1, (\phi_{\mu_1} x^*) e_2, (\phi_{\mu_2} \circ \phi_{\mu_1} x^*) e_3, (\phi_{\mu_3} \circ \phi_{\mu_2} \circ \phi_{\mu_1} x^*) e_4, \ldots,$$
$$(\phi_{\mu_{p-1}} \circ \ldots \circ \phi_{\mu_1} x^*) e_p, x_1^* e_1, \ldots\}.$$

So, vectors of $\omega_F y$ are of the form $u e_i$ where $u \in \omega_{\phi_{\mu_p} \circ \phi_{\mu_{p-1}} \circ \ldots \circ \phi_{\mu_1}} x$, $i = \overline{1, p}$.

The final macro system state is a pair

$$S^*(y) = \{\omega_f y, E\} \quad \text{where } E = \{e_1, \ldots, e_p\}.$$

13.7 Examples

13.7.1 The Dynamics of the Northern Spotted Owl

The algorithm for computing of the population dynamics is implemented in Matlab as a function with the following input data: n-dimensional initial vector $y \geq 0$ and matrix $A \geq 0$ of n order. The final state of the population is given as an output data in the form of two arrays of vectors.

Let us demonstrate this algorithm by simulating the dynamics of the Northern Spotted Owl. As an input data we use the real (3×3)-matrix A from article of Lamberson, McKelvey, et al. [18]. We would like to take into account limited resources for the population. For this purpose, in contrast to the linear model considered in [18], we propose nonlinear models given by the dynamical system $\{f^m, \mathrm{X}, Z_+\}$. In the models a proportional coefficient c is introduced as an input data to make the dynamics nontrivial.

Example 1

1. enter (a) $y = (0.1, 0.1, 0.1)'$,

   (b) $A = c \cdot \begin{pmatrix} 0 & 0 & 0.33 \\ 0.18 & 0 & 0 \\ 0 & 0.71 & 0.94 \end{pmatrix}$.

   The elements in the top row of matrix A are fertility rates; the sub-diagonal elements are survival rates; nonzero diagonal element a_{ii} is the probability that females in stage i remain in the same stage next year;

   (c) $c = 3.1$ (almost maximum available value of c to fulfil $\|A\| \leq 4$);

2. vectors e_j of the set E with accuracy $\epsilon = 10^{-5}$ and parameters $\mu_j, j = \overline{1,p}$, are computed. As a result, after eight iterations, a convergence of the sequence of vectors $e_i(y)$ to E is obtained. The ultimate result is $p = 1$, $(n \times p)$-array $E = \{e\}$ and array $U = \{\mu\}$ where $e = (0.2402, 0.0440, 0.7159)'$, $\mu = 3.0491$;
3. given $x = 0.8$;
4. given accuracy $\epsilon = 10^{-5}$ for the trajectory $\{\psi_\mu^m x\}$ obtain $\omega_{\psi_\mu} x$ as a cycle of period 2 per 56 iterations,

$$\omega_{\psi_\mu} x = \{x^*, \psi_\mu x^*\} = \{0.5909, 0.7371\};$$

5. for the trajectory $\{f^m y\}$

$$\omega_f y = \{0.5909e, 0.7371e\} =$$

$$= \{(0.1419, 0.0260, 0.4230)', (0.1770, 0.0324, 0.5277)'\}.$$

The final population state is

$$S^*(y) = \{\omega_f y, E\} \quad \text{where } E = \{e\}$$

and is shown in Fig. 13.1a.

Example 2

1. enter (a) $y = (0.1, 0.1, 0.1)'$,
   (b) $A = c \cdot \begin{pmatrix} 0 & 0 & 0.33 \\ 0.18 & 0 & 0 \\ 0 & 0.71 & 0 \end{pmatrix}$. In this model we suppose that there are no females remaining in the same stage next year;
   (c) $c = 5$ (almost maximum available value of c to fulfil $\|A\| \leq 4$);
2. vectors e_j with accuracy $\epsilon = 10^{-5}$ and parameters $\mu_j, j = \overline{1,p}$, are computed. As a result, after 3 iterations, a convergence of sequence of vectors e_j to set E is obtained. The ultimate result is $p = 3$, $(n \times p)$-array $E = \{e_1, e_2, e_3\}$ and array $U = \{\mu_1, \mu_2, \mu_3\}$ where $e_1 = (0.3333, 0.3333, 0.3333)'$, $e_2 = (0.2705, 0.1475, 0.5820)'$, $e_3 = (0.5559, 0.1409, 0.3032)'$, $\mu_1 = 2.0333$, $\mu_2 = 1.7275$, $\mu_3 = 1.5009$;
3. as $A^3 = \lambda^3 I$ then y, $\{f^m y\}$ and $\omega_f y$ are located in the same set J_3. Here $\lambda = 1.7404$ is the maximum eigenvalue of $A \geq 0$ and I is identity matrix. So, calculate $x = \sum_1^3 y_i = 0.3$;
4. given accuracy $\epsilon = 10^{-5}$ for the trajectory $\{(\psi_{\mu_3} \circ \psi_{\mu_2} \circ \psi_{\mu_1})^m x\}$ obtain $\omega_{\psi_{\mu_3} \circ \psi_{\mu_2} \circ \psi_{\mu_1}} x$ as a fixed point per 8 iterations,

$$\omega_{\psi_{\mu_3} \circ \psi_{\mu_2} \circ \psi_{\mu_1}} x = \{x^*\} \quad \text{where } x^* = 0.368;$$

5. for the trajectory $\{f^m y\}$

$$\omega_f y = \{x^* e_1,\ (\psi_{\mu_1} x^*) e_2,\ (\psi_{\mu_2} \circ \psi_{\mu_1} x^*) e_3\} = \{(0.1227; 0.1227; 0.1227)',$$
$$(0.1279; 0.0698; 0.2752)', (0.2394; 0.0607; 0.1306)'\}.$$

The final population state is

$$S^*(y) = \{\omega_f y, E\} \quad \text{where } E = \{e_1, e_2, e_3\}$$

and is shown in Fig. 13.1b.

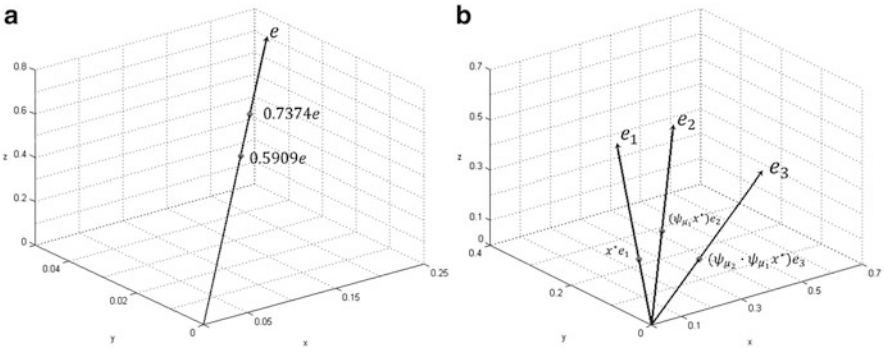

Fig. 13.1 Final state of three-group population: stable population structure characterized by unit vector e and 2-year periodic age-group sizes defined by two vectors $0.5909e$ and $0.7374e$ (**a**); 3-year periodic population structure characterized by unit vectors e_1, e_2, e_3 and 3-year periodic age-group sizes defined by three vectors x^*e_1, $(\psi_{\mu_1}x^*)e_2$, $(\psi_{\mu_2} \circ \psi_{\mu_1}x^*)e_3$ (**b**)

13.7.2 The Dynamics of Macro System Composed of a Large Number of Components

In the next two examples we demonstrate the advantages of the method of one-dimensional superposition in graphic visualization of the final macro system state at $n > 3$ and $p > n$. We briefly summarize the results obtained by the method. Assume that the macro system dynamics is described by the dynamical system $\{f^m, \mathrm{X}, Z_+\}$.

Example 3 Let $n = 10$ and A be (10×10)-matrix of a quasidiagonal form $\{A_1, A_2, A_3\}$ with matrices A_j on the main diagonal,

$$A_1 = \begin{pmatrix} 0 & 3.2 \\ 3.2 & 0 \end{pmatrix}, \quad A_2 = \begin{pmatrix} 0 & 2.56 & 0 \\ 0 & 0 & 3.2 \\ 4 & 0 & 0 \end{pmatrix}, \quad A_3 = \begin{pmatrix} 0 & 2.56 & 0 & 0 & 0 \\ 0 & 0 & 4 & 0 & 0 \\ 0 & 0 & 0 & 4 & 0 \\ 0 & 0 & 0 & 0 & 3.2 \\ 2.56 & 0 & 0 & 0 & 0 \end{pmatrix}.$$

(Matrix A is not a real matrix of the subsystems' relations, just some model matrix). Matrix A has 10 eigenvalues in modulus 3.2.

Enter $y = (0, 0.1, 0.1, 0.1, 0.1, 0.05, 0.05, 0, 0.3, 0.05)'$ and A as an input data.

As an ultimate result we get $p = 15$ and (10×15)-array E consisting of 15 vectors.

Given accuracy $\epsilon = 10^{-10}$ for the trajectory $\{(\psi_{\mu_{15}} \circ \psi_{\mu_{14}} \circ \ldots \circ \psi_{\mu_1})^m x\}$ its ω-limit set is a cycle of period 4.

For the trajectory $\{f^m y\}$ its ω-limit set $\omega_f y$ is a cycle of period $60 = 4 \cdot 15$.

The final macro system state is $S^*(y) = \{\omega_f y, E\}$.

We present graphic visualization of the part of $\omega_f y$ located in J_p along the vector e_1 i.e., four vectors with coordinates x^*, $(\psi_{\mu_p} \circ \ldots \circ \psi_{\mu_1})x^*$, $(\psi_{\mu_p} \circ \ldots \circ \psi_{\mu_1})^2 x^*$, $(\psi_{\mu_p} \circ \ldots \circ \psi_{\mu_1})^3 x^*$. In XY coordinate system four vectors with the same coordinates along the unit vector of the bisector of the first coordinate angle are drawn and their graphic image is shown in Fig. 13.2a. The parts of $\omega_f y$ located in J_p along the vectors $e_2, \ldots, e_p$, are of the same type i.e., each of them consists of four vectors.

Example 4 Change the initial vector to $y = (0.1, 0.1, 0, 0.3, 0.1, 0, 0, 0, 0.3, 0.05)'$.

The ultimate result is $p = 30$ (the maximum possible value at $n = 10$), (10×30)-array E now consists of 30 vectors.

Given accuracy $\epsilon = 10^{-10}$ for the trajectory $\{(\psi_{\mu_{30}} \circ \psi_{\mu_{29}} \circ \ldots \circ \psi_{\mu_1})^m x\}$ we get non-stop iterative process when calculating its ω-limit set. It means that ω-limit set is irregular or a cycle of a very large period. In this case we agreed to accept the last 200 iterations when calculating the trajectory $(\psi_{\mu_{30}} \circ \psi_{\mu_{29}} \circ \ldots \circ \psi_{\mu_1})^m x$ as its ω-limit set.

Graphic visualization of 200 vectors which are the part of $\omega_f y$ located in J_p along the vector e_1, is presented in XY coordinate system by 200 vectors with the same coordinates, along the unit vector of the bisector of the first coordinate angle. The graphic image of these vectors is shown in Fig. 13.2b.

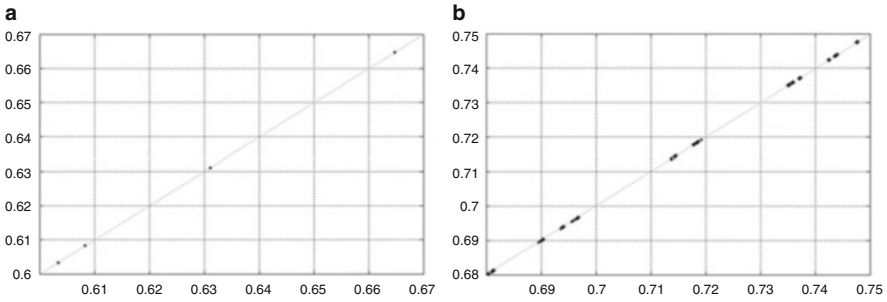

Fig. 13.2 In an XY coordinate system, vectors visualizing the part of the limit set $\omega_f y$ of 10-component macro system with p-periodic structure, along the unit vector e_1 of macro system structure: four vectors when macro system structure is 15-periodic (**a**); 200 vectors when macro system structure is 30-periodic (**b**)

13.7.3 Outcomes of Examples

Examples 1 and 2 show that in the first model the population structure is asymptotically stabilized and does not vary any more and population size, as well as age group sizes change periodically every 2 years. In the second model the structure of the population is stabilized and varies every 3 years along with the population size and age group sizes. Examining the dynamics of the population, one can see the mechanism of regulation or harvestable surplus of the population size without affecting long term stability, or average population size. Indeed, according to the second model all individuals of the third stage may be taken away after the childbearing period ($a_{33} = 0$) every year. In spite of the structure of the population, its size and age group sizes vary periodically, in this case the population remains persistent.

Stabilized periodic structure of macro system is determined by its initial structure and not its initial size. Indeed, by iterating the map F of the form (13.1) m times, we write out $F^m y = \Phi^{(m)}(y)A^m y$ where

$$\Phi^{(m)}(y) = \prod_{i=0}^{m-1} \Phi(F^i y),$$

$y \in \mathrm{X}$. Hence it follows that the directions of $F^m y$ and $A^m y$ coincide, $m = 1, 2, \ldots$ i.e., the directions of nonzero vectors of the trajectory $\{F^m y\}$ as $m \to \infty$ are defined by the linear part of the map F and are independent of the form of $\Phi(y)$.

Let all nonzero entries of the matrix A be equal to 3.2 in the Examples 3 and 4. Then $\mu_1 = \ldots = \mu_p = \mu = 3.2$, $\psi_{\mu_p} \circ \ldots \circ \psi_{\mu_1} = \psi_\mu^p$ and $\omega_{\psi_\mu^p} x$ is a cycle of period 2 for any $x \in \mathrm{I}$ [2, p. 26]. According to [19] there are more than one periodic attractors and therefore more than one different dynamics of the map $\psi_{\mu_p} \circ \ldots \circ \psi_{\mu_1}$, $p \geq 1$ at the fixed parameter values. So, if there is only one asymptotic regime of the map $\psi_{\mu_p} \circ \ldots \circ \psi_{\mu_1}$ in the interval I at the fixed $\mu_1, \ldots, \mu_p$, then macro systems with the same initial structure will have the same final state. If there are more than one asymptotic regimes of the map $\psi_{\mu_p} \circ \ldots \circ \psi_{\mu_1}$ in the interval I at the fixed $\mu_1, \ldots, \mu_p$, then macro systems with the same initial structure will have the same stabilized periodic structure and may have different sizes changed periodically (or not).

13.8 Conclusion

In this article we describe an approach we have developed to study multiparameter nonlinear dynamics. The advantages of applying the results of the qualitative theory and using the method of one-dimensional superpositions in a simulation of the

dynamics are as follows:

1. The dynamical systems considered are nonlinear and thus very sensitive to the data entry errors. The proposed method simplifies computations of the ω-limit set of the system trajectory. Firstly, a stable cycle of rays of period p, which contains the ω-limit set, is identified using the system matrix of the n-th order. Secondly, the ω-limit set is obtained using the non-linear one-dimensional map. As a result, this leads to markedly reduced computing times, especially when the order n and the periods p are large.
2. In an n-dimensional case, $n > 3$ it is impossible to obtain a graphic image of ω-limit sets of the dynamical system, e.g. to realize their types. However, we can get graphic visualization of the part of ω-limit sets consisting of vectors along the first unit vector of the stable invariant set containing the ω-limit set. In an XY coordinate system, vectors along the unit vector of the bisector of the first coordinate angle which have the same coordinates can be easily plotted.
3. Theoretical results of the qualitative theory help us to correctly interpret the numerical results as well as to conduct an accurate computer simulation of the system dynamics. We specify the number of iterations to detect a stable cycle of rays containing the ω-limit set of the system as well as the number of iterations to compute the ω-limit set.
4. The determination of the dynamical parameters and the calculation of their number and values by the formulas provides the description of the system dynamics in stable cycles of rays containing ω-limit sets of the system and therefore, the identification of the regions with different dynamics. Their number may be very large, e.g. greater than the number of the system parameters. However, one can see that this number cannot be reduced without the loss of accuracy of the system behavior description.

Acknowledgements The work is supported by the grant 0292/GF3 of Ministry of Education and Science of the Republic of Kazakhstan.

References

1. A.N. Sharkovskii, Co-existence of cycles of a continuous mapping of the line into itself. Ukr. Math. J. **16**, 61–71 (1964)
2. A.N. Sharkovskii, Y.L. Maistrenko, E.Y. Romanenko, *Difference Equations and Their Applications* (Naukova Dumka, Kiev, 1986) (in Russian)
3. M. Feigenbaum, Quantitative universality for a class of nonlinear transformations. J. Stat. Phys. **19**, 25–52 (1978)
4. R.M. May, Simple mathematical models with very complicated dynamics. Nature **261**(5560), 459–467 (1976)
5. A.G. Radwan, On some generalized discrete logistic maps. J. Adv. Res. **4**(2), 163–171 (2013)
6. G. Tiozzo, Topological entropy of quadratic polynomials and dimension of sections of the Mandelbrot set. Adv. Math. **273**(19), 651–715 (2015). doi:10.1016/j.aim.2014.12.033

7. M. Joglekar, J.A Yorke, Robustness of periodic orbits in the presence of noise. Nonlinearity **28**(3), 697–711 (2015). doi:10.1088/0951-7715/28/3/697
8. Z. Arai, W. Kalies, H. Cocubu, K. Mischaikow et al., A database schema for the analysis of global dynamics of multiparameter systems. SIAM J. Appl. Dyn. Syst. **8**(3), 757–789 (2009)
9. I. Gohberg, P. Lancaster, L. Rodman, *Invariant Subspaces of Matrices with Applications* (Providence, SIAM, 2006)
10. J. Sabuco, M.A.F. Sanjuan, J.A. Yorke, Dynamics of partial control. Chaos, **22**(4), 047507-1-047507-9 (2012)
11. A.S. de Paula, M.A. Savi, State space reconstruction applied to a multiparameter chaos control method. Meccanica **50**, 207–216 (2015). doi: 10.1007/s11012-014-0066-z
12. I.N. Pankratova, Cyclic invariant sets for one class of maps. Sib. Math. J. **50**(1), 107–116 (2009). doi:10.1007/s11202-009-0013-8
13. R. Muradore, R. Foroncelli, P. Fiorini, Statistical methods for estimating the dynamical parameters of manipulators, in *Proceedings of joint 48th IEEE Conference on Decision and Control and 28th Chinese Control Conference*, 2009, pp. 6472–6477. doi: 10.1109/CDC.2009.5400194
14. I.N. Pankratova, Limit sets of manydimensional analogy of nonlinear logistic difference equation. Differ. Equ. **32**(7), 1006–1008 (1996)
15. P.H. Leslie, The use of matrices in certain population mathematics. Biometrika **33**, 183–212 (1945)
16. D.O. Logofet, Projection matrices revisited: a potential-growth indicator and the merit of indication. J. Math. Sci. **193**(5), 671–686 (2013)
17. I.N. Pankratova, On some properties of invariant subspaces of linear operator containing cycles of rays, in *Conference Program and Book of Abstracts of Conference MAT TRIAD*, Herceg Novi, Montenegro, 2013, pp. 49–50. http://mattriad2013.pmf.uns.ac.rs/programme.php
18. R. Lamberson, R. McKelvey, B. Noon, C. Voss, A dynamic analysis of Northern spotted owl viability in a fragmented forest landscape. Conserv. Biol. **6**(4), 505–512 (1992)
19. J. Guckenhemer, G.F. Oster, A. Ipartchi. The dynamics of density dependent population models. J. Math. Biol. **4**, 101–147 (1976)

Chapter 14
Sudden Cardiac Death and Turbulence

Guillaume Attuel, Oriol Pont, Binbin Xu, and Hussein Yahia

Abstract Data acquired from the electrical activity of human hearts during episodes of atrial fibrillation, a disordered arrhythmia that is a major cause of stroke, reveals intriguing features for an excitable media: highly skew symmetric probability distributions with heavy tails, long range correlations, and broad singularity spectra. Interestingly, the relevant exponents extracted from these empirical laws are stable over several minutes but not universal. Their stable values are distributed among patients and areas of the heart. The question of central clinical purpose is whether they might characterise locally the myocardium contingent pathology. To achieve clarification of these peculiar facts, we were led to devise a phenomenological model that departs from the conventional approach to fibrillation. Instead of a defect mediated spiral wave "turbulence" induced by front collisions, fibrillation is pictured here as a highly intermittent modulation of cardiac pulse trains. It is based on the physiology of inter-cellular ionic exchanges, which is associated with the natural degree of freedom of the inter-pulse duration. We infer an experimentally unknown slow dynamics of inter-cellular coupling, that may induce an inter-pulse effective coupling. This interaction creates a modulation that may lead to intermittency in various ways. The exchange of charges occurs at small scales in the model. They are passively advected at each interstitial junction on fast time scales and on average collectively driving the larger scales. In fact, a dimensionless number characterising the dynamics is an analogue of the Rayleigh number. Away from a rapidly beating source, random back scattering and front splitting make pulses follow random hierarchical "percolating" paths in 1D. We discuss very briefly the topological origin of these dynamics. In the light of this model, we don't omit to mention some important physiological aspects of the pathology that are still not well understood and more possibilities for the case which comes to grip with sudden cardiac death.

8*th* CHAOS Conference Proceedings, 26–29 May 2015, Henri Poicaré Institute, Paris France.

G. Attuel (✉) • O. Pont • B. Xu • H. Yahia
GeoStat, "Geometry and Statistics in acquisition data", Centre de recherche INRIA Bordeaux Sud-Ouest, 200 rue de la Vieille Tour, 33405 Talence Cedex, France
e-mail: guillaume.attuel@inria.fr

C. Skiadas (ed.), *The Foundations of Chaos Revisited: From Poincaré to Recent Advancements*, Understanding Complex Systems,
DOI 10.1007/978-3-319-29701-9_14

14.1 Introduction

Sudden cardiac death accounts for about 10 % of all natural deaths in developed countries and for about 50 % of the mortality from cardiovascular diseases. Meanwhile, it is not really a pathology: statistical surveys have found risk factors but which fail to be individually predictive [1]. In our present understanding, it can be considered more as an accident. One cause of sudden cardiac death is fibrillation of the ventricles. Experimental studies are difficult for obvious reasons. The milder case of atrial fibrillation (AF), which is however one major cause of stroke in Europe and North America, can be monitored and studied more easily. In this paper, we give the general scheme of an analysis of AF that we are developing. We will shortly discuss at the end some possible lessons we may learn from it for sudden cardiac death.

The heart muscle is an excitable tissue, long believed to be a syncytium of myocardial cells. Models of excitability for the heart are reaction-diffusion systems that describe the propagation of electrical pulses, called action potentials. They result from ionic exchange cycles between the cytoplasm of excitable cells and their extra-cellular medium. A typical example is an action potential propagating through a nerve axon [2] or throughout the myocardium [3–6]. In the right atrium of a human heart, the sinus node (a pacemaker) ensures a periodic stimulation of the tissue, from where pulses propagate regularly in normal sinus rhythm. In its abnormal states, called arrhythmias, the myocardium is overwhelmed by rapid and irregular patterns of activation. In part for the reasons we are exposing in the text, we consider AF the most irregular arrhythmia, as illustrated in Fig. 14.1.

Chaos has been observed in cultures of automatic cardiac cells, through their coupling to periodic stimulation, and also in the heart via the occurrence of parasystoles. This can be traced to phase locking and chaos of relaxation oscillators with periodic forcing, and could be well modelled by return maps [7–9]. Also, period doubling, called alternans in this context, arises when the adaptation of the

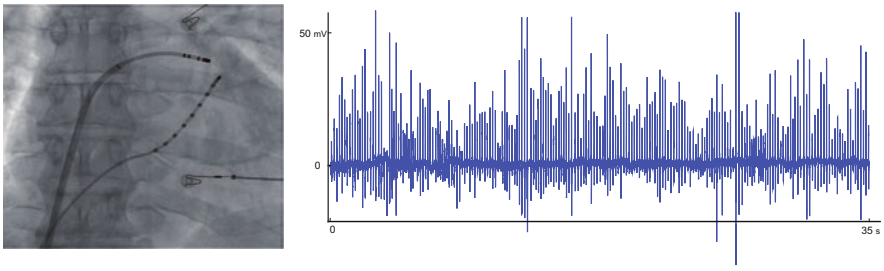

Fig. 14.1 A radiography of the atrium with two bipolar electrodes is shown. Held by a medical practitioner, one runs along the coronary sinus, while the other is located on the septum of the right atrium close to the appendage

action potential duration to an imposed rate becomes unstable [10]. For this reason, alternans are thought in one hypothesis as a route to ventricular fibrillation [11]. Moreover, fibrillation in the atria were in some instances clinically found to follow an inadaptation of the action potential duration [12]. However, an excitable limit cycle is very robust when it comes down to chaos, because its saddle fixed point does not give way to a homoclinic tangle. This can be understood by considering the stable fixed point as an absorbing state, or a phase resetting state. Therefore, even under periodic forcing, no return map can be drawn. In other words, the regularity of the triggering sources is transferred to the limit cycle.

In contrast, as propagation becomes further involved in the arrhythmia, the usual theoretical interpretation is based on a kind of defect mediated turbulence, specific to excitable oscillators. Basically, spiral waves are often found more stable than striped or other patterns in excitable media. This stems from the important fact that an excitable pulse with a free end meets a region in a refractory state and starts wandering about it [13–15]. It is also more fundamentally related to the topological charge of the spiral core [16] and to the chiral symmetry breaking that an excitable pulse carries with itself (a Bloch wall) [17–19]. Low dimensional aperiodicity has again been observed before the onset of fibrillation for meandering spiral cores [20]. To account for spatio-temporal chaos a mechanism of front collisions is put forward. If in oscillatory media spirals may break up due to a modulational instability of the emitted pulse train from its meandering core, in excitable media the breakup seems to amount to direct fore front and back front collisions within the pulse train [21–23]. Notice that when a small diffusivity of the inhibitor is added, a curvature instability may lead to front splitting and spiral turbulence near the Ising-Bloch transition [24].

As successful as low dimensional chaos, and spatio-temporal chaos, in excitable media may look in describing these arrhythmias, we show here why this paradigm is quite inadequate to tackle an essential property of the recorded data, which hasn't been noticed so far.

A crucial aspect about the pathology is the intermittency of bursty occurrences of the arrhythmia. Intermittent alternation of sinus rhythm with fibrillation is what defines paroxysmal AF. This intermittency can be modulated by the external drive of the autonomic nervous system, as shown by P. Coumel and co-workers, see for instance [25]. Moreover, on the myocardium surface, within each episode of fibrillation, the recorded signal is found to be more or less regular: the so called "fragmentation" in clinical lingo. In fact, as we demonstrate in Sect. 14.2, the locally recorded electrical potential exhibits many traits in common with hydrodynamic intermittency. Another poorly understood fact is a reversible process of deterioration of the myocardium during AF called remodelling [26]. It appears that the longer the heart remains in a fibrillatory state, the poorer its conduction properties become, and the more stable this abnormal state gets. We believe that these features are rooted in some underlying chemical modulation of the electrical synapses between the cells. Our model demonstrates this possibility.

We may look for the nucleation of metastable chaotic domains to explain such observations. This has led us to find out a physiological path to the mechanism

described by Pomeau [27]. As illustrated in [28], if a limit cycle is able to reach its homoclinic connection, then bistability with another fixed point, or cycle, may generate spatio-temporal intermittency. The difficulty is that an excitable limit cycle is over-damped and very robust. No such saddle fixed point connecting with another basin of attraction normally exists. Even worse would be to try to find a crisis bifurcation to some strange attractor. Never mind, if the tissue is in fact capable of generating another limit cycle, then the route devised by Y. Pomeau might be reached. For instance a modulation of pulse trains would work. This can be indeed the case as we show. This originates in the electrical coupling between the cells, that under some circumstances which we describe, may grow collectively, versus diffusively. One can thus rephrase the previous findings for oscillatory media in terms of these collective modes, and find a variety of interesting scenarios. For simplicity, we adopt a point of view *à la* Ginzgurg Landau.

We formulate therefore in Sect. 14.3 a derivation from first principles of the yet unknown dynamics of ionic currents at the gap junctions. This dynamical coupling between cells is considered as a synaptic plasticity. The point is to question the importance of intrinsic fluctuations and disorder. We make sure that observing the Ginzburg region of criticality in excitable reaction-diffusion systems is classically impossible. Then, we will find out that cardiac pulses can be pinned where cycles of neighbouring cells become out of phase with one another, because of interstitial plasticity. This unfortunate plasticity may slowly contaminate the whole tissue, which is what we will relate to electrical remodelling.

In Sect. 14.4, we very briefly sketch an interpretation. Due to the intrinsic noise, the critical Ginzburg domain extends widely, leading to self organised criticality (SOC). This maps to multiplicative noise, describing the singularities in the signal.

We will show throughout the text the high level of agreement between the patients data and the model data.

14.2 Time Series, Fluctuations and Limitations of Excitable Models

Surface electrical potentials recorded as time series during AF are called electrograms (egm), such as the one shown in Fig. 14.1. Normal frequency f, in beats per minute, is about $f \approx 60$ bpm, whereas during AF, it is typically in the range of 200 bpm $\lesssim f \lesssim$ 600 bpm. At first sight, egms during AF contrast to normal as they seem to fluctuate randomly. Their amplitude also looks locally abnormally oscillatory, Fig. 14.2. The auto-correlation function starts decreasing rapidly, exponentially fast during the first 60 ms or so, and goes on oscillating with a slow decrease of the envelop, asymptotically as a power law, see Fig. 14.2, where an indicative solid line $\sim t^{-1}$ is drawn. Peaks appear naturally as multiples of the average periodicity of the arrhythmia at about 300 bpm there. The identification of the shorter time scale is expected and indicative of local incoherent oscillations, but

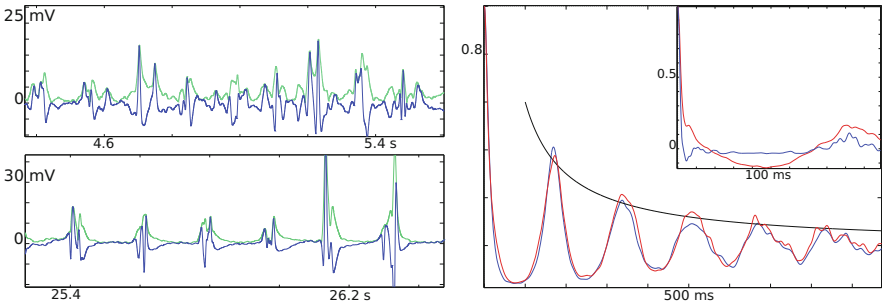

Fig. 14.2 *Left*: two instances of one egm amplitude and its envelop at two different moments in time, where a Hilbert transform was used. *Right*: two auto-correlation functions of egm envelops, and of amplitudes in the inset, for two different locations on the heart

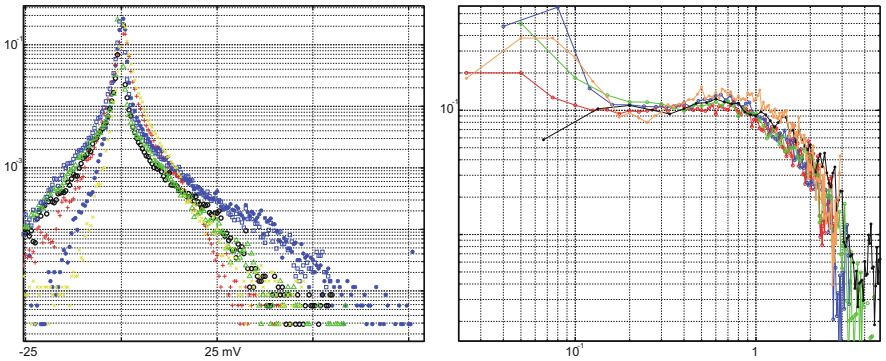

Fig. 14.3 Normalised probability density distributions of egm amplitudes in semilog scale, from all over the atrium of one patient (*left*). Shown in loglog scale the empirical collapse, for positive values and various exponents τ, on a scaling function G of Eq. (14.1) (*right*). $A_c \sim 3 - 5$ mV

the algebraic correlation law of the envelop is more suggestive of some collective phenomena with quasi long-range order. Thus, we are led to look for some collective modulation of the pulses.

We observe that fluctuations are large and their probability density distributions collapse as is seen in Fig. 14.3. The high skewness and heavy tails are a hint of underlying mechanisms. They can be cast into the form

$$P(A, A_c) = A^{-\tau} G\left(\frac{A}{A_c}\right) \tag{14.1}$$

where A is the egm varying amplitude in mV, A_c is a cut-off, τ is a scaling exponent, and a scaling function G decreasing rapidly towards zero. Very briefly summarized, various values of τ have been found. They range roughly between $1.2 < \tau < 3$ among patients, and regions of the atria. To our knowledge, similar fluctuations were not found in excitable systems, but are rather ubiquitous in complex systems.

To name a few instances, they are found in random field Ising models [29], with the Barkhausen noise as a magnetic field is applied to a dirty ferromagnet [30], for magnetic penetration in hard superconductors [31–33], during the firing activity of some neural networks [34–37], or in the intermittent regimes of strong turbulence [38, 39].

Turning to continuous excitable media, they are modelled by reaction-diffusion systems

$$\begin{cases} \frac{\partial}{\partial_t} U_m = \mathcal{R}(U_m, J_m) + D\Delta\left(U_m\right) \\ \frac{\partial}{\partial_t} J_m = \mathcal{G}(U_m, J_m) \end{cases}. \tag{14.2}$$

Here, U_m is associated with the membrane potential of a cell, and J_m is a vector representing (non diffusing) inhibitors, associated with the many ionic currents going through channels across the otherwise impermeable membrane of a cardiac cell. In the limit of interest, time scales are well separated, that is U_m is a fast variable, while J_m is a slow variable. One usually denotes by $\mu^{-1} \approx 1\,\text{ms}$, the typical fast time scale, which corresponds to the time for the insulating membrane, of thickness $\Lambda \approx 100\,\text{nm}$, to depolarise. This is possible at such short time scales because Nernst-Planck thermal equilibrium is reached indeed thanks to facilitated diffusion and active pumping of ions [40]. The slow time scale, associated with repolarisation, is typically of the order of 100 ms or greater.

Now, to be endowed with the property of excitability, the system's null clines, $\mathcal{R} = 0$ and $\mathcal{G} = 0$, basically intersect in a way as to produce locally a kind of saddle-node configuration. Nonlinearities and dissipation (or periodic order parameters) give rise to a limit cycle once an orbit is generated away from the saddle fixed point. It is insightful to draw a straightforward analogy with a Van der Waals diagram. Roughly speaking, the analogy goes as: a cycle "nucleates" each time the "supercooled spinodal branch" is reached by a finite perturbation. The width of the nucleation region corresponds to the degree of excitability. A Ginzburg-Landau description of Eq. (14.2) reads as $\frac{\partial}{\partial t} U_m = -\frac{\delta}{\delta U_m} \mathcal{F}_0$, with a free energy of the form

$$\mathcal{F}_0 = \frac{1}{2} \int dx^d \left\{ -\mu U_m^2 + \frac{\beta}{2} U_m^4 + D\left(\nabla U_m\right)^2 - I U_m \right\} \tag{14.3}$$

where all parameters are positive, $I = J_0 - J_m$ is a source term, and J_0 is an external input of current. Dimension $d = 2$ is appropriate for the atria, since the atrial myocardium is very thin, typically of order 2 mm thick, as it does not contribute much to the pump function of the heart, while $d = 3$ is more adequate for the ventricles. In fact dimension $d = 1$ is quite appropriate also for the description of fast conducting fibres in both chambers.

Since the free energy has two local minima, depending on boundary conditions, domain walls typically form. In source free conditions, their height is $U_0 = 2\sqrt{\frac{\mu}{\beta}} \approx 100\,\text{mV}$ and their thickness is the Ginzburg-Landau correlation length

$l_c \propto \sqrt{\frac{D}{\mu}} \approx 1$ mm. They propagate at constant velocity by diffusion, with a velocity $c \propto \sqrt{D\mu} \approx 1\,\mathrm{ms}^{-1}$. The role of the recovery current J_m is to break the symmetry between the two minima of the energy manifold, by favouring the return to one of them, corresponding to the rest potential. In its most basic version, we have the Fitzhugh-Nagumo model (FhN), with $\mathcal{G}(U_m, J_m) = \gamma U_m - \sigma J_m - \eta$, where σ controls the repolarisation time scale, and η is a leaking current. It defines a cell cycle.

For the sake of simplicity here, let us take $\eta = 0$, the condition of excitability becomes $\mu > \frac{\gamma}{\sigma}$. Let us admit that FhN may spontaneously evolve into locally aperiodic states, for instance with more complicated reactions $\mathcal{G}$ and the spiral breakup mechanism [41]. Then, configuration averaging leads to an effective reparametrization $\mu \to \mu - \frac{\gamma}{\sigma}$, since one expects fast modes to be slaved to slow modes and average as $\langle J_m \rangle = \frac{\gamma}{\sigma} \langle U_m \rangle$. The mean field susceptibility may then increase to very high values $\chi \sim \left(\frac{\gamma}{\sigma} - \mu\right)^{-1} \to \infty$ on the verge of excitability, thereby explaining the large fluctuations and long range correlations observed.

The argument above fails firstly because it only tells us locally that cycles will be triggered almost with no threshold. Secondly, on a global scale, the narrowness of the critical Ginzburg region in parameter space prevents any wild collective effect to become observable [42]. Taking the order of magnitude of the diffusive length of about $l_c \approx 1$ mm and bringing it next to the microscopic cut-off length, the maximum between the gap junction wall thickness $\Lambda \approx 100$ nm and the Debye length, here about $\lambda_D \approx 10$ nm , one obtains a very narrow width of the parameter range, entirely unobservable in practice $\delta\chi^{-1} \sim \Lambda^2 l_c^{-2} \lesssim 10^{-10}$.

This rules out near equilibrium critical fluctuations in ordinary excitable media. We have realized however that mean field arguments break down when the ionic exchange current at the gap junction alters the effective potential energy of the cell, in such a way as to restore a continuous symmetry, and approach an effective critical region.

14.3 Incorporation of Cell to Cell Dynamical Coupling

The works in [43–45] show the crucial role played by the gap junctions, since they are supposed to guarantee good coupling between the cells. However, in excitable models it is not clear how bad conduction can be modelled. According to near equilibrium thermodynamics, the exchange current may simply be written down as $J_e = -g_s \nabla U_m$, where g_s is a stationary conductance. The point is to demonstrate that the perturbation of the opening and closing of the gap junction channels induce some time lag in the activation of the cell.

Typical relaxation times of gap junctions are much larger than those of membrane polarisation, but compare well with membrane repolarisation time scales. On average they are of order $\gtrsim 100$ ms [46]. There is thus no alternative but to consider the full kinetics of the gap junctions, at such high frequencies as found in arrhythmias. This is a crucial aspect missing in common models for arrhythmias.

Applying common wisdom on membrane physico-chemistry to the gap junctions, replacing U_m with ∇U_m, yields a kinetic relaxation equation of the form [2]

$$\frac{\partial}{\partial t} g = a(\nabla U_m)\,(g_0 - g) - b(\nabla U_m) g\ , \tag{14.4}$$

where the functions $a(\nabla U_m)$ and $b(\nabla U_m)$ are the respective average rates of opening and closing of the gap junction channels. The constant g_0 is a typical maximum resting value, essentially $g_s = g_0 \frac{a}{a+b}$. The gradient is the one felt at the gap junctions. So we turn to the question of how the electrical force $-\nabla U_m$ can be strong enough as to perturb a and b in order to make the current deviate from electro-diffusion. Since a pulse front of typical width l_c encompasses many cells, the voltage difference $\sim \Lambda \nabla U_m$ at a gap junction cannot be as strong as the one felt across membranes. Nevertheless, gap junction channels have a very distinctive role in inter-cellular communication. They are open at rest state, and very long molecules permeate through. They are therefore inclined to a modulation of their permeability, depending on the concentration levels of some messenger molecules [47]. We explore here this possibility, letting some ions act on the gap junction properties. This will simply arise from their naturally slow linear response to the presence of high ionic concentration.

In that respect, there exists a point of view that allows us to characterise the ionic flow by a dimensionless number. For certain values of this dimensionless number, an instability will occur for the most unstable mode [48], which eventually will develop dissipative structures [49, 50]. Upon forcing the system to higher values, secondary instabilities may destabilise the primary structures, leading to a broad spectrum of modes [51].

To construct our model, we basically use charge conservation and a kinetic equation for the gap junction channel average opening under proper thermodynamic forcing. As is depicted in Fig. 14.4, we consider an excess charge sitting at the gap junction, and its effect on the equilibrium dynamics. The force is simply the electro-chemical gradient. In 1D, as the sketch suggests, take a finite volume element $\mathcal{V}$ spanning the gap junction, incorporating the excess charge and extending to the membranes. Noting ρ the excess density, charge conservation inside this volume reads $\frac{\partial}{\partial t}\rho = -\tilde{g}\nabla U_m$, where the gradient is understood as a finite difference over the closed surface. We used a perturbed conductance $\tilde{g}$, which is the important assumption in our model. It states that excess charge density variations overrate the stochastic averaging of the opening and closing of the channels, that would otherwise set the conductance to its equilibrium value. Therefore, we need to consider Eq. (14.4), which we will linearise as $a(\nabla U_m) = \alpha\rho + a_0$, with α a control parameter, and $b = b_0$ for the sake of simplicity of the demonstration. This linearisation simply stipulates that the excess charge amounts to $\mathcal{V}\rho \approx C\nabla U_m$, with a gap junction effective capacitance C. Note that the extra cellular medium is supposed to rest at a constant potential reference.

The combined equations basically say that excess charges are swept along the small scale gradients (excess charges will tend to average out over large volume

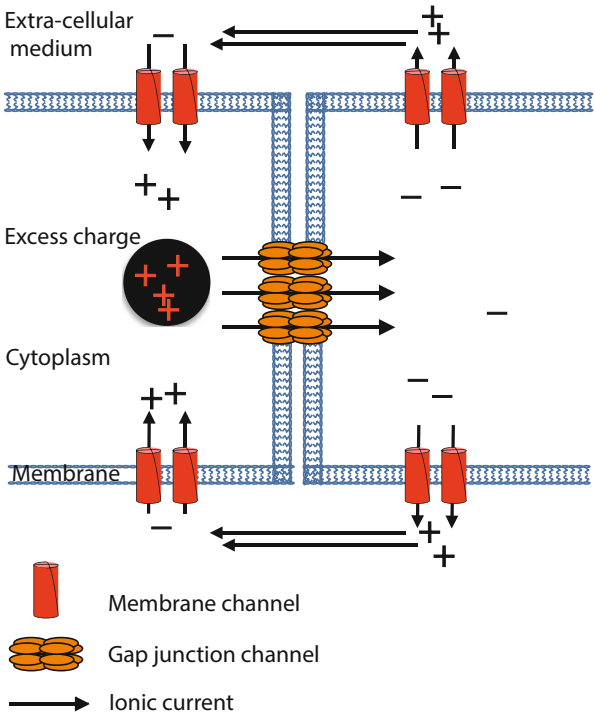

Fig. 14.4 Excess of positive charge (*black*) sitting next to the gap junction channels. *Arrows* indicate inter-cellular flows, which are generally supposed to be diffusive

elements comprising many cells), while variations of the conductance remain local. Denoting $\nu = a_0 + b_0$, dropping the tilde for clarity, we get the following system of equations

$$\begin{cases} \frac{\partial}{\partial t} U_m = \mu U_m - \beta U_m^3 - J_m + D\Delta U_m - \nabla (g\rho) \\ \frac{\partial}{\partial t} J_m = \gamma U_m - \sigma J_m \\ \frac{\partial}{\partial t} g = \alpha \rho - \nu g \\ \frac{\partial}{\partial t} \rho = -g \nabla U_m - \nu_2 \rho \end{cases}, \tag{14.5}$$

where we have let the capacitance and volume $C \equiv 1$, $\mathcal{V} \equiv 1$ without loss of generality. The locally perturbed current is $g\rho$ by construction. The evaporation rate ν_2 is a local simplification of charge diffusion, for a fixed length scale, and is meant to be small. This set is not parity invariant, and by construction one needs to take an opposite α to change directions of front propagation from the location of a source, since the potential gradient will reverse sign.

As we described above, some important perturbations of the dynamics may emerge at slow time scales. Indeed, this simple model is in spirit quite comparable to a kind of Rayleigh instability, where α plays the role of the gravitational pull. Because the interface is fixed at the gap junction, no convective term is present. More precisely, when only two cells are coupled with one free boundary, notice

indeed how the first, third and fourth equations have the same structure as the Lorenz system of ODE (where the opposite limit $\mu \to 0$ holds though). The analogue Rayleigh dimensionless number is here $\mathcal{R}_a \equiv \frac{\alpha\rho}{L\nu\nu_2}$, which controls the effect of thermodynamic forcing over dissipation, where L is an equilibrium length associated with the slow time scales. In fact, we force the system at one end with an automatic cell (a very rapid abnormal pacemaker), or similarly with an abnormal current leak J_0. Now, since on average we will have $D\left\langle\frac{\rho}{L}\right\rangle \approx J_0$, it is possible to rewrite

$$\mathcal{R}_a \equiv \frac{\alpha J_0}{D\nu\nu_2} \,. \tag{14.6}$$

So we expect a transition point towards chaos around $\mathcal{R}_a \sim 1$, for very small arrays, of two to a very few cells, and to turbulence in longer arrays. This transition to high dimensional chaos is illustrated in Fig. 14.5.

It is easy to quickly check the validity of this argument numerically. Starting with parameters for which we observe regularity of beats and rhythm, decreasing D, ν_2 or ν, and raising α makes it possible to reach a domain of turbulent dynamics of ρ and g, that strongly affect U_m and J_m, see Fig. 14.6. Here, we provide an illustration of the turbulent domain with the same numerical values of the parameters as in Fig. 14.6. We do find similar properties for the numerical data as for the experimental data. It seems indeed that long range auto-correlations decrease as $\sim t^{-1}$ power laws. As shown in Fig. 14.7, probability density distributions of the current divergence scale in the same way. Despite that the effect of the system size seems negligible at first glance on the onset of turbulence, we find non universal exponents, which appear to mark the distance from the source. Just as strikingly, the broad singularity spectra, with a substantial contribution of negative exponents, can be superposed completely, see Fig. 14.8. This tends to demonstrate the presence of an identical random cascade process underlying the dynamics.

The transient time that the turbulent state takes to pervade the system could be related to the electrical remodelling. We observe a typical time scale that reads like

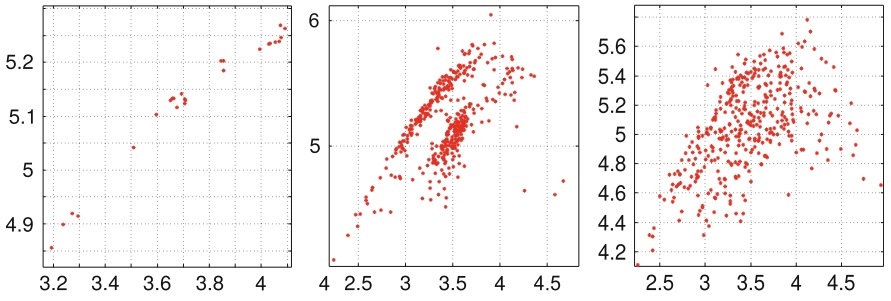

Fig. 14.5 Poincaré section plots (ρ, g), from maxima of U_m, for 2, 3 and 4 cells coupled linearly, in the special case $\mu = 0$ and $\sigma \to \infty$. The section on the *left* is from the famous Lorenz attractor. One notes the spreading of points revealing the increase of the attractor dimension

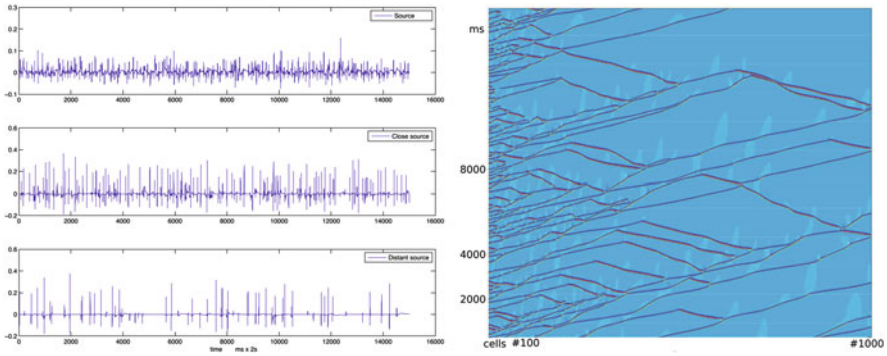

Fig. 14.6 Some traces of the gap current divergence, in the model in 1D, from near a source of abnormal automaticity, cell #0, to further away. Spatio-temporal map of action potentials showing many back-scattering and some front splitting in a hierarchical structure of propagation, since the ones that escape collisions rarefy. $\mu = 1$, $\beta = 1$, $\gamma = 0.008$, $\sigma = 0.02$, $\alpha = 0.01$, $\nu = 0.01$, $\nu_2 = 0.0001$

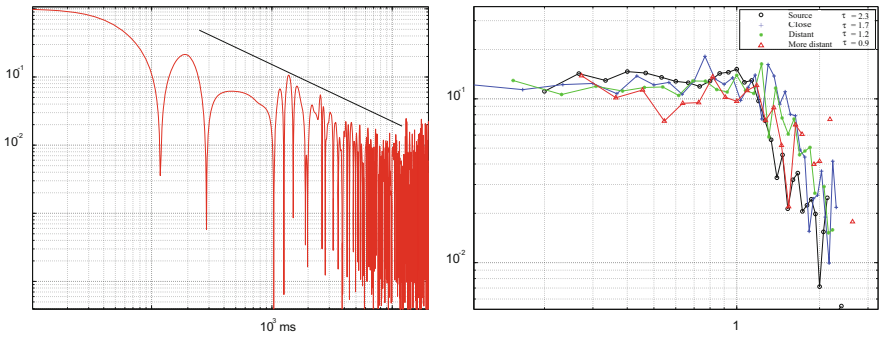

Fig. 14.7 Loglog plot of the auto-correlation of cell #5, with an indicative t^{-1} plot (*left*). Empirical collapse function G for the model (*right*), with non universal exponents, decreasing with distance from the source for arbitrary cells, shown #2, #20, #80, and #400

$T \sim L^z$, with $z \approx 1$. For typical length of human atrial fibres, it happens to fall in the physiologically recorded range of about a few minutes [52]. Finally, system size does affect the onset of turbulence as expected, the distance from the source affects the scaling exponents we have found, see Fig. 14.7. This basically marks the hierarchical propagation pattern. In practice, this could be good news for a quantitative method of finding abnormal sources of activity in the heart, a highly valued goal pursued by medical practitioners and physiologists.

This phenomenology holds in two dimensions with isotropic coupling as well. Note also that the propagation of perturbing charges is like some effective diffusion of the inhibitor. Therefore, considering the anatomical organisation of the myocardium in fibre bundles and the anisotropy of conducting properties, one expects fronts to split along their direction.

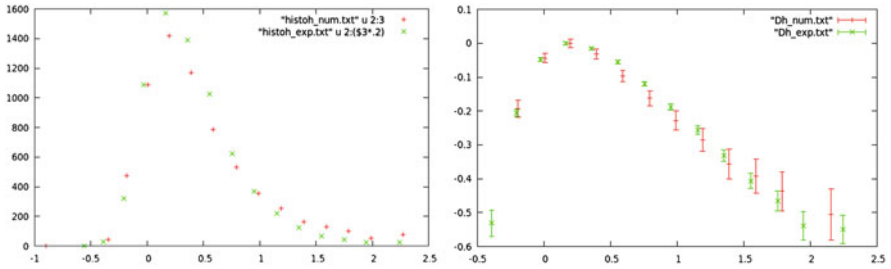

Fig. 14.8 Strikingly good superposition of the broad histograms (*left*) and fractal dimension spectra (*right*) of the sets of singularity exponents h defined locally, for small τ of a few *ms*, as $\left\langle \int^{\tau} dt \, \frac{\partial}{\partial t} \boldsymbol{\nabla} g\rho \right\rangle \sim \tau^{h}$. They were obtained from the same experimental data as in Fig. 14.2 and the 1D numerical data as in the previous figures for an average over ten cells taken at random spanning the first 100 cells

By chance, in three dimensions various topological arguments convey the idea that the ventricles are better equipped to resist such onset of very irregular patterns. Thus far, one may have in mind natural selection to understand the Aschoff-Tawara node, which function is somehow to low-pass filter the activity of the atria, before relaying it to the ventricles.

14.4 Discussion and Conclusion

The large oscillations of pulses and the intermittency are quite intriguing at first, since μ is the dominant parameter, which guarantees the stability of U_0 against any spontaneous fluctuation. In fact, a phase approximation of the dynamics is indeed relevant in this sector. Then, what is seen might signal the restoration of a continuous symmetry for the dynamics of the phase, that finds itself effectively at criticality.

Firstly, upon appropriate rescaling, define a complex scalar $\Psi = U_m + iJ_m = Ae^{i\theta}$. The phase $\theta\,(\mathbf{x}, t)$ is a distribution of ticks recording the passage and shape of pulses. Since μ defines the rapid time scale, it is natural to consider a fixed amplitude of Ψ. Let us model the perturbation caused by the ionic gap currents as some local time delay φ for the onset of depolarisation. The equation for the phase then reads

$$\partial_t \theta = D\Delta\theta - H \sin\left(\theta + \varphi\left(\mathbf{x}\right)\right) + F, \tag{14.7}$$

where H and F define characteristic scales that can be made to match that from $\mathcal{R}$ and $\mathcal{G}$, such as the domain wall thickness $l_c \sim \sqrt{H^{-1}}$. Taking a random distribution of phase in the range $\varphi\,(\mathbf{x}) \in [0, 2\pi]$, random pinning is facilitated. This governs the behaviour of charged density waves in impure magnetic materials [53–56]. Naively, an effective critical state could be reached from the average of random phases $\mu_{eff} \sim \langle H \cos(\varphi)\rangle$, though the model equation does not reduce to critical dynamics, model A in [57]. Basically, one can find in the literature the anomalous scaling of the

velocity jumps of the density waves, that reads like $\delta v \propto F^{\xi}$ with $\xi \neq 1$, near the forcing threshold of the depinning transition (insulating to conducting). SOC is typically found in those systems [58]. Counting consecutive phase slips, one finds a distribution of avalanches that typically scales with system size, a cut-off measuring a distance to a critical point, in a form like Eq. (14.1), where the exponent τ is related to ξ [29, 59].

Hence, one notes that avalanches of phase slips, within a surrounding closed contour, must be related to large amplitude variations of the bulk average. Heuristically, the argument is quite suggestive of multi-scaling. From the slowly varying random aspect of the noise term emerges a random cascade. It is tempting to model this dynamical effect by a mean field multiplicative noise $\mu \mapsto \tilde{\mu}(J_0, \boldsymbol{x}, t)$ acting on top of diffusion, leading to large deviations as captured by the observed singularity spectra [39], and percolating paths [60]. In fact, chaotic coupled map lattices (with a derivative coupling here) are known to show desychronisation patterns, spatio-temporal intermittency in the universality class of the Kardar Parisi Zhang equation or in the class of directed percolation [61, 62].

In conclusion, we have presented data, from humans with a very irregular arrhythmia, that seem to exhibit patterns of hydrodynamic intermittency. We showed that such fluctuations could not emerge from purely excitable dynamics, and found out a good alternative candidate, namely intrinsic modulations. We devised a model of ionic flows through the gap junction channels of a cardiac tissue, that effectively modulate otherwise independent pulses. The observed abnormal patterns finely match the ones from the model, when the flow is intermittent. It is the first to manifest a transient related to the degradation of pulse propagation, called electrical remodelling, and to suggest a relationship between local exponents in the signal with the distance to an abnormal source.

In that respect, we would like to believe that our model may further illustrate Y. Pomeau's conjecture, relating hydrodynamic intermittency with some directed percolation of metastable orbits.

At any rate, these results are clear evidence of the role of the dynamical coupling of the network of cells, which do not form a true syncytium.

References

1. D.P. Zipes, H.J.J. Wellens, Circulation **98**, 2334 (1998)
2. A.L. Hodgkin, A.F. Huxley, J. Physiol. **117**(4), 500 (1952)
3. B. van der Pol, J. van der Mark, Philos. Mag. Suppl. (6), 763 (1928)
4. D. Noble, J. Physiol. **160**, 317 (1962)
5. R. Fitzhugh, in *Mathematical Models of Excitation and Propagation in Nerve*, ed. by H.P. Schwan. Biological Engineering (McGraw-Hill, New York, 1962)
6. J. Nagumo, S. Arimoto, S. Yoshizawa, Proc. IRE **50**, 2061 (1962)
7. M.R. Guevarra, L. Glass, J. Math. Biol. **14**, 1 (1982)
8. L. Glass, M.R. Guevarra, A. Shrier, R. Perez, Physica 7D 89 (1983)
9. U. Parlitz, W. Lauterborn, Phys. Rev. A **(36)**, 1428 (1987)
10. M.R., Guevarra, L. Glass, IEEE Comput. Cardiol. 167 (1984)
11. A. Karma, Chaos **4**, 461 (1994)

12. P. Attuel et al., Int. J. Cardiol. **2**, 179 (1982)
13. M.A. Allessie, F.I.M. Bonke, F.J.G. Schopman, Circ. Res. **41**(1), 9 (1977)
14. E. Meron, P. Pelcé, Phys. Rev. Lett. **60**(18), 1880 (1988)
15. A. Hagberg, E. Meron, Phys. Rev. Lett. **72**(15), 2494 (1994)
16. I.S. Aranson, L. Kramer, Rev. Mod. Phys. **74**(1), 99 (2002)
17. J. Lajzerowicz, J.J. Niez, J. Phys. Lett. **40**(7), 165 (1979)
18. P. Coullet, J. Lega, B. Houchmanzadeh, J. Lajzerowicz, Phys. Rev. Lett. **65**(11), 1352 (1990)
19. T. Frisch, S. Rica, P. Coullet, J.M. Gilli, Phys. Rev. Lett. **72**(10), 1471 (1994)
20. A. Garfinkel et al., J. Clin. Investig. **99**(2), 305 (1997)
21. A. Karma, Phys. Rev. Lett. **71**(7), 1103 (1993)
22. A.T. Winfree, Science **266**(5187), 1003 (1994)
23. F.H. Fenton, E.M. Cherry, H.M. Hastings, S.J. Evans, Chaos **12**(3), 852 (1993)
24. A. Hagberg, E. Meron, Chaos **4**(3), 477 (1994)
25. P. Attuel, P. Coumel, M.J. Janse, *The Atrium in Health and Disease*, 1st edn. (Futura Publishing Co, Mount Kisco, 1989)
26. M.C. Wijffels, C.J. Kirchhof, R.M. Dorland, M. Allessie, Circulation **92**, 1954 (1995)
27. Y. Pomeau, Physica 23D 3 (1986)
28. M. Argentina, P. Coullet, Phys. Rev. E **56**(3), R2359 (1997)
29. K. Dahmen, J.P. Sethna, Phys. Rev. B **53**(22), 14872 (1996)
30. J.C. McClure Jr., K. Schroder, C R C Crit. Rev. Solid State Sci. **6**(1), 45 (1976)
31. J.S. Urbach, R.C. Madison, J.T. Market, Phys. Rev. Lett. **75**(2), 276 (1995)
32. C.J. Olson, C. Reichhardt, F. Nori, Phys. Rev. B **56**(10), 6175 (1997)
33. E. Altshuler et al., Phys. Rev. B **70**, 140505 (2004)
34. J.M. Beggs, D. Plenz, J. Neurosci. **23**(35), 1167 (2003)
35. C.-W. Shin, S. Kim, Phys. Rev. E **74**, 045101(R) (2006)
36. L. de Arcangelis, C. Perrone-Capano, H.J. Herrmann, Phys. Rev. Lett. **96**, 028107 (2006)
37. J. Hesse, T. Gross, Front. Syst. Neurosci. **8**, 166 (2014)
38. S. Ciliberto, P. Bigazzi, Phys. Rev. Lett. **60**(4), 286 (1988)
39. U. Frisch, *Turbulence: The legacy of Kolmogorov* (Cambridge University Press, Cambridge, 1995)
40. B. Hille, *Ion Channels of Excitable Membranes*, 3d edn. (Sinauer Sunderland, 2001)
41. A. Panfilov, P. Hogeweg, Phys. Lett. A **176**, 295 (1993)
42. L. Landau, E.M. Lifchitz, *Physique Statistique*, 4th édn. (Mir ellipse, Moscow, 1994)
43. Y.J. Chen, S.A. Chen, M.S. Chang, C.I. Lin, Cardiovasc. Res. **48**, 265 (2000)
44. G. Bub, A. Shrier, L. Glass, Phys. Rev. Lett. **88**(5), 058101 (2002)
45. G. Bub, A. Shrier, L. Glass, Phys. Rev. Lett. **94**, 028105 (2005)
46. H.-Z. Wang, J.L. Jian, F.L. Lemanski, R.D. Veenstra, Biophys. J. **63**, 39 (1992)
47. J. Neyton, A. Trautmann, J. Exp. Biol. **124**, 93 (1986)
48. M.C. Cross, P.C. Hohenberg, Rev. Mod. Phys. **65**(3), 851 (1993)
49. P. Glansdorff, I. Prigogine, *Thermodynamic Theory of Structure, Stability and Fluctuations*. (Wiley-Interscience & Wiley, New York, 1971)
50. I. Prigogine, G. Nicolis, Q. Rev. Biophys. **4**(2 & 3), 107 (1971)
51. P. Bergé, M. Dubois, J. Phys. Lett. **46**(10), 431 (1985)
52. E.G. Daoud et al., Circulation **94**, 1600 (1996)
53. H. Fukuyama, P.A. Lee, Phys. Rev. B **17**(2), 535 (1978)
54. P.A. Lee, T.M. Rice, Phys. Rev. B **19**(8), 3970 (1979)
55. M.J. Rice, Phys. Rev. Lett. **36**(8), 432 (1976)
56. G. Grüner, Rev. Mod. Phys. **60**(4), 3970 (1979)
57. P.C. Hohenberg, P.C. Hohenberg, Rev. Mod. Phys. **49**(3), 435 (1977)
58. C.R. Myers, J.P. Sethna, Phys. Rev. B **47**(17), 11171 (1993)
59. D.S. Fisher, Phys. Rev. Lett. **50**(19), 1486 (1983)
60. H. Hinrichsen, Adv. Phys. **49**(7), 815–958 (2000)
61. G. Grinstein, D. Mukamel, R. Seidin, C.H. Bennett, Phys. Rev. Lett. **70**(23), 3607 (1993)
62. P. Grassberger, Phys. Rev. E **59**(3), R2520 (1999)

Chapter 15
Absolute Negative Mobility in a Ratchet Flow

Philippe Beltrame

Abstract This paper is motivated by the transport of suspended particles pumped periodically through a modulated channel filled of water. The resulting flow behaves as a ratchet potential, called ratchet flow, i.e. the particle may drift to a preferential direction without bias. We study the deterministic particle dynamics using continuation of periodic orbits and of periodic transport solutions. The transport exists regardless the parity symmetry of the problem and the bifurcation scenario involve chaotic transitions. Moreover, the influence of the noise is discussed and points out a counter-intuitive consequence. The noise triggers a particle transport in the opposite direction to the bias (Absolute Negative Mobility). We show that this phenomenon is generic for slightly biased ratchet flow problem.

15.1 Introduction

The transport of micro-particles through pores in a viscous fluid in absence of mean force gradient finds its motivation in many biological applications as the molecular motor or molecular pump. In the last decade, the literature shows that a periodical pore lattice without the symmetry $x \to -x$ can lead to the so-called ratchet effect allowing an transport in one direction x or $-x$. A review can be found in Hänggi and Marchesoni [12]. We focus on the set-up presented in Matthias and Müller [22] and Mathwig et al.[21] consisting in a macroporous silicon wafer which is connected at both ends to basins. The basins and the pore are filled with liquid with suspended particles (1–10 μm). The experiment shows the existence of an effective transport in a certain range of parameter values. By tuning them, the direction of the effective transport may change and in particular the transport direction is opposite to the particle weight. These results may be interpreted as a ratchet effect by Kettner et al.[14] and Hänggi et al.[13] where "ratchet" refers to the noisy transport of particle without bias (zero-bias). When the transport direction

P. Beltrame (✉)
UMR1114 EMMAH, Department of physics, Université d'Avignon – INRA, F-84914 Avignon, France
e-mail: philippe.beltrame@univ-avignon.fr

C. Skiadas (ed.), *The Foundations of Chaos Revisited: From Poincaré to Recent Advancements*, Understanding Complex Systems,
DOI 10.1007/978-3-319-29701-9_15

is opposite to the bias, then it is called Absolute Negative Mobility (ANM), see e.g. Du and Mei [9] or Spiechowicz et al.[27]. Recently, we show that inertia may induce a directed transport Beltrame et al.[4]. In this deterministic approach where thermal fluctuations are negligible and a small inertia is taken in to account, the transport results from non-linear phenomena. Because of the existence of transport without bias, we called the fluid flow in the micro-pump: ratchet flow. Since the results of the experiment of Mathwig et al.[21] questions the relevance of small fluctuations in the transport, in this paper, we propose to better understand the role of noise in this non-linear dynamics. And especially to focus on a possible Absolute Negative Mobility.

We consider a one-dimensional system where the Stokes force and a small random force due to fluctuations are the only forces acting on the particle. It results a ODE system which is similar to inertia ratchet as found in the literature: Barbi and Salerno [3], Mateos [18], Speer et al.[26] and Alatriste and Mateos[1]. In these latter papers, transport solutions synchronized with the periodic forcing are found for the deterministic case. They show that this dynamics results from a synchronization transition as it occurs for periodically forced oscillator Pitkovsky et al.[24]. This regime can be destroyed via a crisis which appears after a period-doubling cascade. The synchronized transport regime may exist in the symmetric case (parity symmetry $x \to -x$), see Speer et al.[26] or Cubero et al.[6]. Obviously, it implies the existence of an opposite transport solution and then there is no transport in statistical sense. Now, if a small bias is applied, the domain of existence of opposite transport solutions do not match anymore. As consequence by varying the tuning parameter the transport direction may change and in particular the transport opposed to the bias may exist (Wickenbrock et al.[30]). The deterministic dynamics may help to understand ANM too. For instance, in Machura et al.[16], the nonlinear analysis showed that stable periodic solution and unstable periodic transport solution coexist. By adding a small noise, the trajectory may escape from the bounded periodic solution and may follow during few periods the periodic transport solution. As consequence, a drift opposed to the bias is triggered by the noise.

Despite a plethora of study in this topic, there is still open issues as the transition from unbounded dynamics to transport dynamics which seems no to be clearly identified. Moreover, most studies assumed the inertia large or, in contrary, the limit case of overdamped dynamics (Kettner et al.[14] and Lee [15]). Here we consider moderate drag coefficient of the particle. We aim at finding transport transition and possible ANM. In order to tackle this problem we propose to study the deterministic case with inertia particle and then apply a small Gaussian noise. In addition to the time integration, the deterministic case is analyzed with the help of continuation method (Beltrame et al.[5] and Dijkstra et al.[7]). This method appears seldom in the literature dealing with ratchet (see e.g. Pototsky et al.[25]). However, we can follow periodic orbit (or relative periodic orbit for the transport solution) and determine their stability and bifurcation point. Thus, it is powerful to determine onsets and the kind of bifurcation.

In the present work, we consider the physical parameters: particle drag (inverse of the inertia), the mean flow of the fluid, the velocity contrast, the asymmetry of

the flow and the bias (resulting from the particle weight). We analyze firstly the bounded periodic solution (symmetric and asymmetric cases), Secondly, the onset of transport is determined. Finally, we treat the case of the small perturbation due to a Gaussian noise.

15.2 Modeling

Let us consider a L-periodic varying channel along the line (Ox) (Fig. 15.1) through which a viscous fluid containing suspended particles is periodically pumped. We assume that the period of the pumping period is small enough to consider a creeping flow. Such an assumption is relevant for periodicity for $L \simeq 10\,\mu\text{m}$ and $T \geq 1\,\text{ms}$ (Kettner et al.[14]). The particle is centered on the x-axis then the momentum of the particle is neglected and the particle does not rotate. This creeping flow exerts a F_d drag force on the particle along the x axis. The set-up is vertical so that the particle weight, F_w, is oriented to the x negative and the buoyancy force, F_b, to the positive direction. Thus the particle position $x(t)$ is governed by the equation

$$m\ddot{x}(t) = F_d + F_w + F_b \tag{15.1}$$

To simplify, we assume that F_d is approximatively given by the Stokes drag: $F_d = -\gamma(v(x,t) - v_f(x,t))$, where γ is the drag coefficient and v and v_f are the particle velocity and the fluid velocity without particle, respectively. This expression of the drag force requires that the particle is small comparing to the channel radius. Because, it is quasi-static problem, the fluid velocity distribution without particle is proportional to the amplitude pumping so that we may write: $v(x,t) = u_0(x)\sin(2\pi t)$ for a sinusoidal pumping, where $u_0(x)$ depends on the pore profile. We obtain the adimensional governing equation

$$\ddot{x}(t) = \gamma(u_0(x(t))\sin(2\pi t) - \dot{x}(t)) + g \tag{15.2}$$

where the length is scaled by the pore length L, the time by the pumping period T and the drag by m/T and $g = (F_w + F_b)/(mL/T^2)$. This equation admits an unique solution C^2 for a given position and velocity (x_i, v_i, t_i) at a time t_i. In particular,

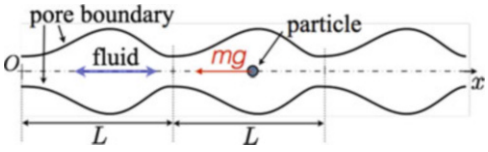

Fig. 15.1 Sketch of the problem: the particle translates along the x-axis of a periodic distribution of pores. It is dragged by a periodic motion of a viscous fluid. The particle weight is oriented to the negative x direction

two different solutions cannot have at a given time the same position and velocity. Another straightforward result shows that particle acceleration $\ddot{x}$ and its velocity $\dot{x}$ remain bounded.

The velocity profile $u_0(x)$ gets the periodicity of the geometry. If the pore geometry is symmetric, we consider a sinusoidal velocity profile:

$$u_0(x) = u_m(1 + a\cos(2\pi x)) \tag{15.3}$$

where u_m is the mean velocity and a the velocity contrast. Otherwise for asymmetric geometry, we consider an additional parameter d related to the asymmetry and then the pore profile is given by:

$$\begin{aligned} u_0(x) = u_m &+ a u_m \cos\left(\pi \frac{\bar{x}}{\frac{1}{2}+d}\right) \mathbb{1}_{[0;\frac{1}{2}+d]}(\bar{x}) \\ &+ a u_m \cos\left(\pi \frac{\bar{x}-1}{\frac{1}{2}-d}\right) \mathbb{1}_{]\frac{1}{2}+d;1]}(\bar{x}) \end{aligned} \tag{15.4}$$

d is the algebraic shift which ranges from $-\frac{1}{2}$ to $\frac{1}{2}$, $\bar{x} = x \mod 1$ and $\mathbb{1}_I$ is the indicator function of the interval I ($\mathbb{1}_I(\bar{x}) = 1$ if $\bar{x} \in I$, otherwise $\mathbb{1}_I(\bar{x}) = 0$). Examples of the velocity profiles are shown in Fig. 15.2. Note that, it is possible to

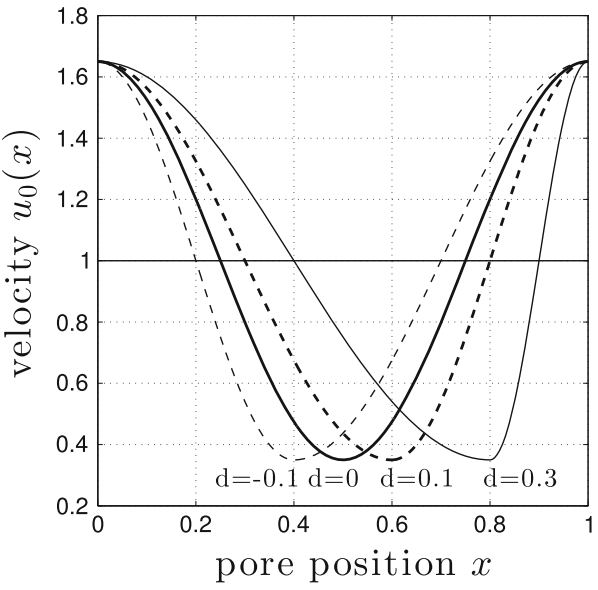

Fig. 15.2 Analytical velocity profiles of the flow $u_0(x)$ for $u_m = 1$, $a = 0.65$ and different values of d

find out pore profiles corresponding to such analytical profiles, see Beltrame et al.[4] and Makhoul et al.[17]. The asymmetry parameter d does not add a bias: if $g = 0$, the bias remains zero even if $d \neq 0$.

As explained in the introduction, we employ continuation method in order to track the periodic orbits of Eq. (15.2) in the parameter space. We use the software AUTO (Doedel et al.[8]). This latter requires an autonomous system. In order to obtain an autonomous system and still periodic orbits, we added an oscillator which converges asymptotically to the sinusoidal functions called φ and ϕ:

$$\dot{x} = v \tag{15.5a}$$

$$\dot{v} = \gamma\,(u_0(x)\phi - v) + g \tag{15.5b}$$

$$\dot{\phi} = 2\pi\varphi + \phi(1 - \varphi^2 - \phi^2) \tag{15.5c}$$

$$\dot{\varphi} = -2\pi\phi + \varphi(1 - \varphi^2 - \phi^2) \tag{15.5d}$$

where the sinusoidal forcing is the asymptotical stable solution of Eqs. (15.5c) and (15.5d), i.e. $\phi \to \sin 2\pi t$ and $\varphi \to \cos(2\pi t)$ [2]. The system (15.5) has the same periodic solutions as Eq. (15.2). This four-dimensional problem can be written

$$\dot{s} = (\dot{x}, \dot{v}, \dot{\varphi}, \dot{\phi}) = F(x, v, \varphi, \phi) = F(s) \tag{15.6}$$

The deterministic transport is only possible if u_0 is not constant, then the velocity field $u_0(x)$ constitutes the ratchet flow. Considering a symmetric problem, i.e. $u_0(-x) = u_0(x)$ and $g = 0$, the function F is equivariant by the central symmetry $F(-s) = -F(s)$. As consequence, s is solution implies $-s$ is solution too. We called symmetric orbit, solution which are invariant by the central symmetry. There is two symmetric solutions: one centered the pore middle ($x = 1/2$), noted s_m and at the second one, centered at the pore inlet ($x = 0$), noted s_0.

For the asymmetric case, it is no longer true. However, for small oscillation amplitude u_m, the problem is similar to charged particles in a non-uniform oscillating electromagnetic force (McNeil and Thompson [23]) and it is possible to prove that there exists periodic solution centered at the extrema of $u_0(x)$. At the maximum it is unstable while it is stable at the minimum and it constitutes the only attractor (Beltrame et al.[4]).

Therefore, the analytical results do not show existence of transport solution. In the following we propose to track the periodic solutions in the parameter space.

15.3 Transitions to Transport Solutions

We study the periodic branches for the symmetric case, i.e., the velocity profile u_0 is symmetric ($d = 0$) and there is no bias ($g = 0$). Besides the solutions s_0 and s_m, we find an asymmetric branch (Fig. 15.3a). This branch is not invariant by the central symmetry and there is two branches s_a^+ and s_a^- copies by the central symmetry.

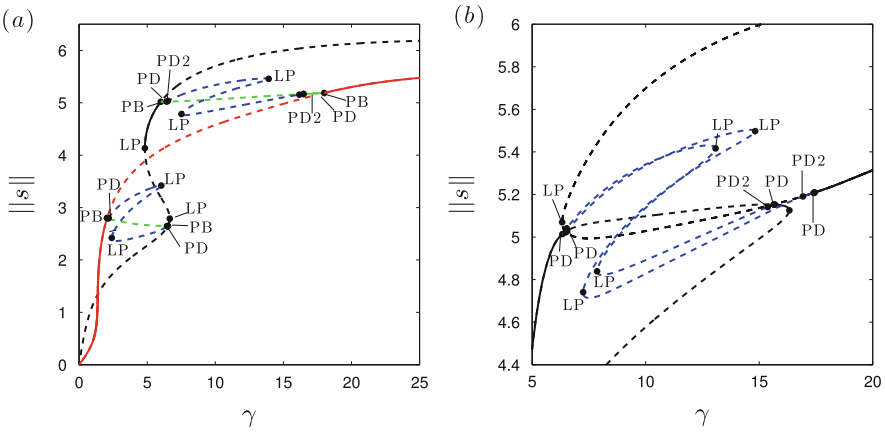

Fig. 15.3 (**a**) Bifurcation diagrams showing the periodic branches as a function of the drag γ for $a = 0.65$, $u_m = 9$ in the symmetric case. The *black color* indicates the s_0 branch, *red* the s_m branch, *green* the s_a branch and *blue* the 2-periodic branch. *Dots* indicate the different bifurcations: Pitchfork bifurcation (PB), Period-Doubling (PD) and (PD2) for the second period-doubling, fold bifurcation (LP). (**b**) Bifurcation diagram for the parameter but in the asymmetric case: $d = 0.1$ and $g = -0.1$. *Black* indicate 1-periodic branch and *blue* 2-periodic branch. In both diagrams, *plain lines* indicate stable orbits while *dashed line* correspond to unstable orbits

Then, they have the same norm and they do not appear in the bifurcation diagram, we note them s_a to simplify. The s_a branch results from a pitchfork bifurcation either from s_0 or s_m and thus connect both branches (Fig. 15.3a). This arises in the intervals $[2.05, 6.52]$ and $[6, 18]$. At each end of the intervals, the same scenario, described below, occurs by varying γ away from the pitchfork bifurcation:

1. The s_a branch is stable in the vicinity of the pitchfork bifurcation but it is destabilized in the via a period doubling. We plotted the bifurcated 2-periodic branch which displays two folds. It becomes unstable via period doubling too. Note that the period-doubling cannot arise on a symmetric branch according to Swift and Wiesenfeld [28].
2. A period doubling cascade follows the first period-doubling and leads to a strange attractor. The present cascade has a behavior similar to one-dimensional map whose the distance between two consecutive bifurcations is divided by the universal Feigenbaum constant [10] $\delta \simeq 4.669$.
3. The strange attractor is bounded till an widening crisis (Grebogi et al.[11]). As consequence, contiguous attractors (shifted by one spatial period) are connected. Because of the spatial shift symmetry, the dynamics is no longer bounded. Of course for the symmetric case no preferential direction of the particle trajectory is observed. This Dynamics is reminiscent of anomalous diffusion (Mateos and Alatriste [20]).

For the asymmetric case, similar transitions from 1-periodic orbit to the onset of the transport are observed. Nevertheless, the pitchfork bifurcations of the 1-periodic

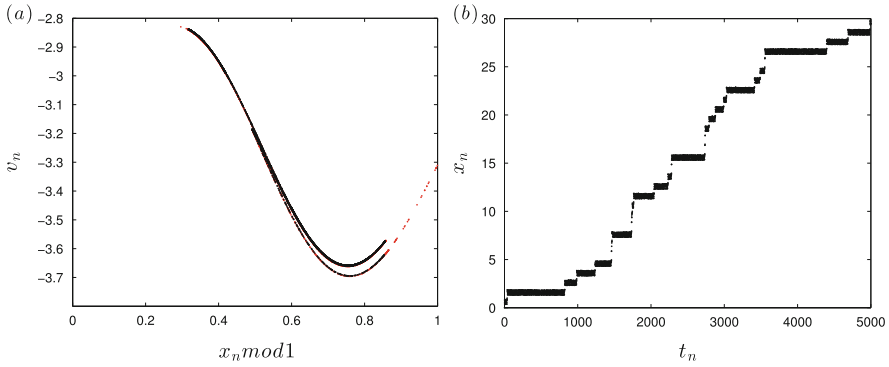

Fig. 15.4 (**a**) Poincaré section ($x_n = x(n) mod 1, v_n = v(n)$) where $n \in \mathbb{N}$ near the onset of transport at (*black dots*) $\gamma = 14.70$ and (*red dots*) $\gamma = 14.69$, other parameters are: $u_m = 9, a = 0.65, d = 0.1, g = -0.1$. The strange attractor in *black* remains in the interval $[0, 1]$ while the *red* strange attractor is no longer bounded. Its representation modulo 1 displays a sudden expansion characteristic of the widening crisis. (**b**) Discrete dynamics $x_n = x(t_n)$ at discrete times $t_n = n$ of the *red* strange attractor of the panel (**a**) at $\gamma = 14.69$. An intermittent drift to positive x appears (Color figure online)

orbits vanish and instead there is two 1-periodic branches formed, firstly, by the coalescence of the s_0, s_a^+ and s_m and, secondly, by the coalescence of s_0, s_a^- and s_m. An example for $d = 0.1$ and $g = -0.1$ (other parameters being the same as for the symmetric case) is displayed in the bifurcation diagram (Fig. 15.3b). From each branch, a period-doubling occurs. Both 2-periodic branches present two folds. A period-doubling cascade arises as for the symmetric case. We focus on the period-doubling cascade which starts at the largest drag coefficient $\gamma \simeq 16.48$. Indeed a drag coefficient smaller than 10 is quite unrealistic for small particles. The period-doubling cascade leads to an asymmetric strange attractor at $\gamma \simeq 15.2$. At $\gamma_c^t \simeq 14.698$, we observe a widening crisis connecting the contiguous attractors (Fig. 15.4a). But this time, because of the asymmetry of the system, there is a non-zero mean drift particle (see Fig. 15.4b). As expected, the dynamics after the crisis is intermittent: the dynamics spends a long time near the "ghost" bounded strange attractor and "jumps" to the other "ghost" attractor shifted by one period length. Note that, it is quite unexpected that we obtain a transport opposite to the bias. Now, we study the transport solutions.

15.4 Transport Solutions

By decreasing further the drag coefficient, the drift velocity increases. In fact, the mean duration of the bounded-like dynamics is shorter. For γ approaching the critical value $\gamma_c^s \simeq 13.41639$, the drift velocity is almost equal to one. The epochs of bounded-like dynamics are very short comparing to the transport events. The

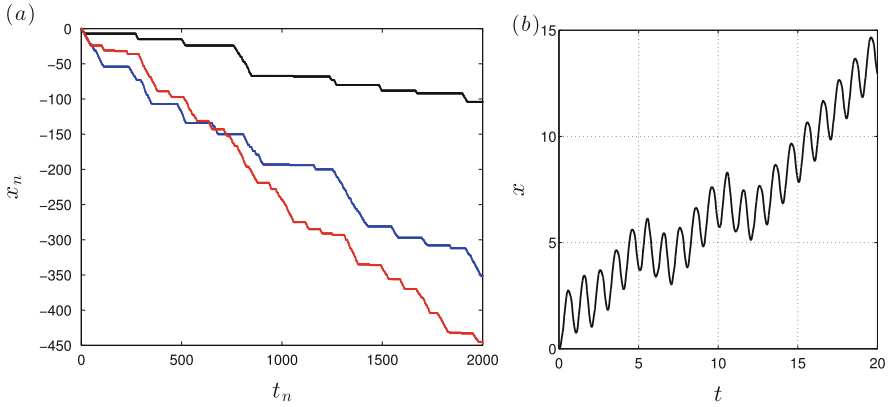

Fig. 15.5 (**a**) Discrete dynamics x_n at entire times t_n in the co-moving frame $c = +1$ near the onset of synchronization at (*red*) $\gamma = 13.4170$, (*blue*) $\gamma = 13.4165$ and (*black*) $\gamma = 13.4164 > \gamma_c^s$. Other parameters are $u_m = 9, a = 0.65, d = 0.1, g = -0.1$. The plateaux correspond to a near synchronized transport with $c = +1$. (**b**) Dynamics $x(t)$ for $\gamma = 13.416 < \gamma_c^s$: after a chaotic transition, the dynamics is the synchronized transport with $c = +1$

discrete particle position $x_n = x(t_n)$ at entire times $t_n = n$ and in the comoving frame with the speed $+1$ is displayed in the Fig. 15.5a. Thus, the long plateaux correspond to the dynamics with drift velocity about one. When γ tends to γ_c^s the longer of the plateaux diverges and then the velocity tends to one. For $\gamma > \gamma_c^s$ the dynamics is periodic in the comoving frame. In other words, the particle advances of one spatial length after one period (Fig. 15.5b). It is the so-called synchronized transport. In point of view of synchronization, it is a synchronization of oscillators with forcing at moderate amplitude Vincent et al.[29]. Then the transition is a saddle-node. Moreover, the chaotic transient observed in Fig. 15.5b suggests the presence of a chaotic repeller as it occurs in this case, see e.g. Pitkovsky et al.[24].

We study the regular transport emerging from the synchronization. Since the transport $x_t(t)$ is periodic in the comoving frame, we introduce the periodic function x_p such as

$$x_t(t) = x_p(t) + ct \tag{15.7}$$

where $c = \pm 1$ depending on the direction of the transport. Then if x_t is solution of Eq. (15.2) then it is solution of the equation:

$$\ddot{x}_p = \gamma \left[u_0(x_p + t)) \sin(2\pi t) - \dot{x}_p - c \right] + g, \tag{15.8}$$

It is a similar equation as Eq. (15.2) with an added bias $-\gamma c$. We found a transport with $c = +1$ and also the opposite transport $c = -1$ (Fig. 15.6b). The coexistence of opposite transport solutions is a consequence of the existence of synchronized transport in the symmetry case. Indeed, for the symmetric case, a similar scenario leads to the synchronized transport (Fig. 15.6a). In this case, according to the

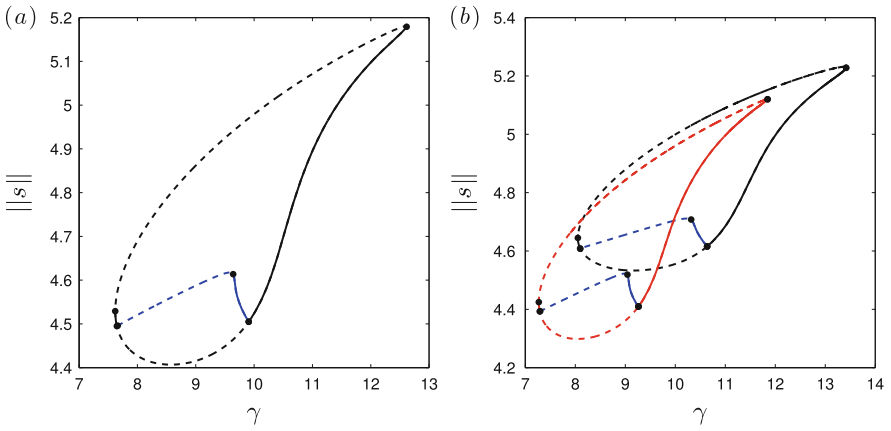

Fig. 15.6 (**a**) Bifurcation diagram of the synchronized transport solution with $c = \pm 1$ for the symmetric case. The solution emerges at saddle-node bifurcations. *Dashed* [*plain*] *line* indicate unstable [stable] solution branch. The stable branch becomes unstable via period-doubling (the blue branch corresponds to 2-periodic orbit), which is again unstable by period-doubling. Other parameters are $u_m = 9, a = 0.65$. (**b**) Bifurcation diagrams of the synchronized transport solution with (*red*) $c = -1$ and (*black*) $c = +1$ for the asymmetric case: $d = 0.1, g = -0.1$, the other parameters being the same as in panel (**a**). A similar bifurcation diagram as for the symmetric case occurs for both branches $c = +1$ and $c = -1$. However, their domains of existence are slightly shifted

equivariance of the problem, if the solution $c = +1$ is found, then a solution $c = -1$ exists, deduced from the central symmetry (Speer et al.[26] and Beltrame et al.[4]). Because the transport solutions are not invariant by the central symmetry, a forced symmetry-breaking of the system do not destroy them, as long as the perturbation is small. Then, we expect that the transport solutions remain when the asymmetry d and the bias g are small.

All the bifurcation diagrams of synchronized transport with $c = \pm 1$ have the same structure (Fig. 15.6). The solution emerges from a saddle-node leading to the birth of a pair of saddle branches. The unstable branch remains unstable over its existence domain. The stable branch becomes unstable via a period doubling bifurcation. As for the bounded periodic solution, a period-doubling cascade occurs leading to a chaotic dynamics. Note however as long as a widening crisis does not occur, the drift velocity remains locked to $c = \pm 1$. After the widening crisis, the strange attractor is no longer bounded in the comoving frame. The resulting dynamics is no longer locked and it is chaotic. Examples for the symmetric and asymmetric cases are displayed in Fig. 15.7. For the symmetric case, there is a competition between opposite transport solutions which are unstable. The trajectory is unbounded but the mean position remains zero. It is an anomalous diffusion like. For the asymmetric case, the dynamics is similar but the resulting drift is non-zero. For the specific example in Fig. 15.7b, we obtain a net transport direction to the negative direction.

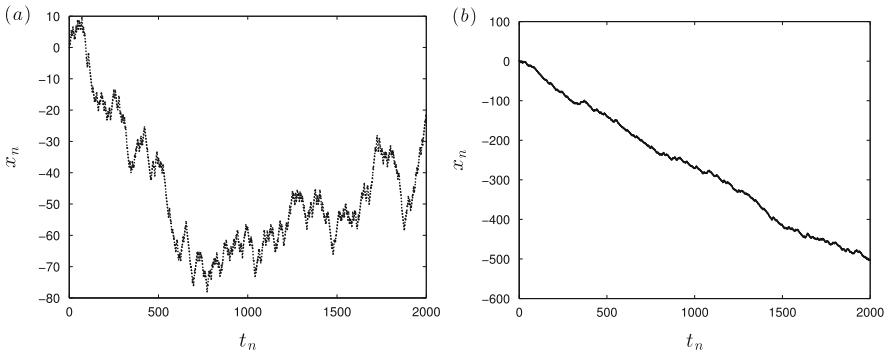

Fig. 15.7 Discrete time evolutions x_n at entire times t_n for $\gamma = 8.5, u_m = 9, a = 0.65$ and (**a**) for the symmetric case and (**b**) the asymmetric case: $d = 0.1, g = -0.1$. The dynamics display a competition between opposite transports. However in the asymmetric case, a net drift to x negative appears

In the asymmetric case, despite the negative bias, there is range where only the upward transport exists ($\gamma \in [11.8457, 13.41639]$). The 'trick" to obtain this unnatural dynamics was, firstly, to introduce the small flow asymmetry d which shifts the existence domains of the transport solutions $c = +1$ and $c = -1$ of the symmetric case (Fig. 15.6a). Then, the region $c = +1$ persists for a small enough negative bias g. Note, without the flow asymmetry d, this region does not exist. In this region, we have a particle motion opposed to the bias like the ANM. To find a upwards dynamics due to the noise, we have to study its influence.

15.5 Absolute Negative Mobility

We consider an additional random force, then the ODE system (15.2) becomes

$$\ddot{x}(t) = \gamma(u_0(x(t))\sin(2\pi t) - \dot{x}(t)) + g + \epsilon\xi(t) \tag{15.9}$$

where ϵ is the amplitude of the fluctuating force, and ξ is a Gaussian stochastic process such as $< \xi(t) >= 0$ and $< \xi(t)\xi(t') >= \delta(t - t')$ where δ is the Dirac delta expressing that the noise is purely Markovian. We propose to study the influence of the noise near the onset of unbounded dynamics at the widening crisis. Indeed, before the crisis and in its vicinity, contiguous strange attractors are close together then a small noise may allow to jump from a strange attractor to another one. The simulation near the strange attractor corroborates this scenario (Fig. 15.8). We observe a dynamics similar to the one which occurs after the crisis. Long epochs of bounded dynamics are interrupted by a jump to the upward pore. We do not observe jump to the downward direction. This is due to the asymmetry of the strange attractor. Note that the simulation in the symmetric case does not display a

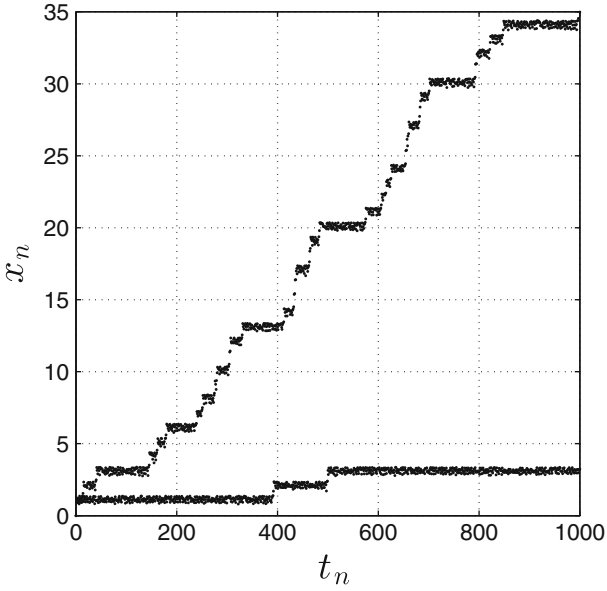

Fig. 15.8 Discrete stochastic particle dynamics at discrete times n governed by the Eq. (15.9) with the fluctuation amplitude $\epsilon = 0.1$ for two different values γ near γ_c^l: $\gamma = 14.7$ and $\gamma = 15$ (long plateaux). Other parameters are fixed to $u_m = 9, a = 0.65, d = 0.1, g = -0.1$

preferential direction. Away from the crisis by taking larger value of γ, the duration of the bounded dynamics events are statically longer. Indeed it is quite difficult to distinguish this noisy dynamics from the deterministic dynamics. The noise triggers the crisis transition leading to the same kind of dynamics. Since the transport is opposed to the bias and it does not exist without noise, we have found an example of Absolute Negative Mobility in this framework.

In contrast, once the deterministic crisis occurred, the noise does not notably modified the dynamics and the drift velocity. It seems to have a negligible influence on the onset of the synchronized dynamics too. Moreover, the small noise does not allow to escape from the attraction basin of the periodic transport solution so that it does not destroy the synchronized transport.

Note that the Absolute Negative Mobility found in Machura et al. [16] results from a different mechanism. Indeed, in their case the ANM dynamics follows during a few periods a deterministic unstable synchronized transport opposed to the bias which allows the drift. Such a behavior can be explained by the coexistence of a stable periodic solution with an unstable synchronized transport for the deterministic case. According to our bifurcation diagrams (Figs. 15.3 and 15.6), the synchronized transport exists only after the widening crisis, thus this kind of ANM cannot occur in our framework.

15.6 Conclusion

In this paper we have examined a nonlinear ODE and its perturbation by a small gaussian noise as a model for inertia particle transport via a micro-pump device. The equation is similar to ratchet problem where the ratchet flow $u_0(x)$ variations play the role of the periodical potential in the ratchet literature.

The deterministic analysis showed that synchronized transport solutions exist for inertia particles with drag coefficient about 10. Their existence is not related to asymmetry. Indeed for the symmetric case, the symmetric solution s_0 or s_m becomes unstable via a pitchfork bifurcation. This latter becomes unstable via period-doubling cascade leading to a bounded strange attractor. This strange attractor is destroyed via a widening crisis allowing the emergence of an unbounded dynamics. Finally, via a synchronization transition the periodic transport appears. In the symmetric case, the transports with $c = +1$ and $c = -1$ emerge at the same onset. A similar scenario occurs in the asymmetric case, but the onset of downward and upward transport no longer coincide. When the asymmetry is small, both transport directions exist but their existence domains are shifted. Thus there is a range of the drag coefficient where only the upward transport exists even if the bias is negative.

A weak noise does not modify the synchronized dynamics. However it may trigger the onset of the unbounded dynamics created via an widening crisis. We show that for subcritical parameters, a net drift may appear due to the noise. Indeed, it allows jumps between consecutive bounded strange attractors. We obtain an Absolute Negative Mobility near the onset of the upward transport. This mechanism differs from Machura et al.[16] and occurs in a very small range. That shows that the study of the deterministic case and the continuation method is powerful to understand and to find such dynamics. The found ANM is generic of slightly biased ratchet problem. In fact, the scenario involves generic non-linear phenomena: symmetric breaking and crisis in a spatial periodic problem. The existence of an upwards-transport opposed to the bias can be understood as a perturbation of the symmetric case where up and down dynamics coexist. Then for a small perturbation both should exist. Finally, it is quite known that the noise allows to escape from an attractor as it occurs in our case. So, the ANM scenario presented in this paper has a quite universal aspect for ratchet problem.

References

1. F.R. Alatriste, J.L. Mateos, Phase synchronization in tilted deterministic ratchets. Physica A: Stat. Mech. Appl. **372**(2), 263–271 (2006)
2. J.C. Alexander, E. Doedel, H.G. Jand Othmer, On the resonance structure in a forced excitable system. SIAM J. Appl. Math. **50**(5), 1373–71418 (1990)
3. M. Barbi, M. Salerno, Phase locking effect and current reversals in deterministic underdamped ratchets. Phys. Rev. E **62**, 1988–1994 (2000)
4. P. Beltrame, M. Makhoul, J. Maminirina, Deterministic particle transport in a ratchet flow. Phys. Rev. E **93**, 012208 (2016)
5. P. Beltrame, E. Knobloch, P. Hänggi, U. Thiele, Rayleigh and depinning instabilities of forced liquid ridges on heterogeneous substrates. Phys. Rev. E **83**(1), 016305 (2011)

6. D. Cubero, V. Lebedev, F. Renzoni, Current reversals in a rocking ratchet: dynamical versus symmetry-breaking mechanisms. Phys. Rev. E **82**, 041116 (2010)
7. H.A. Dijkstra, F.W. Wubs, A.K. Cliffe, E. Doedel, I.F. Dragomirescu, B. Eckhardt, A.Y. Gelfgat, A.L. Hazel, V. Lucarini, A.G. Salinger, E.T. Phipps, J. Sanchez-Umbria, H. Schuttelaars, L.S. Tuckerman, U. Thiele, Numerical bifurcation methods and their application to fluid dynamics: analysis beyond simulation. Commun. Comput. Phys. **15**, 1–45 (2014)
8. E. Doedel, R. Paffenroth, A. Champneys, T. Fairgrieve, Y. Kuznetsov, B. Sandstede, X. Wang, Auto 2000: Continuation and bifurcation software for ordinary differential equations (with homcont). Technical Report, Caltech, 2001
9. L. Du, D. Mei, Absolute negative mobility in a vibrational motor. Phys. Rev. E **85**, 011148 (2012)
10. M.J. Feigenbaum The universal metric properties of nonlinear transformations. J. Stat. Phys. **21**, 669–706 (1979)
11. C. Grebogi, E. Ott, F. Romeiras, J.A. Yorke, Critical exponents for crisis-induced intermittency Phys. Rev. A **36**(11), 5365–5380 (1987)
12. P. Hänggi, F. Marchesoni, Artificial Brownian motors: controlling transport on the nanoscale. Rev. Mod. Phys. **81**, 387–442 (2009)
13. P. Hänggi, F. Marchesoni, F. Nori, Brownian motors. Ann. Phys. **14**, 51–70 (2005). Wiley-VCH Verlag
14. C. Kettner, P. Reimann, P. Hänggi, F. Müller, Drift ratchet. Phys. Rev. E **61**(1), 312–323 (2000)
15. K. Lee, Overdamped transport of particles in a periodic ratchet potential. J. Korean Phys. Soc. **60**(11), 1845–1850 (2012)
16. L. Machura, M. Kostur, P. Talkner, J. Luczka, P. Hanggi, Absolute negative mobility induced by thermal equilibrium fluctuations. Phys. Rev. Lett. **98**(4), 040601 (2007)
17. M. Makhoul, P. Beltrame, M. Joelson, Particle drag force in a periodic channel: wall effects, in *Topical Problems of Fluid Mechanics : Proceedings*, Prague, 2015, pp. 141–148
18. J.L. Mateos, Chaotic transport and current reversal in deterministic ratchets. Phys. Rev. Lett. **84**, 258–261 (2000)
19. J.L. Mateos, Current reversals in deterministic ratchets: points and dimers. Physica D **168–169**, 205–219 (2002). {VII} Latin American Workshop on Nonlinear Phenomena
20. J.L. Mateos, F.R. Alatriste, Phase synchronization in tilted inertial ratchets as chaotic rotators. Chaos **18**, 043125 (2008)
21. K. Mathwig, F. Müller, U. Gösele, Particle transport in asymmetrically modulated pores. New J. Phys. **13**(3), 033038 (2011)
22. S. Matthias, F. Müller, Asymmetric pores in a silicon membrane acting as massively parallel Brownian ratchets. Nature **424**, 53–57 (2003)
23. B.W.J. McNeil, N.R. Thompson, X-ray free-electron lasers. Nat. Photon **4**(12), 814–821 (2010)
24. A. Pitkovsky, M. Rosenblum, J. Kurths, *Synchronization. A Universal Concept in Nonlinear Sciences* (Cambridge University Press, Cambridge, 2001)
25. A. Pototsky, A.J. Archer, S.E. Savel'ev, U. Thiele, F. Marchesoni, Ratcheting of driven attracting colloidal particles: temporal density oscillations and current multiplicity. Phys. Rev. E **83**, 061401 (2011)
26. D. Speer, R. Eichhorn, P. Reimann, Transient chaos induces anomalous transport properties of an underdamped Brownian particle. Phys. Rev. E **76**, 051110 (2007)
27. J. Spiechowicz, P. Hänggi, J. Luczka, Absolute negative mobility of inertial Brownian particles induced by noise, in *IEEE 22nd International Conference on Noise and Fluctuations*, vol. 370, 24–28 June 2013, Montpellier, France, 2013, pp. 446–447
28. J.W. Swift, K. Wiesenfeld, Suppression of period doubling in symmetric systems. Phys. Rev. Lett. **52**, 705–708 (1984)
29. U.E. Vincent, A.N. Njah, O. Akinlade, A.R.T. Solarin, Phase synchronization in unidirectionally coupled chaotic ratchets. Chaos **14**, 1018–1025 (2004)
30. A. Wickenbrock, D. Cubero, N.A.A. Wahab, P. Phoonthong, F. Renzoni, Current reversals in a rocking ratchet: the frequency domain. Phys. Rev. E **84**, 021127 (2011)